Spring 2015

Monoamine Transporter Photoaffinity Ligands Based On Methylphenidate and Citalopram: Rational Design, Chemical Synthesis, and Biochemical Application

Nageswari Yarravarapu

MONOAMINE TRANSPORTER PHOTOAFFINITY LIGANDS BASED ON METHYLPHENIDATE AND CITALOPRAM: RATIONAL DESIGN, CHEMICAL SYNTHESIS, AND BIOCHEMICAL APPLICATION

A Dissertation

Submitted to the Graduate School of Pharmaceutical Sciences

Duquesne University

In partial fulfillment of the requirements for

the degree of Doctor of Philosophy

By

Nageswari Yarravarapu

May 2015

MONOAMINE TRANSPORTER PHOTOAFFINITY LIGANDS BASED ON METHYLPHENIDATE AND CITALOPRAM: RATIONAL DESIGN, CHEMICAL SYNTHESIS, AND BIOCHEMICAL APPLICATION

By

Nageswari Yarravarapu

Approved March 4, 2015

David J. Lapinsky, Ph.D. Associate Professor of Medicinal Chemistry, Graduate School of Pharmaceutical Sciences, Duquesne University, Pittsburgh, PA (Committee Chair)	Michael Cascio, Ph.D Associate Professor of Chemistry and Biochemistry, Bayer School of Natural and Environmental Sciences, Duquesne University, Pittsburgh, PA (Committee Member)
Patrick T. Flaherty, Ph.D. Associate Professor of Medicinal Chemistry, Graduate School of Pharmaceutical Sciences, Duquesne University, Pittsburgh, PA (Committee Member)	Aleem Gangjee, Ph.D. Professor of Medicinal Chemistry, Graduate School of Pharmaceutical Sciences, Duquesne University, Pittsburgh, PA (Committee Member)
Marc W. Harrold, Ph.D. Professor of Medicinal Chemistry, Graduate School of Pharmaceutical Sciences, Duquesne University, Pittsburgh, PA (Committee Member)	J. Douglas Bricker, Ph.D Dean, Mylan School of Pharmacy Professor of Pharmacology-Toxicology

ABSTRACT

MONOAMINE TRANSPORTER PHOTOAFFINITY LIGANDS BASED ON METHYLPHENIDATE AND CITALOPRAM: RATIONAL DESIGN, CHEMICAL SYNTHESIS, AND BIOCHEMICAL APPLICATION

By

Nageswari Yarravarapu

May 2015

Dissertation supervised by Dr. David J. Lapinsky

Monoamine transporters (MATs) are a family of proteins that include the dopamine transporter (DAT), serotonin transporter (SERT), and norepinephrine transporter (NET). Specifically, dysregulation of MAT function is associated with a host of disease states including drug abuse, major depressive disorder, and anxiety. Additionally, several drugs acting as MAT inhibitors are clinically available to treat multiple disorders. However, details regarding the transport inhibition mechanism created by these drugs, as well as their discrete ligand-binding pockets within their target MAT proteins, remains poorly understood. This knowledge gap in turn hinders rational development of novel therapeutics for numerous MAT-associated disorders. The objective of this research dissertation was to develop irreversible chemical probes based

on methylphenidate (MP) and citalopram (CIT), two therapeutically significant MAT inhibitors, in order to map their binding sites and poses within their major MAT target protein. The central hypothesis was that MP and CIT could be rationally derivatized, without significant loss in pharmacological activity, to contain a tag moiety and a photoreactive group capable of forming a covalent bond to their target MAT protein, thus allowing application of a "Binding Ensemble Profiling with (f)Photoaffinity Labeling (BEProFL)" experimental approach. Specifically, BEProFL rationally couples photoaffinity labeling, chemical proteomics, and computational molecular modeling in order to map the binding sites and poses of ligands within their target proteins. This central hypothesis was tested by pursuing three specific aims: 1) identification of non-tropane photoprobes based on MP suitable for DAT structure-function studies, 2) identification of photoprobes based on CIT and (*S*)-CIT suitable for SERT structure-function studies, and 3) development of a tandem photoaffinity labeling-bioorthogonal conjugation protocol for SERT structure-function studies. In the first aim, MP was structurally modified to contain an aryl azide photoreactive group and a ^{125}I radioisotope tag. The compounds were then subjected to DAT pharmacological evaluation in order to identify suitable candidates for DAT structure-function studies. In the second aim, CIT and (*S*)-CIT were structurally modified to contain an aryl azide or benzophenone photoreactive group and ^{125}I, a terminal alkyne, or an aliphatic azide as a tag. Likewise, these compounds were subjected to SERT pharmacological evaluation in order to identify suitable candidates for SERT structure-function studies. Finally, under the third aim, a tandem photoaffinity labeling-bioorthogonal conjugation protocol was developed to label purified hSERT expressed in HEK-293 cells using a (*S*)-CIT-based benzophenone-alkyne

clickable photoprobe. Probe-labeled hSERT samples from this protocol are currently being analyzed by high resolution mass spectrometry in order to map the (*S*)-CIT-binding site(s) within the hSERT.

Dedicated to My Family

ACKNOWLEDGEMENTS

I would like to express my deepest gratitude to my research advisor, Dr. David J. Lapinsky, for his guidance and continuous support throughout these years. He truly takes the success of his students as a priority and invests a huge amount of time and energy in mentoring. He encouraged my interest in chemical biology and provided me with opportunities for professional development. He has taught me to never give up in the face of hardship and nurtured me into a confident researcher.

I sincerely thank Dr. Michael Cascio for giving me an opportunity to learn chemical biology techniques and guiding my research from a chemical biology point of view. I would like to thank my dissertation committee members, Dr. Aleem Gangjee, Dr. Patrick T. Flaherty, and Dr. Marc W. Harrold for their valuable time, encouragement, and advice throughout my graduate school career. I also appreciate the time Dr. J. Douglas Bricker has taken to serve as the school representative for my dissertation defense.

I specially thank Dr. Christopher K. Surratt and Dr. Roxanne Vaughan for the biological evaluation of my compounds. I thank Ms. Jackie Farrer, Ms. Nancy Hosni, Ms. Deborah Willson, and Ms. Mary Caruso for their help and support in administrative affairs. I also wish to thank the Graduate School of Pharmaceutical Sciences at Duquesne University for financial assistance.

I am grateful to all my fellow graduate students at Duquesne University for their time, help, and friendship. I must thank my parents, Aruna and Siva Prasad Yarravarapu, and my brother, Sasi Bhargav for their endless love and support. Finally, I thank my

husband, Bhargava Nalagala, for his unconditional love, encouragement, and emotional support during this experience.

TABLE OF CONTENTS

Page

LIST OF FIGURES

LIST OF SCHEMES

LIST OF ABBREVIATIONS

3D	Three dimensional
5-HT	5-Hydroxytryptamine
ADHD	Attention deficit hyperactivity disorder
APC	Anti-proteolytic cocktail
BEProFL	Binding ensemble profiling with (f)photoaffinity labeling
BSA	Bovine serum albumin
CIT	Citalopram
CNS	Central nervous system
DAT	Dopamine transporter
dDAT	Drosophila dopamine transporter
DEA	Drug enforcement agency
DMEM	Dulbecco's modified eagle medium
DMF	Dimethylformamide
DTT	Dithiothreitol
EDC	1-Ethyl-3-(3-dimethylaminopropyl)carbodiimide
EtOAc	Ethyl acetate
FAAH	Fatty acid amide hydrolase
FBS	Fetal bovine serum
FDA	Food and Drug Administration
HA	Hemagglutinin
HBSS	Hanks buffered salt solution

HDAC	Histone deacetylase
hDAT	Human dopamine transporter
HEK	Human embryonic kidney
HOBT	Hydroxybenzotriazole
HPLC	High performance liquid chromatography
hSERT	Human serotonin transporter
ISC	Intersystem crossing
KRH	Krebs Ringer HEPES
LeuT	Leucine transporter
MAO	Monoamine oxidase
MAOIs	Monoamine oxidase inhibitors
MATs	Monoamine transporters
MDMA	Methylenedioxymethamphetamine
MeOH	Methanol
MP	Methylphenidate
Mp	Melting point
MS	Mass Spectrometry
NDRI	Norepinephrine and dopamine reuptake inhibitor
NET	Norepinephrine transporter
NRI	Norepinephrine reuptake inhibitor
NSS	Neurotransmitter sodium symporter
PBS	Phosphate buffrered saline

PD	Parkinson’s disease
PMSF	Phenylmethylsulfonyl fluoride
PRG	Photoreactive group
PSQ	Penicillin-Streptomycin-Glutamine
RG	Reporter group
SAR	Structure activity relationships
SDS-PAGE	Sodium dodecyl sulfate polyacrylamide gel electrophoresis
SERT	Serotonin transporter
SLC6	Solute carrier family 6
SNRI	Serotonin and noerpinephrine reuptake inhibitor
SSRI	Selective serotonin reuptake inhibitor
TBS	Tris buffrered saline
TBTA	Tris[1-benzyl-1**H**-1,2,3 triazol-4yl)methyl]amine
TCA	Tricyclic antidepressant
TCEP	Tris-2-carboxyethyl phosphine hydrochloride
TEV	Tobacco etch virus
TFA	Trifluoroacetic acid
THF	Tetrahydrofuran
TM	Transmembrane

CHAPTER ONE

1. Biological Literature Review

1.1. Introduction to Monoamine Transporters (MATs)

The neurotransmitters (Figure 1.1) dopamine (**1.1**), serotonin (**1.2**), and norepinephrine (**1.3**) are monoamine chemical messengers that mediate complex functions such as locomotion, memory, appetite, sleep, cognition, mood, reward, fear, sexual drive, and motivation (Grant *et al*., 1988; Barnes and Sharp, 1999; Greengard, 2001; Girault and Greengard, 2004). The duration and intensity of monoamine chemical signaling is dependent on extracellular neurotransmitter levels, which are regulated by monoamine transporters (MATs). MATs are transmembrane proteins located in plasma membranes of monoaminergic neurons, and their main function is to terminate neurotransmission by inward transport of released monoamines (Benarroch, 2013). MATs include dopamine (DAT), serotonin (SERT), and norepinephrine (NET) transporters, and they belong to the Na^+- and Cl^--coupled solute carrier 6 (SLC6) gene family (also known as the neurotransmitter sodium symporter (NSS) family) (Rudnick *et al*., 2014). The size of these three MATs is fairly similar, wherein the DAT, SERT, and NET have 617, 630, and 620 amino acid residues, respectively. These three MATs also share a common membrane topology that is characterized by 12 transmembrane (TM) helices and intracellular N- and C-termini.

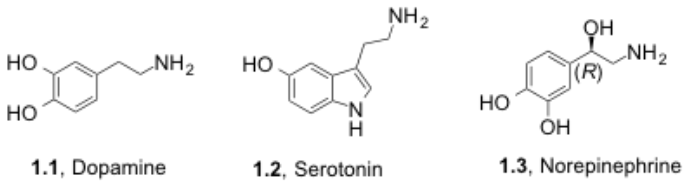

Figure 1.1. The chemical structures of dopamine, serotonin, and norepinephrine as monoamine neurotransmitters.

Dopamine, serotonin, and norepinephrine imbalances are implicated in numerous neurological disorders (Hahn and Blakely, 2002) like anxiety, depression (Klimek *et al*., 1997), alcoholism (Heinz *et al*., 2001), drug abuse (Howell and Negus, 2013), Parkinson's disease (Seeman and Niznik, 1990), and schizophrenia (Abdolmaleky *et al*., 2014). More than thirty MAT inhibitors are Food and Drug Administration (FDA) approved to treat disorders such as anxiety, depression, smoking cessation, and attention deficit hyperactivity disorder (ADHD). While the tricyclic antidepressants (TCAs) target all three MATs, the current standard of treatment for generalized anxiety and depression is to use selective serotonin reuptake inhibitors (SSRIs), whose primary target is the SERT (Stahl *et al*., 2013). Several antidepressants can also bind to DAT and NET with lower affinity. MATs are also targets for drugs of abuse (Figure 1.2) including cocaine (**1.4**), amphetamine ((±)-**1.5**), methaphetamine ((±)-**1.6**), and methylenedioxymethamphetamine ((±)-**1.7**, MDMA, ecstasy) (Howell and Negus, 2013). However, these psychostimulants differ in their relative affinity for DAT, SERT, and NET. For example, cocaine has approximately equal affinity for DAT, SERT, and NET, whereas amphetamine, methamphetamine, and methylphenidate have relatively lower affinity for SERT compared to their affinity for DAT and NET (Howell and Kimmel, 2008).

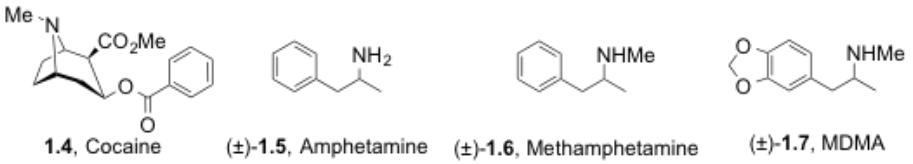

Figure 1.2. Examples of drugs of abuse that target DAT, SERT, and NET.

Over the last few decades, drug discovery efforts for the treatment of mood disorders have mainly focused on drugs targeting the DAT, SERT, or NET. TCAs (*e.g.*, imipramine (**1.8**), clomipramine (**1.9**), and desipramine (**1.10**), Figure 1.3) are the first generation antidepressants that target MATs (Lader, 2004). TCAs can also target G protein-coupled receptors and cardiac sodium channels giving rise to several side effects (Zohar and Westenberg, 2000). In order to avoid these side effects, subsequent drugs were mainly developed to act on specific monoamine transporters. Eventually, selective serotonin (SSRIs) (*e.g.*, citalopram ((±)-**1.11**), escitalopram ((*S*)-**1.11**), fluoxetine (**1.12**), sertraline (**1.13**), paroxetine (**1.14**), and fluvoxamine (**1.15**), Figure 1.3) and norepinephrine reuptake inhibitors (NRIs) (*e.g.*, reboxetine (**1.16**) and atomoxetine (**1.17**), Figure 1.3) were developed. SSRIs generally possess fewer side effects when compared to TCAs, principally due to their high selectivity. As a result, they represent a treatment of first choice for depression (Stahl *et al*., 2013). In contrast, NRIs and DAT inhibitors (*e.g.*, methylphenidate (**1.18**), Figure 1.3) are mainly used for the treatment of ADHD. DAT inhibitors (*e.g.*, benztropine (**1.19**), Figure 1.3 and analogues) are also being pursued for the treatment of cocaine addiction (Howell and Negus, 2013). Additionally, serotonin and noerpinephrine reuptake inhibitors (SNRIs) (*e.g.*, desvenlafaxine (**1.20**) and duloxetine (**1.21**), Figure 1.3) and norepinephrine and dopamine reuptake inhibitors (NDRIs) (*e.g.*, bupropion (**1.22**) and nomifensine (**1.23**), Figure 1.3) represent dual acting MAT inhibitors, wherein the NDRI bupropion is used as

a smoking cessation agent (Jorenby, 2002). Recently, triple reuptake inhibitors that equally target DAT, SERT, and NET (*e.g.*, tesofensine (**1.24**), Figure 1.3) have been developed and pursued for treatment of obesity (Astrup *et al*., 2008).

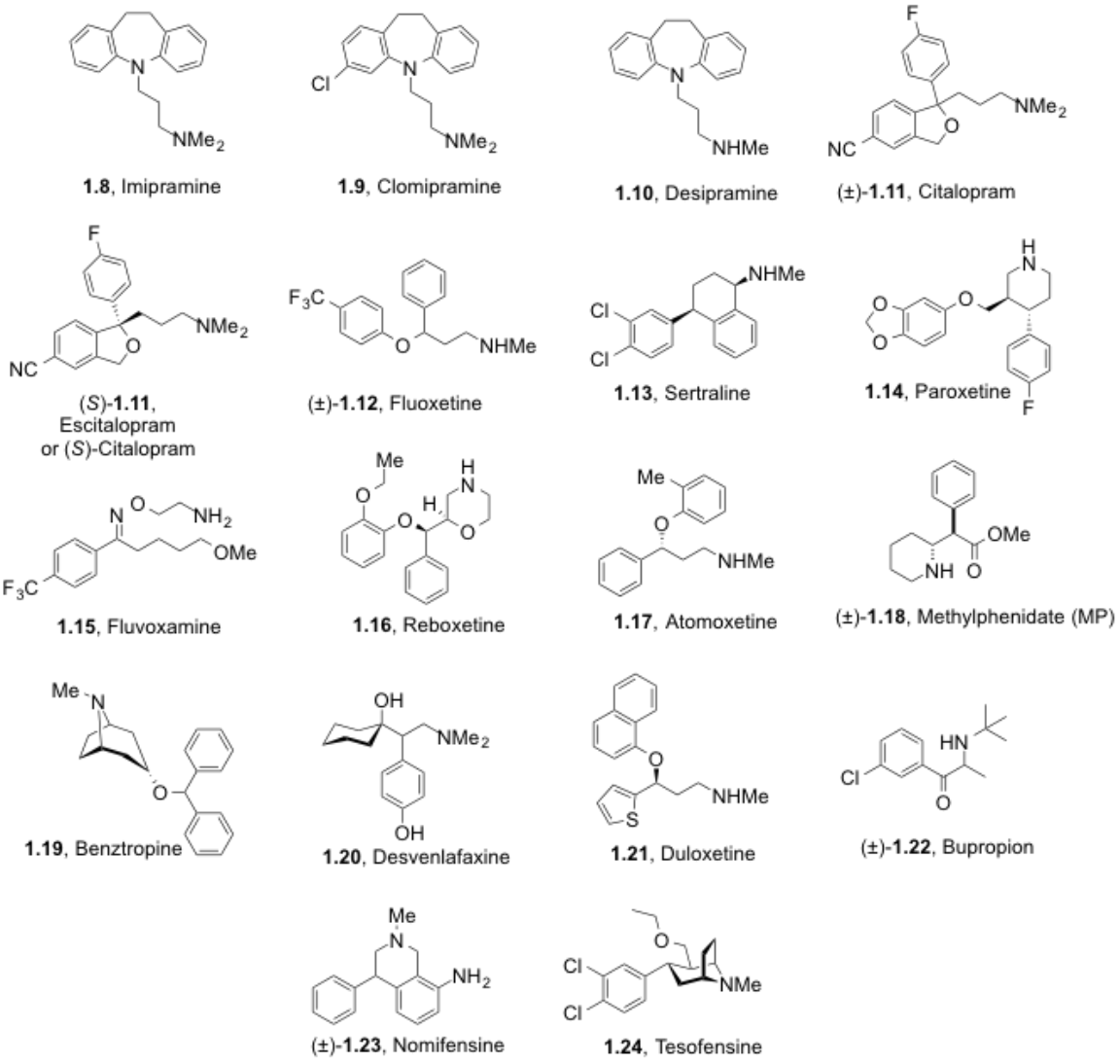

Figure 1.3. Examples of inhibitors that target DAT, SERT, or NET.

Although multiple drugs are available to treat mental illnesses, their drawbacks have fueled the quest for novel agents targeting MATs. For example, currently available antidepressants have several limitations such as late onset of action, a high percentage of non-responding patients, and numerous side effects such as sexual dysfunction, weight

gain, nausea, anxiety, and insomnia (Khawam *et al*., 2006). Despite being clinically important drugs and drug targets, very little is known about the specific drug-protein interactions that lead to their clinical efficacy. As a result, it is important to understand the structural and functional features of MATs, in particular, the binding sites for therapeutic drugs within these proteins. A better understanding of MAT binding sites is expected to enable efforts to discover and develop new and improved therapeutics for the treatment of numerous diseases associated with these proteins (*e.g*., depression, anxiety, post-traumatic stress disorder, obsessive-compulsive disorder, drug abuse, addiction, etc.).

1.2. The Dopaminergic System and the Dopamine Transporter (DAT)

Arvid Carlsson established dopamine as a neurotransmitter in the late 1950's and dopaminergic pathways in the central nervous system were subsequently identified (Iversen and Iversen, 2007). Dopamine neuron cell bodies are localized in the substantia nigra, ventral tegmental area, and hypothalamus, and their axons project to the caudate nucleus, putamen, nucleus accumbens, and prefrontal cortex (Girault and Greengard, 2004). Dopaminergic neurotransmission is involved in important physiological processes such as motor control, cognition, arousal, and reward (Greengard, 2001). Improper functioning of the dopaminergic system can result in severe neurodegenerative and psychiatric disorders, including attention deficit hyperactivity disorder (ADHD), bipolar disorder, Parkinson's disease (PD), and schizophrenia (Mehler-Wex *et al*., 2006; Mazei-Robison *et al*., 2008; Serretti and Mandelli, 2008).

Dopamine is a catecholamine synthesized in dopaminergic neurons from the amino acid tyrosine, and is stored in presynaptic vesicles. In response to a presynaptic action potential, dopamine is released into the synaptic cleft *via* calcium-mediated exocytosis (Westerink, 2006), where it subsequently binds to dopamine receptors to produce chemical impulses signaling reward or satisfaction (Iversen and Iversen, 2007). The dopamine transporter (DAT) is a neuronal membrane protein that mediates the reuptake of dopamine into the presynaptic neuron. It is primarily responsible for regulating the intensity and duration of the dopaminergic neurotransmission (Jaber *et al*., 1997) (Figure 1.4). Once dopamine is transported by the DAT into neurons, it is either degraded by monoamine oxidase (MAO) enzymes or stored in vesicles.

Historically, inhibition of DAT by stimulant drugs was an important finding. The behavioral, reinforcing, and euphorogenic effects of stimulant drugs such as cocaine and amphetamine has been explained *via* a dopamine hypothesis, and numerous studies have identified the DAT as the primary drug target associated with the abuse and addiction potential of these compounds (Koob, 1992; Woolverton and Johnson, 1992; Rothman and Glowa, 1995; Lile and Nader, 2003; Fleckenstein *et al*., 2007; Natarajan and Yamamoto, 2011). In rodents, the self-administration capacity of cocaine-like stimulants is correlated with their potency in inhibiting the DAT (Ritz *et al*., 1987).

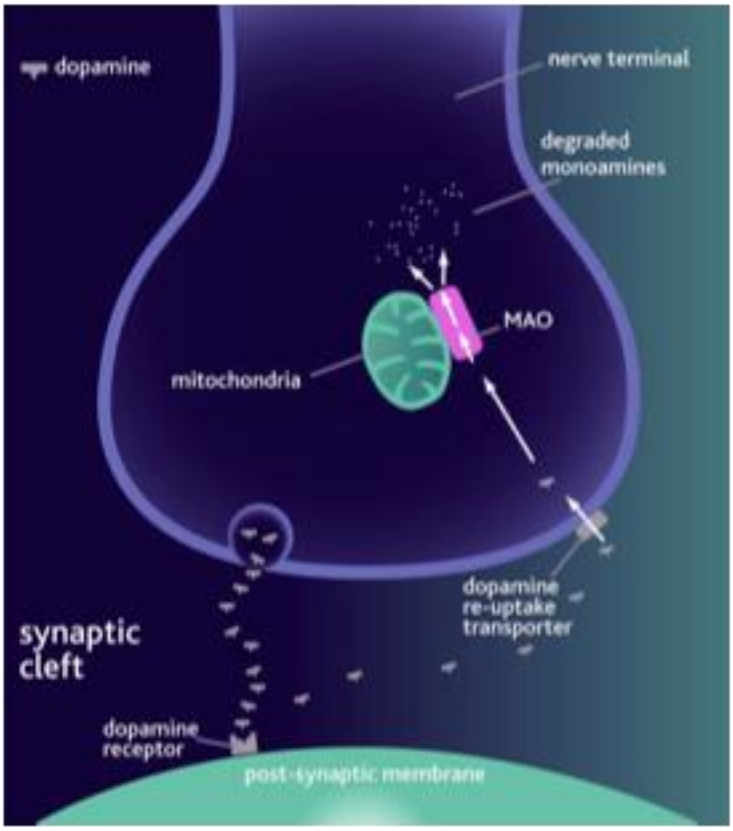

Figure 1.4. Cartoon of dopaminergic neurotransmission (Reprinted with permission from https://www.cnsforum.com/educationalresources/imagebank/substance_abuse/mao_cocaine. Copyright 2015, accessed on 01/26/2015).

It is known that cocaine binds to DAT proteins present on presynaptic membranes and increases extracellular dopamine concentration by blocking the reuptake activity of DAT. The resulting excess dopamine continuously activates dopamine receptors present on postsynaptic membranes. This phenomenon causes an increased activation of the dopaminergic reward pathways resulting in the "high" traditionally associated with cocaine use (Figure 1.5). This "high" reported by cocaine users, appears to be a function of both the rate of DAT occupancy by cocaine and the speed of cocaine delivery into the brain (Volkow *et al*., 2000).

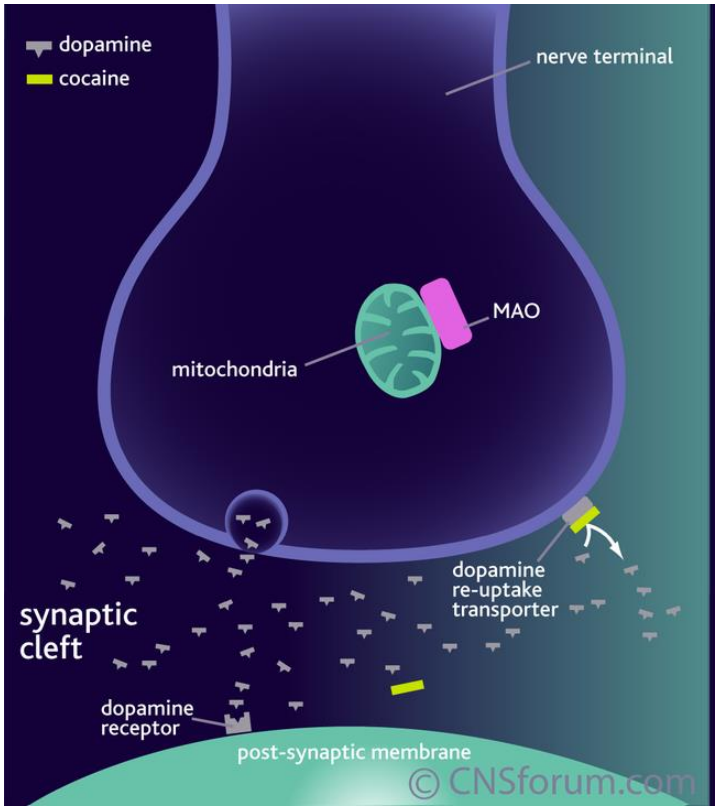

Figure 1.5. Inhibition of dopamine reuptake upon binding of cocaine to the dopamine transporter (Reprinted with permission from https://www.cnsforum.com/educationalresources/imagebank/substance_abuse/mao_cocaine. Copyright 2015, accessed on 01/26/2015).

1.2.1. Chemical Composition and Structure of the Dopamine Transporter

The human dopamine transporter (hDAT) is an 80 kDa integral protein that contains 620 amino acids (Benarroch, 2013). Its size is relatively similar to that of other monoamine transporters, such as the norepinephrine (NET) and serotonin (SERT) transporter, and alignment of the amino acid sequences of these transporters reveals that some segments within these proteins share a high degree of homology. Monoamine transporters belong to the neurotransmitter sodium symporter (NSS) or solute carrier 6 (SLC6) family of proteins, which may account for their homologous sequences (Rudnick *et al*., 2014).

The DAT is composed of 12 transmembrane (TM) domains connected by alternating intracellular and extracellular loops, with the amino and carboxyl-terminals located on the intracellular side of the membrane (Figure 1.6). There are three potential N- glycosylation sites on the large extracellular loop of DAT between TM3 and TM4. Stability and plasma membrane trafficking of the DAT is strongly influenced by glycosylation (Li *et al*., 2004). The DAT also contains a number of potential phosphorylation sites on the intracellular domains, which correlate with the transporter's activity and trafficking (Chen *et al*., 2010). TM1 and TM6 have residues important for transport of the substrate dopamine (Huang and Zhan, 2007; Indarte *et al*., 2008) and are also important for the binding of inhibitiors like cocaine (Vaughan *et al*., 2007; Ukairo *et al*., 2005; Parnas *et al*., 2005; Reith *et al*., 2001).

The hDAT also contains a Zn^{2+}-binding motif between extracellular loop 2, TM7, and TM8 (Norregaard *et al*., 1998). Zn^{2+} serves to mediate conformational changes of hDAT that are critical for the transport process. In addition to having a Zn^{2+}-binding motif, DAT also has a leucine zipper-like motif within TM2 and TM9. Leucine mutations within TM2 and TM9 suggest that the leucine zipper motif in TM2 contributes to the oligomerization and trafficking of DAT, which are essential to the functionality of the transporter (Torres *et al*., 2003). The cellular orientation of DAT, along with its trafficking, contributes significantly to the function of the transporter. Results from these studies show that the proper assembly and trafficking of DAT to the plasma membrane are necessary for the function of the transporter.

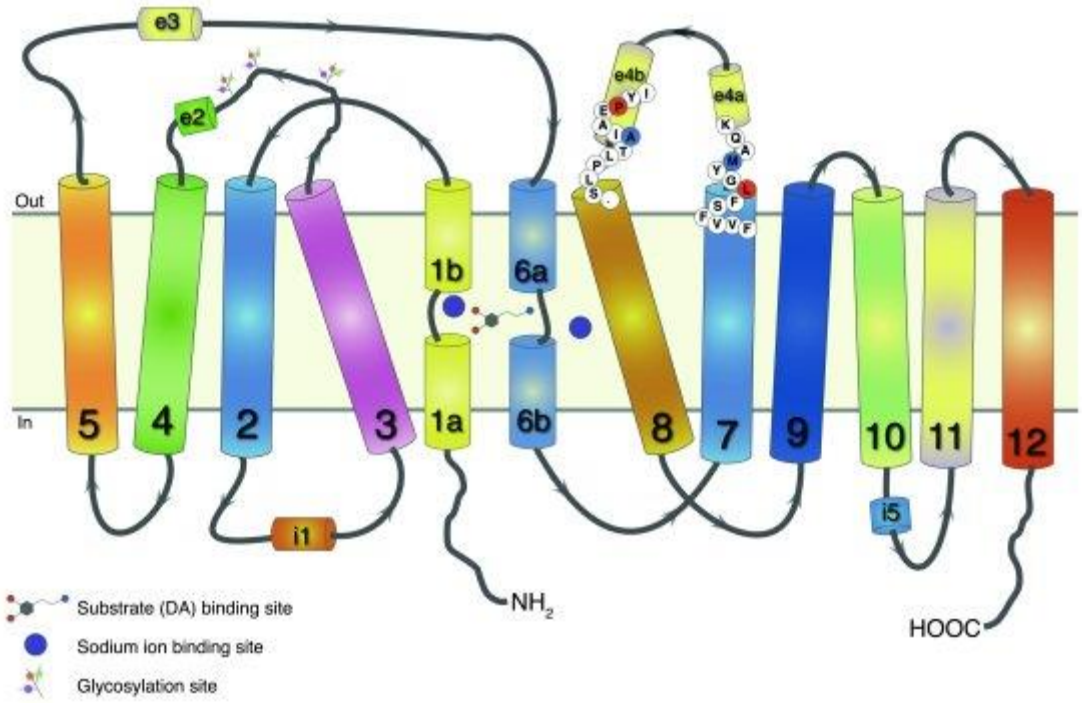

Figure 1.6. Diagram of membrane topology of the human dopamine transporter based upon bacterial leucine transporter crystal structures. Full TM helices are numbered 1–12 and intra- and extracellular loops are numbered 1–5 with prefixes either 'i' or 'e' respectively (Schmitt *et al.*, 2008. Reprinted with permission from *J. Neurochem.* **2008**, *107*, 928-940. Copyright 2008, International Society for Neurochemistry).

Ligand-binding and site-directed mutagenesis studies have been used to characterize DAT structural features such as substrate translocation mode and conformational preferences when bound with different DAT ligands (Chen and Reith, 2003; Uhl and Lin, 2003; Chen *et al*., 2004; Volz and Schenk, 2005; Schmitt *et al*., 2008; Loland *et al*., 2008). Simultaneously, photoaffinity labeling agents based on cocaine and other known DAT inhibitors have been used to identify potential binding sites within the DAT (Grigoriadis *et al*., 1989; Kline *et al*., 1994; Vaughan *et al*., 1998, 1999, 2001, 2005, and 2007; Dutta *et al*., 2001; Zou *et al*., 2001; Newman *et al*., 2006; Parnas *et al*., 2008; Dahal *et al*., 2014). However, the molecular mechanism and exact binding sites of cocaine and other DAT inhibitors, as well as the molecular determinants of inhibitor selectivity, remains largely unknown. In particular, currently it is not possible to

comprehensively understand the DAT at the molecular level due to the lack of three-dimensional (3D) high-resolution DAT structure. In particular, the lack of a DAT crystal structure has hindered the rational drug design of potential DAT ligands. Most recently, x-ray crystal structures of bacterial (Aquifex aeolicus) leucine transporter (LeuT) (Yamashita *et al*., 2005; Zhou *et al*., 2007 and 2009; Quick *et al*., 2009; Singh, *et al*., 2007 and 2008; Nyola *et al*., 2010; Krishnamurthy and Gouaux, 2012; Piscitelli and Gouaux, 2012; Wang and Gouaux, 2012; Kantcheva *et al*., 2013; Loland, 2015; Penmatsa and Gouaux, 2014) and the fly (Drosophila melanogaster) dopamine transporter (dDAT) (Penmatsa *et al*., 2013) have become available as templates for computational DAT homology modeling (Koldso, Christiansen *et al.*, 2013; Stockner *et al.*, 2013; Seddik *et al.*, 2013; Gedeon *et al.*, 2010; Huang *et al.*, 2009; Indarte *et al.*, 2008).

LeuT has a low level of similarity to DAT (20%), SERT (21%), and NET (24%), even though it belongs to the NSS family (Beuming *et al*., 2006). Despite this overall low sequence homology, a few regions in transmembrane domains 1, 3, 6, and 8, which form the ligand-binding site in LeuT, are highly conserved throughout the family, thus providing the opportunity to build potentially reliable homology models (*e.g.*, Indarte *et al*., 2008; Manepalli *et al*., 2012). The LeuT crystal structures have principally revealed two binding pockets termed S1 (primary substrate-binding site) and S2 (antidepressant-binding site), which have been verified by molecular docking studies of DAT inhibitors (Singh *et al*., 2007; Zhou *et al*., 2007). However, the highly potent DAT inhibitor cocaine does not display appreciable inhibitory potency for substrate transport by LeuT (Singh *et al*., 2007). In addition, antidepressants such as desipramine that were cocrystalized with LeuT have little appreciable affinity and inhibitory potency for DAT

(Zhou *et al*., 2007). Most recently, the tricyclic antidepressant nortriptyline was cocrystalized with dDAT and shown to bind in the S1 binding pocket (Penmatsa *et al*., 2013). Though the overall structure of dDAT is similar to that of LeuT, it was observed that these proteins also have multiple divergent features. For example, the transmembrane 12 of dDAT has a twist in its center at Pro 572, which is not observed in LeuT. Furthermore and unlike LeuT, there is a latch-like carboxy-terminal helix capping the intracellular cytoplasmic gate in dDAT. Another distinction between LeuT and dDAT crystal structures is that dDAT has a cholesterol molecule lodged within a pocket surrounded by TMs 1a, 5, and 7. Additionally, dDAT has made accommodations to account for the absence of a carboxylate group in biogenic amine substrates, as compared to the interactions between the carboxylate group of leucine substrate and Tyr108 within the substrate-binding pocket of LeuT. In particular, Asp46 present in TM1 of dDAT forms a hydrogen bond with the hydroxyl group of Tyr 124, which is equivalent to Tyr 108 in LeuT (Penmatsa *et al*., 2013). As a result, these disparities between dDAT and LeuT indicate that more direct and valid experimental approaches are required for hDAT structure and function studies.

1.3. Proposed Mechanism of Dopamine Reuptake by the Human Dopamine Transporter

The function of DAT is to reuptake dopamine into the presynaptic neuron in order to regulate the intensity and duration of the dopaminergic neurotransmission (Jaber *et al*., 1997). Coupling of dopamine influx with an inward flow of Na^+ and Cl^- drives the dopamine reuptake process, as these ions move down a gradient across the cell membrane (Figure 1.7). DAT promotes the transport of dopamine together with Na^+ and Cl^- ions as

co-substrates with a stoichiometric ratio of 2:1:1 for sodium:chloride:dopamine. Na^+K^+-ATPase creates a concentration gradient that moves three Na^+ ions out of the cell for every two K^+ ions into the cell. According to the alternate accessing model, dopamine, Na^+, and Cl^- bind to DAT on the extracellular side in an outward-facing conformation (Jardetzky, 1966). This binding is proposed to induce a conformational change in the transporter such that the dopamine-binding site becomes exposed to the intracellular side of the membrane (*i.e.*, an inward-facing conformation), thus allowing dopamine, Na^+, and Cl^- to be transported to the intracellular side (Figure 1.8). Subsequently, upon simultaneous release of potassium ions into the synaptic cleft, the empty transporter returns to the outward facing conformation in order to initiate another transport cycle (Figure 1.9).

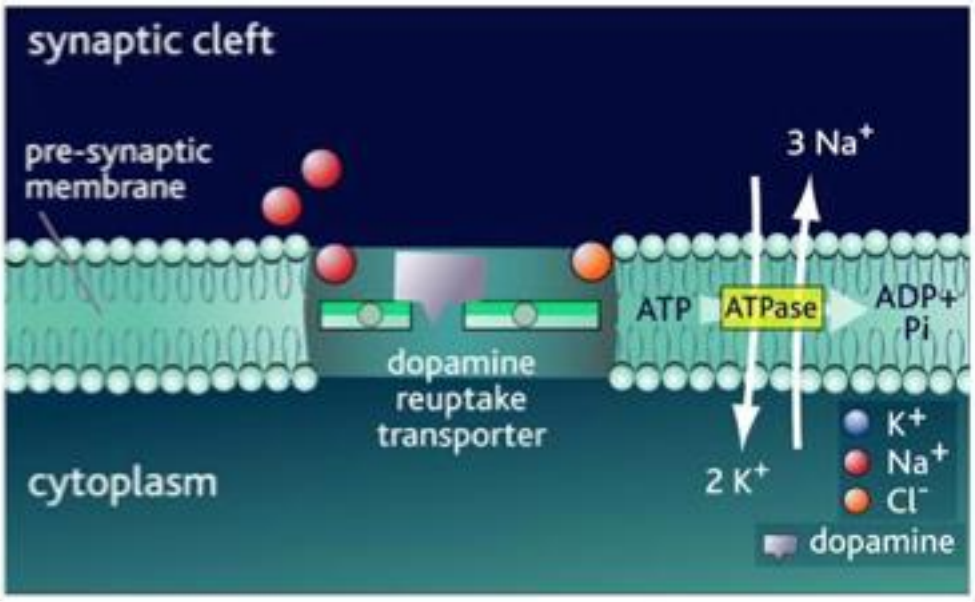

Figure 1.7. Na^+K^+-ATPase-induced concentration gradient in the human dopamine transporter (Reprinted with permission from https://www.cnsforum.com/educationalresources/imagebank/dopaminergic/rcpt_sys_da_reup. Copyright 2015, accessed on 01/26/2015).

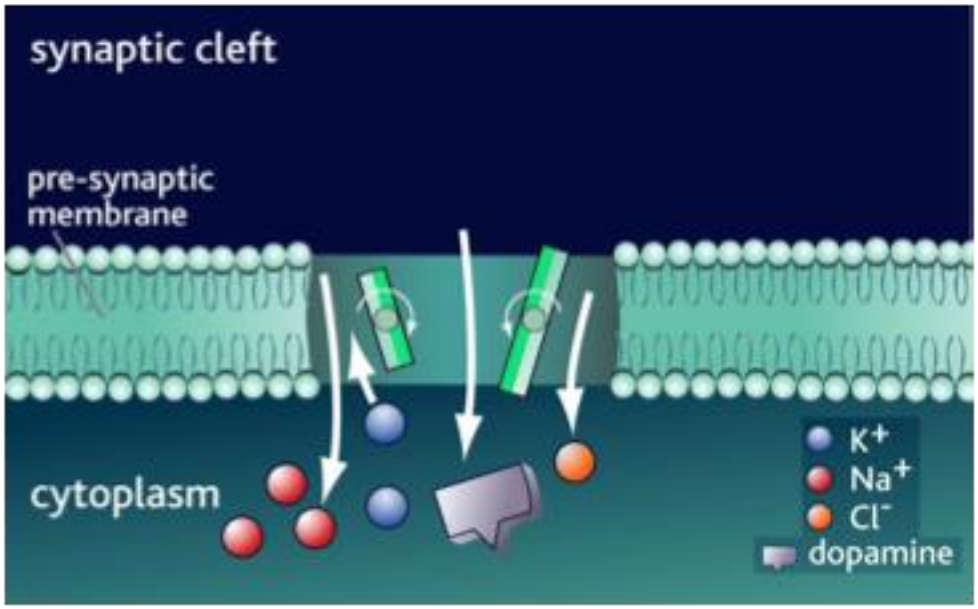

Figure 1.8. Dopamine influx coupled with inward flow of Na^+ and Cl^- ions as part of the reuptake process (Reprinted with permission from https://www.cnsforum.com/educationalresources/imagebank/dopaminergic/rcpt_sys_da_reup. Copyright 2015, accessed on 01/26/2015).

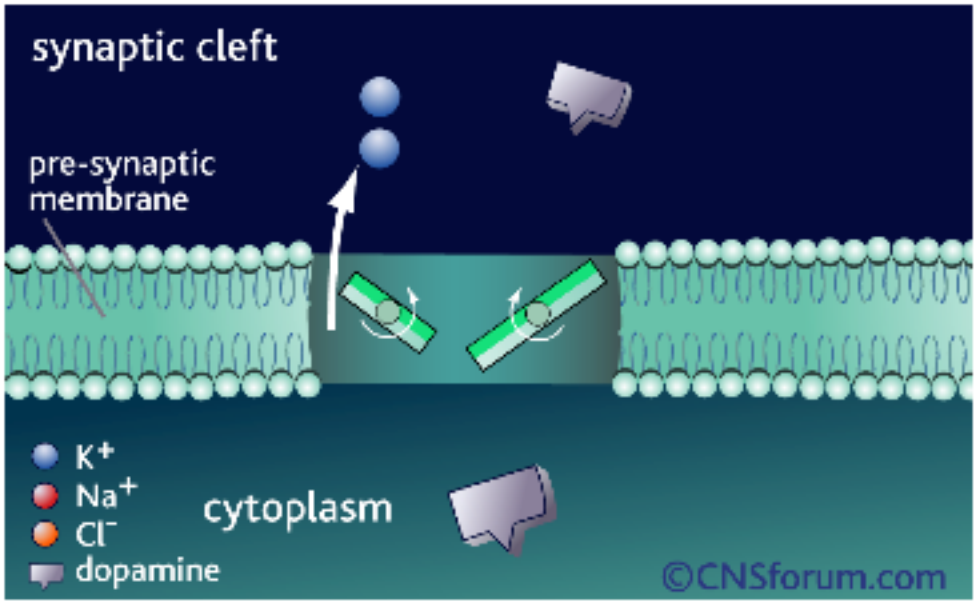

Figure 1.9. The dopamine transporter returns to an outward-facing conformation in order to facilitate another transport cycle (Reprinted with permission from https://www.cnsforum.com/educationalresources/imagebank/dopaminergic/rcpt_sys_da_reup. Copyright 2015, accessed on 01/26/2015).

Single-molecule dynamics studies, molecular simulations, and subsequent crystals of LeuT have further verified this alternate access model. In turn, these studies have revealed a third, low-energy state, a dually occluded, substrate-bound intermediate conformation, while transitioning between outward-open and inward-open conformations during substrate translocation (Penmatsa and Gouaux, 2014; Schmitt *et al*., 2013).

Based on the insights from LeuT, a mechanistic framework for the dopamine transport has been proposed, including an outward-facing conformation for dopamine and ion pickup, an occluded conformation featuring dopamine and ion bound, and an inward-facing conformation allowing dopamine and ion release (Penmatsa and Gouaux, 2014; Schmitt *et al*., 2013). The transport cycle is proposed to start with an ion/substrate-free (apo) outward-facing state of the dopamine transporter (Figure 1.10, A). Binding of Na^+ and Cl^- ions then equilibriates the apo DAT towards a more stabilized outward-facing conformation, which features a fully open extracellular gate readily prepared to bind substrate (Figure 1.10, B) (Claxton *et al*., 2010; Krishnamurthy and Gouaux, 2012). Dopamine then binds at the primary substrate (S1) site (Figure 1.10, C) and closes the extracellular gate *via* salt bridge formation between extracellular gating residues Arg85 and Asp476, thus giving rise to an occluded state. Subsequent, conformational changes in the process promote the transporter from the occluded state towards an inward-facing conformation (Figure 1.10, D). Finally, dopamine, Na^+, and Cl^- ions are released into the cytosol from the inward-facing state of the dopamine transporter due to hydration of its binding sites. Subsequent dopamine transporter changes from the inward- to outward-facing state allow another dopamine transport cycle to commence (Figure 1.10, A and E; Schmitt *et al*., 2013).

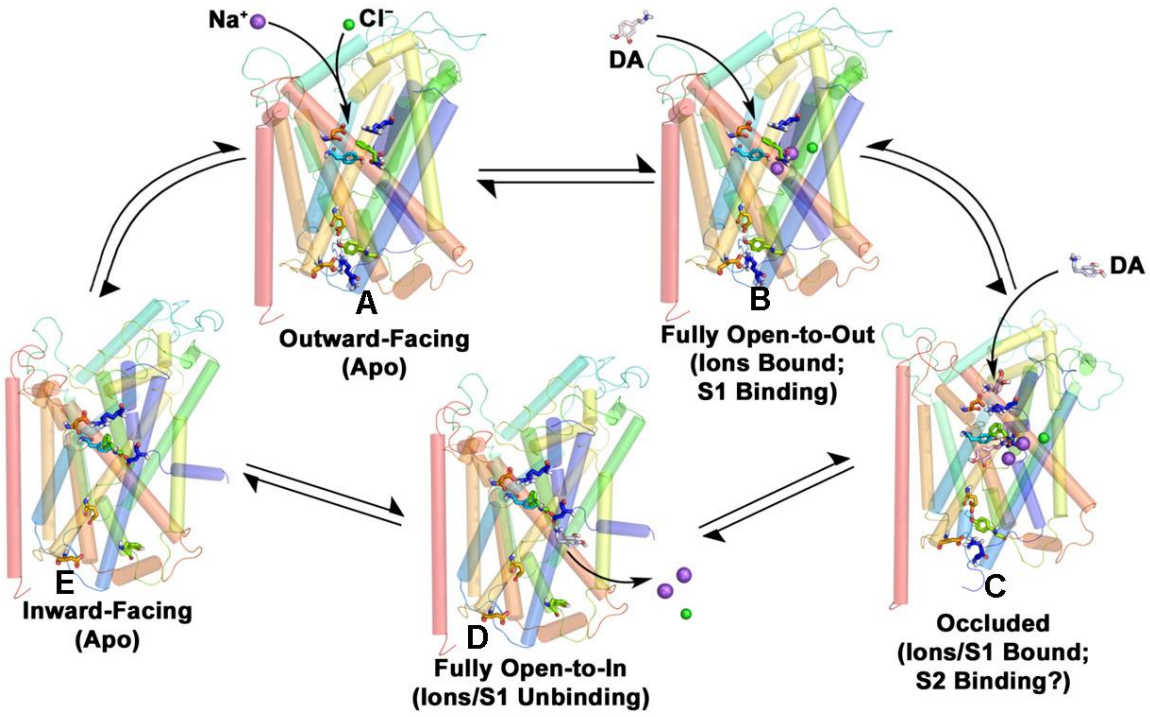

Figure 1.10. Putative dopamine transporter conformational cycle for translocation of dopamine (DA) (Schmitt *et al.*, 2013. Adapted with permission from *J. Pharmacol. Exp. Ther.* **2013**, *346*, 2-10. Copyright 2013, JPET Online by American Society for Pharmacology and Experimental Therapeutics).

Another transport hypothesis features binding of a second dopamine molecule to a secondary allosteric site (S2) located 11Å above the S1 site towards the extracellular side of the membrane. This is proposed to activate the conformational shift from the occluded to inward-facing state (Figure 1.10, C and D) (Shi *et al*., 2008; Quick *et al*., 2012). This secondary allosteric S2 site in LeuT was identified to be the binding site for tricyclic antidepressants and selective serotonin reuptake inhibitors (Zhou *et al*., 2007 and 2009). However, the existence of the S2 site in hDAT and its role with respect to ligand binding is highly debated by researchers in the MAT field.

1.4. Dopamine Transporter Ligands

1.4.1. Dopamine Transporter Substrates

Amphetamines ((±)-**1.5**) - (±)-**1.7**), Figure 1.11) are structurally similar to dopamine and act as substrates at the dopamine transporter (Robertson *et al*., 2009). Amphetamine and methamphetamine are pschostimulants approved for the treatment of ADHD, obesity and narcolepsy (Fleckenstein *et al*., 2007). The Drug Enforcement Agency (DEA) tightly controls these drugs by categorizing them as Schedule II agents, principally because their potential for abuse can lead to severe psychological and physiological dependence. Amphetamines produce their principal effects by increasing synaptic levels of dopamine, norepinephrine, and serotonin through multiple mechanisms. Although amphetamines generally target various transporters, the DAT is primarily implicated in their reinforcing properties and abuse potential (Fleckenstein *et al*., 2007). The exchange diffusion / reverse transport model has been used to explain the mechanism of action of amphetamines and relies on evidence that amphetamines are substrates for the DAT (Figure 1.12). The DAT transports amphetamines into the presynaptic neuron, and this leads to a reverse transport of dopamine into the synaptic cleft, thus enhancing extracellular dopamine levels (Sulzer *et al*., 2005). Another mechanism of amphetamine-mediated dopamine efflux features a channel-like configuration of DAT (Kahlig *et al*., 2005). Similar to DAT inhibitors, amphetamines also increase extracellular dopamine levels by competing with dopamine for the substrate-binding site within DAT, thus preventing dopamine reuptake from the synapse (Figure 1.12) (Wayment *et al*., 1998).

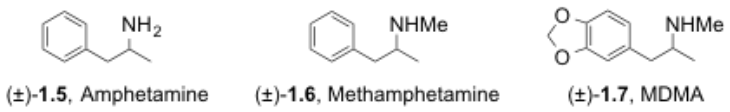

Figure 1.11. Chemical examples of amphetamines as monoamine transporter substrates.

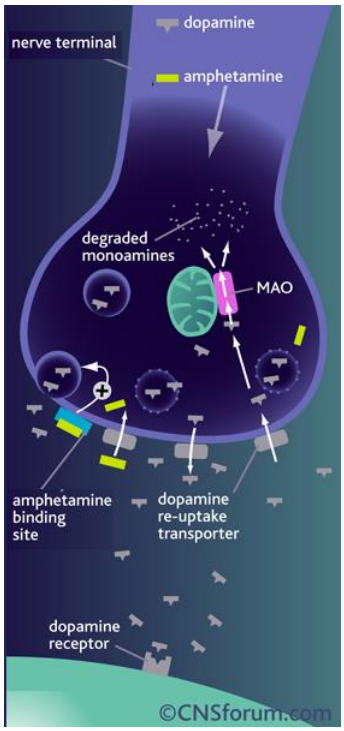

Figure 1.12. Mechanism of action of amphetamine (Adapted with permission from https://www.cnsforum.com/educationalresources/imagebank/substance_abuse/drug_amphet_low. Copyright 2015, accessed on 01/26/2015).

1.4.2. Dopamine Transporter Inhibitors

Since the DAT has been implicated as the primary target associated with cocaine and amphetamines abuse, DAT ligands acting as cocaine antagonists have been pursued for the treatment of psychostimulant abuse (Howell and Negus, 2013). In particular, it has been suggested that the ideal DAT inhibitor for treatment of cocaine abuse should gradually eliminate craving for cocaine and help users maintain abstinence (Rothman *et al*., 1989; Carroll *et al*., 1999). However, a DAT inhibitor has yet to be approved for the treatment of psychostimulant abuse, principally because the rational design of such compounds are hindered due to limited 3D structural information and poor understanding

of the dopamine- and inhibitor-binding sites within the DAT. To date, existing DAT inhibitors have been discovered either by serendipity or ligand-based drug design, and are classified as either "cocaine-like" or "atypical" based on their distinct behavioral effects (Schmitt *et al*., 2013). Earlier, it was believed that both DAT substrates and inhibitors have addiction potential equivalent to cocaine, principally due to their ability to increase extraneuronal dopamine levels. However, recently discovered, "atypical" benztropine-like DAT inhibitors show a lack of addiction potential as compared to cocaine (Woolverton *et al*., 2000; Ferragud *et al*., 2009; Hiranita *et al*., 2009). As a reslut, ligands with different chemical structures have been shown to be capable of inducing specific conformational changes in the DAT, which can be differentially transduced by the cell towards eliciting unique behavioral and psychological effects (Schmitt *et al*., 2013).

1.4.2.1. "Cocaine-Like" Dopamine Transporter Inhibitors

1.4.2.1.1. Tropanes

Cocaine (**1.4**, Figure 1.13) is a powerful CNS stimulant that has been an abused substance for more than 100 years (Ciccarone, 2011). According to a National Survey on Drug Use and Health (NSDUH), the national prevalence of cocaine dependence or abuse was 1.1 million persons in 2012, third in illicit drugs after marijuana and misuse of prescription medications (see http://www.samhsa.gov/data/NSDUH/2012SummNatFind DetTables/NationalFinds/NSDUHresults2012.htm). Cocaine abuse and addiction remains a major health and economic problem that continues to plague our society. Currently,

there are no FDA-approved medications for this type of addiction. As a result, the development of agents for cocaine dependence is vitally important.

Cocaine is a nonselective, competitive inhibitor of monoamine transporters that binds to the DAT, NET, and SERT, and functions to inhibit uptake of dopamine, norepinephrine, and serotonin, respectively (Newman *et al*., 2001; Katz *et al*., 2001). Although cocaine affects all three monoamine transporters, decades of studies have established that binding of cocaine to the DAT is primarily responsible for its reward and reinforcement effects (Koob, 1992; Woolverton and Johnson, 1992; Rothman and Glowa, 1995; Lile and Nader, 2003; Fleckenstein *et al*., 2007; Natarajan and Yamamoto, 2011). Since the neurochemical basis for the dependence-producing properties of cocaine were elucidated, numerous approaches to develop a therapeutic for cocaine addiction have been under investigation (Howell and Negus, 2013). Towards this goal, many researchers have hypothesized a dopamine-sparing cocaine antagonist approach. Such a compound would be expected to partially mimic the effects of cocaine without intense craving, thereby gradually withdrawing abusers into abstinence.

In an attempt to identify dopamine-sparing cocaine antagonists, tropane analogs such as WIN-35,428 (**1.25,** Figure 1.13) and benztropine (**1.19**, Figure 1.14) have been identified. WIN-35,428 has high DAT affinity and inhibitory potency showing approximately 8-fold increased binding affinity towards DAT as compared to cocaine (Clarke *et al*., 1973; Madras *et al*., 1989). The radioisotope [^{3}H]-WIN-35,428 is commonly used to assess binding affinity of novel ligands to the DAT (Carroll *et al*., 1994), mainly because WIN-35,428 has a longer half-life relative to cocaine due to the absence of the metabolically labile benzoate ester.

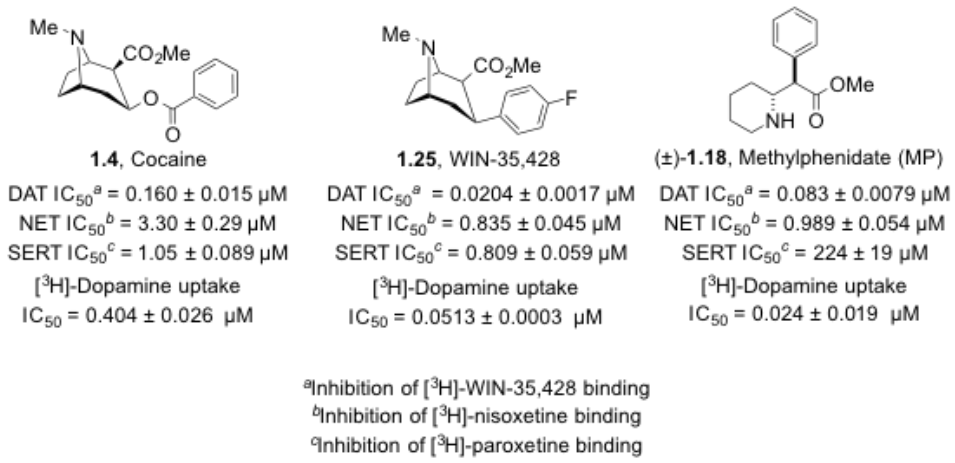

Figure 1.13. Chemical examples of "cocaine-like" DAT inhibitors and their MAT pharmacology (Javanmard *et al*., 1999).

1.4.2.1.2. Methylphenidate

The psychostimulant methylphenidate ((±)-**1.18**), Figure 1.13), a non-tropane DAT inhibitor, has higher binding affinity for DAT than the other monoamine transporters (Gatley *et al*., 1996). The binding affinity of methylphenidate to DAT has been shown to be twice that of cocaine (Gatley *et al*., 1996), even though both compounds have comparable functional groups (*i.e.*, a basic nitrogen, methyl ester, and an aromatic ring). Most importantly, methylphenidate is a U.S. Food and Drug Administration (FDA) approved therapeutic for treatment of attention deficit hyperactivity disorder (ADHD) (Golubchik *et al*., 2014). Animal behavioral studies suggest methylphenidate has reinforcing effects similar to that of cocaine (Bergman *et al*., 1989). However, in humans, methylphenidate's reinforcing ability appears to be substantially lower and has been shown to reduce cocaine cravings (Yano and Steiner, 2007). These results suggest that methylphenidate has the attributes necessary to serve as a lead candidate for the treatment of cocaine dependence, and currently, methylphenidate analogs are being pursued as therapeutics for drug abuse (Misra *et al*., 2010). Recently,

Misra and coworkers have reviewed structure-activity relationships for methyphenidate (Misra *et al*., 2010).

1.4.2.2. "Atypical" Dopamine Transporter Inhibitors

1.4.2.2.1. Benztropines

Benztropine (Cogentin, **1.19**, Figure 1.14) is a tropane-based DAT inhibitor (Zou *et al*., 2003) and anticholinergic agent used in symptomatic treatment of Parkinson's disease (Katzenschlager *et al*., 2002). Benztropine restores the balance between the neurotransmitters acetylcholine and dopamine due to its anticholinergic activity, which may improve the symptoms of early Parkinson's disease. Benztropine is also given to psychotic patients being treated with neuroleptic medications to reduce some of the movement-associated side effects (Soares and McGrath, 2000). Both benztropine (**1.19**) and cocaine (**1.4**) have a *N*-methyl tropane as their structural core. While cocaine is fuctionalized with a methyl ester at the 2-position and β-benzoyl ester at the 3-position of the tropane, benztropine contains only an α-diphenylmethoxy functional group at the 3-position. It has been observed that select benztropines have high binding affinity for DAT, yet these same compounds demonstrate unique behavioral profiles that are significantly different from cocaine. For example, select benztropines do not stimulate locomotor activity as effectively as cocaine, and do not completely substitute for cocaine in rats trained to discriminate cocaine from saline (Katz, *et al*., 1999 and 2004; Newman *et al*., 1995; Sanchez *et al*., 2010). In addition, self-administration of benztropines in rhesus monkeys was less compared to cocaine (Woolverton *et al*., 2000; Ferragud *et al*., 2009; Hiranita *et al*., 2009) and select benztropines have a comparatively slow onset and

longer duration of action relative to cocaine (Tanda *et al*., 2009). Because of these non-addictive behavioral properties, benztropine analogs are currently being pursued as potential agents for the treatment of cocaine abuse (Rothman *et al*., 2008).

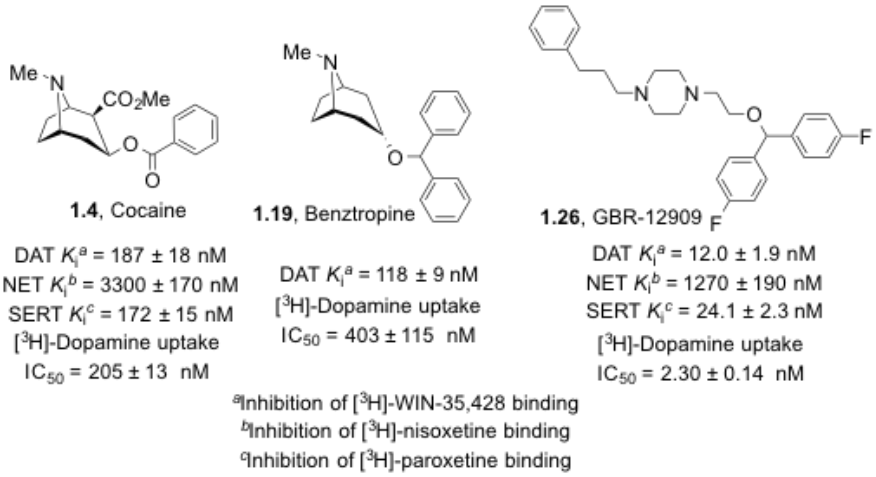

Figure 1.14. Structural and pharmacological comparison of cocaine *versus* benztropine and GBR-12909 "atypical" DAT inhibitors (Newman *et al*., 1995; Husbands *et al*., 1999).

1.4.2.2.2. GBR-12909

Tropane ring-modified benztropine analogs lead to the discovery of GBR-12909 (**1.26**; Figure 1.14), which has a significantly different behavioral profile than cocaine (Tella *et al.*, 1996). Similar to benztropines, GBR-12909 is a high affinity DAT inhibitor with a slow onset and long duration of action compared to cocaine (Rothman *et al.*, 2008). Owing to its ideal pharmacokinetic and pharmacodynamic properties, GBR-12909 was progressed into clinical studies as a potential therapeutic for psychostimulant abuse. However, it was withdrawn eventually due to its association with undesirable long QT syndrome (Goldsmith *et al.*, 2007).

1.4.3. Unique Behavioral Profiles of DAT Inhibitors

DAT inhibitors with different chemical structures have been shown to

preferentially bind to specific conformational states, or induce specific conformational changes in the DAT, which are capable of regulating the behavioral profile of a given DAT ligand (Loland *et al*., 2008). In particular, conformation-specific ligand interactions were initially studied by differentiating the reactivity of DAT extracellular-facing cysteine residues towards membrane-impermeable sulfhydryl-reducing reagents. Using this experimental approach, cocaine and benztropine were subsequently shown to have different effects on the reactivity of particular cysteines, thus indicating that these compounds stabilize different DAT conformations (Reith *et al*., 2001). Apart from accessibility of select DAT cysteine residues to reactive agents, researchers have also employed site-directed mutagenesis to further verify DAT conformation-specific ligand interactions. For example, W84L and D313N are mutations known to lead to an outward-facing stabilized DAT, and these mutants have shown increased binding affinity for both cocaine and methylphenidate. In contrast, decreased or retained binding affinity was observed for benztropine and GBR-12909 in these particular DAT mutants (Chen *et al*., 2001 and 2004).

Simultaneously, DAT mutant Y335A, which stabilizes an inward-facing DAT conformational state, completely disrupted the binding of cocaine-like componds, but increased the affinity of benztropine analogs. These observations indicate that cocaine-like compounds preferentially stabilize an outward-facing DAT conformation state, whereas atypical DAT inhibitors stabilize an inward-facing, closed DAT conformation. Schmitt and coworkers have postulated that atypical DAT inhibitors first enter the S2-binding site in the extracellular DAT vestibule and eventually stabilize the inward-facing conformation of DAT similar to substrates, but unlike substrates, atypical DAT inhibitors

are not released immediately into the intracellular side (Schmitt *et al.*, 2013). Additionally, it was observed that DAT inhibitors with a slow onset of action showed reduced addiction potential compared to DAT inhibitors with a rapid onset of action (Wee *et al.*, 2006). Overall, the preferential interactions of atypical DAT inhibitors with the inward-facing DAT conformation might be responsible for the lower abuse potential, or even complete lack of cocaine-like behavioral responses, typically associated with these compounds (Loland *et al.*, 2008; Kopajtic *et al.*, 2010; Schmitt and Reith, 2011). As a result, further investigation is necessary in order to elucidate the molecular requirements of DAT ligands with respect to their behavioral profiles. Such knowledge is expected to lead to improved drug candidates for DAT-implicated diseases (*e.g.*, ADHD, cocaine addiction, etc.).

1.5. The Serotonin Transporter and Its Importance in the Treatment of Depression

Similar to DAT, the main function of the serotonin transporter (SERT) is to terminate serotonin-mediated neurotransmission by reuptake of serotonin from the synaptic cleft into the presynaptic neuron (Rudnick *et al*., 2014). SERT is also the primary drug target for well-known antidepressants such as selective serotonin reuptake inhibitors (SSRIs) (Stahl *et al*., 2013). Because of drawbacks associated with existing antidepressants, the quest for better antidepressants remains an intense area of research. For example, currently available antidepressants have several limitations, such as late onset of action, a high percentage of non-responding patients, and side effects like sexual dysfunction, weight gain, nausea, anxiety, and insomnia (Khawam *et al*., 2006). Novel strategies to treat depression are currently being pursued that mainly combine SERT inhibition with additional pharmacological mechanisms of action (Stahl *et al*., 2013).

One strategy to achieve this is to combine a SSRI with another drug with a different mechanism of action such as DAT/NET inhibition, $5HT_{2A}$ antagonism, $5HT_{1A}$ partial agonism, and $5HT_{2C}$/$5HT_7$ antagonism. In particular, the combination of an alpha 2 adrenergic receptor antagonist, mirtazapine (**1.27**, Figure 1.15), with SSRIs proved powerful in the recovery of treatment-resistant depressed patients (Benjamin and Doraiswamy, 2011). Apart from alpha 2 antagonism, mirtazapine displays antagonist properties at $5HT_{2A}$, $5HT_{2C}$, $5HT_3$, and H_1 histamine receptors as well. Additionally, the combination of a $5HT_{1A}$ partial agonist, buspirone (**1.28**, Figure 1.15), with an SSRI was shown to increase serotonin levels in rodent brains at a faster rate compared to SSRIs alone (Dawson and Nyugen, 1998).

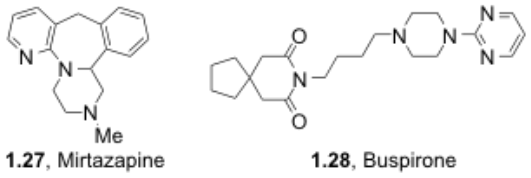

Figure 1.15. Examples of drugs used in combination with SSRIs to treat depression.

A second strategy for new antidepressants is to develop single molecules with multiple mechanisms of action, such as vilazodone (**1.29**, Figure 1.16) (SERT inhibition + $5HT_{1A}$ partial agonism) and vortioxetine (**1.30**, Figure 1.16) (SERT inhibition, $5HT_{1A}$/$5HT_{1B}$ partial agonism, and $5HT_3$/$5HT_7$-antagonism) (Stahl *et al*., 2013). Vilazodone (**1.29**) is an FDA-approved drug for the treatment of major depressive disorder, and its $5HT_{1A}$ binding property seems to lower the incidence of sexual dysfunction in depressed patients *versus* SSRIs (Khan, 2009; Singh and Schwartz, 2012). Given these novel approaches for antidepressant drug development, SERT continues to remain a target of high pharmaceutical interest (Butler and Meegan, 2008; Stahl *et al*.,

2013). However, there are limited details regarding the 3D structure and function of SERT (*e.g.*, the molecular mechanisms of substrate binding and transport, SSRI binding sites, etc.), which are essential for the development of novel antidepressants.

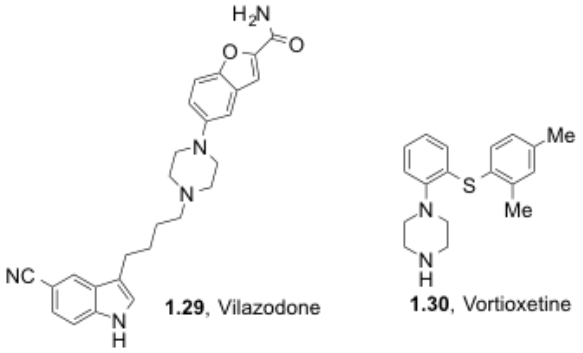

Figure 1.16. Examples of antidepressants with multiple mechanisms of action.

1.5.1. Chemical Composition and Structure of the Serotonin Transporter

As mentioned earlier, SERT and its homologous proteins, DAT and NET, are monoamine transporters (MATs) and members of the neurotransmitter:sodium symporter (NSS) family (Rudnick *et al*., 2014). The genes encoding multiple SERT species were isolated in the early 1990s, and subsequent studies provided evidence that SERT is a hydrophobic protein that contains 630 amino acids (Blakely *et al*., 1991; Demchyshyn *et al*., 1994; Hoffman, 1994; Mortensen *et al*., 1999; Benarroch, 2013). As a NSS family member, SERT shares the common feature of 12 transmembrane (TM) domains connected by alternating intracellular and extracellular loops (IL and EL, respectively), a large second extracellular loop between TM3 and TM4 containing multiple N-linked glycosylation sites, and cytoplasmic N- and C- termini (Demchyshyn *et al*., 1994; Tate and Blakely, 1994; Chen *et al*., 1998; Mortensen *et al*., 1999; Yamashita *et al*., 2005).

Similar to DAT, several computational homology models have been built using LeuT as a template in order to understand the tertiary structure of SERT (Ravna *et al.*, 2006; Jorgensen, Tagmose, Jorgensen, Bogeso *et al*., 2007; Jorgensen, Tagmose, Jorgensen, Topiol *et al*., 2007; Gabrielsen *et al.*, 2012; Manepalli *et al*., 2012; Koldso, Autzen *et al.*, 2013; Koldso, Christiansen *et al.*, 2013; Zhou *et al.*, 2013). Based on this information, SERT is proposed to have a high-affinity binding site termed S1 (primary substrate-binding site) and a low-affinity allosteric site called S2 (extracellular vestibule-located site). In particular, homology molecular modeling (*e.g*., Jorgensen, Tagmose, Jorgensen, Topiol *et al*., 2007), site-directed mutagenesis (*e.g*., Barker *et al.*, 1998; Andersen *et al.*, 2010), and small molecule SAR studies (*e.g*., Zhang *et al.*, 2010) have suggested that TCAs and SSRIs bind to the S1 site with high affinity in a competitive manner (Talvenheimo *et al*., 1979; Henry *et al.*, 2006; Andersen *et al.*, 2009 and 2011; Sinning *et al.*, 2010; Tavoulari *et al.*, 2009; Koldso *et al.*, 2010).

Most recently, LeuT has been engineered to display monoamine/biogenic amine transporter-like pharmacology by mutating key residues near the primary S1 binding pocket (Wang *et al.*, 2013). This mutated LeuT, subsequently named LeuBAT, has also been co-crystallized with sertraline, paroxetine, fluoxetine, and fluvoxamine as SSRIs, as well as the TCA clomipramine, indicating all of these compounds bind in the primary S1 binding pocket. However, and in sharp contrast to LeuBAT, other crystallographic studies with LeuT indicate the TCA desipramine (Zhou *et al.*, 2007), and the SSRIs sertraline and fluoxetine (Zhou *et al.*, 2009), bind in the homologous S2 site as non-competitive inhibitors (Singh *et al.*, 2007). In addition, multiple studies of SERT indicate that the S2 binding site acts as a low-affinity allosteric site, wherein ligands binding to S2

can inhibit the dissociation of S1-bound SSRIs, thus enhancing their efficacy (Plenge *et al.*, 1991, 1997, 2007, and 2012; Chen, Larsen, Neubauer *et al.*, 2005; Chen, Larsen, Sanchez *et al.*, 2005; Zhong *et al.*, 2009 and 2012; Neubauer *et al.*, 2006). Furthermore, characterization of the S2 binding site in SERT using computational modeling, as well as experimental support by site-directed mutagenesis, Zn^{+2}-site engineering, and cysteine-reactivity assays, indicates that binding to the allosteric site impedes dissociation of S1-bound drug, most likely by steric blockade of the exit pathway (Plenge *et al.*, 2012). In short, given the roles of the S1 and S2 binding sites within SERT are not completely understood, there is a significant need for further studies that can elucidate the structural features of SERT at the molecular level.

1.5.2. Proposed Mechanism of Serotonin Reuptake by the Human Serotonin Transporter

In monoamine transporters, the reuptake of substrate is driven by a Na^+K^+-ATPase-generated electrochemical gradient, with movement of Na^+ ions out of the neuron and K^+ ions into the neuron (Figure 1.7). In DAT, the inward transport of one molecule of neurotransmitter substrate is accompanied with two Na^+ ions and one Cl^- ion, whereas SERT co-transports one Na^+ and one Cl^- from outside to inside the cell in order to drive serotonin uptake. However, SERT also counter transports one K^+ ion (inside to outside) in order to make the protein available for another serotonin transport cycle (Rudnick and Clark, 1993; Gu *et al*., 1994).

The substrate translocation by SERT and other NSS family members is thought to occur by an alternating access mechanism as proposed by Jardetzky (Jardetzky, 1966).

As previously explained for the DAT (Section 1.3), this alternating access model for transport is believed to involve the following states: binding of the substrate to the outward-facing state (substarte-free/apo), isomerization of the transporter-substrate complex to the substrate-bound occluded state, isomerization from occluded to inward-facing state, and return to the outward-facing state triggered by substrate dissociation from the inward–facing state (Krishnamurthy and Gouaux, 2012; Penmatsa and Gouaux, 2014).

1.6. Serotonin Transporter Ligands

1.6.1. Serotonin Transporter Substrates

Amphetamines (Figure 1.11) include amphetamine ((±)-**1.5**) and its analogs such as methamphetamine ((±)-**1.6**) and MDMA (3,4-methylenedioxy-*N*-methylamphetamine, ((±)-**1.7** or "ecstasy"). Though amphetamines are used for management of disorders such as attention deficit hyperactivity disorder (ADHD), traumatic brain injury, and narcolepsy, these compounds are more popular as drugs of abuse based on their rewarding and addictive properties (Fleckenstein *et al*., 2007). Amphetamines act as "false substrates" for SERT, NET, and DAT (Robertson *et al*., 2009). In particular, MDMA induces the efflux of [^{3}H] serotonin from membrane vesicles *via* SERT mediated exchange (Rudnick and Wall, 1992). As previously discussed in Section 1.4.1, amphetamine-mediated monoamine efflux is explained by two models: (a) exchange diffusion model (Seidel *et al*., 2005; Sitte and Freissmuth, 2010; Sucic *et al*., 2010), and (b) amphetamine-induced channel-like activity of the transporter (Sonders *et al*., 1997; Sitte *et al*., 1998; Kahlig *et al*., 2005). A recent study on the effects of *p*-

chloroamphetamine and methylenedioxyamphetamine on serotonin-induced currents through SERT corroborated that a multi-state version of the alternate access model explains transporter-mediated efflux of amphetamines (Sandtner *et al*., 2014).

1.6.2. Serotonin Transporter Inhibitors

1.6.2.1. Tricyclic Antidepressants (TCAs)

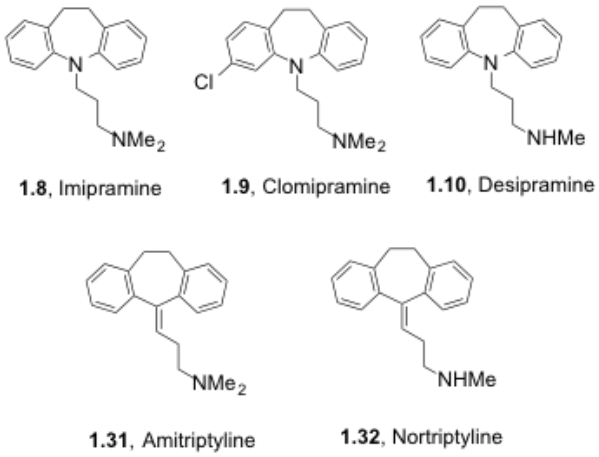

Figure 1.17. Examples of selected tricyclic antidepressants (TCAs).

Tricyclic antidepressants (TCAs, Figure 1.17) such as imipramine (**1.8**), clomipramine (**1.9**), desipramine (**1.10**), amitriptyline (**1.31**), and nortriptyline (**1.32**) have a three- ring molecular core and share the pharmacological property of inhibiting serotonin and norepinephrine uptake. In addition, TCAs also exhibit post-synaptic receptor antagonism at H_1 histamine, α_1 adrenergic, M_1 muscarinic, and 5-HT_{2A} receptors. Gillman has reviewed the pharmacology and drug interactions of TCAs and this information can be used for choosing the right TCA in a clinical setting (Gillman, 2007). Overall, TCAs result in increased synaptic neurotransmitter concentrations (Andersen *et al*., 2009) and are classified as the first-generation antidepressant drugs alongside monoamine oxidase inhibitors (MAOIs).

1.6.2.2. Selective Serotonin Reuptake Inhibitors (SSRIs)

Selective serotonin reuptake inhibitors (SSRIs) started a new era in the treatment of depression, and they are categorized as the second-generation antideressants alongside serotonin-norepinephrine reuptake inhibitors (SNRIs) and norepinephrine reuptake inhibitors (NRIs). SSRIs (Figure 1.18) include citalopram ((±)-**1.11**), *S*-citalopram ((*S*)-**1.11**), fluoxetine ((±)-**1.12**), sertraline (**1.13**), paroxetine (**1.14**), and fluvoxamine (**1.15**). SSRIs are also used for the treatment of generalized anxiety disorder, panic disorder, social anxiety disorder, obsessive-compulsive disorder, premenstrual dysphoric disorder, bulimia, and post-traumatic stress disorder, depending upon the individual drug (Koen and Stein, 2011; Shah *et al*., 2008). Inhibition of SERT is the primary mechanism of SSRIs. However, except for *S*-citalopram, all SSRIs are not entirely selective and display indirect actions (Stahl *et al*., 2013). SSRIs are structurally different *versus* TCAs and selectively bind to SERT with high affinity. As a result, these compounds possess significant advantages over TCAs, namely, similar or improved efficacy, relatively fewer side effects, wider therapeutic window, and safer in cases of overdose (Anderson, 2000; Henry *et al*., 1995). Although SSRIs have no appreciable affinity for α_1-adrenergic receptors, H_1-histamine receptors, and muscarinic cholinergic receptors, and are generally better tolerated than TCAs, SSRIs have their own specific problems, such as aggravation of sexual dysfunction, suicidality, insomnia, pregnancy problems, and, for many, a discontinuation syndrome (Moret *et al*., 2009). SSRIs also cause side effects such as nausea, vomiting, headache, and agitation, which usually subside within 2-3 weeks.

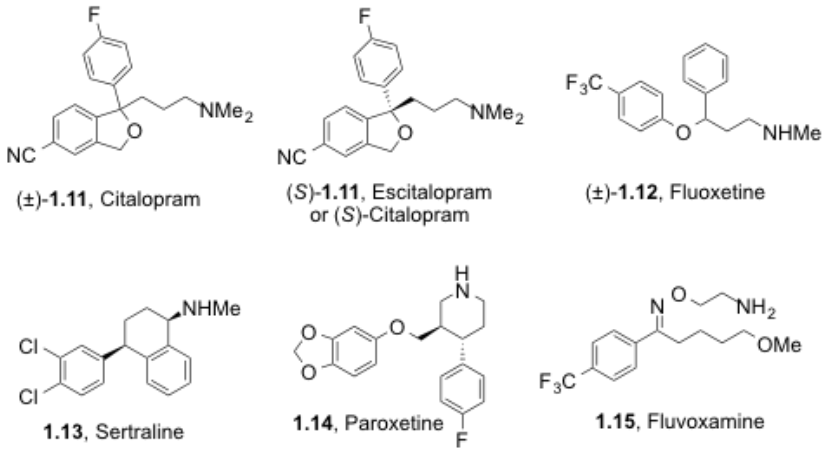

Figure 1.18. Structures of selective serotonin reuptake inhibitors (SSRIs) in clinical use.

In particular, citalopram ((±)-**1.11**)) is a potent selective serotonin reuptake inhibitor (hSERT K_i = 1.6 nM, serotonin uptake IC_{50} = 9.6 nM), and is a racemic mixture composed of (*S*)-citalopram (hSERT K_i = 1.1 nM, serotonin uptake IC_{50} = 2.5 nM) and (*R*)-citalopram (hSERT K_i = 36 nM, serotonin uptake IC_{50} = 67 nM) (Owens *et al*., 2001). Citalopram has gained special attention with respect to the S1 and S2 binding sites of SERT (Sanchez *et al*., 2004). The eutomer, escitalopram ((*S*)-**1.11**) interacts with hSERT uniquely, whereas other SSRIs bind to both the S1 and S2 sites (Chen, Larsen, Sánchez *et al*., 2005). (S)-Citalopram displays ~30 fold higher binding affinity at SERT *versus* its enantiomer, (*R*)-citalopram, and (*R*)-citalopram may attenuate the effects of (*S*)-citalopram *via* allosteric modulation (Chen, Larsen, Sánchez *et al*., 2005; Zhong *et al*., 2009 and 2012). The SERT binding contacts for these citalopram enantiomers are unknown, and the importance of the S2 allosteric site with respect to the pharmacological profile of existing SSRIs is not well understood. Most recently, several analogs of citalopram were synthesized to understand structure-activity relationships and the importance of the allosteric binding site within SERT (Zhang *et al*., 2010; Banala *et al*., 2013).

1.6.2.3. Serotonin-Norepinephrine Reuptake Inhibitors (SNRIs)

Four serotonin-norepinephrine reuptake inhibitors (SNRIs, Figure 1.19) are clinically available in the United States, venlafaxine (**1.33**), desvenlafaxine (**1.20**), duloxetine (**1.21**) and milnacipran (**1.34**). While venlafaxine, desvenlafaxine, and duloxetine are approved for treatment of depression, milnacipran is only approved for treatment of fibromyalgia in the United States. In particular, venlafaxine is approved for the treatment of depression, generalized anxiety disorder, social anxiety disorder, panic disorder, obsessive compulsive disorder, and post traumatic stress disorder (Phleps and Cates, 2005; Pae *et al*., 2007). Duloxetine is also effective in the treatment of diabetic peripheral neuropathic pain, fibromyalgia, osteoarthritis, and low back pain (Bril 2012; Hauser *et al*., 2012; Citrome and Weiss-Citrome 2012). The inhibition of both SERT and NET not only increases serotonin and norepinephrine levels in the brain but also increases dopamine levels in the prefrontal cortex, which potentially adds to the efficacy of SNRIs in treatment of depression (Stahl, 2013). SNRIs are thought to have a faster onset of action compared to SSRIs and are useful for depressed patients resistant to other treatments, mainly due to reasons of their efficacy and tolerability (Kasper and Pail, 2010).

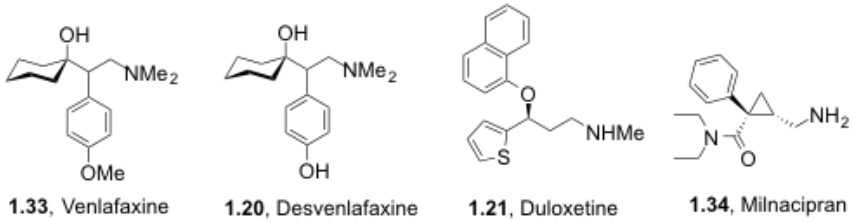

Figure 1.19. Structures of serotonin-norepinephrine reuptake inhibitors (SNRIs) in clinical use.

1.7. References

- Abdolmaleky, H.M., Nohesara, S., Ghadirivasfi, M., Lambert, A.W., Ahmadkhaniha, H., Ozturk, S., and Thiagalingam, S. DNA hypermethylation of serotonin transporter gene promoter in drug naive patients with schizophrenia. *Schizophr. Res.* **2014**, *152*, 373-380.

- Andersen, J., Taboureau, O., Hansen, K.B., Olsen, L., Egebjerg, J., Stromgaard, K., and Kristensen, A.S. Location of the antidepressant binding site in the serotonin transporter: importance of Ser-438 in recognition of citalopram and tricyclic antidepressants. *J. Biol. Chem.* **2009**, *284*, 10276-10284.

- Andersen, J., Olsen, L., Hansen, K.B., Taboureau, O., Jorgensen, F.S., Jorgensen, A.M., and Kristensen, A.S. Mutational mapping and modeling of the binding site for (*S*)-citalopram in the human serotonin transporter. *J. Biol. Chem.* **2010**, *285*, 2051-2063.

- Andersen, J., Stuhr-Hansen, N., Zachariassen, L., Toubro, S., Hansen, S.M., Eildal, J.N., and Kristensen, A.S. Molecular determinants for selective recognition of antidepressants in the human serotonin and norepinephrine transporters. *Proc. Nat. Acad. Sci.* **2011**, *108*, 12137-12142.

- Anderson, I.M. Selective serotonin reuptake inhibitors *versus* tricyclic antidepressants: a meta-analysis of efficacy and tolerability. *J. Affect. Disord.* **2000**, *58*, 19-36.

- Astrup, A., Madsbad, S., Breum, L., Jensen, T.J., Kroustrup, J.P., Larsen, T.M.

Effect of tesofensine on bodyweight loss, body composition, and quality of life in obese patients: a randomised, double-blind, placebo-controlled trial. *Lancet* **2008**, *372*, 1906-1913.

- Banala, A.K., Zhang, P., Plenge, P., Cyriac, G., Kopajtic, T., Katz, J.L., Loland, C.J., and Newman, A.H. Design and synthesis of 1-(3-(dimethylamino)propyl)-1-(4-fluorophenyl)-1,3-dihydroisobenzofuran-5-carbonitrile (citalopram) analogues as novel probes for the serotonin transporter S1 and S2 binding sites. *J. Med. Chem.* **2013**, *56*, 9709-9724.

- Barker, E.L., Perlman, M.A., Adkins, E.M., Houlihan, W.J., Pristupa, Z.B., Niznik, H.B., and Blakely, R.D. High affinity recognition of serotonin transporter antagonists defined by species-scanning mutagenesis an aromatic residue in transmembrane domain I dictates species-selective recognition of citalopram and mazindol. *J. Biol. Chem.* **1998**, *273*, 19459-19468.

- Barnes, N.M. and Sharp, T. A review of central 5-HT receptors and their function. *Neuropharmacology* **1999**, *38*, 1083-1152.

- Benarroch, E.E. Monoamine transporters: structure, regulation, and clinical implications. *Neurology* **2013**, *81*, 761-768.

- Benjamin, S. and Doraiswamy, P.M. Review of the use of mirtazapine in the treatment of depression. *Expert Opin. Pharmacother.* **2011**, *12*, 1623-1632.

- Bergman, J., Madras, B.K., Johnson, S.E., and Spealman, R.D. Effects of cocaine and related drugs in nonhuman primates. III. Self-administration by squirrel monkeys. *J. Pharmacol. Exp. Ther.* **1989**, *251*, 150-155.

- Beuming, T., Shi, L., Javitch, J.A., and Weinstein, H. A comprehensive structure-based alignment of prokaryotic and eukaryotic neurotransmitter/Na^+ symporters (NSS) aids in the use of the LeuT structure to probe NSS structure and function. *Mol. Pharmacol.* **2006**, *70*, 1630-1642.

- Beuming, T., Kniazeff, J., Bergmann, M.L., Shi, L., Gracia, L., Raniszewska, K., and Gether, U. The binding sites for cocaine and dopamine in the dopamine transporter overlap. *Nat. Neurosci.* **2008**, *11*, 780-789.

- Blakely, R.D., Berson, H.E., Fremeau, R.T., Caron, M.G., Peek, M.M., Prince, H.K., and Bradley, C.C. Cloning and expression of a functional serotonin transporter from rat brain. *Nature* **1991**, *354*, 66-70.

- Bril V. Treatments for diabetic neuropathy. *J. Peripher. Nerv. Syst.* **2012**, *17*, 22-27.

- Butler, S.G. and Meegan, M.J. Recent developments in the design of anti-depressive therapies: targeting the serotonin transporter. *Curr. Med. Chem.* **2008**, *15*, 1737-1761.

- Carroll, F.I., Mascarella, S.W., Kuzemko, M.A., Gao, Y., Abraham, P., Lewin, A.H., Boja, J.W., and Kuhar, M.J. Synthesis, ligand binding, and QSAR (COMFA and classical) study of 3-beta-(3'-substituted phenyl)-, 3-beta-(4'-substituted phenyl)-, and

3-beta-(3',4'-disubstituted phenyl)tropane-2-beta-carboxylic acid methyl esters. *J. Med. Chem.* **1994**, *37*, 2865-2873.

- Carroll, F., Howell, L., and Kuhar, M. Pharmacotherapies for treatment of cocaine abuse: preclinical aspects. *J. Med. Chem.* **1999**, *42*, 2721-2736.

- Chen, F., Larsen, M.B., Neubauer, H.A., Sánchez, C., Plenge, P., and Wiborg, O. Characterization of an allosteric citalopram-binding site at the serotonin transporter. *J. Neurochem.* **2005**, *92*, 21-28.

- Chen, F., Larsen, M.B., Sánchez, C., and Wiborg, O. The *S*-enantiomer of *R,S*-citalopram, increases inhibitor binding to the human serotonin transporter by an allosteric mechanism. Comparison with other serotonin transporter inhibitors. *European Neuropsychopharmacology* **2005**, *15*, 193-198.

- Chen, J.G., Liu-Chen, S., and Rudnick, G. Determination of external loop topology in the serotonin transporter by site-directed chemical labeling. *J. Biol. Chem*. **1998**, *273*, 12675-12681.

- Chen, N., Vaughan, R.A., and Reith, M.E. The role of conserved tryptophan and acidic residues in the human dopamine transporter as characterized by site-directed mutagenesis. *J. Neurochem.* **2001**, *77*, 1116-1127.

- Chen, N. and Reith, M.E. Na^+ and the substrate permeation pathway in dopamine transporters. *Eur. J. Pharmacol.* **2003**, *479*, 213-221.

- Chen, N., Rickey, J., Berfield, J.L., and Reith, M.E. Aspartate 345 of the dopamine transporter is critical for conformational changes in substrate translocation and cocaine binding. *J. Biol. Chem.* **2004**, *279*, 5508-5519.

- Chen, R., Furman, C.A., and Gnegy, M.E. Dopamine transporter trafficking: rapid response on demand. *Future Neurol.* **2010**, *5*, 123-141.

- Ciccarone, D. Stimulant abuse: pharmacology, cocaine, methamphetamine, treatment, attempts at pharmacotherapy. *Prim. Care* **2011**, *38*, 41-58.

- Citrome, L. and Weiss-Citrome, A. A systematic review of duloxetine for osteoarthritic pain: what is the number needed to treat, number needed to harm, and likelihood to be helped or harmed? *Postgrad. Med.* **2012**, *124*, 83-93.

- Clarke, R.L., Daum, S.J., Gambino, A.J., Aceto, M.D., Pearl, J., Levitt, M., Cumiskey, W.R., and Bogado, E.F. Compounds affecting the central nervous system. 4. 3 beta-phenyltropane-2-carboxylic esters and analogs. *J. Med. Chem.* **1973**, *16*, 1260-1267.

- Claxton, D.P., Quick, M., Shi, L., de Carvalho, F.D., Weinstein, H., Javitch, J.A., and McHaourab, H.S. Ion/substrate-dependent conformational dynamics of a bacterial homolog of neurotransmitter:sodium symporters. *Nat. Struct. Mol. Biol.* **2010**, *17*, 822-829.

- Dahal, R.A., Pramod, A.B., Sharma, B., Krout, D., Foster, J.D., Cha, J.H., Cao, J., Newman, A.H., Lever, J.R., Vaughan, R.A., and Henry, K. Computational and biochemical docking of the irreversible cocaine analog RTI 82 directly demonstrates

ligand positioning in the dopamine transporter central substrate binding site. *J. Bio. Chem.* **2014**, *298*, 29712-29727.

- Dawson, L.A. and Nguyen, H.Q. Effects of 5-HT1A receptor antagonists on fluoxetine-induced changes in extracellular serotonin concentrations in rat frontal cortex. *Eur. J. Pharmacol.* **1998**, *345*, 41-46.

- Demchyshyn, L.L., Pristupa, Z.B., Sugamori, K.S., Barker, E.L., Blakely, R.D., Wolfgang, W.J., Forte, M.A., and Niznik, H.B. Cloning, expression, and localization of a chloride-facilitated, cocaine-sensitive serotonin transporter from Drosophila melanogaster. *Proc. Natl. Acad. Sci. USA* **1994**, *91*, 5158-5162.

- Dutta, A.K., Fei, X.S., Vaughan, R.A., Gaffaney, J.D., Wang, N., Lever, J.R., and Reith, M.E.A. Design, synthesis, and characterization of a novel, 4-[2-(diphenylmethoxy) ethyl]-1-benzylpiperidine-based, dopamine transporter photoaffinity label. *Life Sci.* **2001**, *68*, 1839-1849.

- Ferragud, A., Sanchez, C.V., Rabaza, V.H., Nacher, A., Merino, V., Carda, M., and Canales, J.J. A dopamine transport inhibitor with markedly low abuse liability suppresses cocaine self-administration in the rat. *Psychopharmacology* **2009**, *207*, 281-289.

- Fleckenstein, A.E., Volz, T.J., Riddle, E.L., Gibb, J.W., and Hanson, G.R. New insights into the mechanism of action of amphetamines. *Annu. Rev. Pharmacol. Toxicol.* **2007**, *47*, 681-698.

- Gabrielsen, M., Ravna, A.W., Kristiansen, K., and Sylte, I. Substrate binding and translocation of the serotonin transporter studied by docking and molecular dynamics simulations. *J. Mol. Model.* **2012**, *18*, 1073-1085.

- Gatley, S.J., Pan, D., Chen, R., Chaturvedi, G., and Ding, Y.S. Affinities of methylphenidate derivatives for dopamine, norepinephrine and serotonin transporters. *Life Sciences* **1996**, *58*, PL231-PL239.

- Gedeon, P.C., Indarte, M., Surratt, C.K., and Madura, J.D. Molecular dynamics of leucine and dopamine transporter proteins in a model cell membrane lipid bilayer. *Proteins: Structure, Function, and Bioinformatics* **2010**, *78*, 797-811.

- Gillman, P.K. Tricyclic antidepressant pharmacology and therapeutic drug interactions updated. *British J. Pharmacol.* **2007**, *151*, 737-748.

- Girault, J.A. and Greengard, P. The neurobiology of dopamine signaling. *Arch. Neurol.* **2004**, *61*, 641-644.

- Goldsmith, P., Golder, Z., Hunt, J., Berghmans, S., Jones, D., Stables, J.P., Murphree, L., Howden, D., Newton, P.E., and Richards, F.M. GBR12909 possesses anticonvulsant activity in zebrafish and rodent models of generalized epilepsy but cardiac ion channel effects limit its clinical utility. *Pharmacology* **2007**, *79*, 250-258.

- Golubchik, P., Sever, J., and Weizman, A. Methylphenidate treatment in children with attention deficit hyperactivity disorder and comorbid social phobia. *Int. Clin. Psychopharmacol.* **2014**, *29*, 212-215.

- Grant, S.J., Aston-Jones, G., and Redmond Jr., D.E. Responses of primate locus coeruleus neurons to simple and complex sensory stimuli. *Brain Research Bulletin* **1988**, *21*, 401-410.

- Greengard, P. The neurobiology of dopamine signaling. *Biosci. Rep.* **2001**, *21*, 247-269.

- Grigoriadis, D.E., Wilson, A.A., Lew, R., Sharkey, J.S., and Kuhar, M.J. Dopamine transport sites selectively labeled by a novel photoaffinity probe: ^{125}I-DEEP. *J. Neurosci.* **1989**, *9*, 2664-2670.

- Gu, H., Wall, S.C., and Rudnick, G. Stable expression of biogenic amine transporters reveals differences in inhibitor sensitivity, kinetics, and ion dependence. *J. Biol. Chem.* **1994**, *269*, 7124-7130.

- Hahn, M. and Blakely, R. Monoamine transporter gene structure and polymorphisms in relation to psychiatric and other complex disorders. *The Pharmacogenomics Journal* **2002**, *2*, 217-235.

- Hauser, W., Wolfe, F., Tolle, T., Uceyler, N., and Somme, C. The role of antidepressants in the management of fibromyalgia syndrome: a systematic review and meta-analysis. *CNS Drugs* **2012**, *26*, 297- 307.

- Heinz, A., Mann, K., Weinberger, D.R., and Goldman, D. Serotonergic dysfunction, negative mood states, and response to alcohol. *Alcoholism: Clinical and Experimental Research* **2001**, *25*, 487-495.

- Henry, J.A., Alexander, C.A., and Sener, E.K. Relative mortality from overdose of antidepressants. *BMJ* **1995**, *310*, 221-224.

- Henry, L.K., Field, J.R., Adkins, E.M., Parnas, M.L., Vaughan, R.A., Zou, M.F., and Blakely, R.D. Tyr-95 and Ile-172 in transmembrane segments 1 and 3 of human serotonin transporters interact to establish high affinity recognition of antidepressants. *J. Biol. Chem.* **2006**, *281*, 2012-2023.

- Hiranita, T., Soto, P.L., Newman, A.H., and Katz, J.L. Assessment of reinforcing effects of benztropine analogs and their effects on cocaine self-administration in rats: comparisons with monoamine uptake inhibitors. *J. Pharmacol. Exp. Ther.* **2009**, *329*, 677-686.

- Hoffman, B.J. Expression cloning of a serotonin transporter: a new way to study antidepressant drugs. *Pharmacopsychiatry* **1994**, *27*, 16-22.

- Howell, L. and Negus, S. Monoamine transporter inhibitors and substrates as treatments for stimulant abuse. *Advances in Pharmacology* **2013**, *69*, 129-176.

- Howell, L.L. and Kimmel, H.L. Monoamine transporters and psychostimulant addiction. *Biochem. Pharmacol.* **2008**, *75*, 196-217.

- Huang, X., and Zhan, C.G. How dopamine transporter interacts with dopamine: insights from molecular modeling and simulation. *Biophys. J.* **2007**, *93*, 3627-3639.

- Huang, X., Gu, H.H., and Zhan, C.G. Mechanism for cocaine blocking the transport of dopamine: Insights from molecular modeling and dynamics simulations. *J. Phys. Chem. B.* **2009**, *113*, 15057-15066.

- Husbands, S.M., Izenwasser, S., Kopajtic, T., Bowen, W.D., Vilner, B.J., Katz, J.L., and Newman, A.H. Structure-activity relationships at the monoamine transporters and σ receptors for a novel series of 9-[3-(*cis*-3,5-dimethyl-1-piperazinyl)-propyl]carbazole (rimcazole) analogues. *J. Med. Chem.* **1999**, *42*, 4446-4455.

- Indarte, M., Madura, J.D., and Surratt, C.K. Dopamine transporter comparative molecular modeling and binding site prediction using the LeuT(Aa) leucine transporter as a template. *Proteins* **2008**, *70*, 1033-1046.

- Iversen, S.D. and Iversen, L.L. Dopamine: 50 years in perspective. *Trends in Neurosciences* **2007**, *30*, 188-193.

- Jaber, M., Jones, S., Giros, B., and Caron, M.G. The dopamine transporter: a crucial component regulating dopamine transmission. *Movement Disorders* **1997**, *12*, 629-633.

- Jardetzky, O. Simple allosteric model for membrane pumps. *Nature* **1966**, *211*, 969-970.

- Javanmard, S., Deutsch, H.M., Collard, D.M., Kuhar, M.J., and Schweri, M.M. Synthesis and pharmacology of site-spesific cocaine abuse treatment agents: 2-substituted-6-amino-5-phenylbicyclo[2.2.2]octanes. *J. Med. Chem.* **1999**, *42*, 4836-4843.

- Jorenby, D. Clinical efficacy of bupropion in the management of smoking cessation. *Drugs* **2002**, *62*, 25-35.

- Jorgensen, A.M., Tagmose, L., Jorgensen, A.M.M., Bogeso, K.P., and Peters, G.H. Molecular dynamics simulations of Na^+/Cl^--dependent neurotransmitter transporters in a membrane-aqueous system. *ChemMedChem* **2007**, *2*, 827-840.

- Jorgensen, A.M., Tagmose, L., Jorgensen, A.M.M., Topiol, S., Sabio, M., Gundertofte, K., and Peters, G. H.. Homology modeling of the serotonin transporter: Insights into the Primary Escitalopram-binding Site. *ChemMedChem* **2007**, *2*, 815-826.

- Kahlig, K.M, Binda, F., Khoshbouei, H., Blakely, R.D., McMahon, D.G., and Javitch, J. Amphetamine induces dopamine efflux through a dopamine transporter channel. *Proc. Natl. Acad. Sci. USA* **2005**, *102*, 3495-3500.

- Kantcheva, A.K., Quick, M., Shi, L., Winther, A.M.L., Stolzenberg, S., Weinstein, H., and Nissen, P. Chloride binding site of neurotransmitter sodium symporters. *Proc. Natl. Acad. Sci. USA* **2013**, *110*, 8489-8494.

- Kasper, S. and Pail, G. Milacipran: a unique antidepressant? *Neuropsychiatric Disease and Treatment* **2010**, *6*, 23-31.

- Katzenschlager, R., Sampaio, C., Costa, J., and Lees, A. Anticholinergics for symptomatic management of Parkinson's disease. *Cochrane Database Syst. Rev.* **2002**, CD003735.

- Katz, J.L., Izenwasser, S., Kline, R.H., Allen, A.C., and Newman, A.H. Novel 3alpha-diphenylmethoxytropane analogs: selective dopamine uptake inhibitors with

behavioral effects distinct from those of cocaine. *J. Pharmacol. Exp. Ther*. **1999**, *288*, 302-315.

- Katz, J.L., Agoston, G.E., Alling, K.L., Kline, R.H., Forster, M.J., Woolverton, W.L., Kopajtic, T.A., and Newman A.H. Dopamine transporter binding without cocaine-like behavioral effects: synthesis and evaluation of benztropine analogs alone and in combination with cocaine in rodents. *Psychopharmacology* **2001**, *154*, 362-374.

- Katz, J.L., Kopajtic, T.A., Agoston, G.E., and Newman, A.H. Effects of *N*-substituted analogs of benztropine: diminished cocaine-like effects in dopamine transporter ligands. *J. Pharmacol. Exp. Ther.* **2004**, *309*, 650-660.

- Khan, A. Vilazodone, a novel dual-acting serotonergic antidepressant for managing major depression. *Expert Opin. Investig. Drugs* **2009**, 18, 1753-1764.

- Khawam, E.A., Laurencic, G., and Malone Jr., D.A. Side effects of antidepressants: an overview. *Clev. Clin. J. Med.* **2006**, *73*, 351-361.

- Klimek, V., Stockmeier, C., Overholser, J., Meltzer, H.Y., Kalka, S., Dilley, G., and Ordway, G.A. Reduced levels of norepinephrine transporters in the locus coeruleus in major depression. *J. Neurosci.* **1997**, *17*, 8451-8458.

- Kline, R.H., Eshleman, A.J., Eldefrawi, M.E., and Wright, J. Synthesis of substituted 3-carbamoylecgonine methyl ester analogs: Irreversible and photoaffinity ligands for the cocaine receptor/dopamine transporter. *J. Med. Chem.* **1994**, *37*, 2249-2252.

- Koen, N. and Stein, D.J. Pharmacotherapy of anxiety disorders: a critical review. *Dialogues Clin. Neurosci.* **2011**, *13*, 423-437.

- Koldso, H., Severinsen, K., Tran, T.T., Celik, L., Jensen, H.H., Wiborg, O., and Sinning, S. The two enantiomers of citalopram bind to the human serotonin transporter in reversed orientations. *J. Am. Chem. Soc.* **2010**, *132*, 1311-1322.

- Koldso, H., Autzen, H.E., Grouleff, J., and Schiott, B. Ligand induced conformtational changes of the human serotonin transporter revealed by molecular dynamics simulations. *PLoS One* **2013**, *8*, e63635.

- Koldso, H., Christiansen, A.B., Sinning, S., and Schioett, B. Comparative modeling of the human monoamine transporters: Similarities in substrate binding. *ACS Chem. Neurosci.* **2013**, *4*, 295-309.

- Koob, G.F. Neural mechanisms of drug reinforcement. *Annals of the New York Academy of Sciences* **1992**, *654*, 171-191.

- Kopajtic, T.A., Liu, Y., Surratt, C.K., Donovan, D.M., Newman, A.H., and Katz, J.L. Dopamine transporter-dependent and -independent striatal binding of the benztropine analog JHW 007, a cocaine antagonist with low abuse liability. *J. Pharmacol. Exp. Ther.* **2010**, *335*, 703-714.

- Krishnamurthy, H. and Gouaux, E. X-ray structures of LeuT in substrate-free outward-open and apo inward-open states. *Nature* **2012**, *481*, 469-474.

- Lader, M. Tricyclic antidepressants. *Handbook of Experimental Pharmacology.* **2004**, *157*, 185-208.

- Li, L.B., Chen, N., Ramamoorthy, S., Chi, L., Cui, X.N., Wang, L.C., and Reith, M.E. The role of N-glycosylation in function and surface trafficking of the human dopamine transporter. *J. Biol. Chem.* **2004**, *279*, 21012-21020.

- Lile, J.A. and Nader, M.A. The abuse liability and therapeutic potential of drugs evaluated for cocaine addiction as predicted by animal models. *Curr. Neuropharmacol.* **2003**, *1*, 21-46.

- Loland, C.J., Desai, R.I., Zou, M.F., Cao, J., Grundt, P., Gerstbrein, K., Sitte, H.H., Newman, A.H., Katz, J.L., and Gether, U. Relationship between conformational changes in the dopamine transporter and cocaine-like subjective effects of uptake inhibitors. *Mol. Pharmacol.* **2008**, *73*, 813-823.

- Loland, C.J. The use of LeuT as a model in elucidating binding sites for substrates and inhibitors in neurotransmitter transporters. *Biochim. Biophys. Acta* **2015**, *1850*, 500-510.

- Madras, B.K., Spealman, R.D., Fahey, M.A., Neumeyer, J.L., Saha, J.K., and Milius, R.A. Cocaine receptors labeled by [^{3}H]2β-carbomethoxy-3β-(4-fluorophenyl)tropane. *Mol. Pharmacol.* **1989**, *36*, 518-524.

- Manepalli, S., Surratt, C.K., Madura, J.D., and Nolan, T.L. Monoamine transporter structure, function, dynamics, and drug discovery: a computational perspective. *AAPS J.* **2012**, *14*, 820-831.

- Mazei-Robison, M.S., Bowton, E., Holy, M., Schmudermaier, M., Freissmuth, M., Sitte, H.H., and Blakely, R.D. Anomalous dopamine release associated with a human dopamine transporter coding variant. *J. Neurosci.* **2008**, *28*, 7040-7046.

- Mehler-Wex, C., Riederer, P., and Gerlach, M. Dopaminergic dysbalance in distinct basal ganglia neurocircuits: implications for the pathophysiology of Parkinson's disease, schizophrenia and attention deficit hyperactivity disorder. *Neurotoxicity Research* **2006**, *10*, 167-179.

- Misra, M., Shi, Q., Ye, X., Gruszecka-Kowalik, E., Bu, W., Liu, Z., and Venanzi, C.A. Quantitative structure-activity relationship studies of threo-methylphenidate analogs. *Bioorg. Med. Chem.* **2010**, *18*, 7221-7238.

- Moret, C., Isaac, M., and Briley, M. Problems associated with long-term treatment with selective serotonin reuptake inhibitors. *J. Psychopharmacol.* **2009**, *23*, 967-974.

- Mortensen, O.V., Kristensen, A.S., Rudnick, G., and Wiborg, O. Molecular cloning, expression and characterization of a bovine serotonin transporter. *Brain Res. Mol. Brain Res.* **1999**, *71*, 120-126.

- Natarajan, R. and Yamamoto, B.K. The basal ganglia as a substrate for the multiple actions of amphetamines. *Basal Ganglia* **2011**, *1*, 49-57.

- Neubauer, H.A., Hansen, C.G., and Wiborg, O. Dissection of an allosteric mechanism on the serotonin transporter: a cross-species study. *Mol. Pharmacol.* **2006**, *69*, 1242-1250.

- Newman, A.H., Kline, R.H., Allen, A.C., Izenwasser, S., George, C., and Katz, J.L. Novel 4'-substituted and 4',4''-disubstituted 3-alpha-(diphenylmethoxy)tropane analogs as potent and selective dopamine uptake inhibitors. *J. Med. Chem.* **1995**, *38*, 3933-3940.

- Newman, A.H., Robarge, M.J., Howard, I.M., Wittkopp, S.L., Kopajtic, T., Izenwasser, S., and Katz, J.L. Structure activity relationships at the monoamine transporters and muscarinic receptors for *N*-substituted-3α-[(3'-Cl-, 4'-Cl-, 4',4''-diCl-substituted) diphenyl] methoxytropanes. *J. Med. Chem.* **2001**, *44*, 633–640.

- Newman, A.H. and Kulkarni, S. Probes for the dopamine transporter: new leads toward a cocaine-abuse therapeutic--A focus on analogues of benztropine and rimcazole. *Med. Res. Rev.* **2002**, *22*, 429-464.

- Newman, A.H., Cha, J.H., Cao, J., Kopajtic, T., Katz, J.L., Parnas, M.L., Vaughan, R., and Lever, J.R. Design and synthesis of a novel photoaffinity ligand for the dopamine and serotonin transporters based on 2β-carbomethoxy-3β-biphenyltropane. *J. Med. Chem.* **2006**, *49*, 6621-6625.

- Norregaard, L., Frederiksen, D., Nielsen, E.O., and Gether, U. Delineation of an endogenous zinc-binding site in the human dopamine transporter. *The EMBO journal* **1998**, *17*, 4266-4273.

- Nyola, A., Karpowich, N.K., Zhen, J., Marden, J., Reith, M.E., and Wang, D.N. Substrate and drug binding sites in LeuT. *Curr. Opin. Struct. Biol.* **2010**, *20*, 415-422.

- Owens, M.J., Knight, D.L., and Nemeroff, C.B. Second-generation SSRIs: human monoamine transporter binding profile of escitalopram and R-fluoxetine. *Biol. Psychiatry* **2001**, *50*, 345–350.

- Pae, C.U., Lim, H.K., Ajwani, N., Lee, C., and Patkar, A.A. Extended-release formulation of venlafaxine in the treatment of post-traumatic stress disorder. *Expert Rev. Neurother.* **2007**, 7, 603-615.

- Parnas, M.L., Gaffaney, J.D., Zou, M.F., Lever, J.R., Newman, A.H., and Vaughan, R.A. Labeling of dopamine transporter transmembrane domain 1 with the tropane ligand *N*-[4-(4-azido-3-[^{125}I]iodophenyl)butyl]-2beta-carbomethoxy-3beta-(4-chlorophenyl) tropane implicates proximity of cocaine and substrate active sites. *Mol. Pharmacol.* **2008**, *73*, 1141-1150.

- Penmatsa, A., Wang, K.H., and Gouaux, E. X-ray structure of dopamine transporter elucidates antidepressant mechanism. *Nature* **2013**, *503*, 85-90.

- Penmatsa, A. and Gouaux, E. How LeuT shapes our understanding of the mechanisms of sodium-coupled neurotransmitter transporters. *J. Physiol.* **2014**, *592*, 863-869.

- Piscitelli, C.L. and Gouaux, E. Insights into transport mechanism from LeuT engineered to transport tryptophan. *EMBO J.* **2012**, *31*, 228-235.

- Phelps, N.J. and Cates, M.E. The role of venlafaxine in the treatment of obsessive-compulsive disorder. *Ann. Pharmacother*. **2005**, *39*, 136-140.

- Plenge, P., Mellerup, E.T., and Laursen, H. Affinity modulation of [^{3}H] imipramine, [^{3}H] paroxetine and [^{3}H] citalopram binding to the 5-HT transporter from brain and platelets. *Eur. J. Pharmacol.* **1991**, *206*, 243-250.

- Plenge, P. and Mellerup, E.T. An affinity-modulating site on neuronal monoamine transport proteins. *Pharmacology & Toxicology* **1997**, *80*, 197-201.

- Plenge, P., Gether, U., and Rasmussen, S.G. Allosteric effects of R-and S-citalopram on the human 5-HT transporter: evidence for distinct high- and low-affinity binding sites. *Eur. J. Pharmacol.* **2007**, *567*, 1-9.

- Plenge, P., Shi, L., Beuming, T., Te, J., Newman, A.H., Weinstein, H., and Loland, C.J. Steric hindrance mutagenesis in the conserved extracellular vestibule impedes allosteric binding of antidepressants to the serotonin transporter. *J. Biol. Chem.* **2012**, *287*, 39316-39326.

- Quick, M., Lund-Winther, A.M., Shi, L., Nissen, P., Weinstein, H., and Javitch, J.A. Binding of an octylglucoside detergent molecule in the second substrate (S2) site of LeuT establishes an inhibitor-bound conformation. *Proc. Natl. Acad. Sci. USA* **2009**, *106*, 5563-5568.

- Quick, M., Shi, L., Zehnpfennig, B., Weinstein, H., and Javitch, J.A. Experimental conditions can obscure the second high-affinity site in LeuT. *Nat. Struct. Mol. Biol.* **2012**, *19*, 207-211.

- Ravna, A.W., Jaronczyk, M., and Sylte, I. A homology model of SERT based on the LeuTAa template. *Bioorg. Med. Chem. Lett.* **2006**, *16*, 5594-5597.

- Reith, M.E., Berfield, J.L., Wang, L.C., Ferrer, J.V., and Javitch, J.A. The uptake inhibitors cocaine and benztropine differentially alter the conformation of the human dopamine transporter. *J. Biol. Chem.* **2001**, *276*, 29012-29018.

- Ritz, M.C., Lamb, R., and Kuhar, M. Cocaine receptors on dopamine transporters are related to self-administration of cocaine. *Science* **1987**, *237*, 1219-1223.

- Robertson, S., Matthies, H., and Galli, A. A closer look at amphetamine-induced reverse transport and trafficking of the dopamine and norepinephrine transporters. *Mol. Neurobiol.* **2009**, *39*, 73-80.

- Rothman, R., Mele, A., Reid, A., Akunne, H., Greig, N., Thurkauf, A., Rice, K., and Pert, A. Tight binding dopamine reuptake inhibitors as cocaine antagonists. A strategy for drug development. *FEBS Lett.* **1989**, *257*, 341-344.

- Rothman, R. and Glowa, J. A review of the effects of dopaminergic agents on humans, animals, and drug-seeking behavior, and its implications for medication development. *Mol. Neurobiol.* **1995**, *11*, 1-19.

- Rothman, R.B., Baumann, M.H., Prisinzano, T.E., and Newman, A.H. Dopamine transport inhibitors based on GBR12909 and benztropine as potential medications to treat cocaine addiction. *Biochem. Pharmacol.* **2008**, *75*, 2-16.

- Rudnick, G. and Wall, S.C. The molecular mechanism of ‘‘ecstasy’’ [3,4-methylenedioxymethamphetamine (MDMA)]: serotonin transporters are targets for MDMA-induced serotonin release. *Proc. Natl. Acad. Sci. USA* **1992**, 89, 1817–1821.

- Rudnick, G. and Clark, J. From synapse to vesicle: the reuptake and storage of biogenic amine neurotransmitters. *Biochim. Biophys. Acta.* **1993**, 1144, 249-263.

- Rudnick, G., Kramer, R., Blakely, R.D., Murphy, D.L., and Verrey, F. The SLC6 transporters: perspectives on structure, functions, regulation, and models for transporter dysfunction. *Pfluegers Arch.* **2014**, *466*, 25-42.

- Sanchez, C., Bogeso, K.P., Ebert, B., Reines, E.H., and Braestrup, C. Escitalopram *versus* citalopram: the surprising role of the R-enantioner. *Psychopharmacology* **2004**, *174*, 163-176.

- Sanchez, C.V., Ferragud, A., Murga, J., Carda, M., and Canales, J.J. The high affinity dopamine uptake inhibitor, JHW 007, blocks cocaine-induced reward, locomotor stimulation and sensitization. *Eur. Neuropsychopharmacol.* **2010**, *20*, 501-508.

- Sandtner, W., Schmid, D., Schicker, K., Gerstbrein, K., Koenig, X., Mayer, F.P., Boehm, S., Freissmuth, M., and Sitte, H.H. A quantitative model of amphetamine action on the 5-HT transporter. *Br. J. Pharmacol.* **2014**, *171*, 1007-1018.

- Schmitt, K.C., Zhen, J., Kharkar, P., Mishra, M., Chen, N., Dutta, A.K., and Reith, M.E. Interaction of cocaine-, benztropine-, and GBR12909-like compounds with wild-type and mutant human dopamine transporters: molecular features that differentially determine antagonist-binding properties. *J. Neurochem.* **2008**, *107*, 928-940.

- Schmitt, K.C. and Reith, M.E.A. The atypical stimulant and nootropic modafinil interacts with the dopamine transporter in a different manner than classical cocaine-like inhibitors. *PLoS One* **2011**, *6*, e25790.

- Schmitt, K.C., Rothman, R.B., and Reith, M.E. Nonclassical pharmacology of the dopamine transporter: atypical inhibitors, allosteric modulators, and partial substrates. *J. Pharmacol. Exp. Ther.* **2013**, *346*, 2-10.

- Seddik, A., Holy, M., Weissensteiner, R., Zdrazil, B., Sitte, H.H., and Ecker, G.F. Probing the selectivity of monoamine transporter substrates by means of molecular modeling. *Mol. Inf.* **2013**, *32*, 409-413.

- Seeman, P. and Niznik, H.B. Dopamine receptors and transporters in Parkinson's disease and schizophrenia. *FASEB J.* **1990**, *4*, 2737-2744.

- Seidel, S., Singer, E.A., Just, H., Farhan, H., Scholze, P., and Kudlacek, O. Amphetamines take two to tango: an oligomer-based counter-transport model of neurotransmitter transport explores the amphetamine action. *Mol. Pharmacol.* **2005**, *67*, 140–151.

- Serretti, A. and Mandelli, L. The genetics of bipolar disorder: genome 'hot regions', genes, new potential candidates and future directions. *Molecular Psychiatry* **2008**, *13*, 742-771.

- Shah, N.R., Jones, J.B., Aperi, J., Shemtov, R., Karne, A., and Borenstein, J. Selective serotonin reuptake inhibitors for premenstrual syndrome and premenstrual dysphoric disorder: a meta-analysis. *Obstet. Gynecol.* **2008**, *111*, 1175-1182.

- Shi, L., Quick, M., Zhao, Y., Weinstein, H., and Javitch, J.A. The mechanism of a neurotransmitter:sodium symporter--inward release of Na^+ and substrate is triggered by substrate in a second binding site. *Mol. Cell.* **2008**, *30*, 667-677.

- Singh, M. and Schwartz, T.L. Clinical utility of vilazodone for the treatment of adults with major depressive disorder and theoretical implications for future clinical use. *Neuropsychiatr. Dis. Treat.* **2012**, *8*, 123-130.

- Singh, S.K., Yamashita, A., and Gouaux, E. Antidepressant binding site in a bacterial homologue of neurotransmitter transporters. *Nature* **2007**, *448*, 952-956.

- Singh, S.K., Piscitelli, C.L., Yamashita, A., and Gouaux, E. A competitive inhibitor traps LeuT in an open-to-out conformation. *Science* **2008**, *322*, 1655-1661.

- Sinning, S., Musgaard, M., Jensen, M., Severinsen, K., Celik, L., Koldsø, H., and Schiøtt, B. Binding and orientation of tricyclic antidepressants within the central substrate site of the human serotonin transporter. *J. Biol. Chem.* **2010**, *285*, 8363-8374.

- Sitte, H.H., Huck, S., Reither, H., Boehm, S., Singer, E.A., and Pifl, C. Carrier-mediated release, transport rates, and charge transfer induced by amphetamine, tyramine, and dopamine in mammalian cells transfected with the human dopamine transporter. *J. Neurochem.* **1998**, *71*, 1289–1297.

- Sitte, H.H. and Freissmuth, M. The reverse operation of Na(+)/Cl(-)-coupled neurotransmitter transporters-why amphetamines take two to tango. *J. Neurochem.* **2010**, *112*, 340–355.

- Soares, K.V. and McGrath, J.J. Anticholinergic medication for neuroleptic-induced tardive dyskinesia. *Cochrane Database Syst. Rev.* **2000**, CD000204.

- Sonders, M.S., Zhu, S.J., Zahniser, N.R., Kavanaugh, M.P., and Amara, S.G. Multiple ionic conductances of the human dopamine transporter: the actions of dopamine and psychostimulants. *J. Neurosci.* **1997**, *17*, 960–974.

- Stahl, S.M., Lee-Zimmerman, C., Cartwright, S., and Morrissette, D.A. Serotonergic drugs for depression and beyond. *Current Drug Targets* **2013**, *14*, 578-585.

- Stahl, S.M. Stahl's Essential Psychopharmacology. 4th ed. New York: Cambridge University Press, **2013**.

- Stockner, T., Montgomery, T.R., Kudlacek, O., Weissensteiner, R., Ecker, G.F., Freissmuth, M., and Sitte, H.H. Mutational analysis of the high-affinity zinc binding site validates a refined human dopamine transporter homology model. *PLoS Computational Biology* **2013**, *9*, e1002909.

- Sucic, S., Dallinger, S., Zdrazil, B., Weissensteiner, R., Jorgensen, T.N., and Holy, M. The N-terminus of monoamine transporters is a lever required for the action of amphetamines. *J. Biol. Chem.* **2010**, *285*, 10924-10938.

- Sulzer, D., Sonders, M.S., Poulsen, N.W., and Galli, A. Mechanisms of neurotransmitter release by amphetamines: a review. *Prog. Neurobiol.* **2005**, *75*, 406-433.

- Talvenheimo, J., Nelson, P.J., and Rudnick, G. Mechanism of imipramine inhibition of platelet 5-hydroxytryptamine transport. *J. Biol. Chem.* **1979**, *254*, 4631-4635.

- Tanda, G., Newman, A.H., and Katz, J.L. Discovery of drugs to treat cocaine dependence: behavioral and neurochemical effects of atypical dopamine transport inhibitors. *Adv. Pharmacol.* **2009**, *57*, 253-289.

- Tate, C.G. and Blakely, R.D. The effect of N-linked glycosylation on activity of the Na(+)- and Cl(-)-dependent serotonin transporter expressed using recombinant baculovirus in insect cells. *J. Biol. Chem.* **1994**, *269*, 26303-26310.

- Tavoulari, S., Forrest, L.R., and Rudnick, G. Fluoxetine (Prozac) binding to serotonin transporter is modulated by chloride and conformational changes. *J. Neurosci.* **2009**, *29*, 9635-9643.

- Tella, S.R., Ladenheim, B., Andrews, A.M., Goldberg, S.R., and Cadet, J.L. Differential reinforcing effects of cocaine and GBR-12909: Biochemical evidence for divergent neuroadaptive changes in the mesolimbic dopaminergic system. *J. Neurosci.* **1996**, *16*, 7416-7427.

- Torres, G.E., Carneiro, A., Seamans, K., Fiorentini, C., Sweeney, A., Yao, W.D., and Caron, M.G. Oligomerization and trafficking of the human dopamine transporter. Mutational analysis identifies critical domains important for the functional expression of the transporter. *J. Biol. Chem.* **2003**, *278*, 2731-2739.

- Uhl, G.R. and Lin, Z. The top 20 dopamine transporter mutants: structure-function relationships and cocaine actions. *Eur. J. Pharmacol.* **2003**, *479*, 71-82.

- Ukairo, O.T., Bondi, C.D., Newman, A.H., Kulkarni, S.S., Kozikowski, A.P., Pan, S., and Surratt C.K. Recognition of benztropine by the dopamine transporter (DAT)

differs from that of the classical dopamine reuptake inhibitors cocaine, methylphenidate and mazindol as a function of DAT transmembrane 1 aspartic acid residue. *J. Pharmacol. Exp. Ther*. **2005**, *314*, 575-583.

- Vaughan, R.A. Cocaine and GBR photoaffinity labels as probes of dopamine transporter structure. *Methods Enzymol.* **1998**, *296*, 219-230.

- Vaughan, R.A., Agoston, G.E., Lever, J.R., and Newman, A.H. Differential binding of tropane-based photoaffinity ligands on the dopamine transporter. *J. Neurosci.* **1999**, *19*, 630-636.

- Vaughan, R.A., Gaffaney, J.D., Lever, J.R., Reith, M.E.A., and Dutta, A.K. Dual incorporation of photoaffinity ligands on dopamine transporters implicates proximity of labeled domains. *Mol. Pharmacol.* **2001**, *59*, 1157-1164.

- Vaughan, R.A., Parnas, M.L., Gaffaney, J.D., Lowe, M.J., Wirtz, S., Pham, A., and Justice, J.B. Affinity labeling the dopamine transporter ligand binding site. *J. Neurosci. Methods* **2005**, *143*, 33-40.

- Vaughan, R.A., Sakrikar, D.S., Parnas, M.L., Adkins, S., Foster, J.D., Duval, R.A., and Newman, A.H. Localization of cocaine analog [^{125}I]RTI 82 irreversible binding to transmembrane domain 6 of the dopamine transporter. *J. Biol. Chem.* **2007**, *282*, 8915-8925.

- Volkow, N.D., Wang, G.J., Fischman, M.W., Foltin, R., Fowler, J.S., Franceschi, D., and Pappas, N. Effects of route of administration on cocaine induced dopamine transporter blockade in the human brain. *Life Sci.* **2000**, *67*, 1507-1515.

- Volz, T.J. and Schenk, J.O. A comprehensive atlas of the topography of functional groups of the dopamine transporter. *Synapse* **2005**, *58*, 72-94.

- Wang, H. and Gouaux, E. Substrate binds in the S1 site of the F253A mutant of LeuT, a neurotransmitter sodium symporter homologue. *EMBO Rep.* **2012**, *13*, 861-866.

- Wang, H., Goehring, A., Wang, K.H., Penmatsa, A., Ressler, R., and Gouaux, E. Structural basis for action by diverse antidepressants on biogenic amine transporters. *Nature* **2013**, *503* , 141-145.

- Wayment, H., Meiergerd, S.M., and Schenk, J.O. Relationships between the catechol substrate binding site and amphetamine, cocaine, and mazindol bindingsites in a kinetic model of the striatal transporter of dopamine in vitro. *J. Neurochem*. **1998**, *70*, 1941-1949.

- Wee, S., Carroll, F.I., and Woolverton, W.L. A reduced rate of in vivo dopamine transporter binding is associated with lower relative reinforcing efficacy of stimulants. *Neuropsychopharmacology* **2006**, *31*, 351-362.

- Westerink, R.H. Targeting exocytosis: ins and outs of the modulation of quantal dopamine release. *CNS Neurol. Disord. Drug Targets* **2006**, *5*, 57-77.

- Woolverton, W.L., and Johnson, K.M. Neurobiology of cocaine abuse. *Trends in Pharmacol. Sci.* **1992**, *13*, 193-200.

- Woolverton, W.L., Rowlett, J.K., Wilcox, K.M., Paul, I.A., Kline, R.H., Newman, A.H., and Katz, J.L. 3'- and 4'-chloro-substituted analogs of benztropine: intravenous

self-administration and in vitro radioligand binding studies in rhesus monkeys. *Psychopharmacology* **2000**, *147*, 426-435.

- Yamashita, A., Singh, S.K., Kawate, T., Jin, Y., and Gouaux, E. Crystal structure of a bacterial homologue of Na^+/Cl^--dependent neurotransmitter transporters. *Nature* **2005**, *437*, 215-223.

- Yano, M. and Steiner, H. Methylphenidate and cocaine: the same effects on gene regulation? *Trends Pharmacol. Sci.* **2007**, *28*, 588-596.

- Zhang, P., Cyriac, G., Kopajtic, T., Zhao, Y., Javitch, J.A., Katz, J.L., and Newman, A.H. Structure−Activity relationships for a novel series of citalopram (1-(3-(dimethylamino) propyl)-1-(4-fluorophenyl)-1, 3-dihydroisobenzofuran-5-carbonitrile) analogues at monoamine transporters. *J. Med. Chem.* **2010**, *53*, 6112-6121.

- Zhong, H., Hansen, K.B., Boyle, N.J., Han, K., Muske, G., Huang, X., and Sánchez, C. An allosteric binding site at the human serotonin transporter mediates the inhibition of escitalopram by R-citalopram: Kinetic binding studies with the ALI/VFL–SI/TT mutant. *Neurosci. Lett.* **2009**, *462*, 207-212.

- Zhong, H., Haddjeri, N., and Sánchez, C. Escitalopram, an antidepressant with an allosteric effect at the serotonin transporter—a review of current understanding of its mechanism of action. *Psychopharmacology* **2012**, *219*, 1-13.

- Zhou, Z., Zhen, J., Karpowich, N.K., Goetz, R.M., Law, C.J., Reith, M.E., and Wang, D.N. LeuT-desipramine structure reveals how antidepressants block neurotransmitter reuptake. *Science* **2007**, *317*, 1390-1393.

- Zhou, Z., Zhen, J., Karpowich, N.K., Law, C.J., Reith, M.E., and Wang, D.N. Antidepressant specificity of serotonin transporter suggested by three LeuT–SSRI structures. *Nat. Struct. Mol. Bio.* **2009**, *16*, 652-657.

- Zhou, Z.L., Liu, H.L., Wu, J.W., Tsao, C.W., Chen, W.H., Liu, K.T., and Ho. Y. Combining structure-based pharmacophore and in silico approaches to discover novel selective serotonin reuptake inhibitors. *Chem. Biol. Drug Des.* **2013**, *82*, 705-717.

- Zohar, J. and Westenberg, H.G.M. Anxiety disorders: a review of tricyclic antidepressants and selective serotonin reuptake inhibitors. *Acta. Psychiatr. Scand.* **2000**, *101*, 39-49.

- Zou, M.F., Kopajtic, T., Katz, J.L., Wirtz, S., Justice, J.B., and Newman, A.H. Novel tropane-based irreversible ligands for the dopamine transporter. *J. Med. Chem.* **2001**, *44*, 4453-4461.

- Zou, M., Kopajtic, T., Katz, J.L., and Newman, A.H. Structure-activity relationship comparison of (*S*)-2β-substituted 3α-(bis[4-fluorophenyl]methoxy)tropanes and (*R*)-2β-substituted 3β-(3,4-dichlorophenyl)tropanes at the dopamine transporter. *J. Med. Chem.* **2003**, *46*, 2908-2916.

CHAPTER TWO

2. Irreversible Chemical Labeling of Protein Drug Targets with Small Molecules

2.1. Introduction

Monoamine transporters (MATs) are associated with several mental health disorders (Hahn and Blakely, 2002) such as anxiety (Plieger *et al*., 2014), depression (Stahl *et al*., 2013), drug addiction (Howell and Negus, 2013), Parkinson's disease (Grachev, 2014), and schizophrenia (Abdolmaleky *et al*., 2014). Although many drugs are available to treat mental health disorders, attempts are being made to develop novel treatments targeting MATs in order to address shortcomings associated with current agents. For example, currently available antidepressants have several limitations including late onset of action, a high percentage of non-responding patients, and side effects such as sexual dysfunction, weight gain, nausea, anxiety, and insomnia (Khawam *et al*., 2006). Despite representing important drug targets, very little is known about specific drug-protein interactions that lead to the clinical efficacy of agents targeting MATs. In particular, the bottleneck in producing MAT crystal structures is associated with an inability to obtain sufficient amounts of pure and stable protein required for protein crystallization (Bill *et al*., 2011). Apart from X-ray crystallography (Garman, 2014), other approaches for acquiring detailed 3D structural information of proteins include site-directed mutagenesis (Shortle *et al*., 1981), computational modeling (Rodrigues and Bonvin, 2014), and photoaffinity labeling (Sumranjit and Chung, 2013).

Historically, MAT structure-function information has been obtained *via* biophysical, pharmacological, and molecular biology studies (*e.g*., characterization of

MAT site-directed mutants). Such techniques have elucidated the general topology of MAT proteins in the plasma membrane and indicate two or three probable substrate binding sites. However, these experimental techniques have offered little towards elucidating transmembrane domains that are juxtaposed, how substrates are translocated, or the size and shape of ligand-binding pockets. Most recently, crystal structures of a leucine transporter (LeuT) (*e.g.*, Yamashita *et al*., 2005), a bacterial MAT homolog, have paved a way for multiple research groups to build computational human MAT molecular models (*e.g.*, Manepalli *et al*., 2012; Stockner *et al*., 2013). In turn, these computer homology models have aided in characterizing ligand-binding sites within the dopamine transporter (DAT) (*e.g.*, Beuming *et al*., 2008; 2006; Bisgaard *et al*., 2011; Indarte *et al*., 2008) and serotonin transporter (SERT) (*e.g.*, Andersen *et al*., 2010; Celik *et al*., 2008; Henry *et al*., 2006; Kaufmann *et al*., 2009; Ravna, *et al*., 2006; Sarker *et al*., 2010). However, due to significant evolutionary differences between the human DAT, SERT, and bacterial LeuT protein template used for computational homology modeling, careful experimental validation and critical refinement of these molecular models is necessary in order to understand the structure, function, and pharmacological properties of MAT proteins.

To date, DAT and SERT homology models have been experimentally investigated mainly by site-directed mutagenesis studies (*e.g.*, for DAT see Severinsen *et al.*, 2014; Stockner *et al.*, 2013; Guptaroy *et al.*, 2011; Bisgaard *et al.*, 2011; Schmitt *et al.*, 2008; for SERT see Andersen *et al*., 2010 and 2011; Koldso *et al*., 2010; Sorensen *et al*., 2012). In particular, mutagenesis of amino acids in many regions of these proteins results in a reduction or loss of transporter activity and/or inhibitor binding (*e.g.*, Henry,

et al., 2006; Newman *et al*., 2006; Zhang *et al*., 2010). However, it is difficult in the absence of structural information to confirm if the effects of mutations are due to disruptions of specific ligand-protein interaction sites, or to alterations of MAT structure that indirectly impact ligand-binding sites. A positive functional approach to address these concerns is to use photoreactive irreversible ligands to directly identify binding site(s) of MAT inhibitors.

2.2. Photoaffinity Labeling

Photoaffinity labeling (PAL) has contributed significantly to our understanding of how a ligand interacts with its biological target, principally because this experimental approach allows direct determination of the spatial proximity of molecular components (Xu and Wu, 2014). A photoaffinity probe is typically designed from a ligand of interest by rationally incorporating a photoreactive group (PRG) and a reporter group (RG) into the chemical structure of the lead compound (Scheme 2.1). The PRG is inert under normal conditions; however, upon irradiation with UV light, it gets converted into highly reactive radical intermediate, which is capable of forming a covalent bond between the biological target and the photoprobe. The RG is useful for detection of covalent attachment to the biological macromolecule and consequently the site(s) of photoprobe modification. Typically, the irreversible, covalent probe-target complex is then digested or fragmented *via* proteolysis and/or chemical cleavage methods. Probe-labeled fragments can then be analyzed using epitope-specific immunoprecipitation, high-performance liquid chromatography (HPLC), and mass spectrometry (MS) in order to identify the amino acid composition / sequence surrounding the covalent point of

attachment of the probe to the biological target (Dorman and Prestwich, 2000; Geurink *et al.*, 2012).

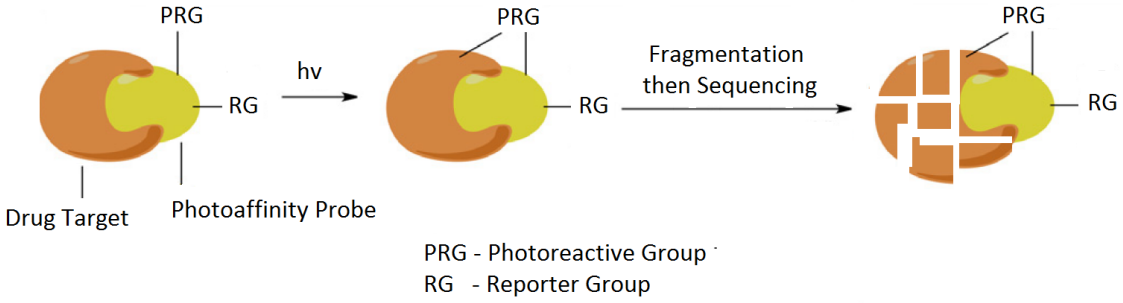

Scheme 2.1. Photoaffinity labeling towards mapping the binding site of a ligand within a drug target. (Lapinsky, 2012. Adapted with permission from *Bioorg. Med. Chem.* **2012**, *20*, 6237-6247. Copyright 2012, Elsevier)

The following set of characteristics has been attributed to ideal photoprobes, specifically: (a) they utilize a wavelength-selective activation that does not damage other components in the biological testing system; (b) they possess high stability in the dark under various pH conditions; (c) they form a stable adduct with their target biological macromolecule(s) and survive subsequent characterization and detection methodology; (d) they bear a structural resemblance to the parent ligand with similar binding affinity and pharmacology; (e) they have the ability to react with any type of bond or residue without any preference; and (f) they generate highly reactive, short-lived photo-intermediates upon irradiation with UV light (Das, 2011; Vodovozova, 2007). Despite extensive research in developing photoaffinity labeling agents, so far there are no reports of photoprobes that possess all of these desired criteria.

Photoaffinity labeling represents one the most direct approaches towards elucidating ligand-binding sites within target proteins. Although this experimental approach has been employed extensively with the DAT (*e.g.*, Agoston *et al.*, 1997; Lever *et al.*, 2005; Newman *et al.*, 2006; Parnas *et al.*, 2008; Vaughan *et al.*, 1999, 2005, and

2007; Vaughan and Kuhar, 1996; Zou *et al.*, 2001; Lapinsky *et al.*, 2009, 2011, and 2012), this dissertation has contributed the first ever clickable photoprobes for SERT and a method to conduct SERT photoaffinity labeling using these probes.

Arguably, the nature of the photoreactive group (PRG) is the most important design component of a photoaffinity probe. The most widely used PRGs in photoaffinity ligands are aromatic azides, benzophenones and acetophenones, and aliphatic (Das, 2011) and aromatic diazirines (*e.g.*, Dubinsky *et al.*, 2012; Hashimoto and Hatanaka, 2008). Photoreactive functional groups can also be characterized according to their photochemically-generated reactive species, principally nitrenes, diradicals, and carbenes (Fleming, 1995). Given this dissertation features chemical probes containing either an aromatic azide or benzophenone photoreactive group, only these functional groups in terms of photoaffinity labeling are reviewed below.

2.2.1. Select Photoreactive Groups Employed in MAT Structure-Function Studies

2.2.1.1. Aryl Azides

Among a wide number of photoreactive functional groups, aryl azides are the most widely used in photoaffinity probes, mainly because of their comparatively small structural variation relative to a parent compound and ease of synthetic incorporation. Upon irradiation at a wavelength of 254 nm, aryl azides generate reactive nitrene intermediates that can form covalent bonds with amino acid functional groups (Scheme 2.2). In general, exposure of an aryl azide (**2.1,** Scheme 2.2) to UV light (250-350 nm) leads to the formation of a nitrene species (**2.2**) that can either: (1) undergo ring expansion to form a ketenimine/azepine (**2.3**) that can react with a nucleophile (**2.4**), (2) insert into C-H or N-H sites (**2.7**), or (3) undergo intersystem conversion (ISC) to a

triplet state (**2.5**) that can subsequently dimerize (**2.6**) (Preston and Wilson, 2013). One non-productive reaction pathway of aryl-azides is that they can also react with thiols to form aryl amines (**2.8**). In particular, the singlet nitrene species (**2.2**) has electrophilic character, and therefore incorporation of electron-withdrawing groups on an aromatic ring bearing a photoreactive azide is typically used as a strategy to stabilize singlet nitrene formation. For example, (per)fluorinated aryl azides avoid undesirable ring expansion reactions and favor bond insertion reactions in a desirable manner (Schnapp *et al.*, 1993). Additionally, the triplet nitrene (**2.5**) can behave as a diradical and form an azobenzene (**2.6**) leading to an undesirable side reaction during photoaffinity labeling. Finally, 1,2-didehydroazepine **2.3** is a key intermediate that can selectively react with particular protein functional groups. In aqueous media, 1,2-didehydroazepine **2.3** has been shown to preferentially react with amines over hydrocarbon groups (Rizk *et al*., 2006).

The wavelength at which aryl azides are photolysed (typically < 300nm) produces a high amount of energy that could potentially damage the biological system being exposed to the UV radiation during photoaffinity labeling. Additionally, due to the lack of reaction specificity and side reactions possible (*e.g*., **2.5** to **2.6**), photoaffinity labeling with aryl azides often results in low yields of the probe-target complex (<30%). In order to address these issues, the absorption wavelength of a photoreactive azide is typically shifted to a higher wavelength, once again by incorporating electron-withdrawing groups such as fluorine and nitro groups on the aromatic ring bearing the photoreactive aryl azide (Mohr, 2004).

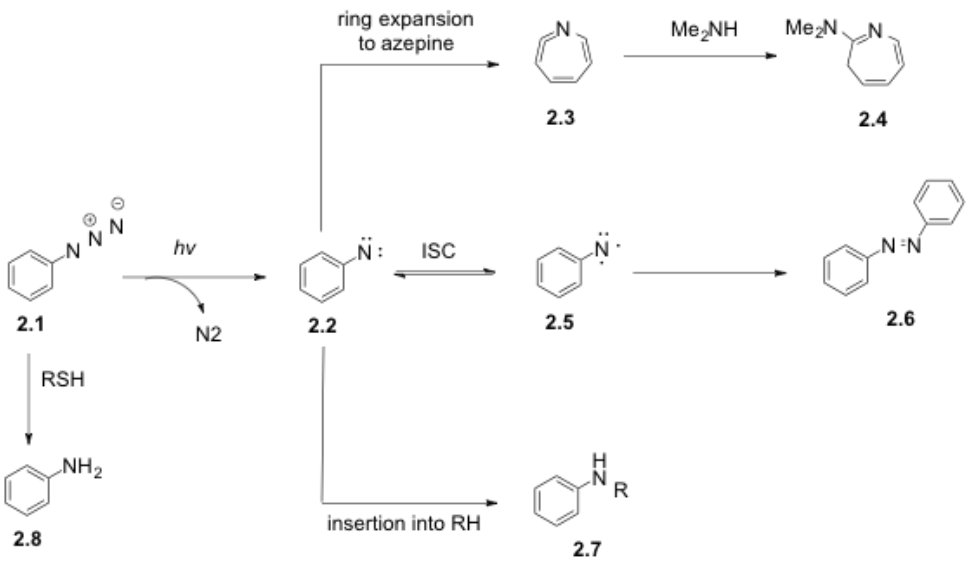

Scheme 2.2. Reaction pathways of aryl azides upon photoactivation.

2.2.1.2. Benzophenones

Upon irradiation with a wavelength of approximately 350 nm, benzophenones (**2.9** in Scheme 2.3) generate a ketyl biradical (**2.10**), which can form a covalent bond with protein functional groups *via* a sequential proton abstraction-radical recombination mechanism (Dorman and Prestwich, 1994; Preston and Wilson, 2013). Ketyl biradical formation occurs as the benzophenone absorbs UV radiation and excites a non-bonding electron into the carbonyl π* orbital. In the diradical state, the electron deficient oxygen has an empty n-orbital that is electrophilic and capable of interacting with C-H bonds in the protein. This results in hydrogen abstraction and produces two ketyl radicals that can readily combine to generate a new C-C bond (**2.12**). The excitation of benzophenones is reversible, and therefore can return to the ground state if hydrogen abstraction does not take place.

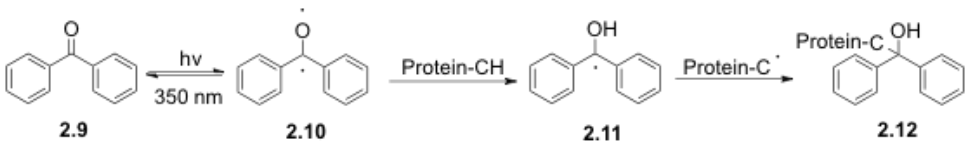

Scheme 2.3. Activation pathway of benzophenone photoreactive group.

Even though the benzophenone photoreactive functional group introduces a significant amount of bulkiness and hydrophobicity to the analog (*i.e.*, relative to the lead compound), thus potentially affecting proper formation of the reversible photoprobe-protein complex before photolysis, benzophenones have several advantages over other photoaffinity labeling groups (Dorman and Prestwich, 1994). Benzophenones are generally more chemically stable than aryl azides and diazirines, and can be activated at 350-360 nm, which is safe for photoaffinity labeling cell cultures or other living systems. Additionally, benzophenones can preferentially react with inactive C-H bonds even in the presence of water and other nucleophiles. Furthermore, benzophenone derivatives are more efficient in labeling the proteome, as they can be repeatedly excited until they generate covalent adducts, without loss of their chemical integrity. Adding to these advantages, a number of benzophenone-containing building blocks are commercially available, and this functional group is stable in most organic solvents and compatible with multiple synthetic reagents for photoprobe synthesis.

2.2.2. Select Reporter Groups Employed in MAT Structure-Function Studies

2.2.2.1. Radioactive Isotopes

Radioactive isotopes are widely used for the detection of a variety of biomolecules in proteomic applications. In particular, ^{125}I has been utilized in many photoprobes because of its ease of incorporation *via* simple synthetic steps, relatively small size, and highly sensitive signal for easy detection and quantification (Sadaghiani *et*

al., 2007). However, ^{125}I has a relatively short half-life ($t_{1/2}$ = ~60 days), which doesn't allow radio-iodinated probes to be stored for long periods of time without significant chemical degradation (Seevers and Counsell, 1982). Additionally, radioisotopes are often harmful entities, thus demanding extra care in their handling and use in a laboratory environment. Finally, radio-iodinated probes are mostly used with known targets, or when specific antibodies can be used to confirm the identity of the target using gel-based read outs (Lapinsky, 2012; Sadaghiani *et al*., 2007).

2.2.2.2. 'Clickable' Handles in Tandem Photoaffinity Labeling-Bioorthogonal Conjugation

In addition to radioactive isotopes, alternative tagging methods are available to facilitate proteomic analysis after photoaffinity labeling. Photoaffinity probes can also include reporter groups such as biotin, epitope tags (*e.g*., FLAG peptide), or fluorophores to allow easy enrichment, detection, and/or isolation of photolabeled products after labeling. However, biotin, epitope tags, and fluorophores are rather large in size, cell impermeable, and may adversely affect pharmacological activity relative to a parent compound, principally by sterically disrupting key interactions between the photoprobe and target biological macromolecule. Most recently, the field of photoaffinity labeling has been advanced by the introduction of small surrogate tags (*e.g*., a terminal alkyne or aliphatic azide) into photoprobes that serve as click chemistry/'clickable' handles thus facilitating the attachment of reporter tags to a photoprobe by using highly specific bioorthogonal ligation chemistry after photoaffinity labeling. These 'clickable' handles are relatively small, easily installed into a parent ligand, and have minimal effects on biological activity and cell permeability when compared to a parent compound. As a

result, these significant advantages make clickable handles the current reporter group of choice in designing photoprobes for studying biological macromolecules of interest (Sadaghiani *et al*., 2007; Lapinsky, 2012).

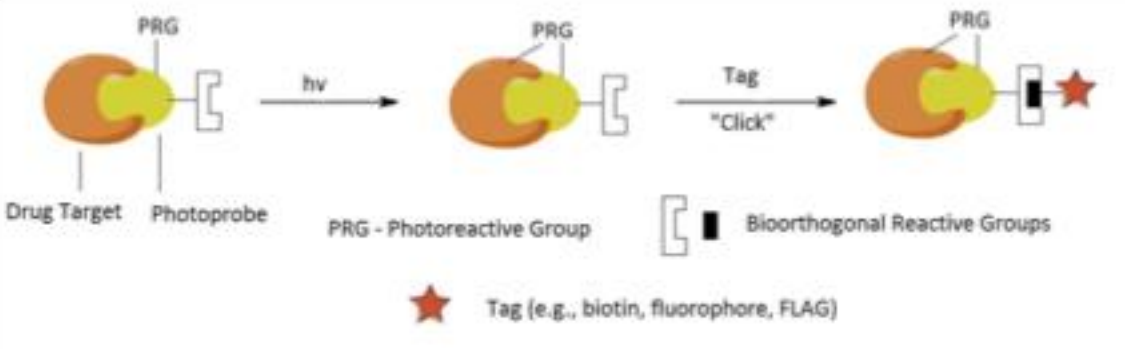

Scheme 2.4. Tandem photoaffinity labeling-bioorthogonal conjugation. (Lapinsky, 2012. Reprinted with permission from *Bioorg. Med. Chem.* **2012**, *20*, 6237-6247. Copyright 2012, Elsevier).

In particular, a new proteomic strategy termed "tandem photoaffinity labeling–bioorthogonal conjugation" (Scheme 2.4) has recently emerged that first involves covalent bond formation between a photoprobe and a biological target *via* photoirradiation (Step 1 in Scheme 2.4), followed by a bioorthogonal conjugation reaction (Step 2 in Scheme 2.4). In particular, bioorthogonal conjugation chemistry is traditionally employed using either a Staudinger-Bertozzi ligation (Saxon and Bertozzi, 2000) or copper-catalyzed Huisgen 1,3-dipolar cycloaddition ('click' reaction or CuAAC) (Rostovtsev *et al*., 2002) (Scheme 2.5). The only apparent concern with this tandem photoaffinity labeling–bioorthogonal conjugation strategy is that yields of the bioorthogonal conjugation step (Step 2, Scheme 2.4) can vary in different systems. In particular, it has been reported that higher yields are often observed when copper-catalyzed Huisgen 1,3-dipolar cycloaddition is employed in the bioorthogonal conjugation step *versus* Staudinger-Bertozzi ligation (Speers *et al*., 2003). However,

regardless of this variability in bioorthogonal conjugation yield, the noteworthy advantages of tag flexibility, high-throughput analysis, and *in vivo* use makes this strategy the current method of choice for analysis of probe-labeled products after photoaffinity labeling.

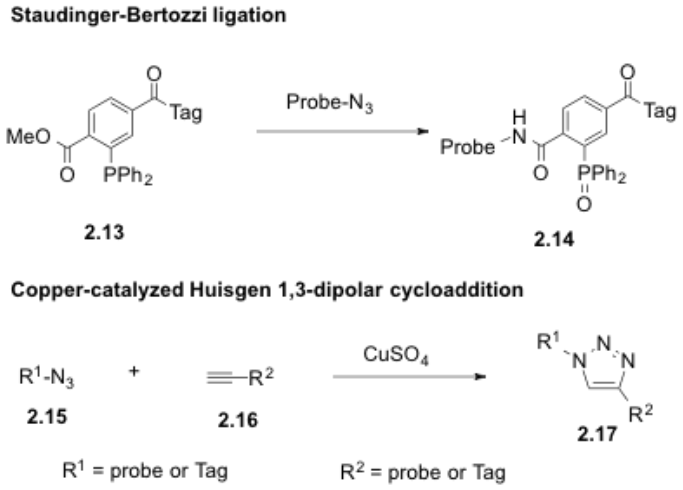

Scheme 2.5. Bioorthogonal conjugation strategies traditionally employed after photoaffinity labeling.

2.2.2.3. Binding Ensemble Profiling with (f)Photoaffinity Labeling (BEProFL)

Binding Ensemble Profiling with (f)Photoaffinity Labeling (BEProFL) represents a novel experimental approach wherein tandem photoaffinity labeling–bioorthogonal conjugation can be coupled with LC–MS and molecular modeling studies in order to accurately determine the three-dimensional structure of a ligand–target complex (He *et al.*, 2009). In particular, BEProFL can be used to facilitate identification of key ligand–target binding interactions, conformational-preferences for both the ligand and biological target, and facilitate obtainment of valuable information for structure-based drug design. Furthermore, detailed molecular information obtained from this combined experimental approach can aid in the validation or refinement of biological target molecular models to

be used for computer-aided drug discovery and development (*e.g.*, virtual / *in silico* screening, structure-based drug design).

In particular, our strategy towards understanding the 3D structural features of monoamine transporters is by developing photoprobes based on established drugs that target DAT or SERT. Furthermore, utilizing the BEProFL experimental approach with these probes is expected to experimentally validate and refine DAT and SERT homology models (Scheme 2.6). Briefly, a DAT or SERT therapeutic agent is functionalized with both a photoreactive group (PRG) and a reporter group (RG). First, the probes are pharmacologically tested in order to evaluate binding affinity at their respective target. Selection criteria for probes for subsequent photoaffinity labeling experiments are those compounds whose binding affinity is < 100 nM and within 10-fold of an appropriate parent compound. Selected candidate probes are then incubated with their natural target, allowed to reversibly bind, and then irradiated with UV light. The resulting irreversible ligand-target complex can then be subjected to traditional proteomic experiments such as SDS-PAGE, proteolysis, and LC-MS/MS, followed by computational studies in order to map the ligand-binding poses and sites of DAT or SERT ligands within their protein targets. Utilization of the BEProFL approach is expected to further refine and/or validate DAT or SERT homology models *via* experimental support, thereby enabling more confident computer-aided drug discovery efforts aimed at these targets (*e.g.*, virtual / *in silico* screening, structure-based drug design) (Indarte *et al.*, 2010; Nolan *et al.*, 2011 and 2014).

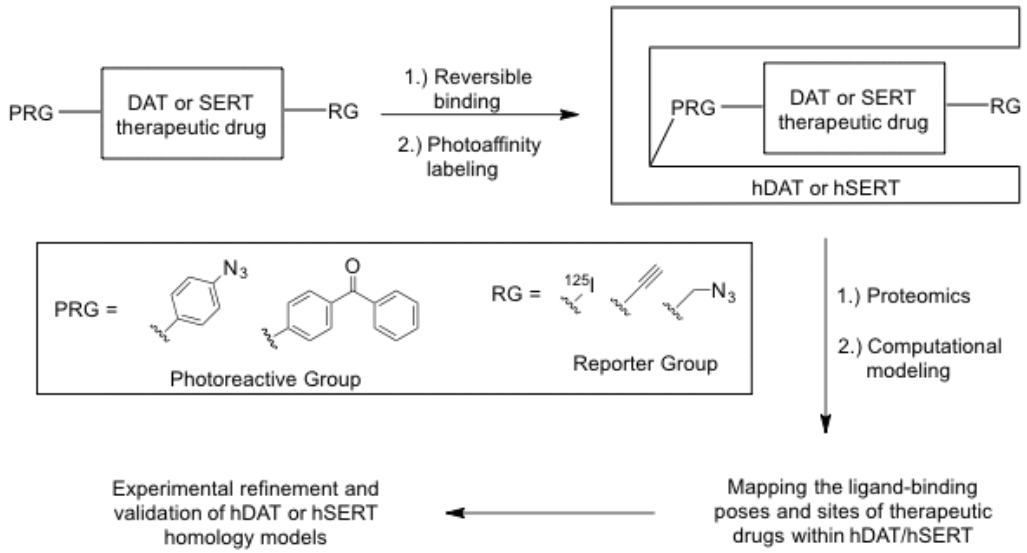

Scheme 2.6. Binding ensemble profiling with (f)photoaffinity labeling (BEProFL) towards experimental validation and refinement of DAT or SERT homology models.

2.3. References

- Abdolmaleky, H.M., Nohesara, S., Ghadirivasfi, M., Lambert, A.W., Ahmadkhaniha, H., Ozturk, S., and Thiagalingam, S. DNA hypermethylation of serotonin transporter gene promoter in drug naive patients with schizophrenia. *Schizophr. Res.* **2014**, *152*, 373-380.

- Agoston, G.E., Vaughan, R., Lever, J.R., Izenwasser, S., Terry, P.D., and Newman, A.H. A novel photoaffinity label for the dopamine transporter based on *N*-substituted 3α-[bis(4'-fluorophenyl)methoxy]tropane. *Bioorg. Med. Chem. Lett.* **1997**, *7*, 3027-3032.

- Andersen, J., Olsen, L., Hansen, K.B., Taboureau, O., Jorgensen, F.S., Jorgensen, A.M., and Kristensen, A.S. Mutational mapping and modeling of the binding site for (S)-citalopram in the human serotonin transporter. *J. Biol. Chem.* **2010**, *285*, 2051-2063.

- Andersen, J., Stuhr-Hansen, N., Zachariassen, L., Toubro, S., Hansen, S.M., Eildal, J.N., and Kristensen, A.S. Molecular determinants for selective recognition of antidepressants in the human serotonin and norepinephrine transporters. *Proc. Natl. Acad. Sci.* **2011**, *108*, 12137-12142.

- Beuming, T., Shi, L., Javitch, J.A., and Weinstein, H. A comprehensive structure-based alignment of prokaryotic and eukaryotic neurotransmitter/Na+ symporters (NSS) aids in the use of the LeuT structure to probe NSS structure and function. *Mol. Pharmacol.* **2006**, *70*, 1630-1642.

- Beuming, T., Kniazeff, J., Bergmann, M.L., Shi, L., Gracia, L., Raniszewska, K., and Gether, U. The binding sites for cocaine and dopamine in the dopamine transporter overlap. *Nature Neurosci.* **2008**, *11*, 780-789.

- Bill, R.M., Henderson, P.J., Iwata, S., Kunji, E.R., Michel, H., Neutze, R., and Vogel, H. Overcoming barriers to membrane protein structure determination. *Nature Biotechnology* **2011**, *29*, 335-340.

- Bisgaard, H., Larsen, M.A., Mazier, S., Beuming, T., Newman, A.H., Weinstein, H., and Gether, U. The binding sites for benztropines and dopamine in the dopamine transporter overlap. *Neuropharmacology* **2011**, *60*, 182-190.

- Celik, L., Sinning, S., Severinsen, K., Hansen, C.G., Møller, M.S., Bols, M., and Schiøtt, B. Binding of serotonin to the human serotonin transporter. Molecular modeling and experimental validation. *J. Am. Chem. Soc.* **2008**, *130*, 3853-3865.

- Das, J. Aliphatic diazirines as photoaffinity probes for proteins: recent developments. *Chem. Rev.* **2011**, *111*, 4405-4417.

- Dorman, G. and Prestwich, G.D. Benzophenone photophores in biochemistry. *Biochemistry* **1994**, *33*, 5661-5673.

- Dorman, G. and Prestwich, G.D. Using photolabile ligands in drug discovery and development. *Trends in Biotechnology* **2000**, *18*, 64-77.

- Dubinsky, L., Krom, B.P., and Meijler, M.M. Diazirine based photoaffinity labeling. *Bioorg. Med. Chem.* **2012**, *20*, 554-570.

- Fleming, S.A. Chemical reagents in photoaffinity labeling. *Tetrahedron* **1995**, *51*, 12479-12520.

- Garman, E.F. Developments in X-ray crystallographic structure determination of biological macromolecules. *Science* **2014**, *343*, 1102-1108.

- Geurink, P.P., Prely, L.M., van der Marel, G.A., Bischoff, R., and Overkleeft, H.S. Photoaffinity labeling in activity based protein profiling. *Top. Curr. Chem.* **2012**, *324*, 85-114.

- Grachev, I.D. Dopamine transporter imaging with [^{123}I]FP-CIT (DaTSCAN) in Parkinson's disease with depressive symptoms: a biological marker for causal relationships? *J. Neurol. Neurosurg. Psychiatry* **2014**, *85*, 130-131.

- Guptaroy, B., Fraser, R., Desai, A., Zhang, M., and Gnegy, M.E. Site-directed mutations near transmembrane domain 1 alter conformation and function of norepinephrine and dopamine transporters. *Mol. Pharmacol.* **2011**, *79*, 520-532.

- Hahn, M. and Blakely, R. Monoamine transporter gene structure and polymorphisms in relation to psychiatric and other complex disorders. *The Pharmacogenomics Journal* **2002**, *2*, 217-235.

- Hashimoto, M. and Hatanaka, Y. Recent progress in diazirine-based photoaffinity labeling. *Eur. J. Org. Chem.* **2008**, *15*, 2513-2523.

- He, B., Velaparthi, S., Pieffet, G., Pennington, C., Mahesh, A., Holzle, D.L., Brunsteiner, M., van Breemen, R., Blond, S.Y., and Petukhov, P.A. Binding ensemble profiling with photoaffinity labeling (BEProFL) approach: Mapping the binding poses of HDAC8 inhibitors. *J. Med. Chem*. **2009**, *52*, 7003-7013.

- Henry, L.K., Field, J.R., Adkins, E.M., Parnas, M.L., Vaughan, R.A., Zou, M.F., and Blakely, R.D. Tyr-95 and Ile-172 in transmembrane segments 1 and 3 of human serotonin transporters interact to establish high affinity recognition of antidepressants. *J. Biol. Chem.* **2006**, *281*, 2012-2023.

- Howell, L. and Negus, S. Monoamine transporter inhibitors and substrates as treatments for stimulant abuse. *Adv. Pharmacol.* **2013**, *69*, 129-176.

- Indarte, M., Madura, J.D., and Surratt, C.K. Dopamine transporter comparative molecular modeling and binding site prediction using the LeuT(Aa) leucine transporter as a template. *Proteins* **2008**, *70*, 1033-1046.

- Indarte, M., Liu, Y., Madura, J.D., and Surratt, C.K. Receptor-based discovery of a plasmalemmal monoamine transporter inhibitor *via* high-throughput docking and pharmacophore modeling. *ACS Chem. Neurosci.* **2010**, *1*, 223-233.

- Kaufmann, K.W., Dawson, E.S., Henry, L.K., Field, J.R., Blakely, R.D., and Meiler, J. Structural determinants of species-selective substrate recognition in human and drosophila serotonin transporters revealed through computational docking studies. *Proteins: Structure, Function, and Bioinformatics* **2009**, *74*, 630-642.

- Khawam, E.A., Laurencic, G., and Malone, D.A. Side effects of antidepressants: an overview. *Clev. Clin. J. Med.* **2006**, *73*, 351-353, 356-361.

- Koldso, H., Severinsen, K., Tran, T.T., Celik, L., Jensen, H.H., Wiborg, O., and Sinning, S. The two enantiomers of citalopram bind to the human serotonin transporter in reversed orientations. *J. Am. Chem. Soc.* **2010**, *132*, 1311-1322.

- Lapinsky, D.J., Aggarwal, S., Huang, Y., Surratt, C.K., Lever, J.R., Foster, J.D., and Vaughan, R.A. A novel photoaffinity ligand for the dopamine transporter based on pyrovalerone. *Bioorg. Med. Chem.* **2009**, *17*, 3770-3774.

- Lapinsky, D.J., Velagaleti, R., Yarravarapu, N., Liu, Y., Huang, Y., Surratt, C.K., Lever, J.R., Foster, J.D., Acharya, R., Vaughan, R.A., and Deutsch, H.M. Azido-iodo-*N*-benzyl derivatives of threo-methylphenidate (Ritalin, Concerta): Rational design, synthesis, pharmacological evaluation, and dopamine transporter photoaffinity labeling. *Bioorg. Med. Chem.* **2011**, *19*, 504-512.

- Lapinsky, D.J., Aggarwal, S., Nolan, T.L., Surratt, C.K., Lever, J.R., Acharya, R., Vaughan, R.A., Pandhare, A., and Blanton, M.P. (+/-)-2-(*N*-tert-Butylamino)-3'-[(125)I]-iodo-4'-azidopropiophenone: a dopamine transporter and nicotinic acetylcholine receptor photoaffinity ligand based on bupropion (Wellbutrin®, Zyban). *Bioorg. Med. Chem. Lett.* **2012**, *22*, 523-526.

- Lapinsky, D.J. Tandem photoaffinity labeling-bioorthogonal conjugation in medicinal chemistry. *Bioorg. Med. Chem.* **2012**, *20*, 6237-6247.

- Lever, J.R., Zou, M.F., Parnas, M.L., Duval, R.A., Wirtz, S.E., Justice, J.B., Vaughan, R.A., and Newman, A.H. Radioiodinated azide and isothiocyanate derivatives of cocaine for irreversible labeling of dopamine transporters: Synthesis and covalent binding studies. *Bioconjugate Chem.* **2005**, *16*, 644-649.

- Manepalli, S., Surratt, C.K., Madura, J.D., and Nolan, T.L. Monoamine transporter structure, function, dynamics, and drug discovery: a computational perspective. *AAPS J.* **2012**, *14*, 820-831.

- Mohr, G.J. Tailoring the sensitivity and spectral properties of a chromoreactand for the detection of amines and alcohols. *Anal. Chim. Acta* **2004**, *508*, 233-237.

- Newman, A.H., Cha, J.H., Cao, J., Kopajtic, T., Katz, J.L., Parnas, M.L., and Lever, J. R. Design and synthesis of a novel photoaffinity ligand for the dopamine and serotonin transporters based on 2β-carbomethoxy-3β-biphenyltropane. *J. Med. Chem.* **2006**, *49*, 6621-6625.

- Nolan, T.L., Lapinsky, D.J., Talbot, J.N., Indarte, M., Liu, Y., Manepalli, S., and Surratt, CK. Identification of a novel selective serotonin reuptake inhibitor by coupling monoamine transporter-based virtual screening and rational molecular hybridization. *ACS Chem. Neurosci.* **2011**, *2*, 544-552.

- Nolan, T.L., Geffert, L.M., Kolber, B.J., Madura, J.D., and Surratt, C.K. Discovery of novel-scaffold monoamine transporter ligands *via* in silico screening with the S1 pocket of the serotonin transporter. *ACS Chem. Neurosci.* **2014**, *5*, 784-792.

- Parnas, M.L., Gaffaney, J.D., Zou, M.F., Lever, J.R., Newman, A.H., and Vaughan, R.A. Labeling of dopamine transporter transmembrane domain 1 with the tropane ligand*N*-[4-(4-azido-3-[^{125}I]iodophenyl)butyl]-2β-carbomethoxy-3β-(4-chlorophenyl)tropane implicates proximity of cocaine and substrate active sites. *Mol. Pharmacol.* **2008**, *73*, 1141-1150.

- Plieger, T., Montag, C., Felten, A., and Reuter, M. The serotonin transporter polymorphism (5-HTTLPR) and personality: response style as a new endophenotype for anxiety. *Int. J. Neuropsychopharmacol.* **2014**, *17*, 851-858.

- Preston, G.W. and Wilson, A.J. Photo-induced covalent cross-linking for the analysis of biomolecular interactions. *Chem. Soc. Rev.* **2013**, *42*, 3289-3301.

- Ravna, A.W., Jaronczyk, M., and Sylte, I. A homology model of SERT based on the LeuTAa template. *Bioorg. Med. Chem. Lett.* **2006**, *16*, 5594-5597.

- Rizk, M.S., Shi, X., and Platz, M.S. Lifetimes and reactivities of some 1,2-didehydroazepines commonly used in photoaffinity labeling experiments in aqueous solutions. *Biochemistry* **2006**, *45*, 543-551.

- Rodrigues, J.P. and Bonvin, A.M. Integrative computational modeling of protein interactions. *FEBS Journal* **2014**, *281*, 1988-2003.

- Rostovtsev, V.V., Green, L.G., Fokin, V.V., and Sharpless, K.B. A stepwise Huisgen cycloaddition process: copper (I)-catalyzed regioselective "ligation" of azides and terminal alkynes. *Angew. Chem. Int. Ed.* **2002**, *41*, 2596-2599.

- Sadaghiani, A.M., Verhelst, S.H., and Bogyo, M. Tagging and detection strategies for activity-based proteomics. *Curr. Opin. Chem. Biol.* **2007**, *11*, 20-28.

- Sarker, S., Weissensteiner, R., Steiner, I., Sitte, H.H., Ecker, G.F., Freissmuth, M., and Sucic, S. The high-affinity binding site for tricyclic antidepressants resides in the outer vestibule of the serotonin transporter. *Mol. Pharmacol.* **2010**, *78*, 1026-1035.

- Saxon, E. and Bertozzi, C.R. Cell surface engineering by a modified Staudinger reaction. *Science* **2000**, *287*, 2007-2010.

- Schmitt, K.C., Zhen, J., Kharkar, P., Mishra, M., Chen, N., Dutta, A.K., and Reith, M.E. Interaction of cocaine-, benztropine-, and GBR12909-like compounds with wild-type and mutant human dopamine transporters: molecular features that differentially determine antagonist-binding properties. *J. Neurochem.* **2008**, *107*, 928-940.

- Schnapp, K.A., Poe, R., Leyva, E., Soundararajan, N., and Platz, M.S. Exploratory photochemistry of fluorinated aryl azides. Implications for the design of photoaffinity labeling reagents. *Bioconjugate Chem.* **1993**, *4*, 172-177.

- Seevers, R.H. and Counsell, R.E. Radioiodination techniques for small organic molecules. *Chem. Rev.* **1982**, *82*, 575-590.

- Severinsen, K., Koldso, H., Thorup, K.A., Schjoth-Eskesen, C., Moller, P.T., Wiborg, O., and Schiott, B. Binding of mazindol and analogs to the human serotonin and dopamine transporters. *Mol. Pharmacol.* **2014**, *85*, 208-217.

- Shortle, D., DiMaio, D., and Nathans, D. Directed mutagenesis. *Ann. Rev. Gen.* **1981**, *15*, 265-294.

- Sorensen, L., Andersen, J., Thomsen, M., Hansen, S.M., Zhao, X., Sandelin, A., and Kristensen, A.S. Interaction of antidepressants with the serotonin and norepinephrine transporters: mutational studies of the S1 substrate binding pocket. *J. Biol. Chem.* **2012**, *287*, 43694-43707.

- Speers, A.E., Adam, G.C., and Cravatt, B.F. Activity-based protein profiling in vivo using a copper (I)-catalyzed azide-alkyne [3+2] cycloaddition. *J. Am. Chem. Soc.* **2003**, *125*, 4686-4687.

- Stahl, M.S., Lee-Zimmerman, C., Cartwright, S., and Ann Morrissette, D. Serotonergic drugs for depression and beyond. *Current Drug Targets* **2013**, *14*, 578-585.

- Stockner, T., Montgomery, T.R., Kudlacek, O., Weissensteiner, R., Ecker, G.F., Freissmuth, M., and Sitte, H.H. Mutational analysis of the high-affinity zinc binding site validates a refined human dopamine transporter homology model. *PLoS Comput. Biol.* **2013**, *9*, e1002909.

- Sumranjit, J. and Chung, S.J. Recent advances in target characterization and identification by photoaffinity probes. *Molecules* **2013**, *18*, 10425-10451.

- Vaughan, R.A. and Kuhar, M.J. Dopamine transporter ligand binding domains. Structural and functional properties revealed by limited proteolysis. *J. Biol. Chem.* **1996**, *271*, 21672-21680.

- Vaughan, R.A., Agoston, G.E., Lever, J.R., and Newman, A.H. Differential binding of tropane-based photoaffinity ligands on the dopamine transporter. *J. Neurosci.* **1999**, *19*, 630-636.

- Vaughan, R.A., Parnas, M.L., Gaffaney, J.D., Lowe, M.J., Wirtz, S., Pham, A., Reed, B., Dutta, S.M., Murray, K.K., and Justice, J.B. Affinity labeling the dopamine transporter ligand binding site. *J. Neurosci. Methods* **2005**, *143*, 33-40.

- Vaughan, R.A., Sakrikar, D.S., Parnas, M.L., Adkins, S., Foster, J.D., Duval, R.A., Lever, J.R., Kulkarni, S.S., and Newman, A.H. Localization of cocaine analog [125I]RTI-82 irreversible binding to transmembrane domain 6 of the dopamine transporter. *J. Biol. Chem.* **2007**, *282*, 8915-8925.

- Vodovozova, E.L. Photoaffinity labeling and its application in structural biology. *Biochemistry (Moscow)* **2007**, *72*, 1-20.

- Xu, B. and Wu, L. Analysis of receptor-ligand binding by photoaffinity cross-linking. *Science China Chemistry* **2014**, *57*, 232-242.

- Yamashita, A., Singh, S.K., Kawate, T., Jin, Y., and Gouaux, E. Crystal structure of a bacterial homologue of Na^+Cl^--dependent neurotransmitter transporters. *Nature* **2005**, *437*, 215-223.

- Zhang, P., Cyriac, G., Kopajtic, T., Zhao, Y., Javitch, J.A., Katz, J.L., and Newman, A.H. Structure−activity relationships for a novel series of citalopram (1-(3-(dimethylamino)propyl)-1-(4-fluorophenyl)-1,3-dihydroisobenzofuran-5-carbonitrile) analogues at monoamine transporters. *J. Med. Chem.* **2010**, *53*, 6112-6121.

- Zou, M.F., Kopajtic, T., Katz, J.L., Wirtz, S., Justice, J.B., and Newman, A.H. Novel tropane-based irreversible ligands for the dopamine transporter. *J. Med. Chem.* **2001**, *44*, 4453-4461.

CHAPTER THREE

3. Chemical Literature Review

3.1. Review of Synthetic Approaches for Racemic *threo*-Methylphenidate, a Lead Compound for DAT Photoprobe Design

A number of synthetic approaches to (±)-*threo*-methylphenidate have been previously described in the chemical literature. For example, Deutsch and coworkers reported an improved synthesis of racemic *threo*-methylphenidate ((±)-**1.18**) (Scheme 3.1) (Deutsch *et al*., 1996) that was originally developed by Panizzon in 1944 (Panizzon, 1944). This improved synthesis is 9 steps in length and produces (±)-*threo*-MP in 18% overall yield. The synthesis begins with alkylation of 2-bromopyridine (**3.2**) with the anion derived from phenylacetonitrile (**3.1**) to give diaryl nitrile **3.3** in 50% yield. Nitrile **3.3** was then hydrolyzed to amide **3.4** using concentrated HCl. Hydrogenation of pyridine **3.4** then provided the piperidine derivative, which was then subjected to salt formation to obtain a diastereomeric mixture of piperidine hydrochloride salts (**3.5)** in good yield (90%). Subsequently, amide **3.5** was hydrolyzed to the carboxylic acid, followed by a 50% KOH epimerization procedure and HCl salt formation, to generate a diastereomeric mixture of ritanilic acid (**3.6**) in 64% yield. The mixture of ritanilic acid stereoisomers was then subjected to esterification followed by recrystallization to provide racemic *threo*-methylphenidate ((±)-**1.18**) in moderate yield (84%).

This synthetic method has been used to generate aromatic ring-substituted analogs of racemic *threo*-methylphenidate in order to establish structure-activity relationships (SAR) with respect to the dopamine transporter (Deutsch *et al*., 1996). One of the

disadvantages of this methodology is that it usually gives a mixture of products that are difficult to purify *via* chromatography.

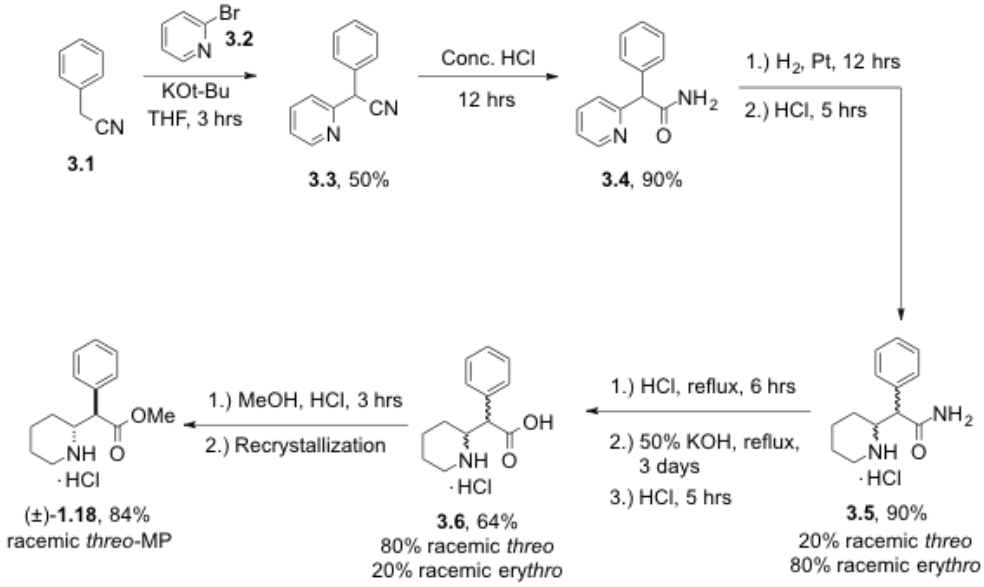

Scheme 3.1. Synthesis of racemic *threo*-methylphenidate (MP) according to Deutsch *et al*., 1996.

Another synthesis of racemic *threo*-methylphenidate ((±)-**1.18**) was reported by Axten *et al*. in 1998 (Axten *et al*., 1998) and later improved by Gutman *et al*. in 2004 (Gutman *et al*., 2004). When compared to the synthesis developed by Deustch *et al*. in 1996 (Scheme 3.1), this particular synthesis method (Scheme 3.2) is relatively short and efficient (5 steps, 56% overall yield). This synthesis begins with condensation of α-keto ester **3.7** with piperidine to give α-keto amide **3.8** in high yield (91%). Under acidic conditions, ketone **3.8** was then treated with tosylhydrazine to provide tosylhydrazone **3.9** in moderate yield (85%). Subsequently, with the aid of phase transfer catalyst Aliquat 336® under aqueous basic conditions, hydrazone **3.9** underwent thermal cyclization to provide lactam **3.10** as a diastereomeric mixture. In turn, recrystallization in ether gave pure racemic *threo*-β-lactam (±)-**3.10** as the major product in 68% yield. Finally, lactam methanolysis yielded racemic *threo*-methylphenidate ((±)-**1.18**).

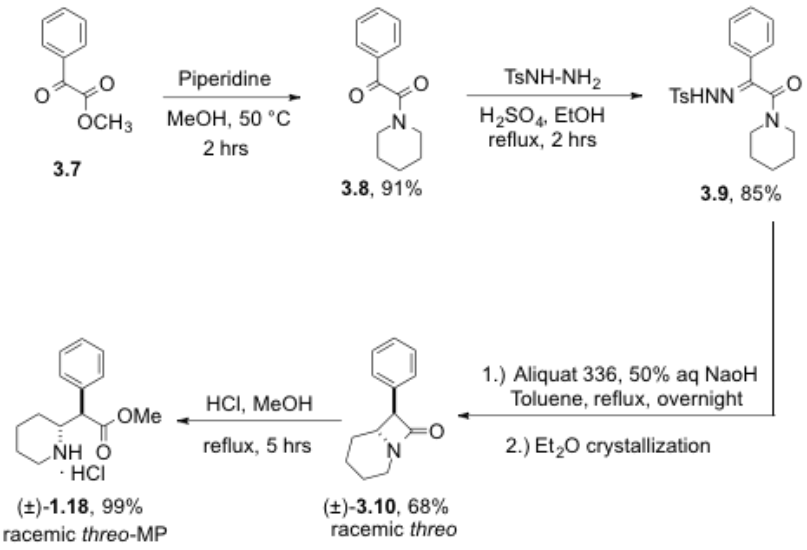

Scheme 3.2. Synthesis of racemic *threo*-methylphenidate (MP) according to Gutman *et al*., 2004.

Concurrently, a synthesis of racemic *threo*-methylphenidate ((±)-**1.18**) (7 steps, 35% overall yield) was reported by Dias and De Piloto Fernandes (Dias and De Piloto Fernandes, 2000). This synthesis utilizes known α-ethoxy carbamate **3.14** (Nagasaka *et al*., 1986) and silyl ketene acetal **3.16** (Tanaka and Fuji, 1992) (Scheme 3.3). The synthesis begins with protection of lactam **3.11** as its carbamate **3.13**, which is then reduced with $NaBH_4$ followed by treatment with EtOH in HCl to give α-ethoxy carbamate **3.14** in 63% overall yield (Scheme 3.3-A, Nagasaka *et al*., 1986). Silyl ketene acetal **3.16** was synthesized in 90% yield by treating ester **3.15** with LDA followed by quenching with TMSCl (Scheme 3.3-B, Tanaka and Fuji, 1992). Subsequent, treatment of α-ethoxy carbamate **3.14** with silyl ketene acetal **3.16** in the presence of TESOTf then provided a distereomeric mixture of *N*-protected racemic *threo*-methylphenidate derivatives (**3.17**) in high yield (90%). Carbamate **3.17** was then subjected to hydrogenolysis to provide a mixture of racemic *threo*- and *erythro*-methylphenidate free bases, which were separable by column chromatography. Finally, treatment of racemic

threo-methylphenidate free base with methanolic HCl provided the hydrochloride salt (±)-**1.18** in moderate yield (69%) (Scheme 3.3-A, Dias and De Piloto Fernandes, 2000).

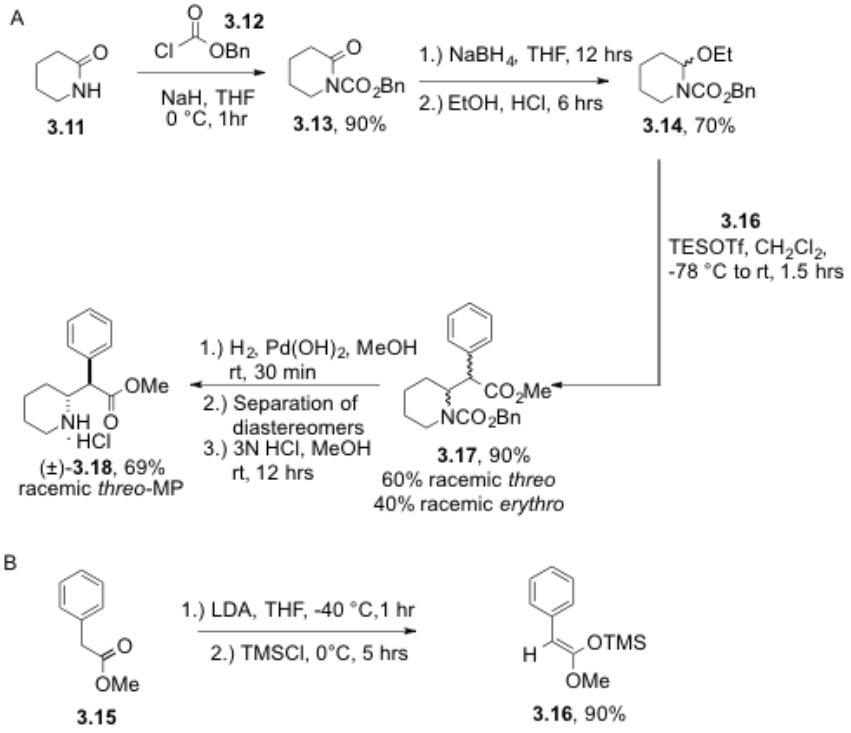

Scheme 3.3. Synthesis of (A) racemic *threo*-methylphenidate (MP) according to Dias and De Piloto Ferandes, 2000 and (B) silyl ketene acetal **3.16** precursor according to Tanaka and Fuji, 1992.

In 2001, Deutsch and colleagues reported a new synthetic method for racemic *threo*-methylphenidate ((±)-**1.18**) (8 steps, 7% overall yield) based on the Blaise reaction (Scheme 3.4, Deutsch *et al*., 2001). In particular, this methodology was used to synthesize methylphenidate analogs in which the amine ring size and aromatic ring were varied in order to develop SAR with respect to the dopamine transporter. The synthesis began with treatment of 4-chloro-1-butanol (**3.18**) with KCN in water-ethanol, to provide 4-cyano-1-butanol, whose alcohol was converted to the corresponding mesylate **3.19** in low yield (25%). A Blaise reaction of mesylate **3.19** with methyl 2-bromo-2-phenylacetate (**3.20**) in the presence of zinc provided imine **3.21**, which subsequently rearranged to form Z-enamine **3.22** in moderate yield (63%). Enamine **3.22** was then

reduced with sodium cyanoborohydride at pH 6, wherein piperidine cyclization occurred spontaneously under basic work-up conditions to give a diastereomeric mixture of racemic *threo*- and *erythro*-methylphenidates **3.23** in moderate yield (78%). Finally, 50% KOH epimerization of the diastereomeric mixture of racemic *threo*- and *erythro*-methylphenidates (**3.23**), followed by salt formation using methanolic HCl and recrystallization, provided racemic *threo*-methylphenidate ((±)-**1.18**) in 55% yield (Scheme 3.4).

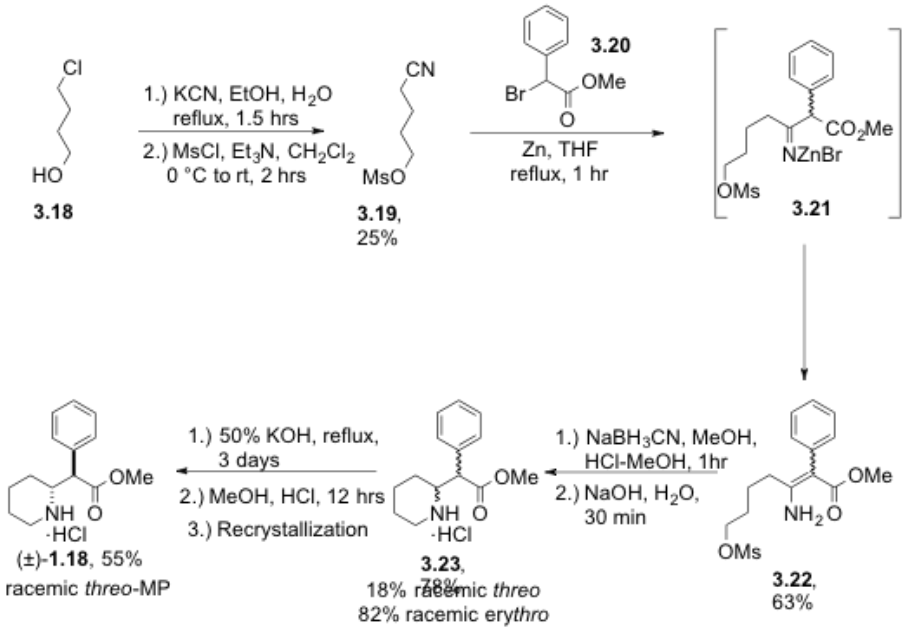

Scheme 3.4. Synthesis of racemic *threo*-methylphenidate (MP) according to Deutsch *et al*., 2001.

3.2. Known Synthesis of Racemic *threo*-4-Iodo-Methylphenidate as a Lead Compound for DAT Photoprobe Design

Racemic *threo*-methyl-2-(4-iodophenyl)-2-(piperidin-2-yl)acetate (4-iodo-methylphenidate, (±)-**3.29**) represents a lead compound for DAT photoprobe design because it displays 6-fold higher DAT binding affinity when compared to methylphenidate ((±)-**1.18**) (Deutsch *et al*., 1996). In particular, Pan and coworkers (Pan

et al., 1996) reported a synthesis of racemic *threo*-4-iodo-methylphenidate ((±)-**3.29**) from racemic *threo*-methylphenidate ((±)-**1.18**) (Scheme 3.5). The synthesis began with *N*-benzoylation of methylphenidate to give amide (±)-**3.24** in 96% yield. Amide (±)-**3.24** was then subjected to electrophilic aromatic nitration to provide *p*-nitro methylphenidate derivative (±)-**3.25** in 85% yield. Conversion of the nitro group to aniline (±)-**3.26** was then accomplished using iron powder under acidic conditions, followed by diazotization and displacement with potassium iodide to provide *p*-iodo methylphenidate derivative (±)-**3.27** in 51% overall yield. Subsequently, strong acidic conditions were required to hydrolyse the amide and ester in (±)-**3.27** to give racemic *threo*-4-iodo-ritinilic acid ((±)-**3.28**) in 40% yield, which was esterified using methanolic-HCl to provide racemic *threo*-4-iodo-methylphenidate ((±)-**3.29**) in quantitative yield (Scheme 3.5).

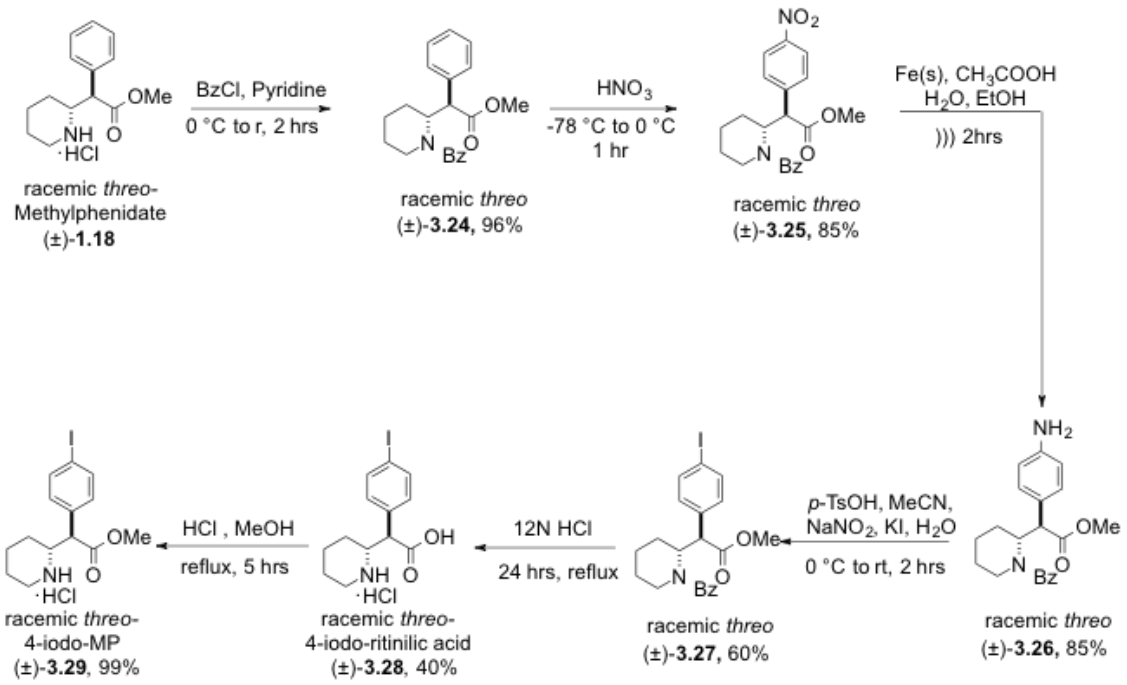

Scheme 3.5. Synthesis of racemic *threo*-4-iodo-methylphenidate (MP) according to Pan *et al*., 1996.

3.3. Known Synthesis of Racemic *threo*-3,4-Dichloro-Methylphenidate as a Lead Compound for DAT Photoprobe Design

Racemic *threo*-methyl-2-(3,4-dichlorophenyl)-2-(piperidin-2-yl)acetate (3,4-dichloro-methylphenidate, (±)-**3.35**) represents a lead compound for DAT photoprobe design because it displays 15-fold higher DAT binding affinity when compared to methylphenidate ((±)-**1.18**) (Deutsch *et al*., 1996). As previously mentioned, Deutsch and colleagues synthesized aromatic ring-substituted analogs of methylphenidate using the methodology in Scheme 3.1 (Deutsch *et al*., 1996). In particular, their synthesis of racemic *threo*-3,4-dichloro-methylphenidate ((±)-**3.35**) began with treatment of 3,4-dichlorophenylacetonitrile (**3.30**) with 2-bromopyridine (**3.2**) under basic conditions to provide nitrile **3.31**, which was then subjected to acidic hydrolysis to provide amide **3.32** in 40% overall yield. Hydrogenation of pyridine **3.32** and subsequent treatment with HCl provided a mixture of diastereomeric piperidine salts (**3.33**) in good yield (80%). Acidic hydrolysis of amide **3.33**, followed by epimerization under basic conditions and subsequent salt formation, provided a diastereomeric mixture of racemic *threo*-ritanilic acid derivatives (**3.34**) in moderate yield (54%). Finally, esterification of **3.34** with methanolic HCl and subsequent recrystallization provided racemic *threo*-3,4-dichloro-methylphenidate ((±)-**3.35**) in good yield (80%) (Scheme 3.6).

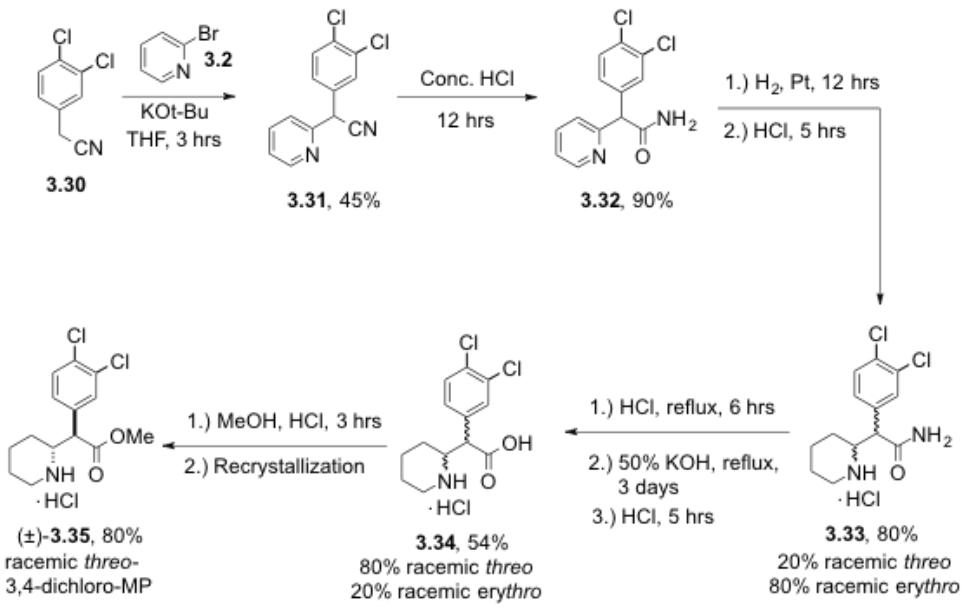

Scheme 3.6. Synthesis of racemic *threo*-3,4-dichloro-methylphenidate (MP) according to Deutsch *et al*., 1996.

3.4. References

- Axten, J.M., Krim, L., Kung, H.F., and Winkler, J.D. A stereoselective synthesis of *dl-threo*-methylphenidate: preparation and biological evaluation of novel analogues. *J. Org. Chem.* **1998**, *63*, 9628-9629.

- Deutsch, H.M., Shi, Q., Gruszecka-Kowalik, E., and Schweri, M.M. Synthesis and pharmacology of potential cocaine antagonists. 2. Structure−activity relationship studies of aromatic ring-substituted methylphenidate analogs. *J. Med. Chem.* **1996**, *39*, 1201-1209.

- Deutsch, H.M., Ye, X., Shi, Q., Liu, Z., and Schweri, M.M. Synthesis and pharmacology of site specific cocaine abuse treatment agents: a new synthetic methodology for methylphenidate analogs based on the Blaise reaction. *Eur. J. Med. Chem.* **2001**, *36*, 303-311.

- Dias, L.C. and De Piloto Fernandes, A.M.A. Short synthesis of methylphenidate and its *p*-methoxy derivative. *Synth. Commun*. **2000**, *30*, 1311-1318.

- Gutman, A., Zaltsman, I., Shalimov, A., Sotrihin, M., Nisnevich, G., Yudovich, L., and Fedotev, I. Process for the preparation of dexmethylphenidate hydrochloride. Patent US 20040180928 A1, **2004**.

- Nagasaka, T., Tamano, H., and Hamaguchi, F. Reduction of *N*-alkoxycarbonyl lactams with sodium borohydride-ethanol-H+: a facile synthesis of α-ethoxyurethanes *Heterocycles* **1986**, *24*, 1231-1232.

- Pan, D., Gatley, S.J., Chen, R., and Ding, Y.S. Iodine-123 labeled derivatives of methylphenidate: potential SPECT radiopharmaceuticals for brain dopamine transporters. *J. Labelled Compds. Radiopharm.* **1996**, *38*, 523-532.

- Panizzon, L. Preparation of pyridyl- and piperidylarylacetonitriles and some derivatives (Part I). *Helv. Chim. Acta*. **1944**, *27*, 1748-1756.

- Tanaka, F.J. and Fuji, K. Stereochemistry of the enolate from methyl phenylacetate. *Tetrahedron Lett.* **1992**, *33*, 7885-7888.

CHAPTER FOUR

4. Statement of Research Problems

4.1. Current Knowledge Gaps

4.1.1. Dopamine Transporter Structure-Function Knowledge Gap

Although LeuT-based DAT homology models (*e.g.*, Koldso, Christiansen *et al.*, 2013; Stockner *et al.*, 2013; Seddik *et al.*, 2013; Gedeon *et al.*, 2010; Huang *et al.*, 2009; Indarte *et al.*, 2008) have provided significant insights into the three-dimensional structure of the dopamine transporter, details regarding the transport inhibition mechanism, conformational states, and ligand-binding sites associated with this protein remain poorly understood. In particular, the molecular mechanisms by which the DAT discriminates substrates (*e.g.*, dopamine and amphetamines) *versus* inhibitors (*e.g.*, cocaine, cathinones, methylphenidate, bupropion, benztropine, and GBR-12909) and highly abused compounds (*e.g.*, cocaine, amphetamines, and cathinones) *versus* therapeutic compounds (*e.g.*, methylphenidate, bupropion, and benztropine) at the molecular level remain unknown. Additionally, it is not clear how structurally distinct dopamine transporter inhibitor classes (*e.g.*, tropane *versus* non-tropane DAT inhibitors) specifically interact with the dopamine transporter leading to specific behavioral and/or phenomenological effects (*e.g.*, addictive *versus* non-addictive behavioral responses).

4.1.2. Serotonin Transporter Structure-Function Knowledge Gap

Selective serotonin reuptake inhibitors (SSRIs) represent first-line antidepressants in the treatment of anxiety disorders and major depressive disorder (Fuller, 1995).

However, despite the well-documented clinical success of SSRIs, the specific drug-protein interactions that dictate the affinity, potency, and selectivity of these compounds remain poorly characterized.

Similar to the DAT, X-ray crystal structures of the bacterial homolog leucine transporter (LeuT) (*e.g.*, Yamashita *et al.*, 2005) have provided insight into the tertiary structure of hSERT *via* homology modeling (*e.g.*, Ravna *et al.*, 2006; Jorgensen *et al.*, 2007; Zhou *et al.*, 2013; Koldso, Autzen *et al.*, 2013; Koldso, Christiansen *et al.*, 2013; Gabrielsen *et al.*, 2012). Based on these studies, the serotonin transporter is proposed to contain a high-affinity binding site termed "S1" (also known as the primary substrate-binding site) and a low-affinity allosteric site termed "S2" (also known as the extracellular vestibule-located site). In particular, homology molecular modeling (*e.g.*, Jorgensen *et al.*, 2007), site-directed mutagenesis (*e.g.*, Barker *et al.*, 1998; Andersen *et al.*, 2010), and small molecule structure-activity relationship (SAR) studies (*e.g.*, Zhang *et al.*, 2010) have suggested that TCAs and SSRIs bind to the S1 site with high affinity in a competitive manner (Talvenheimo *et al.*, 1979; Henry *et al.*, 2006; Andersen *et al.*, 2009 and 2011; Sinning *et al.*, 2010; Tavoulari *et al.*, 2009; Koldso *et al.*, 2010).

Most recently, LeuT has been engineered to display monoamine/biogenic amine transporter-like pharmacology by mutating key residues near the primary S1 binding pocket (Wang *et al.*, 2013). This mutated LeuT, subsequently named LeuBAT, has also been co-crystallized with sertraline, paroxetine, fluoxetine, and fluvoxamine as SSRIs, as well as the TCA clomipramine, indicating all of these compounds bind in the primary S1 binding pocket. However, and in sharp contrast to LeuBAT, other crystallographic studies with LeuT indicate the TCA desipramine (Zhou *et al.*, 2007), and the SSRIs

sertraline and fluoxetine (Zhou *et al.*, 2009), bind in the homologous S2 site as non-competitive inhibitors (Singh *et al.*, 2007). In addition, multiple studies of SERT indicate that the S2 binding site acts as a low-affinity allosteric site, wherein ligands binding to S2 can inhibit the dissociation of S1-bound SSRIs, thus enhancing their efficacy (Plenge *et al.*, 1991, 1997, 2007, and 2012; Chen, Larsen, Neubauer *et al.*, 2005; Chen, Larsen, Sanchez *et al.*, 2005; Zhong *et al.*, 2009 and 2012; Neubauer *et al.*, 2006). Furthermore, characterization of the S2 binding site in SERT using computational modeling, as well as experimental support by site-directed mutagenesis, Zn^{+2}-site engineering, and cysteine-reactivity assays, indicates that binding to the allosteric site impedes dissociation of S1-bound drug, most likely by steric blockade of the exit pathway (Plenge *et al.*, 2012). In short, given the roles of the S1 and S2 binding sites within SERT are not completely understood, there is a significant need for tool compounds and experimental methods that can directly interrogate the microenvironments of hSERT binding sites.

4.2. Long-Term Goal of This Research

The long-term goal of this research is to understand how clinically significant monoamine transporter inhibitors (*e.g.*, methylphenidate as a hDAT inhibitor and citalopram as a SSRI) interact with their major drug targets (*i.e.*, hDAT for methylphenidate and hSERT for citalopram) at the molecular level, thus ultimately facilitating correlation of primary ligand-protein molecular interactions with CNS behavioral effects. Additionally, acquisition of detailed 3D protein structure-function information is expected to validate and further refine MAT molecular models currently used in computer-aided drug discovery efforts (*i.e.*, virtual / *in silico* screening (*e.g.*, Indarte *et al.*, 2010; Nolan *et al.*, 2011 and 2014) and structure-based drug design)

targeting disease states associated with MAT proteins (*e.g.*, depression, anxiety, post-traumatic stress disorder, obsessive-compulsive disorder, drug abuse, and addiction).

4.3. Overall Objective of This Research Dissertation

The overall objective of this research dissertation was to rationally design, chemically synthesize, and biochemically utilize irreversible chemical probes based on methylphenidate as a hDAT inhibitor, and citalopram as a SSRI, in order to map their corresponding binding sites and poses within their major drug targets (*i.e.*, hDAT for methylphenidate and hSERT for citalopram).

4.4. Central Hypothesis of This Research Dissertation

The central hypothesis of this research dissertation was that methylphenidate as a hDAT inhibitor, and citalopram as a SSRI, could be rationally derivatized, without significant loss in pharmacological activity, to contain: 1.) a photoreactive group (PRG; *e.g.*, an aryl azide, benzophenone, etc.) capable of forming a covalent bond to a target protein (*i.e.*, hDAT or hSERT), and 2.) a tag entity (*e.g.*, ^{125}I or a bioorthogonal chemistry handle), thus allowing a "Binding Ensemble Profiling with (f)Photoaffinity Labeling (BEProFL)" experimental approach (He *et al.*, 2009) to map the binding sites and poses of these clinically significant compounds within their major target protein. In short, the premise of the BEProFL approach begins with the employment of appropriate photoprobes (*i.e.*, those compounds whose protein binding affinity is no lower than 10-fold *versus* an appropriate lead parent compound) in traditional photoaffinity labeling experiments to generate covalent ligand-target complexes (Scheme 4.1). This is followed by chemical proteomic experiments, whose results are coupled with computational

molecular modeling of non-covalent or covalent ligand-target complexes in order to directly map the ligand-binding sites and poses of lead compounds within their target proteins. As proof of concept, the BEProFL approach has been successfully used to understand the binding modes of histone deacetylase (HDAC) inhibitors as epigenetic modulators (Abdelkarim *et al.*, 2013; Vaidya *et al.*, 2012; Neelarapu *et al.*, 2011; He *et al.*, 2009) and to probe the microenvironment of fatty acid amide hydrolase (FAAH) (Saario *et al*., 2012), a drug target implicated in the development of pain therapeutics.

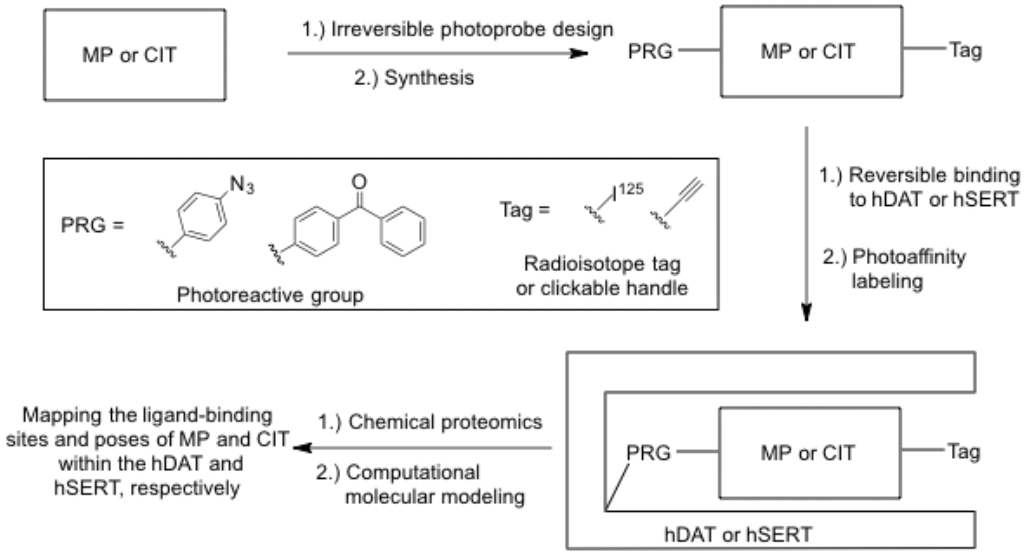

Scheme 4.1. Schematic representation of the BEProFL experimental approach for mapping the ligand-binding sites and poses of methylphenidate (MP) and citalopram (CIT) within hDAT and hSERT, respectively.

4.5. Rationale of This Research Dissertation

The rationale associated with this research dissertation is that, once it is known how clinically relevant drugs targeting the dopamine transporter or serotonin transporter specifically interact with these proteins at the molecular level, this detailed 3D structure-function information can then be rationally used to validate and further refine 3D MAT molecular models currently used in computer-aided drug discovery efforts (*i.e.*,

improved, confident virtual / *in silico* screening and entrance into rational structure-based drug design). Such efforts in turn are expected to generate improved drug candidates for a host of disease states traditionally associated with monoamine transporter proteins (*e.g.*, depression, anxiety, post-traumatic stress disorder, obsessive-compulsive disorder, drug abuse, and addiction).

4.6. Rational Design of Methylphenidate-Based Photoprobes Suitable for Dopamine Transporter Structure-Function Studies

Methylphenidate ((±)-**1.18**, MP, Ritalin, Concerta; Scheme 4.2) is a well known, U.S. Food and Drug Administration (FDA) approved drug for the treatment of attention-deficit hyperactivity disorder (ADHD), narcolepsy, and postural orthostatic tachycardia syndrome (Challman and Lipsky, 2000). Methylphenidate acts as a mild CNS stimulant, principally by functioning as an inhibitor of dopamine and norepinephrine transporter proteins, thus blocking the reuptake of dopamine and norepinephrine neurotransmitters into the presynaptic neuron.

With respect to the dopamine transporter, methylphenidate displays 2-fold higher binding affinity upon comparison to cocaine (*e.g.*, see Pan *et al.*, 1994 as one source of representative DAT pharmacology data for methylphenidate). Additionally, methylphenidate is structurally similar to cocaine in that both compounds contain a basic nitrogen (*i.e.*, a 3˚ amine in cocaine *versus* a 2˚ amine in methylphenidate), a methyl ester, and an aromatic ring. With these structural similarities in mind, perhaps it is not surprising that the reinforcing effects of methylphenidate in animal models are comparatively similar to that of cocaine. However, methylphenidate has been shown to

possess decreased reinforcing effects in humans and facilitates lower cocaine cravings (Yano and Steiner, 2007). Additionally and in sharp contrast to cocaine, methylphenidate does not function as a sodium channel blocker and does not produce harmful effects on nerve conductance when taken in excess (Schwartz *et al.*, 2010). Furthermore, methylphenidate is generally considered to be relatively safe drug that has been used for decades. As a result of the established success of methylphenidate as a safe and effective clinical entity, coupled with its decreased abuse potential, methylphenidate analogs are currently being pursued as potential candidates for the treatment of cocaine abuse (*e.g.*, Misra *et al.*, 2010).

However, it should be noted that despite the long-term significance of methylphenidate in the clinic, the specific molecular contacts this compound makes with the dopamine transporter, which are directly responsible for the affinity, potency, selectivity, and behavioral effects associated with this compound, remain unknown. As a result, several methylphenidate-based dopamine transporter inhibitor photoprobes were rationally developed during the course of this dissertation for potential use in dopamine transporter structure-function studies.

4.6.1. A Call for Racemic *threo*-3-Iodo-Methylphenidate ((±)-4.29) as a Lead Compound and Rational Design of Racemic *threo*-*N*-Azidobenzyl-4-Iodo/3-Iodo-Methylphenidate Compounds (±)-4.17 - (±)-4.22 as Potential Dopamine Transporter Photoaffinity Ligands

At the beginning of this research dissertation, it was observed that an overwhelming number of dopamine transporter inhibitor photoaffinity probes (*e.g.*, Sallee

et al., 1989; Grigoriadis *et al.*, 1989; Carroll *et al.*, 1992; Agoston *et al.*, 1997; Dutta *et al.*, 2001; Zou *et al.*, 2001 and 2003; Cao *et al.*, 2004; Lever *et al.*, 2005; Newman *et al.*, 2006; Chen *et al.*, 2007; Lapinsky *et al.*, 2009; Lapinsky, Aggarwal *et al.*, 2012) published before the development of methylphenidate-based photoprobes (Lapinsky *et al.*, 2011; Lapinsky, Yarravarapu *et al.*, 2012) contain a common 3-iodo-4-azido aromatic ring-substituted structural motif (Figure 4.1). In particular, the 4-azido functional group within this common photoaffinity labeling structural motif represents a photoreactive group for facilitating covalent bond formation of the DAT photoprobe to the DAT. Additionally, the 3-iodine atom represents a position for a future radioisotope tag (*i.e.*, ^{125}I) to detect probe-labeled DAT after DAT photoaffinity labeling, and also serves as an electron-withdrawing group proposed to stabilize the singlet nitrene of an aryl azide upon photodecomposition (Soundararajan and Platz, 1990). In particular, electronic stabilization of highly reactive nitrenes generated upon aryl azide photoactivation is desired and has been shown to prevent undesirable rearrangement of nitrenes to azepines, which can subsequently result in non-specific protein labeling upon nucleophilic attack (see Section 2.2.1.1 for previous discussion). However, DAT photoprobes containing this common 3-iodo-4-azido aromatic ring-substituted structural motif have frequently resulted in low DAT labeling efficiency (*e.g.*, <1%) during photoaffinity labeling (Vaughan *et al.*, 2005).

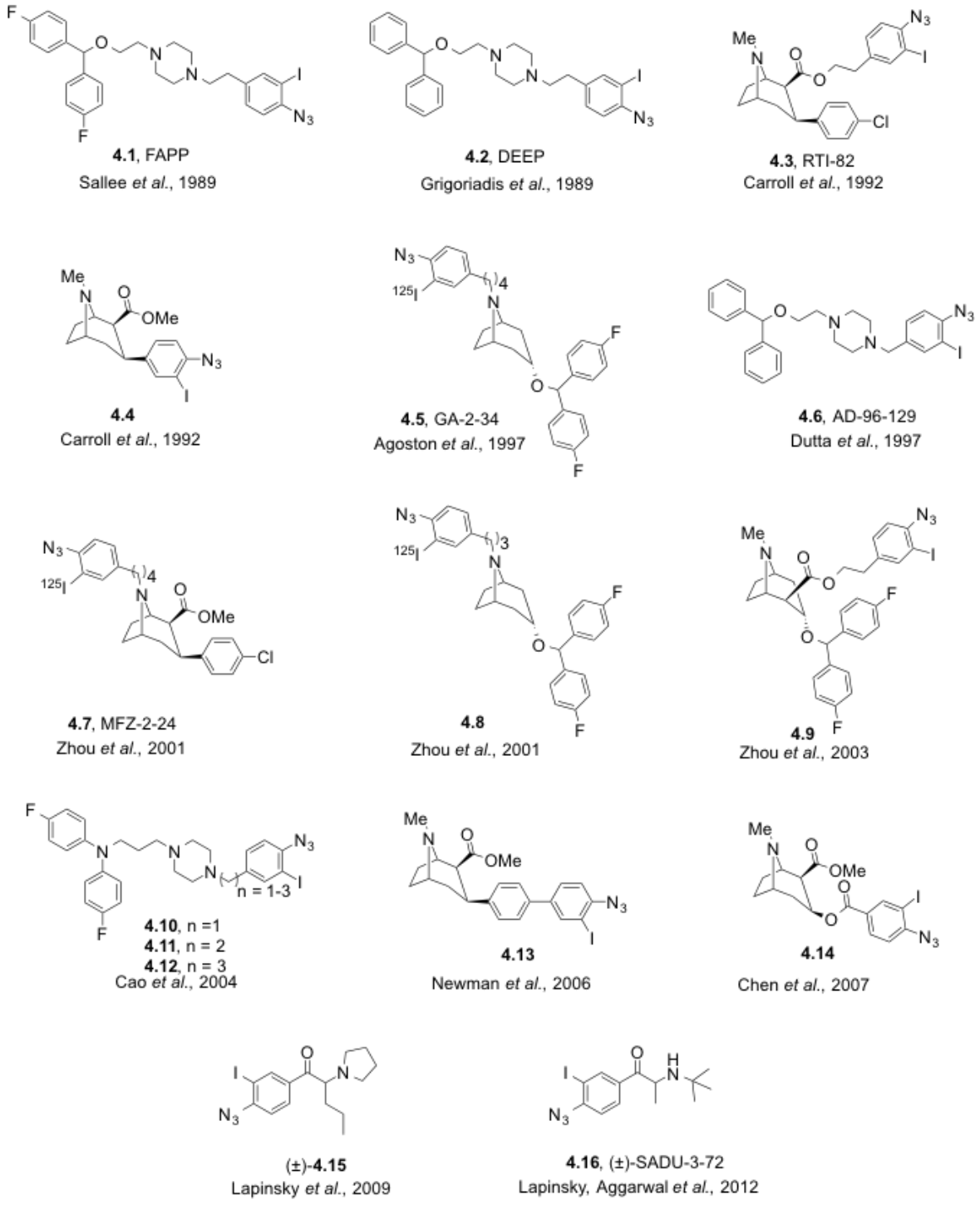

Figure 4.1. DAT photoaffinity probes containing a 3-iodo-4-azido aromatic ring-substituted structural motif that were published before the development of methylphenidate-based photoprobes.

In particular, it has been hypothesized that the low hDAT labeling efficiency of photoprobes containing the 3-iodo-4-azido aromatic ring-substituted motif results from the photoreactive aryl azide being juxtapositioned adjacent to a sterically bulky iodine atom (Vaughan *et al.*, 2005). In order to test this hypothesis and expand the arsenal of non-tropane DAT photoprobes known at the time (Lapinsky *et al.*, 2009; Lapinsky, Aggarwal *et al.*, 2012), a novel, alternative strategy was subsequently pursued wherein the photoreactive aryl azide functional group and the bulky ^{125}I radiotracer tag were placed on different parts of a methylphenidate scaffold (Lapinsky *et al.*, 2011) (Figure 4.2).

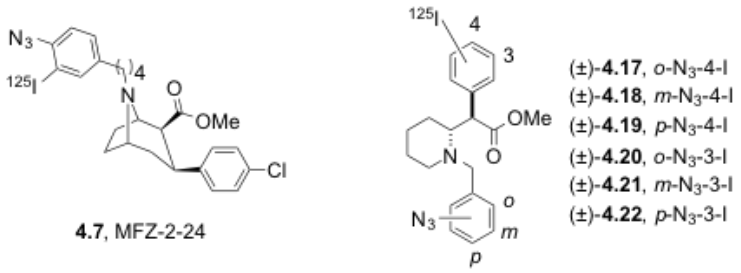

Figure 4.2. Structural comparison of a tropane-based hDAT photoprobe (**4.7**) containing the traditional 3-iodo-4-azido aromatic ring-substituted structural motif *versus* a series of non-tropane methylphenidate-based probes featuring the photoreactive aryl azide and radioisotope ^{125}I tag on separate parts of the chemical scaffold.

The rational design of target methylphenidate-based DAT photoprobes (±)-**4.17** - (±)-**4.22** (Scheme 4.2; Lapinsky *et al.*, 2011) stemmed from several lead methylphenidate analogs (Scheme 4.2). In particular, *threo*-methyl 2-(4-iodophenyl)-2-(piperidin-2-yl)acetate (4-iodomethylphenidate, **(±)-3.29**; hDAT IC_{50} = 14.0 ± 0.1 nM (*i.e.*, inhibition of [^{3}H]-WIN-35,428, a radioactive cocaine analog, binding to hDAT)) was initially chosen as a lead compound for rational DAT photoprobe design, principally because this analog displayed ~6-fold higher DAT binding affinity when compared to (±)-methylphenidate ((±)-**1.18**; hDAT IC_{50} = 83.0 ± 7.9 nM; pharmacology data from

Deutsch *et al*., 1996), thus suggesting the 4-position of methylphenidate's aromatic ring as a logical place to anchor a bulky iodine atom as a future radiotracer tag (*i.e.*, ^{125}I) within rationally designed methylphenidate-based DAT photoaffinity probes. Additionally, *N*-benzyl methylphenidate analogs (±)-**4.30 -** (±)-**4.34** (Misra *et al*., 2010) were considered lead compounds for rational photoprobe design, given these analogs displayed either improved or retained DAT binding affinity when compared to methylphenidate ((±)-**1.18**). Furthermore, improved DAT binding affinity was observed for methylphenidate analogs bearing halogens at the 3-position of the aromatic ring ((±)-**4.26** - (±)-**4.28**) when compared to the 4-position ((±)-**4.23** - (±)-**4.25**) (Deutsch *et al*., 1996); however, *threo*-methyl 2-(3-iodophenyl)-2-(piperidin-2-yl)acetate (3-iodomethylphenidate, (±)-**4.29**) was unknown at the time. This subsequently prompted the Lapinsky group to rationally pursue 3-iodomethylphenidate ((±)-**4.29**) as an additional lead compound for potential DAT photoprobe design, principally under the hope that the 3-position of methylphenidate's aromatic ring could represent an alternative location to potentially anchor a bulky iodine atom as a future ^{125}I radiotracer tag.

As part of this research dissertation, racemic *threo*-3-iodo-methylphenidate ((±)-**4.29**) was synthesized as described in Section 5.1.1 and sent to the Surratt laboratory for pharmacological determination of this compound's hDAT binding affinity in N2A neuroblastoma cells. As expected, an ~6-fold improvement in hDAT binding affinity was observed upon substituting the 3-position of methylphenidate's aromatic ring with an iodine atom (hDAT K_i = 25 ± 1 nM (once again, inhibition of [^{3}H]-WIN-35,428 (a radioactive cocaine analog) binding to hDAT) for racemic *threo*-methylphenidate ((±)-**1.18**) *versus* hDAT K_i = 4.5 ± 1 nM for racemic *threo*-3-iodo-methylphenidate ((±)-**4.29**);

Lapinsky *et al*., 2011). Given that this DAT pharmacological result was consistent with the previous observation that halogens are well-tolerated at the 3-position of methylphenidate's aromatic ring (Deutsch *et al*., 1996), it further suggested another rational anchoring position for an ^{125}I atom as a future radiotracer tag within methylphenidate-based DAT photoaffinity probes.

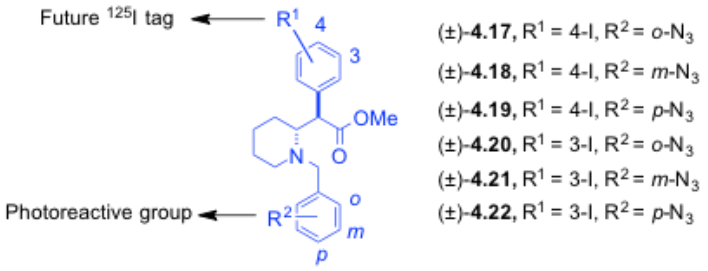

racemic *threo*
N-Azidobenzyl-4-iodo/3-iodo-MP photoprobes

Molecular hybridization

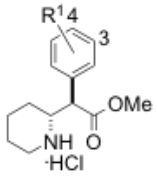

racemic *threo*
MP analogs

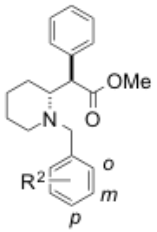

racemic *threo*
N-Bn-MP analogs

IC_{50} = inhibition of [^{3}H]-WIN-35,428 binding to hDAT

R^1	IC_{50} (nM)	R^1	IC_{50} (nM)	R^2	IC_{50} (nM)
(±)-**1.18**, -H (MP)	83.0 ± 7.9			(±)-**4.30**, -H	52.9 ± 2.3
(±)-**4.23**, 4-Br	6.90 ± 0.10	(±)-**4.26**, 3-Br	4.18 ± 0.17	(±)-**4.31**, *p*-Cl	31.2 ± 5.7
(±)-**4.24**, 4-Cl	20.6 ± 3.4	(±)-**4.27**, 3-Cl	5.10 ± 1.6	(±)-**4.32**, *p*-OMe	79.1 ± 1.4
(±)-**4.25**, 4-F	35.0 ± 3.0	(±)-**4.28**, 3-F	40.5 ± 4.5	(±)-**4.33**, *m*-Cl	106 ± 24
(±)-**3.29**, 4-I	14.0 ± 0.1	(±)-**4.29**, 3-I	???	(±)-**4.34**, *p*-NO_2	113 ± 3.0

Scheme 4.2. Rational design of a series of *N*-azidobenzyl-4-iodo/3-iodo-methylphenidate compounds ((±)-**4.17** - (±)-**4.22**) as potential dopamine transporter photoaffinity ligands.

Given these established structure–activity relationships for methylphenidate, a series of photoaffinity ligands ((±)-**4.17** - (±)-**4.22**) was designed *via* molecular hybridization of iodomethylphenidates ((±)-**3.29**, (±)-**4.29**, Scheme 4.1) with *N*-

benzylmethylphenidates ((±)-**4.30** to (±)-**4.34**, Scheme 4.2). These target probes ((±)-**4.17** to (±)-**4.22**, Scheme 4.2) feature systematic placement of a photoreactive azide on the aromatic ring of the *N*-benzyl group. Racemic *threo*-3-iodo-methylphenidate ((±)-**4.29**, Scheme 4.2) was synthesized in bulk and submitted for the synthesis of target probes ((±)-**4.20**, (±)-**4.21**, Scheme 4.2). The final target probe ((±)-**4.22**, Scheme 4.1) was synthesized as described in Section 5.1.2 and was sent for pharmacological determination of hDAT binding affinity in N2A neuroblastoma cells. Thus, this dissertation partially contributed towards a series of *threo*-*N*-azidobenzyl-3-iodo-methylphenidate photoaffinity ligands.

4.6.2. Rational Design of Racemic *threo*-4-Azido-3-Iodo-Methylphenidate as a Potential Photoaffinity Ligand for Dopamine Transporter Structure-Function Studies

The traditional design of DAT photoprobes features incorporation of a 3-I, 4-N_3-phenyl substituent attached to an inhibitor scaffold by means of a variable-length linker. For example, [^{125}I]-MFZ-2−24 (**4.7**, Figure 4.3) has been prepared and found to covalently attach to transmembrane domain 1 (TM1) of the DAT (Parnas *et al*., 2008), while similar results have also been achieved with benztropine probe [^{125}I]-GA-2−34 (**4.5**, Figure 4.3) (Parnas *et al*., 2003). However, phenyltropane-based probe [^{125}I]-RTI-82 (**4.3**, Figure 4.3) covalently ligates to TM6 of the DAT (Vaughan *et al*., 2007). Multiple studies suggest not all tropane-based inhibitors bind to the same conformation or binding site within the DAT, and that covalent conjugation to the DAT protein can occur in different TM regions depending on the position of the photoreactive group within the probe (Parnas *et al*., 2008; Vaughan *et al*., 2005 and 2007). In this regard, photoprobes

4.3, **4.5**, and **4.7** may be viewed as potentially possessing an inherent disadvantage when trying to definitively map the amino acids of the inhibitor-binding pocket, or optimally model the photoprobe−DAT complex, *via* the BEProFL approach (He *et al*., 2009). That is, the covalent point of probe attachment to the DAT, which is dictated by the location of the photoreactive azide group, is somewhat removed from the inhibitor scaffold by means of a conformationally flexible, variable-length methylene linker. In particular, molecular modeling studies of photoprobe **4.7** (Figure 4.3) indicate distances of 10.5 and 15.5 Å between the azide and the pharmacophore tropane nitrogen, and 3β-phenyl ring, respectively. Given that the azide is not directly appended to the tropane pharmacophore for probes **4.3**, **4.5**, and **4.7** (Figure 4.3), adduction may occur at a residue near, but not at, a direct inhibitor contact point, thus representing a significant limitation when trying to delineate the discrete molecular interactions between the probe and the DAT protein. Toward potentially addressing this point, 3-(4′-azido-3′-iodo-phenyl)-8-methyl-8-aza-bicyclo[3.2.1]octane-2-carboxylic acid methyl ester (**4.4**, Figure 4.3) has been synthesized and displays high affinity, wash-resistant binding to the DAT (Carroll *et al*., 1992), but fails to label the DAT in subsequent immunoprecipitation and proteolysis experiments (Vaughan *et al*., unpublished observations). These results, coupled with those from previous DAT photolabeling experiments, have collectively indicated that azide must be some distance away from the tropane pharmacophore to covalently attach to the DAT protein near, but not within, the ligand-binding domain (Newman *et al*., 2006).

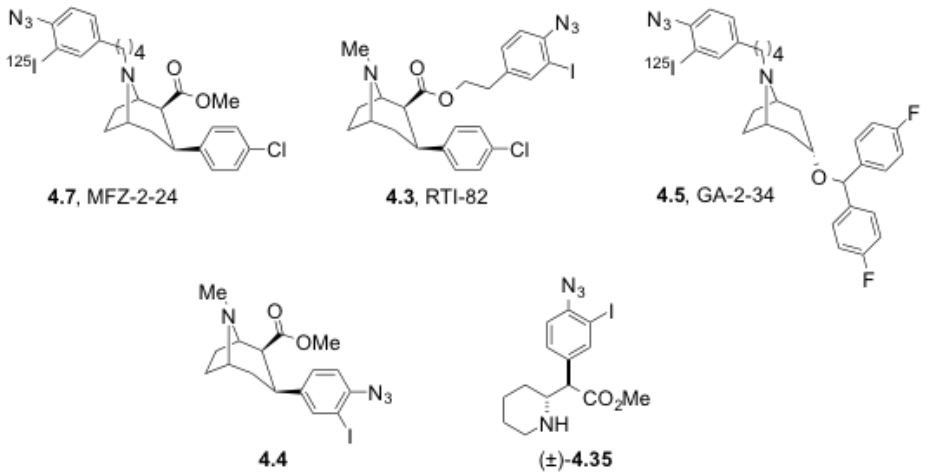

Figure 4.3. Structural comparison of a tropane-based hDAT photoprobes *versus* a compact non-tropane methylphenidate-based probe containing the traditional 3-iodo-4-azido aromatic ring-substituted structural motif.

However, it was later successfully shown that direct substitution of the photoreactive azide group on the aromatic ring of the inhibitor scaffold is tolerated for non-tropane-based DAT photoaffinity labeling agents (Lapinsky *et al*., 2009). The compact pyrovelorone probe (±)-**4.15** (Figure 4.1) was shown to successfully label the dopamine transporter in contrast to tropane-based irreversible compounds where in the azide has to be placed at a distance (usually *via* a linker) from the inhibitor pharmacophore in order to achieve successful protein labeling (Newman *et al*., 2006). Given these previous observations, this research dissertation features the design and synthesis of a compact photoprobe based on MP as a non-tropane DAT inhibitor (Scheme 4.3). Previous SAR studies (Misra *et al*., 2010) indicated the 3- and 4-positions of the aromatic ring within (±)-**1.18** could potentially be modified to include the 3-I-4-N_3 motif without adversely affecting DAT binding affinity (Scheme 4.3). The 4-position of methylphenidate's aromatic ring was envisioned as a logical place to anchor an azide as photoreactive functional group as indicated by analogs (±)-**4.36**, (±)-**4.37**, (±)-**4.24**, and (±)-**3.29** (Scheme 4.3) whose binding affinity increased or was retained when compared

to a parent compound. Additionally, improved DAT binding affinity was observed for methylphenidate analogs bearing halogens at the 3-position of the aromatic ring ((±)-**4.26** to (±)-**4.29**, Scheme 4.3), thus suggesting a potential position for a future ^{125}I radiotracer tag. Furthermore, improved DAT affinity was observed for a methylphenidate analog bearing lipophilic chlorine atoms at both the 3- and 4-positions of the aromatic ring ((±)-**3.35**, thus indicating that methylphenidate analogs bearing this type of disubstitution pattern could possess increased affinity. With these thoughts in mind, compound (±)-**4.35** was rationally designed and envisioned as a compact DAT photoprobe bearing no linker functionality (Scheme 4.3). Such a photoprobe is expected to covalently attach to an amino acid residue directly within the methylphenidate-binding pocket of the hDAT, and also result in a more conformationally restricted photoprobe-protein complex in 3D hDAT molecular modeling studies.

Target compact photoprobe (±)-**4.35** was synthesized as described in Section 5.1.3, and alongside all intermediate methylphenidate analogs, was subjected to DAT pharmacological evaluation. Analogous to previous reports, substituting the 4-position of (±)-*threo*-methylphenidate with a nitro group resulted in an ~4.8-fold loss in hDAT affinity, whereas NH_2 substitution at this position increased affinity ~2.5-fold (Table 4.1) (Misra *et al*., 2010). The addition of a 3-I group to aniline derivative (±)-**4.36** resulted in only a slight decrease (~1.4-fold) in binding affinity for hDAT. However, replacing the aniline of compound (±)-**4.40** with a photoreactive azide group, resulting in target probe (±)-**4.35**, gave an ~2.3-fold increase in hDAT affinity.

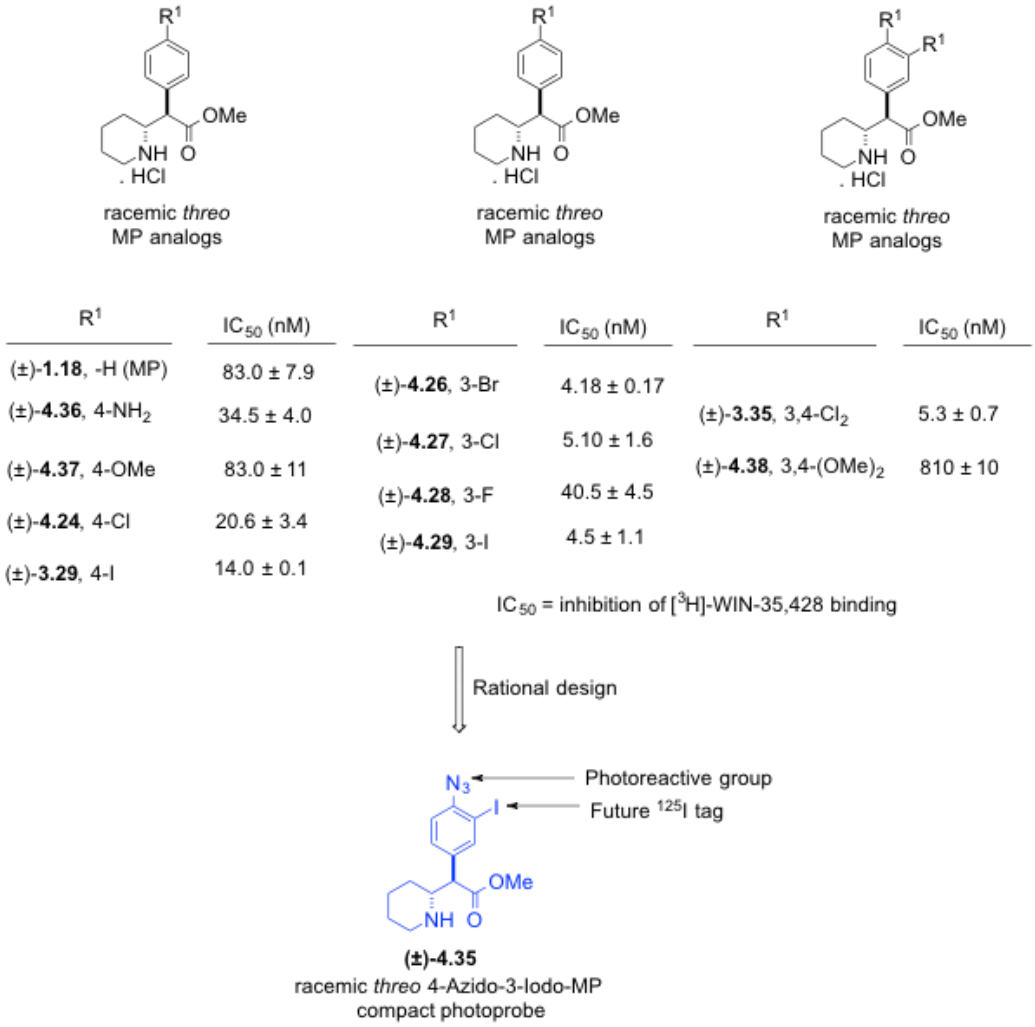

Scheme 4.3. Rational design of racemic *threo* 4-azido-3-iodo-methylphenidate as a compact dopamine transporter photoprobe.

These results indicate that (±)-**4.35** (K_i = 4.0 ± 0.8 nM) displays 6-fold higher hDAT affinity than (±)-*threo*-methylphenidate (±)-**1.18** (K_i = 16.0 ± 2.8 nM), thus representing one of the highest affinity DAT photoprobes synthesized to date (Lapinsky, Yarravarapu *et al*., 2012). In particular, an ~91-fold improvement in hDAT affinity is seen relative to our previously reported best methylphenidate photoprobe, (±)-*threo*-*N*-(*p*-azido-benzyl)-4-iodomethylphenidate (K_i = 363 ± 28 nM), which features the photoreactive azide appended to the pharmacophore *via* an *N*-benzyl linker (Lapinsky *et*

al., 2011). Finally, a ^{125}I version of target photoprobe (±)-**4.35** was synthesized and shown to bind specifically and irreversibly to rDAT and hDAT upon UV irradiation, in the absence or presence of cocaine and methyphenidate as competitors (Lapinsky, Yarravarapu *et al*., 2012) (see Appendix, Section A.1).

Table 4.1. Inhibition of [^{3}H]-WIN-35,428 binding by methylphenidate compounds at hDAT N2A neuroblastoma cells. (Lapinsky, Yarravarapu *et al*., 2012. Adapted with permission from *ACS Med. Chem. Lett.* **2012**, *3*, 378-382. Copyright 2012, American Chemical Society)

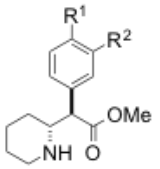

racemic *threo* MP analogs

	R^1	R^2	DAT K_i (nM) [^{3}H]-WIN-35,428 binding inhibition
(±)-**1.18**	-H	-H	16 ± 2.8
(±)-**4.35**	-N_3	-I	4.0 ± 0.8
(±)-**4.39**	-NO_2	-H	77 ± 14
(±)-**4.36**	-NH_2	-H	6.3 ± 2.0
(±)-**4.40**	-NH_2	-I	9.1 ± 1.5
(±)-**4.41**	-N_3	-H	35 ± 5.4
(±)-**4.29**	-H	-I	4.5 ± 1.1

4.7. Rational Design of Citalopram-Based Photoprobes Suitable for Serotonin Transporter Structure-Function Studies

Citalopram ((±)-**1.11**, Figure 4.4) is a well-known, FDA-approved selective serotonin reuptake inhibitor (SSRI) that has been available as an antidepressant since the 1980's. It is well-established that citalopram exerts its therapeutic effects mainly by binding to, and inhibiting, SERT as a neurotransmitter reuptake transporter, resulting in increased synaptic concentrations of serotonin (5-HT) (Stahl *et al*., 2013). In particlar, citalopram has gained special attention in reference to the S1 and S2 binding sites of SERT. The eutomer, escitalopram ((*S*)-**1.11**, Figure 4.4), interacts with the hSERT uniquely, as compared to other 5-HT inhibitors, which interact at both the S1 and S2 sites (Chen, Larsen, Sánchez *et al*., 2005). Furthermore, (*S*)-citalopram has ~30-fold higher

binding affinity at SERT *versus* its enantiomer, (*R*)-citalopram ((*R*)-**1.11**, Figure 4.4), and (*R*)-citalopram may attenuate the effects of (*S*)-citalopram *via* allosteric modulation (Sanchez *et al*., 2004; Chen, Larsen, Sánchez *et al*., 2005; Zhong *et al*., 2009 and 2012). The exact binding contacts for these enantiomers with SERT is unknown, and the importance of allosteric site binding is not well-understood due to the lack of appropriate tool compounds and methods for interrogating the microenvironment of hSERT. In order to address these issues, this dissertation features development of multiple citalopram-based photoprobes potentially capable of elucidating the binding site information within SERT.

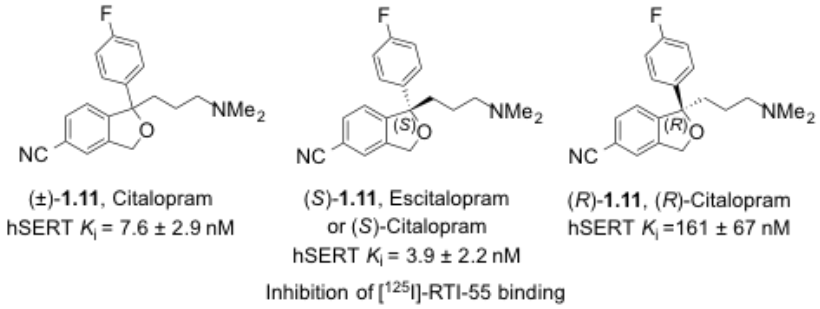

Figure 4.4. Chemical structures of (±)-citalopram, (*S*)-citalopram, and (*R*)-citalopram and their inhibition of [^{125}I]-RTI-55 binding to hSERT in COS-1 cells (Chen, Larsen, Sánchez *et al*., 2005).

4.7.1. Rational Design of Racemic/(*S*)-Citalopram-Based Photoprobes Containing a Clickable Benzophenone-Alkyne Labeling Motif

One of the most common ways to create a clickable photoaffinity ligand is to utilize a benzophenone as a photoreactive group and a terminal alkyne as a click chemistry handle (*e.g*., **4.43**, Scheme 4.4) (Van Scherpenzeel *et al*., 2009 and 2010; Chen *et al*., 2010; Ban *et al*., 2010; Eirich *et al*., 2011 and 2012; Park *et al*., 2012; Cisar and Cravatt, 2012; Saario *et al*., 2012). With this observation in mind, 5-substituted, citalopram-based benzophenone-alkyne SERT photoprobe (±)-**4.44** (Scheme 4.4) was

rationally designed *via* the structure-activity relationship that bulky substituents at the 5-position of citalopram (±)-**1.11** are tolerated (*i.e.*, no large reduction in SERT binding affinity) (Zhang *et al*., 2010 and 2013; Banala *et al*., 2013; Kumar *et al*., 2014). For example, 5-substituted analog (±)-**4.42** (K_i = 23.6 ± 1.54 nM) displayed only a 12-fold loss in binding affinity towards rSERT when compared to (±)-citalopram (K_i = 1.94 ± 0.198 nM) (Banala *et al*., 2013), which is borderline acceptable affinity for designing a future SERT photoaffinity label.

Target citalopram photoprobe (±)-**4.44** was successfully synthesized (see Chapter 5), and submitted to Dr. Christopher Surratt's laboratory (Duquesne University) for hSERT pharmacological evaluation. Binding affinity results indicated that probe (±)-**4.44** (K_i = 4.3 ± 3.5 nM) displays similar hSERT binding affinity as (±)-citalopram ((±)-**1.11**, K_i = 4.4 ± 1.3 nM), thus representing a high affinity potential SERT photoprobe. Even though this photoprobe was initially utilized to develop a photoaffinity labeling protocol for hSERT (see Section 5.3), our subsequent efforts were immediately directed towards synthesizing the enantiomerically pure (*S*)-enantiomer of this probe ((*S*)-**4.44**, Scheme 4.4), primarily because this would remove ambiguity associated with hSERT labeling by a racemic mixture (*i.e.*, two compounds) and also allow use of (*S*)-citalopram as a competitor during photoaffinity labelling experiments. With these thoughts in mind, (*S*)-citalopram-based photoprobe ((*S*)-**4.44**), containing the same clickable benzophenone-alkyne motif, was synthesized as described in Section 5.2.1 and submitted to Dr. Christopher Surratt's laboratory (Duquesne University) for SERT pharmacological evaluation. It was found that (*S*)-**4.44** (K_i = 0.16 ± 0.04 nM) displays 11-fold higher hSERT binding affinity than (*S*)-citalopram ((*S*)-**1.11**, K_i = 1.77 ± 1.14 nM) and 27-fold

higher hSERT binding affinity than (±)-citalopram probe (±)-**4.44**. (*S*)-Probe **4.44** was subsequently utilized to label purified hSERT as discussed in Section 5.3.6. As of the writing of this dissertation, purified hSERT (*S*)-citalopram-benzophenone-alkyne photoprobe-labeled samples were run on a SDS gel, and the labeled bands were excised, trypsin digested (see chapter 6), and submitted to Dr. Michael Cascio's laboratory (Duquesne University) for mass spectrometry analysis.

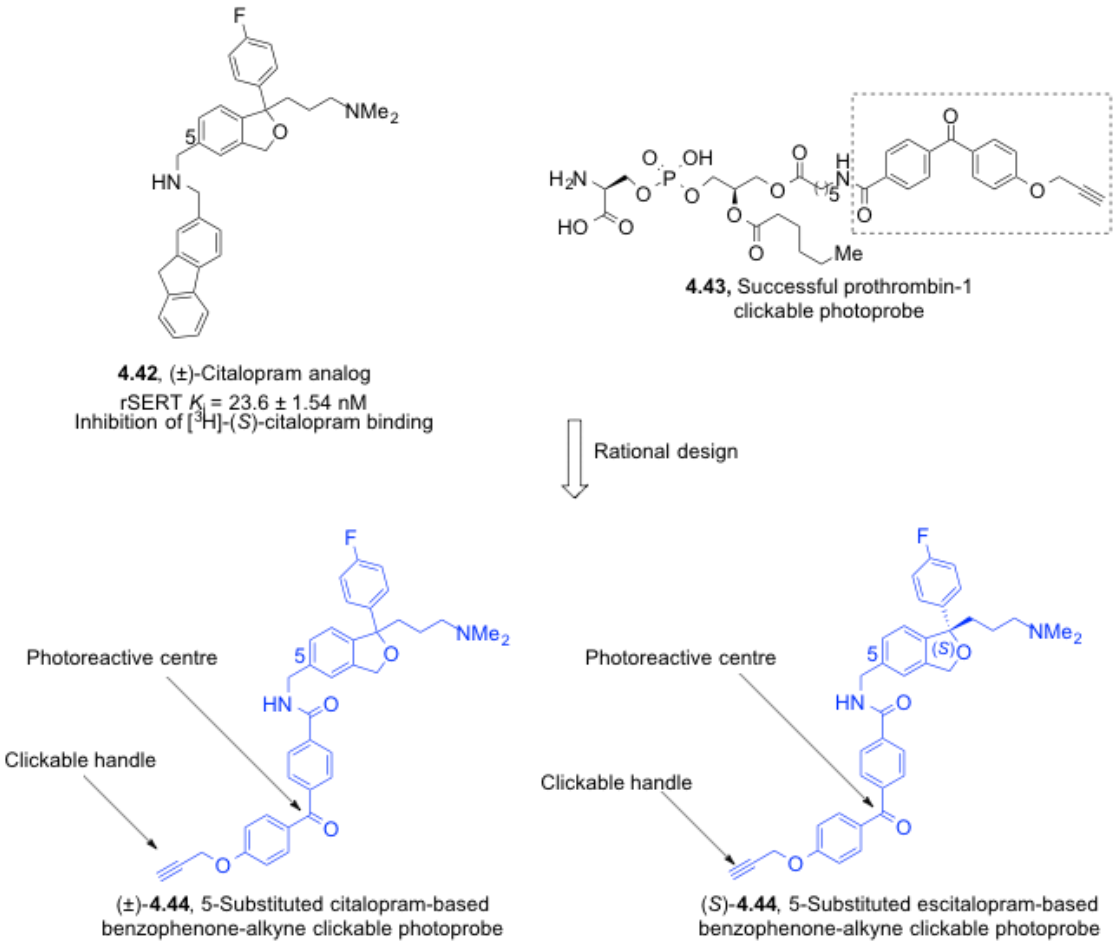

Scheme 4.4. Rational design of 5-substituted, citalopram/escitalopram-based benzophenone-alkyne clickable SERT photoprobes.

One of the goal of this dissertation was to develop multiple (*S*)-citalopram photoprobes featuring systematic placement of different photoreactive functional groups at different positions off on the (*S*)-citalopram scaffold, thus allowing potential

systematic mapping of the (*S*)-citalopram-binding site within hSERT *via* BEProFL. Towards achieving this goal, another point of attachment for the benzophenone-alkyne moiety to (*S*)-citalopram scaffold was pursued in order to potentially gain additional 3D information regarding the (*S*)-citalopram-binding site within SERT. In particular, previous SAR indicated that *N*-substituted analogs of citalopram maintained relatively good binding affinity for SERT (Banala *et al*., 2013). For example, *N*-substituted analog (±)-**4.45** (K_i = 19 ± 2.65 nM) displayed a 10-fold loss in affinity towards rSERT when compared to (±)-citalopram (K_i = 1.94 ± 0.198 nM) (Banala *et al*., 2013), thus suggesting substituting the nitrogen of *N*-desmethyl citalopram with photoreactive group and tag entity could potentially result in a photoprobe with appropriate binding affinity for SERT photoaffinity labeling experiments. Therefore, *N*-substituted-escitalopram-based benzophenone-alkyne photoprobe (*S*)-**4.47** was rationally designed considering (±)-**4.45** as a lead compound (Scheme 4.5). Initially, synthetic methodology for this target probe was established by successful synthesis of escitalopram *N*-substituted benzophenone analog (*S*)-**4.46** (see Chapter 5). Escitalopram *N*-substituted benzophenone analog (*S*)-**4.46** was submitted to Dr. Christopher Surratt's laboratory (Duquesne University) for SERT pharmacological evaluation to see if the bulky benzophenone is tolerable off of citalopram's tertiary nitrogen with respect to maintaining high SERT binding affinity. Later, similar chemistry was utilized to synthesize escitalopram *N*-substituted benzophenone-alkyne clickable photoprobe (*S*)-**4.47** (Section 5.2.1) and likewise this compound was submitted to Dr. Christopher Surratt's laboratory (Duquesne University) for SERT pharmacological evaluation. However, SERT pharmacology results indicated that photoprobe (*S*)-**4.47** (K_i = 487 ± 97 nM) displayed 275-fold loss in SERT binding

affinity when compared to (*S*)-citalopram ((*S*)-**1.11**, K_i = 1.77 ± 1.14 nM). As a result of this significant loss in SERT binding affinity, photoprobe (*S*)-**4.47** was not advanced to SERT photoaffinity labeling studies. At the time of writing this dissertation, a SERT photoaffinity labeling protocol has been optimized using clickable high affinity (*S*)-citalopram-based photoprobes (K_i < 1 nM).

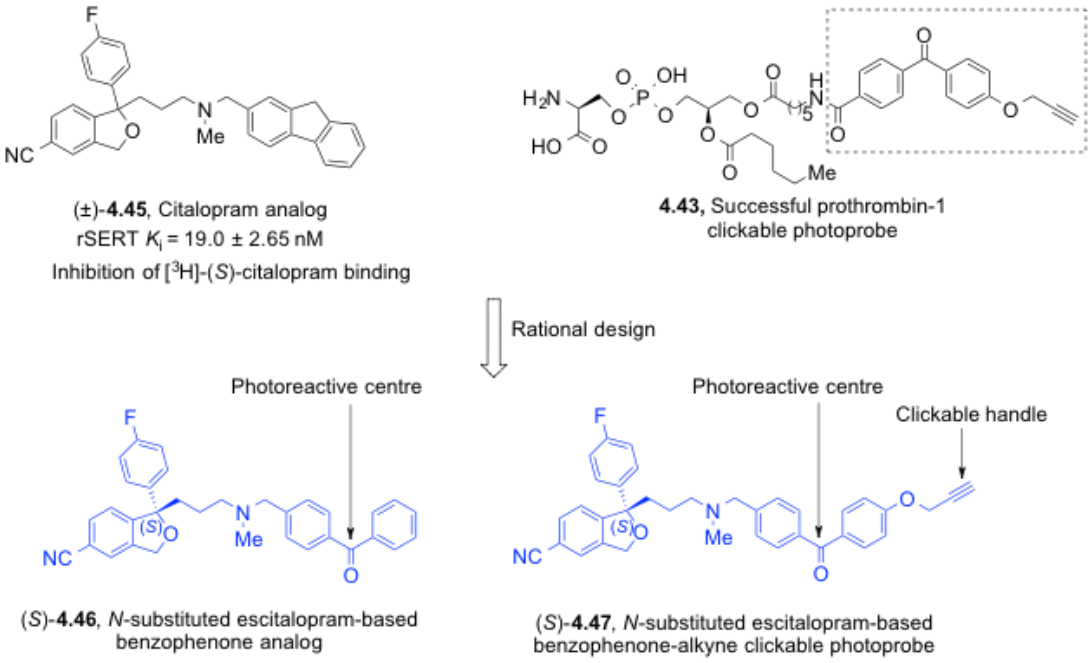

Scheme 4.5. Rational design of *N*-substituted escitalopram benzophenone-based SERT photoprobes.

4.7.2. Rational Design of a Diazido-Based (*S*)-Citalopram Analog as a Potential Photoprobe for Serotonin Transporter Structure-Function Studies

Another common approach to turn lead compounds into clickable photoaffinity ligands is to utilize a 1,3,5-trisubstituted phenyl moiety bearing an aryl azide as a photoreactive group and a methylene aliphatic azide as a click chemistry handle (*e.g.*, **4.49**, Scheme 4.6) (Abdelkarim *et al.*, 2013; Hosoya *et al.*, 2004, 2005, and 2009; Sun *et al.*, 2006; He *et al.*, 2009; Gandy *et al.*, 2011; Neelarapu *et al.*, 2011; Vaidya *et al.*,

2012). In particular, the design of target probe (*S*)-**4.50** is based on 5-substituted high-affinity fluorescent (*S*)-citalopram analog (*S*)-**4.48** (K_i = 3 nM), which maintained equal binding affinity towards hSERT when compared to (*S*)-citalopram (K_i = 2.6 nM) (Kumar *et al*., 2014). Based on this SAR information, diazido-based 5-substituted-(*S*)-citalopram analog (*S*)-**4.50** (Scheme 4.6) was rationally designed by incorporating the known 1,3,5-trisubstituted-phenyl diazide moiety at the 5-position of (*S*)-citalopram.

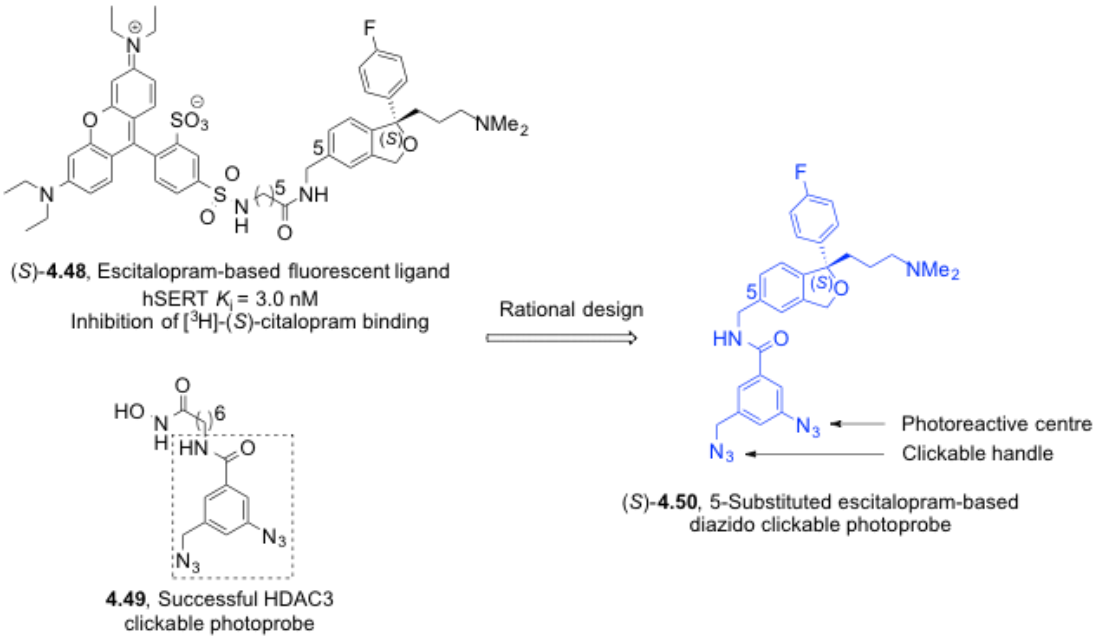

Scheme 4.6. Rational design of a 5-substituted escitalopram-based diazido clickable photoprobe for SERT structure-function studies.

This (*S*)-citalopram-based clickable photoprobe was subsequently synthesized as described in Section 5.2.2 and submitted to Dr. Christopher Surratt's laboratory (Duquesne University) for SERT pharmacological evaluation. It was subsequently found that diazido probe (*S*)-**4.50** (K_i = 10.7 ± 7.5 nM) shows 6-fold higher SERT binding affinity when compared to (*S*)-citalopram ((*S*)-**1.11**, K_i = 1.77 ± 1.14 nM). These pharmacology results indicate that (*S*)-citalopram-based diazide photoprobe (*S*)-**4.50** is a suitable candidate for SERT photoaffinity labeling studies in Dr. Michael Cascio's

laboratory (Duquesne University), principally because the probe maintains high SERT binding affinity (*i.e.*, K_i < 100 nM) and is within a 10-fold SERT binding affinity range when compared to an appropriate parent compound (*i.e.*, (*S*)-citalopram).

4.7.3. Rational Design of a (*S*)-Citalopram-Based Photoaffinity Ligands Containing the Traditional 3-Iodo-4-Azido Labeling Motif

In addition to photoprobes containing a clickable handle, the success of methylphenidate-based probe **4.35**, which contains the traditional 3-iodo-4-azido phenyl ring, prompted us to apply this common Photoaffinity labeling motif to (*S*)-citalopram. (*S*)-Citalopram-based photoprobe (*S*)-**4.51** containing the traditional 3-iodo-4-azido phenyl ring was designed based on the SAR that bulky substituents at the 5-position of the (*S*)-citalopram are well tolerated, as exemplified by (*S*)-citalopram fluorecent ligand (*S*)-**4.48** (Scheme 4.7). The other important factor contributing to the design of probe *S*)-**4.51** was the fact that the synthetic methodology developed for (*S*)-citalopram-based photoprobes (*S*)-**4.44** and (*S*)-**4.50** could be utilized to synthesize (*S*)-citalopram-based 3-iodo-4-azido photoprobe (*S*)-**4.51**. Photoprobe (*S*)-**4.51** was successfully synthesized as described in Section 5.2.3 and was submitted to Dr. Christopher Surratt's laboratory (Duquesne University) for SERT pharmacological evaluation. It was subsequently found that azido-iodo (*S*)-**4.51** (K_i = 3.45 ± 2.04 nM) displays 2-fold higher SERT binding affinity than (*S*)-citalopram ((*S*)-**1.11**, K_i = 1.77 ± 1.14 nM), once again confirming the SAR that bulky substituents at the 5-position of the (*S*)-citalopram are tolerated. Probe (*S*)-**4.51** was subsequently synthesized in its ^{125}I form in the laboratory of Dr. John Lever (University of Missouri – Columbia) and advanced to SERT photoaffinity labeling

studies in the laboratory of Dr. Roxanne Vaughan (University of North Dakota) (see Appendix, Section A.2).

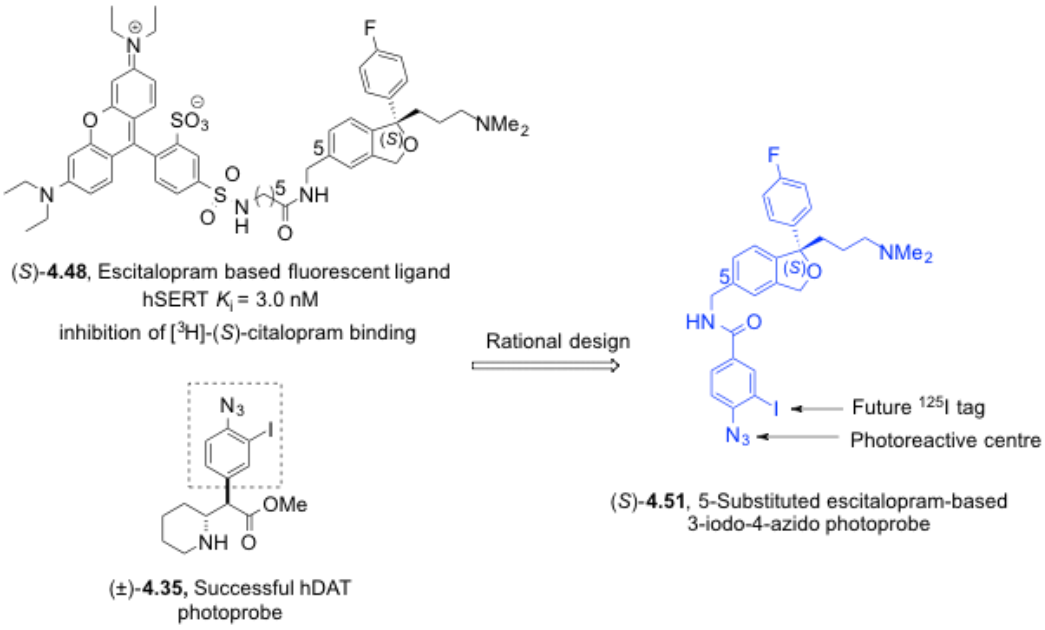

Scheme 4.7. Rational design of a 5-substituted escitalopram-based SERT photoprobe containing a traditional 3-iodo-4-azido photoaffinity labeling motif.

4.8. References

- Abdelkarim, H., Brunsteiner, M., Neelarapu, R., Bai, H., Madriaga, A., van Breemen, R.B., Blond, S.Y., Gaponenko, V., and Petukhov, P.A. Photoreactive "nanorulers" detect a novel conformation of full length HDAC3-SMRT complex in solution. *ACS Chem. Bio*. **2013**, *8*, 2538-2549.

- Agoston, G.E., Vaughan, R., Lever, J.R., Izenwasser, S., Terry, P.D., and Newman, A.H. A novel photoaffinity label for the dopamine transporter based on *N*-substituted-4',4''-difluoro-3α-(diphenylmethoxy)tropane. *Bioorg. Med. Chem. Lett.* **1997**, *7*, 3027-3032.

- Andersen, J., Taboureau, O., Hansen, K.B., Olsen, L., Egebjerg, J., Stromgaard, K., and Kristensen, A.S. Location of the antidepressant binding site in the serotonin transporter: importance of Ser-438 in recognition of citalopram and tricyclic antidepressants. *J. Biol. Chem*. **2009**, *284*, 10276-10284.

- Andersen, J., Olsen, L., Hansen, K.B., Taboureau, O., Jorgensen, F.S., Jorgensen, A.M., Bang-Andersen, B., Egebjerg, J., Stromgaard, K., and Kristensen, A.S. Mutational mapping and modeling of the binding site for (S)-citalopram in the human serotonin transporter. *J. Biol. Chem*. **2010**, *285*, 2051-2063.

- Andersen, J., Stuhr-Hansen, N., Zachariassen, L., Toubro, S., Hansen, S.M., Eildal, J.N., Bond, A.D., Bøgesø, K.P., Bang-Andersen, B., and Kristensen, A.S. Molecular determinants for selective recognition of antidepressants in the human serotonin and norepinephrine transporters. *Proc. Natl. Acad. Sci*. **2011**, *108*, 12137-12142.

- Ban, H.S., Shimizu, K., Minegishi, H., and Nakamura, H. Identification of HSP60 as a primary target of o-carboranylphenoxyacetanilide, an HIF-1α inhibitor. *J. Am. Chem. Soc.* **2010**, *132*, 11870-11871.

- Banala, A.K., Zhang, P., Plenge, P., Cyriac, G., Kopajtic, T., Katz, J.L., Loland, C.J., and Newman, A.H. Design and synthesis of 1-(3-(dimethylamino)propyl)-1-(4-fluorophenyl)-1,3-dihydroisobenzofuran-5-carbonitrile (citalopram) analogues as novel probes for the serotonin transporter S1 and S2 binding sites. *J. Med. Chem*. **2013**, *56*, 9709-9724.

- Barker, E.L., Perlman, M.A., Adkins, E.M., Houlihan, W.J., Pristupa, Z.B., Niznik, H.B., and Blakely, R.D. High affinity recognition of serotonin transporter antagonists defined by species-scanning mutagenesis an aromatic residue in transmembrane domain I dictates species-selective recognition of citalopram and mazindol. *J. Biol. Chem*. **1998**, *273*, 19459-19468.

- Cao, J., Lever, J.R., Kopajtic, T., Katz, J.L., Pham, A.T., Holmes, M.L., Justice, J.B., and Newman, A.H. Novel azido and isothiocyanato analogues of [3-(4-phenylalkylpiperazin-1-yl)propyl]bis(4-fluorophenyl)amines as potential irreversible ligands for the dopamine transporter. *J. Med. Chem*. **2004**, *47*, 6128-6136.

- Carroll, F.I., Gao, Y., Abraham, P., Lewin, A.H., Lew, R., Patel, A., Boja, J.W., and Kuhar, M.J. Probes for the cocaine receptor. Potentially irreversible ligands for the dopamine transporter. *J. Med. Chem*. **1992**, *25*, 1813-1817.

- Challman, T.D. and Lipsky, J.J. Methylphenidate: its pharmacology and uses. *Mayo Clin. Proc*. **2000**, *75*, 711-721.

- Chen, F., Larsen, M.B., Neubauer, H.A., Sánchez, C., Plenge, P., and Wiborg, O. Characterization of an allosteric citalopram-binding site at the serotonin transporter. *J. Neurochem.* **2005**, *92*, 21-28.

- Chen, F., Larsen, M.B., Sánchez, C., and Wiborg, O. The S-enantiomer of R,S-citalopram, increases inhibitor binding to the human serotonin transporter by an allosteric mechanism. Comparison with other serotonin transporter inhibitors. *European Neuropsychopharmacology* **2005**, *15*, 193-198.

- Chen, Y., Hajipour, A.R., Sievert, M.K., Arbabian, M., and Ruoho, A.E. Characterization of the cocaine binding site on the sigma-1 receptor. *Biochemistry* **2007**, *46*, 3532-3542.

- Chen, Y., Wu, Y., Henklein, P., Li, X., Hofmann, K.P., Nakanishi, K., and Ernst, O.P. A photo-cross-linking strategy to map sites of protein-protein interactions. *Chem. Eur. J.* **2010**, *16*, 7389-7394.

- Cisar, J.S. and Cravatt, B.F. Fully functionalized small-molecule probes for integrated phenotypic screening and target identification. *J. Am. Chem. Soc*. **2012**, *134*, 10385-10388.

- Deutsch, H.M., Shi, Q., Gruszecka-Kowalik, E., and Schweri, M. Synthesis and pharmacology of potential cocaine antagonists. 2. structure-activity relationship studies of aromatic ring-substituted methylphenidate analogs. *J. Med. Chem*. **1996**, *39*, 1201-1209.

- Dutta, A.K., Fei, X.S., Vaughan, R.A., Gaffaney, J.D., Wang, N.N., Lever, J.R., and Reith, M.E.A. Design, synthesis, and characterization of a novel, 4-[2-(diphenylmethoxy)ethyl]-1-benzylpiperidine-based, dopamine transporter photoaffinity label. *Life Sci*. **2001**, *68*, 1839-1849.

- Eirich, J., Orth, R., and Sieber, S.A. Unraveling the protein targets of vancomycin in living S. aureus and E. faecalis cells. *J. Am. Chem. Soc*. **2011**, *133*, 12144-12153.

- Eirich, J., Burkhart, J.L., Ullrich, A., Rudolf, G.C., Vollmar, A., Zahler, S., Kazmaier, U., and Sieber, S.A. Pretubulysin derived probes as novel tools for monitoring the

microtubule network *via* activity-based protein profiling and fluorescence microscopy. *Mol. Biosyst*. **2012**, *8*, 2067-2075.

- Fuller, R.W. Serotonin uptake inhibitors: uses in clinical therapy and in laboratory research. *Prog. Drug Res*. **1995**, *45*, 167-204.

- Gabrielsen, M., Ravna, A.W., Kristiansen, K., and Sylte, I. Substrate binding and translocation of the serotonin transporter studied by docking and molecular dynamics simulations. *J. Mol. Model*. **2012**, *18*, 1073-1085.

- Gandy, M.N., Debowski, A.W., and Stubbs, K.A. A general method for affinity-based proteomic profiling of exo-α-glycosidases. *Chem. Commun*. **2011**, *47*, 5037-5039.

- Gedeon, P.C., Indarte, M., Surratt, C.K., and Madura, J.D. Molecular dynamics of leucine and dopamine transporter proteins in a model cell membrane lipid bilayer. *Proteins: Structure, Function, and Bioinformatics* **2010**, *78*, 797-811.

- Grigoriadis, D.E., Wilson, A.A., Lew, R., Sharkey, J.S., and Kuhar, M.J. Dopamine transport sites selectively labeled by a novel photoaffinity probe: ^{125}I-DEEP. *J. Neurosci.* **1989**, *9*, 2664-2670.

- He, B., Velaparthi, S., Pieffet, G., Pennington, C., Mahesh, A., Holzle, D.L., Brunsteiner, M., van Breemen, R., Blond, S.Y., and Petukhov, P.A. Binding ensemble profiling with photoaffinity labeling (BEProFL) approach: Mapping the binding poses of HDAC8 inhibitors. *J. Med. Chem*. **2009**, *52*, 7003-7013.

- Henry, L.K., Field, J.R., Adkins, E.M., Parnas, M.L., Vaughan, R.A., Zou, M.F., Newman, A.H., and Blakely, R.D. Tyr-95 and Ile-172 in transmembrane segments 1 and 3 of human serotonin transporters interact to establish high affinity recognition of antidepressants. *J. Biol. Chem*. **2006**, *281*, 2012-2023.

- Hosoya, T., Hiramatsu, T., Ikemoto, T., Nakanishi, M., Aoyama, H., Hosoya, A., Iwata, T., Maruyama, K., Endo, M., and Suzuki, M. Novel bifunctional probe for radioisotope-free photoaffinity labeling: compact structure comprised of photospecific ligand ligation and detectable tag anchoring units. *Org. Biomol. Chem*. **2004**, *2*, 637-641.

- Hosoya, T., Hiramatsu, T., Ikemoto, T., Aoyama, H., Ohmae, T., Endo, M., and Suzuki, M. Design of dantrolene-derived probes for radioisotope-free photoaffinity labeling of proteins involved in the physiological Ca^{2+} release from sarcoplasmic reticulum of skeletal muscle. *Bioorg. Med. Chem. Lett*. **2005**, *15*, 1289-1294.

- Hosoya, T., Inoue, A., Hiramatsu, T., Aoyama, H., Ikemoto, T., and Suzuki, M. Facile synthesis of diazido-functionalized biaryl compounds as radioisotope-free photoaffinity probes by Suzuki-Miyaura coupling. *Bioorg. Med. Chem*. **2009**, *17*, 2490-2496.

- Huang, X., Gu, H.H., and Zhan, C.G. Mechanism for cocaine blocking the transport of dopamine: Insights from molecular modeling and dynamics simulations. *J. Phys. Chem. B*. **2009**, *113*, 15057-15066.

- Indarte, M., Madura, J.D., and Surratt, C.K. Dopamine transporter comparative molecular modeling and binding site prediction using the LeuT(Aa) leucine transporter as a template. *Proteins: Structure, Function, and Bioinformatics* **2008**, *70*, 1033-1046.

- Indarte, M., Liu, Y., Madura, J.D., and Surratt, C.K. Receptor-based discovery of a plasmalemmal monoamine transporter inhibitor *via* high throughput docking and pharmacophore modeling. *ACS Chem. Neurosci*. **2010**, *1*, 223-233.

- Jorgensen, A.M., Tagmose, L., Jorgensen, A.M.M., Topiol, S., Sabio, M., Gundertofte, K., Bogeso, K.P., and Peters, G.H. Homology modeling of the serotonin transporter: Insights into the primary escitalopram-binding site. *ChemMedChem* **2007**, *2*, 815-826.

- Koldso, H., Severinsen, K., Tran, T.T., Celik, L., Jensen, H.H., Wiborg, O., Schiøtt, B., and Sinning, S. The two enantiomers of citalopram bind to the human serotonin transporter in reversed orientations. *J. Am. Chem. Soc*. **2010**, *132*, 1311-1322.

- Koldso, H., Autzen, H.E., Grouleff, J., and Schiott, B. Ligand induced conformtational changes of the human serotonin transporter revealed by molecular dynamics simulations. *PLoS One* **2013**, *8*, e63635.

- Koldso, H., Christiansen, A.B., Sinning, S., and Schioett, B. Comparative modeling of the human monoamine transporters: Similarities in substrate binding. *ACS Chem. Neurosci*. **2013**, *4*, 295-309.

- Kumar, V., Rahbek-Clemmensen, T., Billesbølle, C.B., Jorgensen, T.N., Gether, U., and Newman, A.H. Novel and high affinity fluorescent ligands for the serotonin transporter based on (S)-citalopram. *ACS Med. Chem. Lett*. **2014**, *5*, 696-699.

- Lapinsky, D.J., Aggarwal, S., Huang, Y., Surratt, C.K., Lever, J.R., Foster, J.D., and Vaughan, R.A. A novel photoaffinity ligand for the dopamine transporter based on pyrovalerone. *Bioorg. Med. Chem*. **2009**, *17*, 3770-3774.

- Lapinsky, D.J., Velagaleti, R., Yarravarapu, N., Liu, Y., Huang, Y., Surratt, C.K., Lever, J.R., Foster, J.D., Acharya, R., Vaughan, R.A., and Deutsch, H.M. Azido-iodo-*N*-benzyl derivatives of threo-methylphenidate (Ritalin, Concerta): rational design, synthesis, pharmacological evaluation, and dopamine transporter photoaffinity labeling. *Bioorg. Med. Chem.* **2011**, *19*, 504-512.

- Lapinsky, D.J., Aggarwal, S., Nolan, T.L., Surratt, C.K., Lever, J.R., Acharya, R., Vaughan, R.A., Pandhare, A., and Blanton, M.P. (±)-2-(*N*-tert-Butylamino)-3'-[(^{125}I]-iodo-4'azidopropiophenone: a dopamine transporter and nicotinic acetylcholine receptor photoaffinity ligand based on bupropion (Wellbutrin, Zyban). *Bioorg. Med. Chem. Lett*. **2012**, *22*, 523-526.

- Lapinsky, D.J., Yarravarapu, N., Nolan, T.L., Surratt, C.K., Lever, J.R., Tomlinson, M., Vaughan, R.A., and Deutsch, H.M. Evolution of a compact photoprobe for the dopamine transporter based on (±)-threo-methylphenidate. *ACS Med. Chem. Lett*. **2012**, *3*, 378-382.

- Lever, J.R., Zou, M-F, Parnas, M.L., Duval, R.A., Wirtz, S.E., Justice, J.B., Vaughan, R.A., and Newman, A.H. Radioiodinated azide and isothiocyanate derivatives of cocaine for irreversible labeling of dopamine transporters: synthesis and covalent binding studies. *Bioconjugate Chem*. **2005**, *16*, 644-649.

- Misra, M., Shi, Q., Ye, X., Gruszecka-Kowalik, E., Bu, W., Liu, Z., Schweri, M.M., Deutsch, H.M., and Venanzi, C.A. Quantitative structure-activity relationship studies of threo-methylphenidate analogs. *Bioorg. Med. Chem*. **2010**, *18*, 7221-7238.

- Neelarapu, R., Holzle, D.L., Velaparthi, S., Bai, H., Brunsteiner, M., Blond, S.Y., and Petukhov, P.A. Design, synthesis, docking, and biological evaluation of novel diazide-containing isoxazole- and pyrazole-based histone deacetylase probes. *J. Med. Chem*. **2011**, *54*, 4350-4364.

- Neubauer, H.A., Hansen, C.G., and Wiborg, O. Dissection of an allosteric mechanism on the serotonin transporter: a cross-species study. *Mol. Pharmacol*. **2006**, *69*, 1242-1250.

- Newman, A.H., Cha, J.H., Cao, J., Kopajtic, T., Katz, J.L., Parnas, M.L., Vaughan, R., and Lever, J.R. Design and synthesis of a novel photoaffinity ligand for the dopamine and serotonin transporters based on 2β-carbomethoxy-3β-biphenyltropane. *J. Med. Chem*. **2006**, *49*, 6621-6625.

- Nolan, T.L., Lapinsky, D.J., Talbot, J.N., Indarte, M., Liu, Y., Manepalli, S., Geffert, L.M., Amos, M.E., Taylor, P.N., Madura, J.D., and Surratt, C.K. Identification of a novel selective serotonin reuptake inhibitor by coupling monoamine transporter-based

virtual screening and rational molecular hybridization. *ACS Chem. Neurosci*. **2011**, *2*, 544-552.

- Nolan, T.L., Geffert, L.M., Kolber, B.J., Madura, J.D., and Surratt, C.K. Discovery of novel-scaffold monoamine transporter ligands *via* in silico screening with the S1 pocket of the serotonin transporter. *ACS Chem. Neurosci*. **2014**, *5*, 784-792.

- Pan, D., Gatley, S.J., Dewey, S.L., Chen, R., Alexoff, D.A., Ding, Y.S., and Fowler, J.S. Binding of bromine-substituted analogs of methylphenidate to monoamine transporters. *Eur. J. Pharm*. **1994**, *264*, 177-182.

- Park, J., Oh, S., and Park, S.B. Discovery and target identification of an antiproliferative agent in live cells using fluorescence difference in two-dimensional gel electrophoresis. *Angew. Chem. Int. Ed*. **2012**, *51*, 5447-5451.

- Parnas, M.L., Gaffaney, J.D., Newman, A.H., Zou, M.F., Lever, J.R., and Vaughan, R.A. Irreversible cocaine analogs map to multiple sites on the dopamine transporter. Program No. 253.18 2003 Abstract; *Society for Neuroscience*: Washington, DC, **2003**.

- Parnas, M.L., Gaffaney, J.D., Zou, M.F., Lever, J.R., Newman, A.H., and Vaughan, R.A. Labeling of dopamine transporter trans-membrane domain 1 with the tropane ligand*N*-[4-(4-azido-3-[^{125}I]iodophenyl)butyl]-2β-carbomethoxy-3β-(4-chlorophenyl)-tropane implicates proximity of cocaine and substrate active sites. *Mol. Pharmacol*. **2008**, *73*, 1141−1150.

- Plenge, P., Mellerup, E.T., and Laursen, H. Affinity modulation of [3H] imipramine, [3H] paroxetine and [3H] citalopram binding to the 5-HT transporter from brain and platelets. *Eur. J. Pharmacol*. **1991**, *206*, 243-250.

- Plenge, P. and Mellerup, E.T. An affinity-modulating site on neuronal monoamine transport proteins. *Pharmacology & Toxicology* **1997**, *80*, 197-201.

- Plenge, P., Gether, U., and Rasmussen, S.G. Allosteric effects of R-and S-citalopram on the human 5-HT transporter: evidence for distinct high-and low-affinity binding sites. *Eur. J. Pharmacol*. **2007**, *567*, 1-9.

- Plenge, P., Shi, L., Beuming, T., Te, J., Newman, A.H., Weinstein, H., Gether, U., and Loland, C.J. Steric hindrance mutagenesis in the conserved extracellular vestibule impedes allosteric binding of antidepressants to the serotonin transporter. *J. Biol. Chem*. **2012**, *287*, 39316-39326.

- Ravna, A.W., Jaronczyk, M., and Sylte, I. A homology model of SERT based on the LeuTAa template. *Bioorg. Med. Chem. Lett*. **2006**, *16*, 5594-5597.

- Saario, S.M., McKinney, M.K., Speers, A.E., Wang, C., and Cravatt, B.F. Clickable, photoreactive inhibitors to probe the active site microenvironment of fatty acid amide hydrolase. *Chem. Sci.* **2012**, *3*, 77-83.

- Sallee, F.R., Fogel, E.L., Schwartz, E., Choi, S.M., Curran, D.P., and Niznik, H.B. Photoaffinity labeling of the mammalian dopamine transporter. *FEBS Lett.* **1989**, *256*, 219-224.

- Sanchez, C., Bogeso, K.P., Ebert, B., Reines, E.H., and Braestrup, C. Escitalopram *versus* citalopram: the surprising role of the R-enantioner. *Psychopharmacology* **2004**, *174*, 163-176.

- Schwartz, B.G., Rezkalla, S., and Kloner, R.A. Cardiovascular effects of cocaine. *Circulation*. **2010**, *122*, 2558-2569.

- Seddik, A., Holy, M., Weissensteiner, R., Zdrazil, B., Sitte, H.H., and Ecker, G.F. Probing the selectivity of monoamine transporter substrates by means of molecular modeling. *Mol. Inf.* **2013**, *32*, 409-413.

- Singh, S.K., Yamashita, A., and Gouaux, E. Antidepressant binding site in a bacterial homologue of neurotransmitter transporters. *Nature* **2007**, *448*, 952-956.

- Sinning, S., Musgaard, M., Jensen, M., Severinsen, K., Celik, L., Koldsø, H., Meyer, T., Bols, M., Jensen, H.H., and Schiøtt, B. Binding and orientation of tricyclic antidepressants within the central substrate site of the human serotonin transporter. *J. Biol. Chem.* **2010**, *285*, 8363-8374.

- Stahl, S.M., Lee-Zimmerman, C., Cartwright, S., and Ann Morrissette, D. Serotonergic drugs for depression and beyond. *Current Drug Targets* **2013**, *14*, 578-585.

- Stockner, T., Montgomery, T.R., Kudlacek, O., Weissensteiner, R., Ecker, G.F., Freissmuth, M., and Sitte, H.H. Mutational analysis of the high-affinity zinc binding site validates a refined human dopamine transporter homology model. *PLoS Comput. Biol*. **2013**, *9*, e1002909.

- Soundararajan, N. and Platz, M.S. Descriptive photochemistry of polyfluorinated azide derivatives of methyl benzoate. *J. Org. Chem*. **1990**, *55*, 2034-2044.

- Sun, P., Wang, G.X., Furuta, K., and Suzuki, M. Synthesis of a bis-azido analogue of acromelic acid for radioisotope-free photoaffinity labeling and biochemical studies. *Bioorg. Med. Chem. Lett*. **2006**, *16*, 2433-2436.

- Talvenheimo, J., Nelson, P.J., and Rudnick, G. Mechanism of imipramine inhibition of platelet 5-hydroxytryptamine transport. *J. Biol. Chem*. **1979**, *254*, 4631-4635.

- Tavoulari, S., Forrest, L.R., and Rudnick, G. Fluoxetine (Prozac) binding to serotonin transporter is modulated by chloride and conformational changes. *J. Neurosci*. **2009**, *29*, 9635-9643.

- Vaidya, A.S., Karumudi, B., Mendonca, E., Madriaga, A., Abdelkarim, H., van Breemen, R.B., and Petukhov, P.A. Design, synthesis, modeling, biological evaluation and photoaffinity lableing studies of novel series of photoreactive benzamide probes for histone deacetylase 2. *Bioorg. Med. Chem. Lett*. **2012**, *22*, 5025-5030.

- Van Scherpenzeel, M., Moret, E.E., Ballell, L., Liskamp, R.M., Nilsson, U.J., Leffler, H., and Pieters, R.J. Synthesis and evaluation of new thiodigalactoside-based chemical probes to label galectin-3. *ChemBioChem* **2009**, *10*, 1724-1733.

- Van Scherpenzeel, M., Vanden Berg, R.J.B.H.N., Donker-Koopman, W.E., Liskamp, R.M.J., Aerts, J.M.F.G., Overkleeft, H.S., and Pieters, R.J. Nanomolar affinity,

iminosugar-based chemical probes for specific labeling of lysosomal glucocerebrosidase. *Bioorg. Med. Chem*. **2010**, *18*, 267-273.

- Vaughan, R.A., Parnas, M.L., Gaffaney, J.D., Lowe, M.J., Wirtz, S., Pham, A., Reed, B., Dutta, S.M., Murray, K.K., and Justice, J.B. Affinity labeling the dopamine transporter ligand binding site. *J. Neurosci. Meth*. **2005**, *143*, 33-40.

- Vaughan, R.A., Sakrikar, D.S., Parnas, M.L., Adkins, S., Foster, J.D., Duval, R.A., Lever, J.R., Kulkarni, S.S., and Newman, A.H. Localization of cocaine analog [^{125}I]RTI 82 irreversible binding to transmembrane domain 6 of the dopamine transporter. *J. Biol. Chem*. **2007**, *282*, 8915-8925.

- Wang, H., Goehring, A., Wang, K.H., Penmatsa, A., Ressler, R., and Gouaux, E. Structural basis for action by diverse antidepressants on biogenic amine transporters. *Nature* **2013**, *503*, 141-145.

- Yamashita, A., Singh, S.K., Kawate, T., Jin, Y., and Gouaux, E. Crystal structure of a bacterial homologue of Na^+/Cl^--dependent neurotransmitter transporters. *Nature* **2005**, *437*, 215-223.

- Yano, M. and Steiner, H. Methylphenidate and cocaine: The same effects on gene regulation? *Trends Pharmacol. Sci*. **2007**, *28*, 588-596.

- Zhang, P., Cyriac, G., Kopajtic, T., Zhao, Y., Javitch, J.A., Katz, J.L., and Newman, A.H. Structure-activity relationships for a novel series of citalopram (1-(3-(dimethylamino)propyl)-1-(4-fluorophenyl)-1,3-dihydroisobenzofuran-5-carbonitrile) analogues at monoamine transporters. *J. Med. Chem*. **2010**, *53*, 6112-6121.

- Zhang, P., Jorgensen, T.N., Loland, C.J., and Newman, A.H. A rhodamine-labeled citalopram analogue as a high-affinity fluorescent probe for the serotonin transporter. *Bioorg. Med. Chem. Lett*. **2013**, *23*, 323-326.

- Zhong, H., Hansen, K.B., Boyle, N.J., Han, K., Muske, G., Huang, X., Egebjerg, J., and Sánchez, C. An allosteric binding site at the human serotonin transporter mediates the inhibition of escitalopram by R-citalopram: Kinetic binding studies with the ALI/VFL–SI/TT mutant. *Neurosci. Lett.* **2009**, *462*, 207-212.

- Zhong, H., Haddjeri, N., and Sánchez, C. Escitalopram, an antidepressant with an allosteric effect at the serotonin transporter - a review of current understanding of its mechanism of action. *Psychopharmacology* **2012**, *219*, 1-13.

- Zhou, Z., Zhen, J., Karpowich, N.K., Goetz, R.M., Law, C.J., Reith, M.E., and Wang, D.N. LeuT-desipramine structure reveals how antidepressants block neurotransmitter reuptake. *Science* **2007**, *317*, 1390-1393.

- Zhou, Z., Zhen, J., Karpowich, N.K., Law, C.J., Reith, M.E., and Wang, D.N. Antidepressant specificity of serotonin transporter suggested by three LeuT–SSRI structures. *Nat. Struct. Mol. Bio.* **2009**, *16*, 652-657.

- Zhou, Z.L., Liu, H.L., Wu, J.W., Tsao, C.W., Chen, W.H., Liu, K.T., and Ho, Y. Combining structure-based pharmacophore and in silico approaches to discover novel selective serotonin reuptake inhibitors. *Chem. Biol. Drug Des*. **2013**, *82*, 705-717.

- Zou, M.F., Kopajtic, T., Katz, J.L., Wirtz, S., Justice, J.B., and Newman, A.H. Novel tropane-based irreversible ligands for the dopamine transporter. *J. Med. Chem*. **2001**, *44*, 4453-4461.

- Zou, M.F., Kopajtic, T., Katz, J.L., and Newman, A.H. Structure-activity relationship comparison of (*S*)-2β-substituted-3α-(bis[4-fluorophenyl]methoxy)tropanes and (*R*)-2β-substituted-3β-(3,4-dichlorophenyl)tropanes at the dopamine transporter. *J. Med. Chem*. **2003**, *46*, 2908-2916.

CHAPTER FIVE

5. Chemical Discussion

5.1. Synthesis of Methylphenidate-Based Photoprobes Suitable for Dopamine Transporter Structure-Function Studies

As previously discussed in Section 4.6, we desired photoprobes for dopamine transporter structure-function studies based on the well-known attention deficit hyperactivity disorder (ADHD) drug, (±)-*threo*-methylphenidate ((±)-**1.18**, Ritalin®, Concerta®), analogs of which have received significant attention as potential cocaine abuse therapeutics (*e.g.*, Kim *et al.*, 2007). In particular, previous SAR studies have indicated structural features leading to high DAT binding affinities for a number of methylphenidate analogs (reviewed in Misra *et al*., 2010), thus aiding in rational DAT photoprobe design from a ligand-based perspective.

5.1.1. Synthesis of Racemic *threo*-3-Iodo-Methylphenidate as an Intermediate for the Synthesis of Racemic *threo*-*N*-Azidobenzyl-3-Iodo-Methylphenidate Photoaffinity Ligands for Dopamine Transporter Structure-Function Studies

As previously discussed in Section 4.6.1, in order to overcome inefficient DAT photoaffinity labeling associated with probes containing the traditional 3-iodo-4-azido labeling motif, racemic *threo*-*N*-azidobenzyl-4-iodo/3-iodo-methylphenidate analogs were pursued as potential photoaffinity ligands for dopamine transporter structure-function studies (Lapinsky *et al.*, 2011). In particular, the synthesis of a series of racemic *threo*-*N*-azidobenzyl-4-iodo/3-iodo-methylphenidate (MP) analogs ((±)-**4.17**-**4.22**) as potential DAT photoaffinity ligands was envisioned *via N*-alkylation of either 4-iodo-

methylphenidate ((±)-**3.29**) or 3-iodo-MP ((±)-**4.29**) with a series of known azido benzyl bromides (**5.1**-**5.3**; Mornet *et al*., 1984) (Scheme 5.1). As a contribution towards the synthesis of these desired methylphenidate analogs, an efficient, relatively large-scale synthesis of 3-iodo-methylphenidate ((±)-**4.29**) was pursued as part of this dissertation.

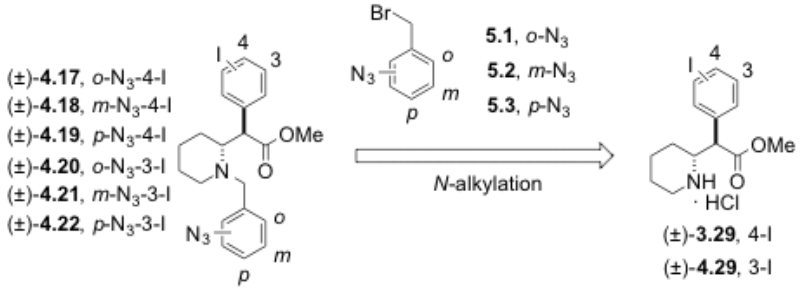

Scheme 5.1. Proposed retrosynthesis of a series of racemic *threo*-*N*-azidobenzyl-4-iodo/3-iodo-methylphenidate analogs as potential DAT photoaffinity ligands.

In short, synthetic methodology previously described in Section 3.1 for the synthesis of racemic *threo*-MP ((±)-**1.18**, Scheme 3.2) (Axten *et al*., 1998; Gutman *et al*., 2004) was modified in order to access racemic *threo*-3-iodo-MP ((±)-**4.29**) (Scheme 5.2). The synthesis began with regioselective *meta*-iodination of known α-keto amide **3.8** (Gutman *et al*., 2004) using a solution of *N*-iodosuccinimide in concentrated sulfuric acid to provide iodo α-keto amide **5.4** in 77% yield. Subsequent condensation of ketone **5.4** with tosylhydrazine under acidic conditions then provided tosylhydrazone **5.5** in moderate yield (72%). Next, thermal cyclization of iodo tosylhydrazone **5.5** under aqueous basic conditions using Aliquat 336® as a phase transfer catalyst, followed by column chromatography and recrystallization from diethyl ether, provided diastereomerically pure racemic *threo*-β-lactam (±)-**5.6** as the major product in moderate yield (55%). Finally, *threo*-β-lactam (±)-**5.6** was converted to 3-iodo-MP ((±)-**4.29**) in quantitative yield by ring opening with methanol under acidic conditions (Lapinsky *et al*.,

2011). In particular, racemic *threo*-3-iodo-MP ((±)-**4.29**) synthesized by this route was determined to be ≥95% diastereomerically pure by ^{1}H NMR upon comparison to the known spectroscopic data for enantiomerically pure *threo*- and *erythro*-methylphenidate and its *para*-substituted derivatives (Thai *et al*., 1998).

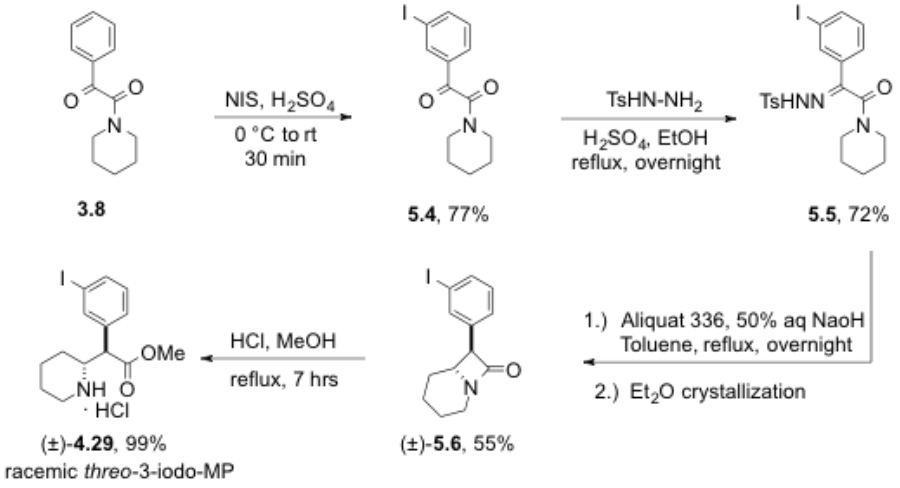

Scheme 5.2. Synthesis of racemic *threo*-3-iodo-methylphenidate (MP) by applying methodology previously described for the synthesis of racemic *threo*-MP (Axten *et al*., 1998).

The chemistry described in Scheme 5.2 worked fairly well yielding 3-iodo-methylphenidate ((±)-**4.29**) in 4 steps and 30 % overall yield. The only troublesome reaction during scale up of this chemistry was the electrophilic aromatic *meta*-iodination (*i.e.*, **3.8** to **5.4**), which was initially done in multiple small batches to avoid large volumes of sulfuric acid. This drawback was subsequently addressed by reducing the volume of sulfuric acid required for the reaction to proceed to completion. Initially, the reaction was attempted on 0.5 mmol of α-keto amide **3.8** (Gutman *et al*., 2004) using 2 equivalents of *N*-iodosuccinimide dissolved in 3 mL of concentrated sulfuric acid (conditions adapted from Chaikovskii *et al*., 2207). As a result, the 5 mmol scale reaction (second attempt) required using 30 mL of concentrated sulfuric acid, which

necessitated tedious and careful quenching in order to isolate the product. In order to address this practical concern on an even larger scale, a 5 mmol scale reaction was attempted and proved successful by using a minimum volume of sulfuric acid (4.5 mL) required for dissolving the *N*-iodosuccinimide (10 mmol). Finally, the meta-iodination could be scaled up to a 10 mmol scale of amide **3.8** using a minimum amount of sulfuric acid (9 mL) required to generate a 20 mmol *N*-iodosuccinimide solution. Overall, the chemistry described in Scheme 5.2 was scaled up to provide 3-iodo-methylphenidate ((±)-**4.29**) in multigram amounts, which was utilized by Dr. Ranganadh Velagaleti for synthesis of racemic *threo*-*N*-azidobenzyl-3-iodo-methylphenidate probes (±)-**4.20** and (±)-**4.21** *via N*-alkylation (Lapinsky *et al*., 2011).

5.1.2. Synthesis of Racemic *threo*-*N*-*para*-Azidobenzyl-3-Iodo-Methylphenidate as a Potential Photoprobe for Dopamine Transporter Structure-Function Studies

As part of this dissertation, racemic *threo*-*N*-*para*-azidobenzyl-3-iodo-methylphenidate ((±)-**4.22**) was pursued as a potential DAT photoaffinity ligand (Lapinsky *et al*., 2011). In particular, this compound was synthesized in moderate yield (65%) by *N*-alkylation of 3-iodo-MP with *para*-azido benzyl bromide (**5.3**, Mornet *et al*., 1984) (Scheme 5.3). Unfortunately, despite support for its rational design as described in Section 4.6.1, probe (±)-**4.22** showed significantly higher DAT binding affinity (DAT K_i = 658 ± 70 nM; ~26-fold loss in DAT binding affinity when compared to (±)-MP (DAT K_i = 25 ± 1 nM)) and did not meet our criteria (*i.e.*, DAT $K_i \leq 100$ nM and $\leq$ 10-fold loss in DAT binding affinity when compared to an appropriate parent compound) for further pursuit of a radioiodinated version for formal DAT photoaffinity labeling.

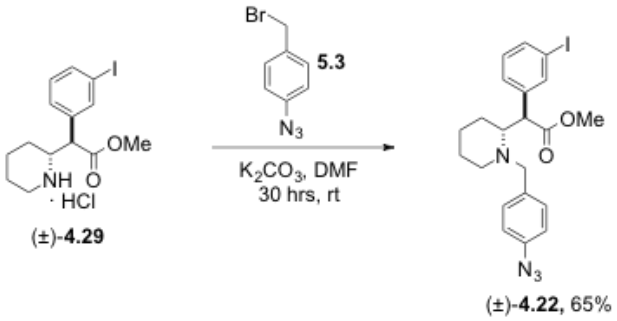

Scheme 5.3. Synthesis of racemic *threo*-*N*-*para*-azidobenzyl-3-iodo-methylphenidate by *N*-alkylation of racemic *threo*-3-iodo-methylphenidate with *para*-azido benzyl bromide.

5.1.3. Synthesis of Racemic *threo*-4-Azido-3-Iodo-Methylphenidate as a Compact Photoaffinity Ligand for Dopamine Transporter Structure-Function Studies

As previously described in Section 4.6.2, racemic *threo*-4-azido-3-iodo methylphenidate ((±)-**4.35**) was desired and pursued as a compact DAT photoaffinity probe featuring a photoreactive aryl azide placed directly on methylphenidate's aromatic ring. Additionally, since attempted *N*-benzylation of iodo-methylphenidates (±)-**3.29** and (±)-**4.29** resulted in a significant decrease in DAT binding affinity upon comparison to racemic *threo*-MP, (±)-**1.18** was pursued in the hopes of obtaining a methylphenidate-based photoprobe with significantly improved DAT binding affinity (*i.e.*, target goal DAT K_i < 100 nM) relative to our first successful probe in this area (*i.e.*, [^{125}I]-(±)-**4.19**; Lapinsky *et al*., 2011).

In terms of retrosynthesis, racemic *threo*-4-azido-3-iodo-methylphenidate ((±)-**4.35**) as a potential DAT photoaffinity ligand was initially envisioned from known methylphenidate analog *N*-benzoyl-4-amino-methylphenidate ((±)-**3.24**, Pan *et al*., 1996) *via* 4 steps: electrophilic aromatic iodination of the aniline, conversion of the aniline to an azide *via* diazotization and azide displacement, then global hydrolysis of a benzamide

methyl ester analog followed by final methyl esterification of a ritalinic acid derivative (Scheme 5.4). In turn, it is known that *N*-benzoyl-4-amino-methylphenidate analog (±)-**3.26** can be accessed from racemic *threo*-methylphenidate ((±)-**1.18**, Axten *et al*., 1998; Gutman *et al*., 2004) using methodology previously reported (*i.e.*, a sequence of *N*-benzoylation, nitration, and reduction; Pan *et al*., 1996). With this particular retrosynthesis in mind, the synthesis of racemic *threo-4*-azido-*3*-iodo-methylphenidate ((±)-**4.35**) was pursued according to this strategy.

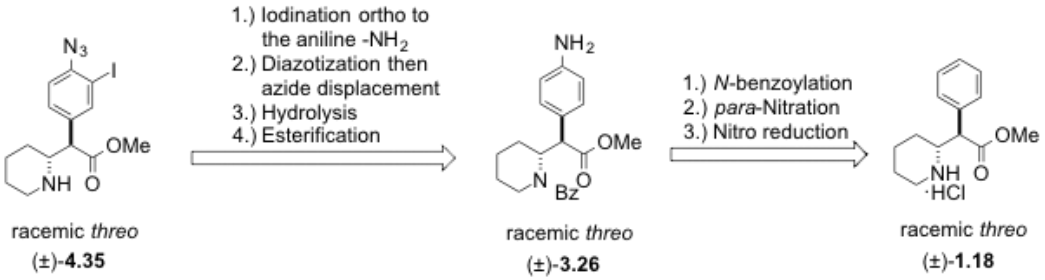

Scheme 5.4. Proposed retrosynthesis of racemic *threo*-4-azido-3-iodo-methylphenidate as a potential DAT photoaffinity ligand from known methylphenidate analog (±)-**3.26** (Pan *et al*., 1996).

This attempted synthesis first began with efficient *N*-benzoylation of racemic *threo*-methylphenidate ((±)-**1.18**) to provide amide (±)-**3.24** in quantitative yield (Scheme 5.5). The aromatic ring of amide analog (±)-**3.24** was then subsequently nitrated with nitric acid to give *p*-nitro isomer (±)-**3.25** as the major product in moderate yield (75%). The nitro functional group was then reduced using iron under sonicating acid conditions to provide aniline (±)-**3.26**, which was subjected to iodination using iodine monochloride to provide *p*-amino-*m*-iodo *N*-protected methylphenidate derivative (±)-**5.7** in 50% yield. Next, aniline (±)-**5.7** was diazotized and displaced with sodium azide to produce *p*-azido-*m*-iodo derivative (±)-**5.8** in moderate yield (60%). However, attempted global hydrolysis of benzamide methyl ester (±)-**5.8** under strong acidic conditions

unfortunately resulted in degradation of the azide functional group, thus forcing subsequent pursuit of an alternative synthetic strategy.

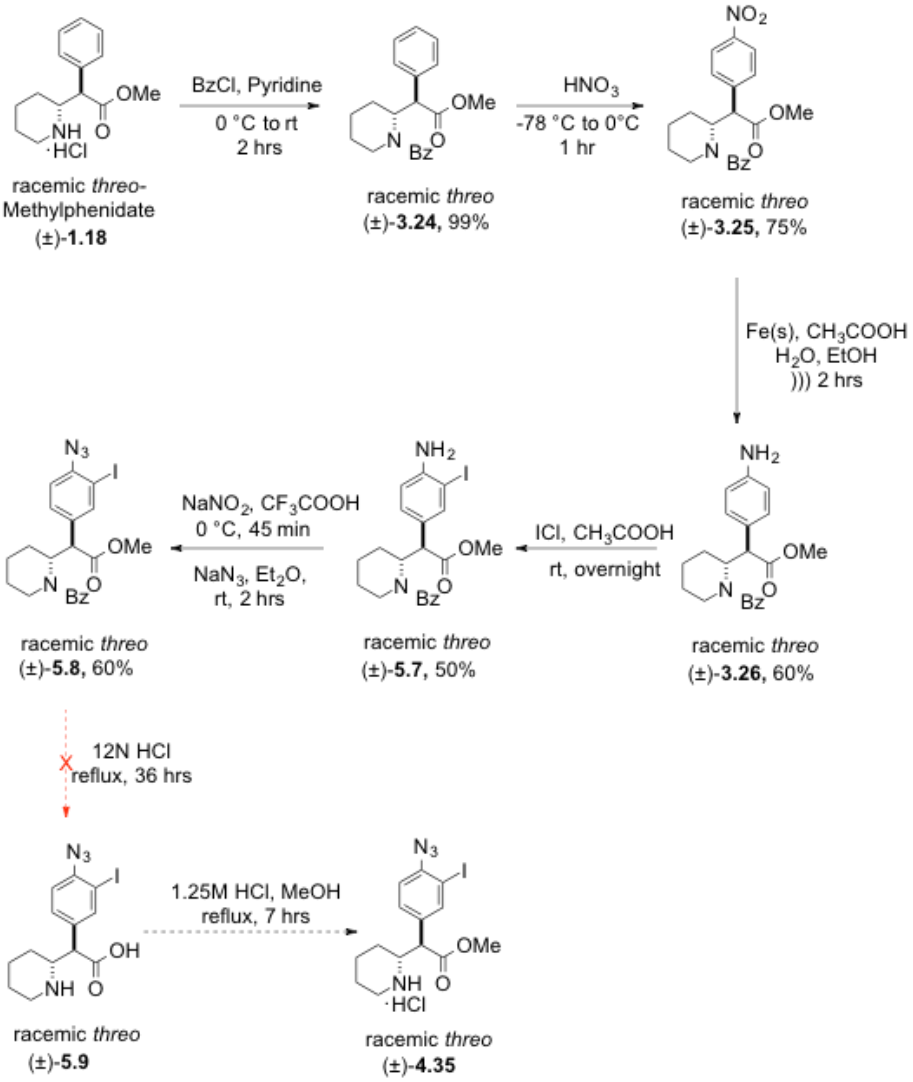

Scheme 5.5. Attempted synthesis of racemic *threo*-4-azido-3-iodo-methylphenidate photoprobe (±)-**4.35** from racemic *threo*-*N*-benzoyl-methylphenidate ((±)-**3.24**).

In order to avoid azide decomposition *via* the harsh acidic global hydrolysis conditions depicted in Scheme 5.5, an alternative retrosynthesis was to first pursue global hydrolysis of *p*-nitro-benzamide (±)-**3.25** to provide 4-nitro-ritalinilic acid, which could then potentially be converted to 4-nitro-methylphenidate ((±)-**4.39**) *via* Fischer

esterification (Scheme 5.6). In turn, the synthesis of target compound racemic *threo*-4-azido-3-iodo-methylphenidate ((±)-**4.35**) was then envisioned from 4-nitro-methylphenidate ((±)-**4.39**) *via* three steps: reduction of the nitro group to the aniline, electrophilic aromatic iodination, then conversion of the aniline to the azide *via* diazotization and azide displacement.

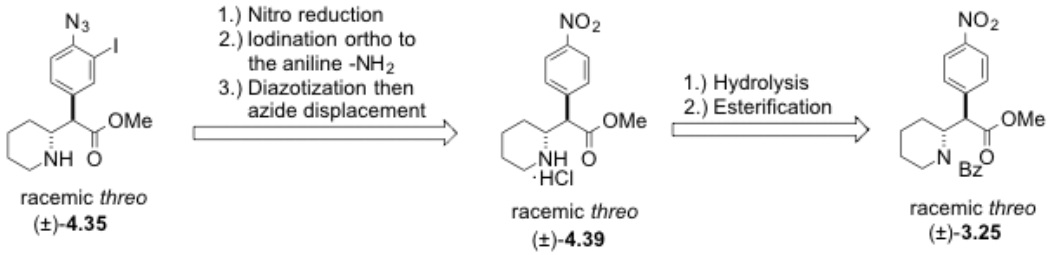

Scheme 5.6. Alternative proposed retrosynthesis of racemic *threo*-4-azido-3-iodo-methylphenidate from racemic *threo*-4-nitro-methylphenidate analog (±)-**5.10**.

With this alternative retrosynthesis in mind, nitro derivative (±)-**3.25** (from Scheme 5.5) was subjected to global hydrolysis to provide 4-nitro-ritalinilic acid, followed by esterification to yield 4-nitro-methylphenidate ((±)-**4.39**) (Scheme 5.7). However, these acidic reaction conditions resulted in a loss of the desired *threo* stereochemistry, generating a mixture of inseparable *erythro*- and *threo*-4-nitro-methylphenidate diastereomers ((±)-**5.10** and (±)-**4.39**). In order to confirm this undesirable epimerization, the mixture of *erythro*- and *threo*- nitro diastereomers was subjected to nitro reduction to obtain a mixture of *erythro*- and *threo*-4-amino-methylphenidate diastereomers ((±)-**5.11** and (±)-**4.36**), whose individual literature ^{1}H NMR data was available for analytical comparison (Deutsch *et al*., 1996). Alternatively, global hydrolysis of 4-amino-*N*-benzoyl-methylphenidate ((±)-**3.26**) followed by esterification also resulted in a mixture of *erythro*- and *threo*-4-amino-methylphenidate diastereomers ((±)-**5.11** and (±)-**4.36**), wherein once again, undesirable epimerization was

confirmed by comparing ^{1}H NMR data to that known in the chemical literature (Deutsch *et al*., 1996).

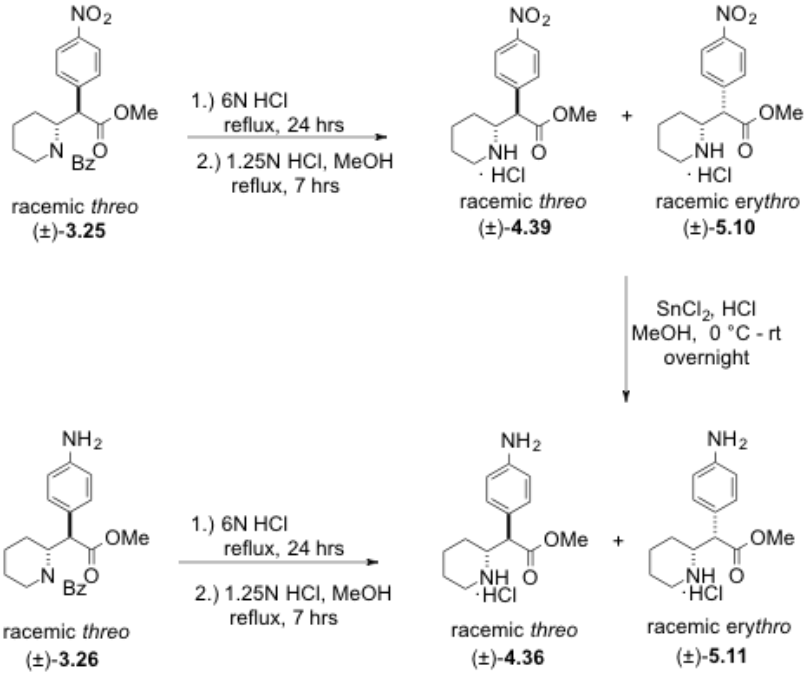

Scheme 5.7. Attempted synthesis of racemic *threo*-4-nitro or 4-amino-methylphenidate leads to epimerization and inseparable diastereomeric mixtures under acidic reaction conditions.

Another potential approach to access racemic *threo*-4-nitro-methylphenidate ((±)-**4.39**) is by nitration of ritalinilic acid ((±)-**5.12**) followed by esterification as previously reported by Deutsch *et al*., 1996 (Scheme 5.8). This attempted synthesis began with acidic hydrolysis of racemic *threo*-methylphenidate ((±)-**1.18**) to provide ritalinilic acid ((±)-**5.12**). Racemic *threo*-ritalinilic acid ((±)-**5.14**) was then subjected to nitration and esterification to provide a mixture of racemic *threo*-nitro-methylphenidates in 50% yield over three steps. In particular, the nitration reaction in this route resulted in formation of an undesirable positional isomer, *i.e.*, *threo*-3-nitro-ritalinilic acid ((±)-**5.14**) (10-20% based on ^{1}H NMR), alongside the desired *threo*-4-nitro-ritalinilic acid ((±)-**5.13**). All attempts to purify the desired *threo*-4-nitro-methylphenidate ((±)-**4.39**) from the

undesirable positional isomer proved futile given their similar retention times during column chromatography and solubility in various solvent systems for attempted recrystallization. As a result, synthesis of target compound racemic *threo*-4-azido-3-iodo-methylphenidate using methylphenidate as a starting material was abandoned in pursuit of alternative synthetic strategy.

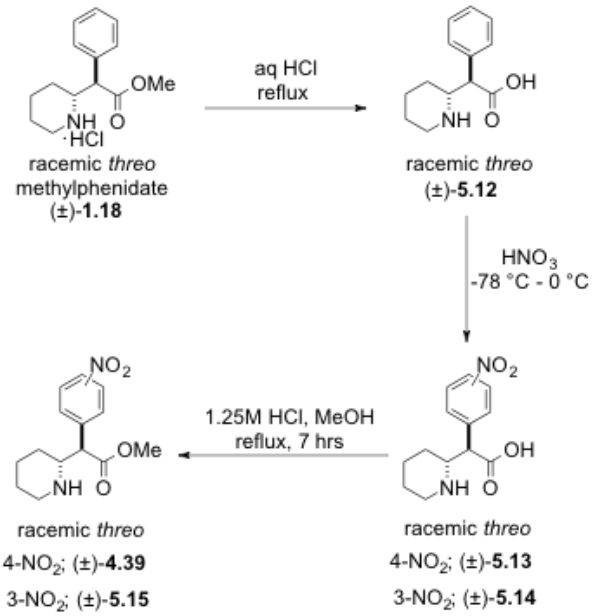

Scheme 5.8. Attempted synthesis of *threo*-4-nitro-methylphenidate *via* nitration of ritalinic acid leads to an inseparable mixture of positional nitro isomers.

Ultimately, application of synthetic methodology previously developed (Axten *et al*., 1998 and Gutman *et al*., 2004) for the synthesis of racemic *threo*-methylphenidate (see Scheme 3.2) proved successful for the synthesis of target photoprobe racemic *threo*-4-azido-3-iodo-methylphenidate (Scheme 5.9). Ketoamide **5.17** was initially prepared in 91% yield from commercially available nitro ester **5.16** by treatment with piperidine in ethanol. Tosylhydrazone **5.18** was then generated in 59% yield by allowing ketoamide **5.17** to react with *p*-toluenesulfonyl hydrazide under refluxing acidic ethanol conditions. Next, utilization of Aliquat 336® as a phase transfer catalyst in refluxing toluene under

basic conditions provided α-diazo amide **5.19** in 95% yield, which subsequently underwent thermal cyclization to provide a diastereomeric mixture of racemic *threo*- and *erythro*-β-lactams. In turn, recrystallization from Et_2O provided diastereomerically pure racemic *threo*-β-lactam (±)-**5.20** as the major product in moderate yield (53% yield from **5.19**). *threo*-β-Lactam (±)-**5.20** was then converted to (±)-*threo*-4-nitromethylphenidate ((±)-**4.39**) in quantitative yield by ring-opening with methanol under acidic conditions.

It should be noted that the synthesis of racemic *threo*-4-nitro-methylphenidate ((±)-**4.39**) *via* Scheme 5.9 definitively sets the position of the nitro functional group *via* starting keto-ester **5.16**. In turn, nitro reduction of racemic *threo*-4-nitro-methylphenidate yielded aniline (±)-**4.36** in moderate yield (61%), followed by subsequent iodination and azidization using previously reported procedures (Zou *et al*., 2001) provided target probe (±)-**4.35**. All (±)-*threo*-methylphenidate analogs *via* this synthetic methodology were determined to be ≥95% diastereomerically pure by ^{1}H NMR upon comparison to the known data for enantiomerically pure *threo*- and *erythro*-methylphenidates and their aromatic ring-substituted derivatives (Thai *et al*., 1998). This particular synthetic strategy also provided aniline intermediate (±)-**4.36** as a valuable synthetic precursor to a radio-iodinated version of target probe (±)-**4.35** synthesized *via* a collaborator of the Lapinsky group, Dr. John Lever (University of Missouri-Columbia; see Appendix, Section A.1).

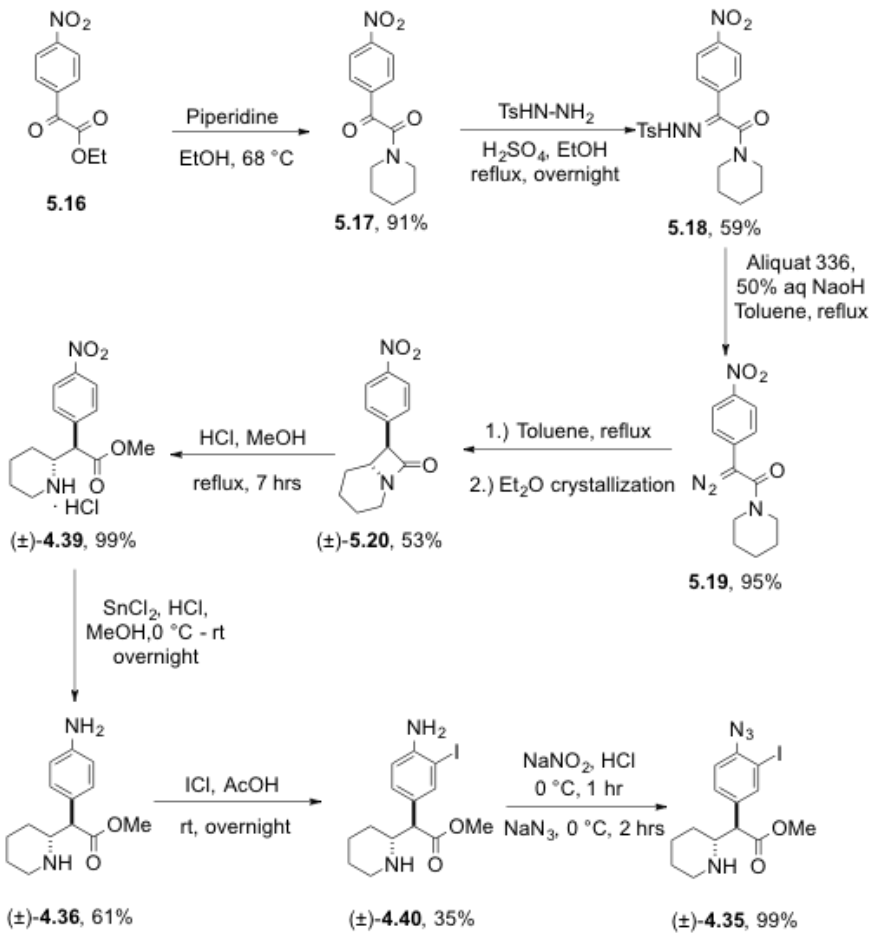

Scheme 5.9. Synthesis of racemic *threo*-4-azido-3-iodo-methylphenidate as a compact DAT photoprobe by applying methodology previously developed by Axten *et al*., 1998 and Gutman *et al*., 2004.

5.2. Synthesis of Citalopram-Based Photoprobes Suitable for Serotonin Transporter Structure-Function Studies

As previously discussed in Section 4.7, a series of SSRI-based photoprobes was desired in order to map the binding sites and poses of these clinically relevant drugs within their major target protein, the serotonin transporter (SERT). In particular, this dissertation focused on the well-known SSRI (±)-citalopram ((±)-**1.11**, Celexa) and its eutomer, escitalopram ((*S*)-**1.11**), as the enantiomers of citalopram are proposed to interact at unique binding sites within the serotonin transporter (Chen *et al*., 2005).

Additionally, previous SAR studies of citalopram analogs (*e.g.*, Banala *et al.*, 2013; Kumar *et al.*, 2014) indicate a number of structural positions or features that lead to high SERT binding affinities, thus potentially aiding in rational photoprobe design from a ligand-based perspective.

5.2.1. Synthesis of Racemic and (*S*)-Citalopram-Based Photoprobes for Serotonin Transporter Structure-Function Studies That Contain a Clickable Benzophenone-Terminal Alkyne Labeling Motif

As previously discussed in Section 4.7.1, photoprobe (±)-**4.44** was rationally designed based on the success of a previous photoprobe containing an identical benzophenone-terminal alkyne labeling motif and established SAR for 5-substituted analogs of (±)-citalopram. In particular, the synthesis of target (±)-citalopram-based photoprobe (±)-**4.44** was envisioned *via* coupling of amino citalopram analog (±)-**5.21** (Banala *et al.*, 2013) with benzophenone carboxylic acid **5.22** (Van Scherpenzeel *et al.*, 2009) (Scheme 5.10).

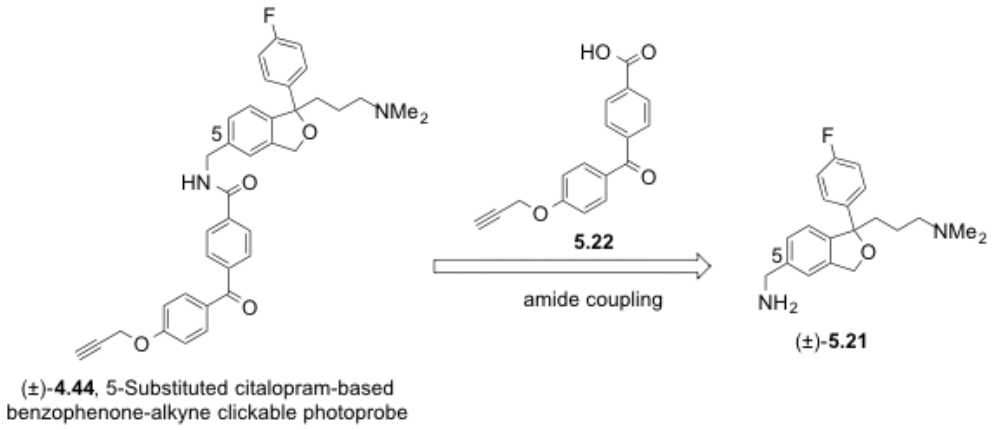

Scheme 5.10. Proposed retrosynthesis of a citalopram-based SERT photoprobe containing a benzophenone photoreactive group and a terminal alkyne click chemistry handle.

Using a previously described literature procedure (Van Scherpenzeel *et al*., 2009), initial synthetic attempts towards obtaining carboxylic acid **5.22** began with propargylation of phenol (Scheme 5.11). However, this previously described work proved troublesome, as attempted Friedel-Crafts acylation of propargyl ether **5.24** with terepthaloylchloride (**5.25)** resulted in an inseparable mixture of desired benzophenone-alkyne carboxylic acid **5.22** and terepthalic acid (**5.26)** (based on ^{1}H NMR) as an impurity.

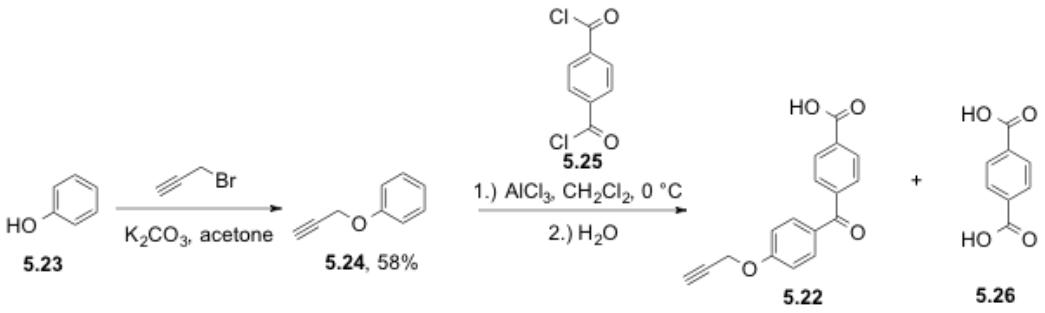

Scheme 5.11. Attempted synthesis of benzophenone-alkyne carboxylic acid **5.22** according to Van Scherpenzeel *et al*., 2009.

In order to avoid terepthalic acid (**5.26**) as an inseparable, undesired impurity as previously noted, the synthesis towards benzophenone-alkyne carboxylic acid **5.22** was subsequently modified (Scheme 5.12). In this regard, the propargyl ether of phenol (**5.24**) was subjected to Friedel-Crafts acylation reaction with commercially available acid chloride **5.27** to generate a mixture of benzophenone positional isomers **5.28** and **5.29**. The desired *para*-substituted compound **5.28** was isolated *via* column chromatography in low yield (27%). Finally, ester **5.28** could be hydrolyzed to generate benzophenone-alkyne carboxylic acid **5.22** in quantitative yield.

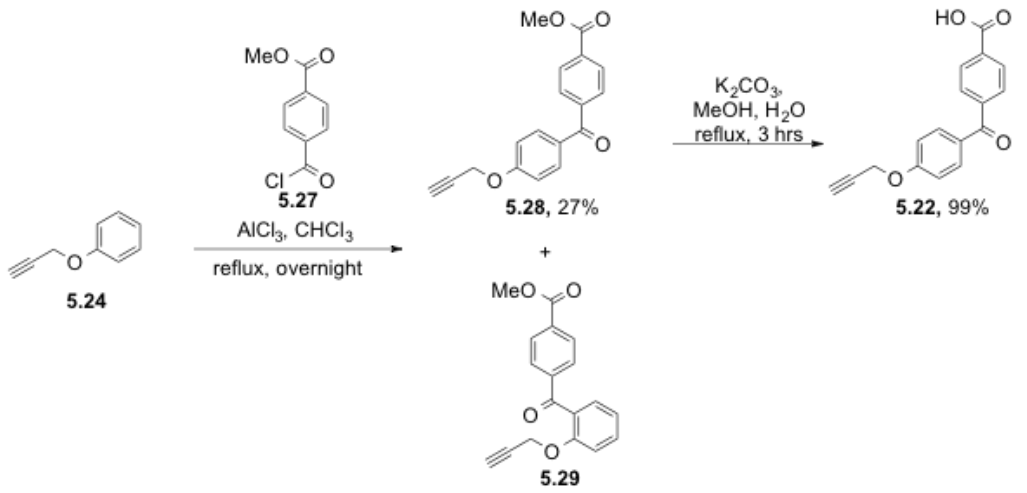

Scheme 5.12. Small-scale synthesis of benzophenone-alkyne carboxylic acid **5.22** *via* Friedel-Crafts acylation of 4-(methoxycarbonyl)benzoyl chloride.

It should be noted that the chemistry depicted in Scheme 5.12 was not particularly useful for generating large quantities of desired carboxylic acid **5.22**, principally due to difficulty separating **5.28** from positional isomer **5.29**. As a result, a previously reported synthetic protocol (Bandyopadhyay and Bong, 2011) was slightly modified in order to synthesize benzophenone-alkyne carboxylic acid **5.22** large quantities (Scheme 5.13). This synthesis began with Friedel-Crafts acylation of anisole using mono-methylterepthalate (**5.30**) and methanesulfonic anhydride in order to obtain 72 % yield of benzophenone **5.32** (Wilkinson, 2011), which could easily be isolated from any positional isomers formed *via* filtration. Benzophenone **5.32** was then demethylated and propargylated to obtain methyl ester **5.28** in 87% yield over two steps. Subsequently, carboxylic acid **5.22** was accessed in quantitative yield by ester hydrolysis using lithium hydroxide.

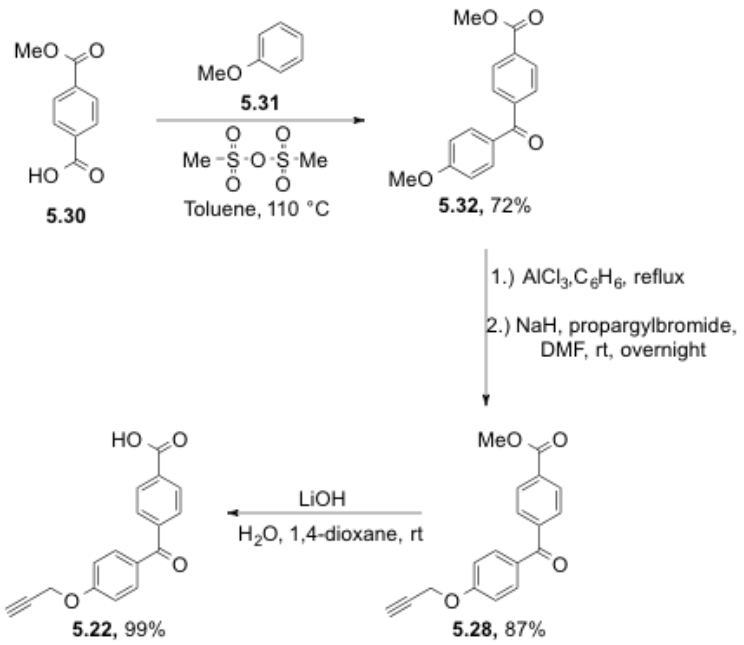

Scheme 5.13. Large-scale synthesis of benzophenone-alkyne carboxylic acid **5.22** starting from anisole.

With benzophenone-alkyne carboxylic acid **5.22** in hand, attention was turned to generating **5.21** as the desired primary amine coupling partner needed for synthesis of (±)-citalopram-based photoprobe (±)-**4.44** (Scheme 5.14). Initially, the nitrile functional group of (±)-citalopram was reduced using lithium aluminium hydride to provide primary amine (±)-**5.21** in 98% yield (Banala *et al*., 2013). This amine was then coupled with carboxylic acid **5.22** using 1-ethyl-3-(3-dimethylaminopropyl)carbodiimide (EDC) and hydroxybenzotriazole (HOBT) to provide target citalopram-based photoprobe (±)-**4.44** in moderate yield (63%).

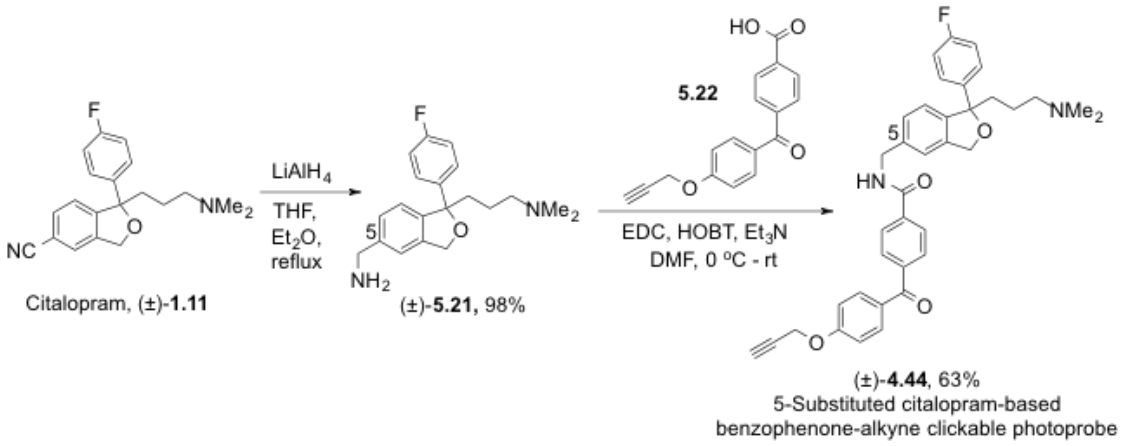

Scheme 5.14. Synthesis of a (±)-citalopram-based photoprobe containing a benzophenone as a photoreactive functional group and a terminal alkyne as a click chemistry handle.

In turn, (*S*)-citalopram-based photoprobe (*S*)-**4.44**, which contains the same benzophenone-alkyne labeling motif as found in the racemic version (*i.e.*, (±)-**4.44**), was synthesized in a similar manner (Scheme 5.15). Initially, (*S*)-citalopram was subjected to nitrile reduction in order to obtain enantiomerically pure amine (*S*)-**5.21** (Kumar *et al*., 2014). Subsequent EDC and HOBT coupling of enantiomerically pure amine (*S*)-**5.21** with carboxylic acid **5.22** provided target photoprobe (*S*)-**4.44** in good yield (80%).

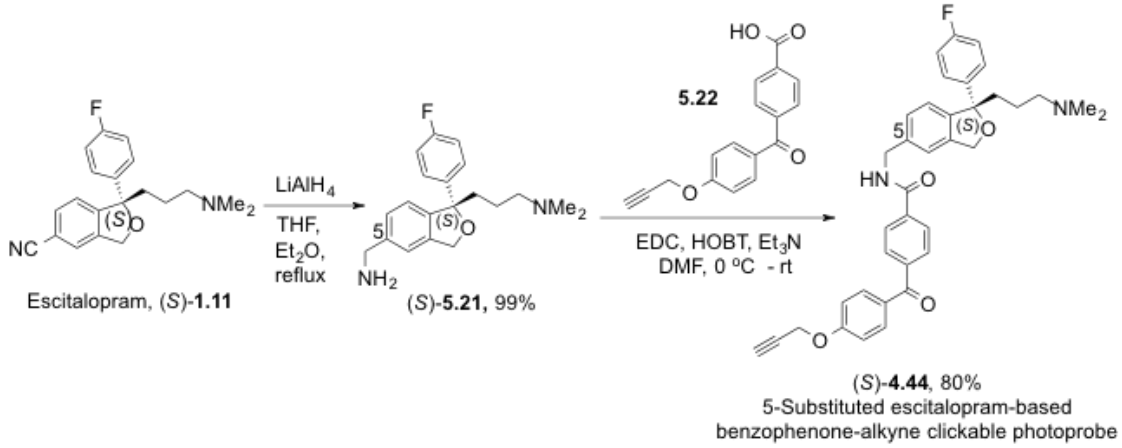

Scheme 5.15. Synthesis of an escitalopram-based photoprobe containing a benzophenone as a photoreactive functional group and a terminal alkyne as a click chemistry handle.

Attention was next turned to escitalopram *N*-substituted benzophenone-alkyne clickable photoprobe (*S*)-**4.47** in order systematically map the (*S*)-citalopram binding site within SERT *via* BEProFL. The rational design of target probe (*S*)-**4.47** was previously described in Section 4.7.1. In particular, initial methodology for the synthesis target probe (*S*)-**4.47** was established by successful synthesis of escitalopram *N*-substituted benzophenone analog (*S*)-**4.46** (Scheme 5.16). In this regard, *N*-desmethylation of escitalopram was initially carried out according to a previously established protocol (Jin *et al*., 2007) to generate (*S*)-desmethylcitalopram ((*S*)-**5.33**). In brief, escitalopram was treated with 1-chloroethylchloroformate to generate a carbamate, which was further subjected to methanolysis to obtain (*S*)-desmethylcitalopram ((*S*)-**5.33**) in 30 % yield over three steps. In particular, the methanolysis also hydrolysed a small amount of the nitrile functional group to a methyl ester, which was separated by converting this ester into a carboxylate salt by treatment with sodium hydroxide. Subsequent *N*-alkylation (conditions adapted from Moore *et al.*, 2005) of (*S*)-desmethylcitalopram with commercially available benzylbromide **5.34** gave escitalopram analog (*S*)-**4.46** in moderate yield (59%).

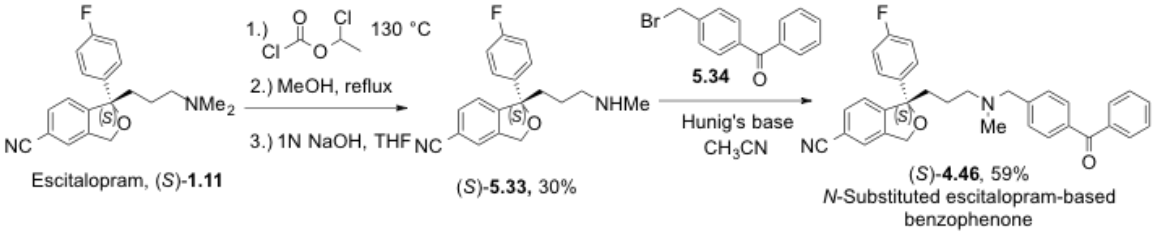

Scheme 5.16. Synthesis of a *N*-substituted escitalopram analog containing a benzophenone photoreactive group.

Towards synthesizing a *N*-substituted escitalopram-based benzophenone-alkyne clickable SERT photoprobe *via* this *N*-alkylation methodology, mesylate **5.38** was

desired and pursued as a proposed key synthetic building block (Scheme 5.17). In this regard, the ketone functional group in previously synthesized benzophenone alkyne **5.28** (see Scheme 5.13) was initially protected as a ketal using ethylene glycol, 1,2-bis(trimethylsiloxy)ethane, and a catalytic amount of *p*-toluenesulfonic acid (conditions adapted from Lippert *et al*., 2009). The ester within benzophenone alkyne **5.35** was then reduced to benzyl alcohol **5.36** using lithium aluminum hydride. The ketal was subsequently converted back to the ketone under acidic hydrolysis conditions to provide benzophenone **5.37** in moderate yield (67%). Finally, the benzyl alcohol was converted into a mesylate leaving group (conditions adapted from Oyelere *et al*., 2009).

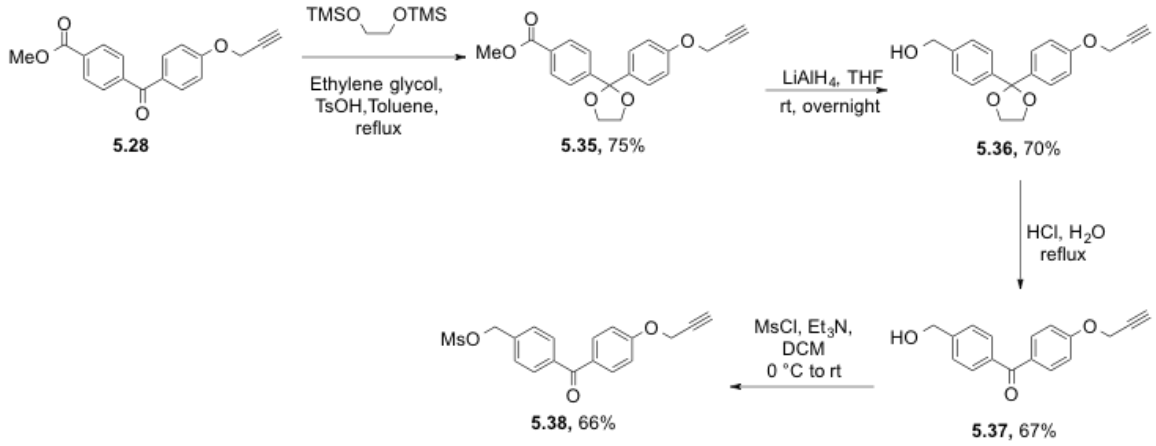

Scheme 5.17. Synthesis of a benzophenone-alkyne mesylate required for the synthesis of a *N*-substituted (*S*)-citalopram-based photoprobe.

With benzophenone-alkyne mesylate **5.38** in hand, the synthesis of *N*-substituted benzophenone-alkyne clickable SERT photoprobe (*S*)-**4.47** was achieved analogous to methodology previously described in Scheme 5.16 for the synthesis of escitalopram benzophenone analog (*S*)-**4.46**. In particular, *N*-alkylation of (*S*)-desmethylcitalopram (synthesized as described in Scheme 5.16) with benzophenone mesylate **5.38** provided target probe (*S*)-**4.47** in relatively low yield (31%) (Scheme 5.18).

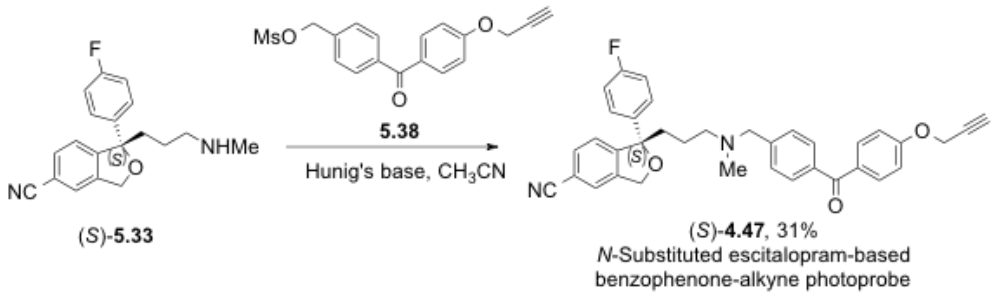

Scheme 5.18. Synthesis of a *N*-substituted escitalopram-based benzophenone-alkyne clickable photoprobe for SERT structure-function studies.

5.2.2. Synthesis of a Diazido-Based Escitalopram Analog as a Potential Photoprobe for Serotonin Transporter Structure-Function Studies

As previously discussed in Section 4.7.2, target photoprobe (*S*)-**4.50** was rationally designed based on the success of a well-known aryl diazido photoaffinity labeling motif and well-established citalopram SAR indicating a wide variety of 5-substituted escitalopram analogs retain high SERT binding affinity. In particular, synthesis of escitalopram-based diazide photoprobe (*S*)-**4.50** was envisioned by coupling previously described amino citalopram analog (*S*)-**5.21** with 3-azido-5-(azidomethyl)benzoic acid (**5.39**) (Scheme 5.19).

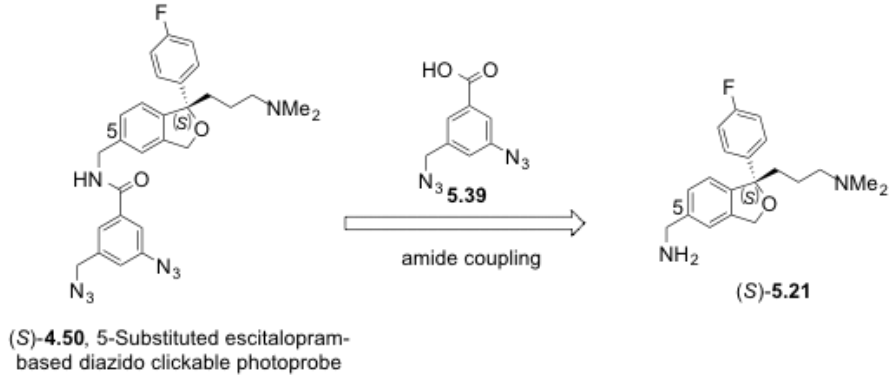

Scheme 5.19. Proposed retrosynthesis of an escitalopram-based diazido clickable photoprobe for SERT structure-function studies.

With this retrosynthesis in mind, the synthesis of 3-azido-5-(azidomethyl)benzoic acid (**5.39**) was pursued according to that previously described (Neelarapu *et al*., 2011) (Scheme 5.20). This synthesis was initiated from a commercially available dimethyl-5-amino-isophthalate (**5.40**), which was subjected to mono-reduction using lithium borohydride to provide amino ester **5.41** in 53% yield. Aniline **5.41** was then converted to the azide **5.42** using *t*-BuONO and TMS-N_3. Next, the one step conversion of benzyl alcohol **5.43** to the corresponding aliphatic azide was performed using bis(2,4-dichlorophenyl)chlorophosphate, DMAP, and NaN_3. Subsequent hydrolysis of ester **5.43** under basic conditions then provided diazido-acid **5.39** in near quantitative yield.

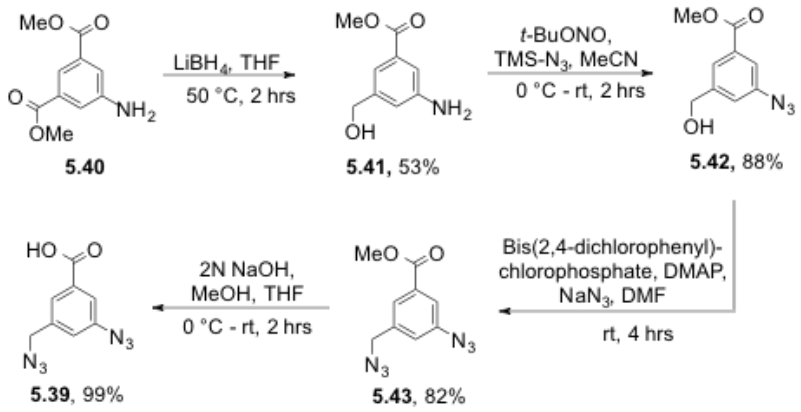

Scheme 5.20. Synthesis of 3-azido-5-(azidomethyl)benzoic acid as a key building block for generating an escitalopram-based diazido SERT photoprobe.

With diazido carboxylic acid **5.43** in hand, coupling with 5-aminomethyl substituted (*S*)-citalopram ((*S*)-**5.21**) (see Scheme 5.14 for synthesis) was performed using EDC and HOBT to provide target photoprobe (*S*)-**4.50** in 75% yield (Scheme 5.21).

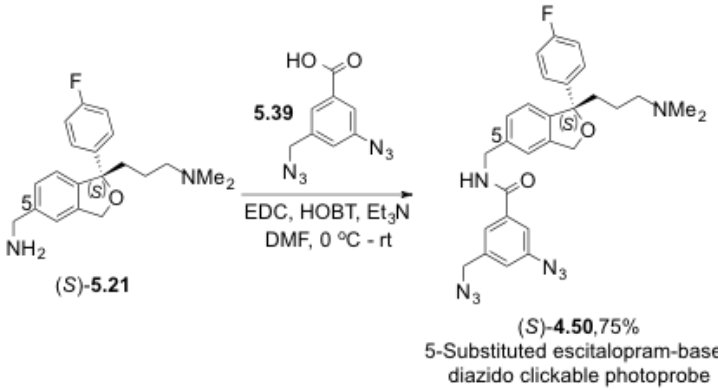

Scheme 5.21. Synthesis of an escitalopram-based diazido photoprobe for SERT structure-function studies.

5.2.3. Synthesis of an Escitalopram-Based Photoaffinity Ligand for Serotonin Transporter Structure-Function Studies Containing the Traditional 4-Azido-3-Iodo Photoaffinity Labeling Motif

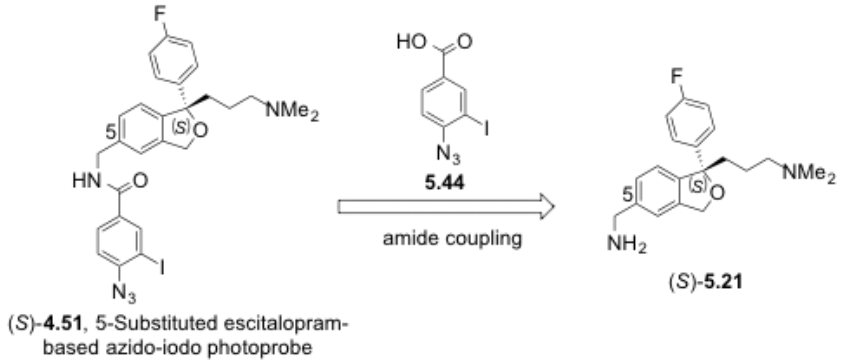

Scheme 5.22. Proposed retrosynthesis of an escitalopram-based photoprobe containing a traditional 4-azido-3-iodo photoaffinity labeling motif.

As previously discussed in Section 4.7.3, target photoprobe (*S*)-**4.51** was rationally designed based on previously established citalopram SAR with respect to SERT and a number of successful DAT structure-function studies employing photoprobes that contain a traditional 4-azido-3-iodo photoaffinity labeling motif. In particular, synthesis of target (*S*)-citalopram-based photoprobe (*S*)-**4.51** containing the traditional 4-azido-3-iodo photoaffinity labeling motif was envisioned by coupling amino

escitalopram analog (*S*)-**5.21** with 4-azido-3-iodobenzoic acid (**5.44**) (Scheme 5.22). With this retrosynthesis in mind, synthesis of 4-azido-3-iodobenzoic acid (**5.44**) was pursued according to that previously described in the chemical literature (Shu *et al*., 1996) (Scheme 5.23). In particular, monoiodination of commercially available methyl 4-aminobenzoate (**5.45**) using N-iodosuccinimide provided iodoester **5.46** in 67 % yield. Subsequent conversion of aniline **5.46** to the diazonium salt followed by displacement with NaN_3 provided azide **5.47** in 40% yield. Final hydrolysis of ester **5.47** under basic conditions provided 4-azido-3-iodobenzoic acid (**5.44**) in near quantitative yield.

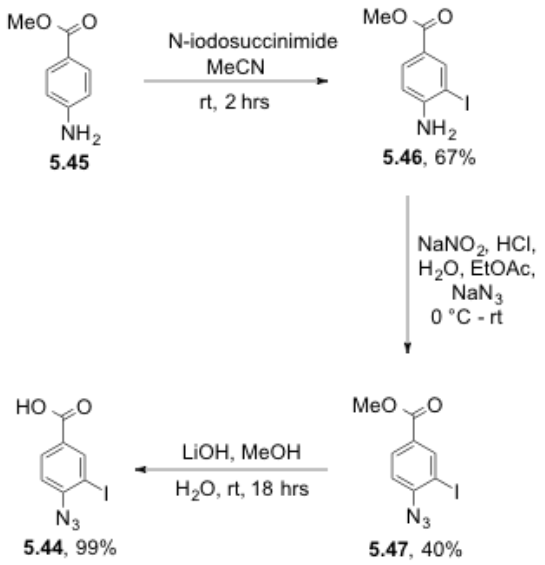

Scheme 5.23. Synthesis of 4-azido-3-iodobenzoic acid as a key building block for synthesizing an escitalopram-based azido-iodo SERT photoprobe.

Analogous to methodology previously described for the synthesis of amide-containing citalopram analogs, 5-aminomethyl substituted (*S*)-citalopram ((*S*)-**5.21**) was coupled with 4-azido-3-iodobenzoic acid (**5.44**) using EDC and HOBT to give target photoprobe (*S*)-**4.51** in 67% yield (Scheme 5.24). In particular, photoprobe (*S*)-**4.51** retained high SERT binding affinity (K_i = 3.45 ± 2.04 nM) when compared to

escitalopram (K_i = 1.77 ± 1.14 nM) as a lead compound, thus justifying further development of this probe into a radioiodinated version for SERT photoaffinity labeling experiments. In this regard, tri-*n*-butyl stannyl analog (*S*)-**5.48** was synthesized as a precursor to (*S*)-[^{125}I]-**4.51**. Specifically, azido-iodo photoprobe (*S*)-**4.51** was subjected to Pd-catalyzed Stille coupling with bis(tributyltin) to provide tri-*n*-butyl stannyl derivative (*S*)-**5.48** in 52% yield. Dr. John Lever (University of Missouri-Columbia) then synthesized (*S*)-[^{125}I]-**4.51** *via* a radio-iodo destannylation protocol (see Appendix, Section A.2).

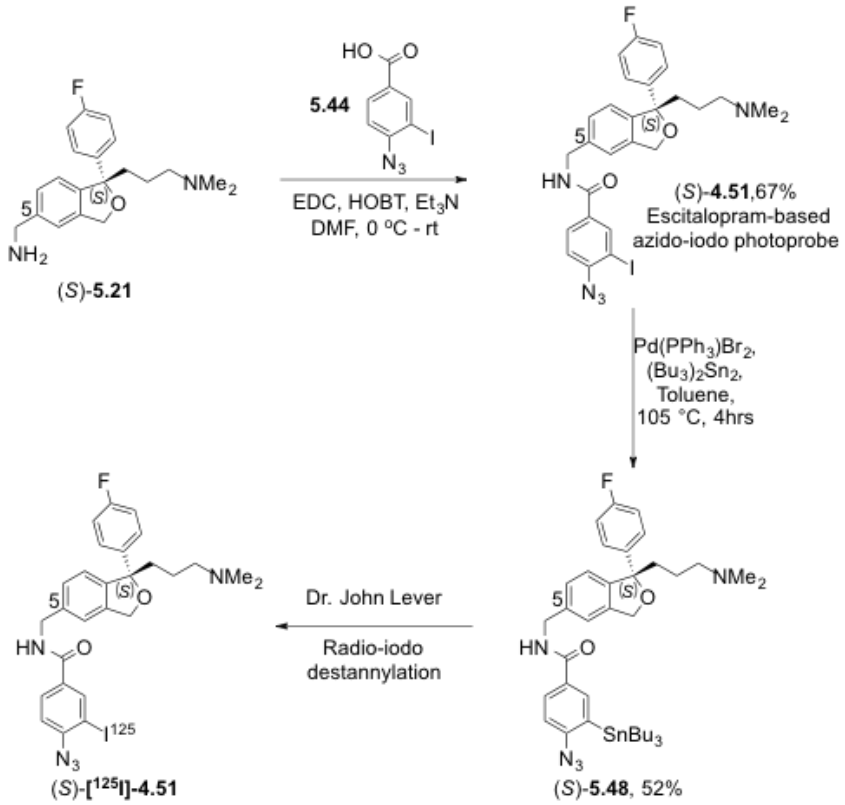

Scheme 5.24. Synthesis of escitalopram-based azido-iodo photoprobe (*S*)-[^{125}I]-**4.51** for SERT structure-function studies.

5.3. Development of a Protocol for Serotonin Transporter Tandem Photoaffinity Labeling-Bioorthogonal Conjugation Using Citalopram-Based Clickable Photoprobes

As previously discussed in Section 4.7, a strategy towards potentially understanding the 3D structural features of SERT is expected to be achieved by developing and applying citalopram-based SSRI photoprobes in a BEProFL experimental approach. Specifically, application of the BEProFL approach to SERT is proposed to feature rational coupling of proteomic results from photoaffinity labeling of SERT with SSRI-based photoprobes and SERT computational homology modeling, towards the goal of mapping the binding sites and poses of SSRIs within their major drug target (*i.e.*, SERT). In particular, this experimental approach is expected to validate and refine current SERT computational homology models for future drug discovery and development.

Therefore, in order to practically pursue the BEProFL experimental approach with respect to SERT, (±)-citalopram and (*S*)-citalopram as SSRIs were functionalized with a photoreactive group (PRG) (*i.e.*, a benzophenone or an aryl azide) and a reporter group (RG) (*i.e.*, a terminal alkyne or an aliphatic azide as click chemistry handles, or ^{125}I) as previously described in this dissertation. In turn, the next research goal of this dissertation was to develop a practical protocol for SERT tandem photoaffinity labeling-bioorthogonal conjugation by employing clickable high affinity citalopram-based photoprobes.

5.3.1. Initial Attempts of SERT Tandem Photoaffinity Labeling-Bioorthogonal Conjugation Using a Racemic Citalopram-Based Photoprobe Containing a Benzophenone-Alkyne Structural Motif

As previously described in Section 5.2.1, 5-substituted citalopram-based benzophenone alkyne photoprobe (±)-**4.44** was synthesized as part of this research dissertation for BEProFL purposes. Given citalopram-based photoprobe (±)-**4.44** displayed very high SERT binding affinity (K_i = 4.3 ± 3.5 nM) comparable to that of (±)-citalopram (K_i = 4.4 ± 1.3 nM), this compound was identified as a suitable candidate photoprobe for attempted SERT tandem photoaffinity labeling-bioorthogonal conjugation.

Initially, a protocol developed in Dr. Michael Cascio's lab (Duquesne University) was attempted to try and photolabel hSERT overexpressed in T-Rex 293 (HEK293) cells (Takayama and Sugio, 2011) (Scheme 5.25). Briefly, T-Rex 293 cells in phosphate buffer (25 mM potassium phosphate buffer, anti-proteolytic cocktail) were lysed using a dounce homogenizer (3 x 15 strokes at 4˚C) and ultra-centrifuged (100,000g, 45 min) to obtain the membrane fraction. This process was repeated twice in order to make sure all cells were lysed. The membrane fraction was then dispersed in phosphate buffer (25 mM potassium phosphate buffer), to which (±)-citalopram photoprobe (±)-**4.44**, dissolved in DMSO (concentration: 500 µM), was added. The mixture was then transferred to quartz cuvettes and exposed to UV light (350-450 nm) for 20 minutes (2 X 10 minutes on ice) with 5 minutes cooling in between. Following this covalent ligation step, the mixture was ultra-centrifuged to remove any excess probe that was not covalently labeled to the proteome using phosphate buffer. Later, the membrane fraction was dispersed in

phosphate saline buffer (PBS) and reacted with biotin azide in the presence of $CuSO_4$ and TCEP as a click chemistry reaction. Excess click reagents were then removed *via* ultracentrifugation and the membrane fraction was solubilized in 50 mM Tris containing 0.1% Triton. Samples were then subsequently analyzed using a Western blot to detect biotinylated proteins *via* streptavidin IR dye (Figure 5.1). Additionally, the solubilized membrane fraction was also subjected to avidin column chromatography in an attempt to purify biotinylated proteins. Proteins on the avidin resin were digested using trypsin and the eluents were treated with C-18 ziptips for mass spectrometry sample preparation. In particular, mass spectrometry data indicated that there were polymers peaks, and as a result for subsequent experiments, trypsin digestion on avidin beads was avoided. Instead, mass spectrometry samples were prepared by excising bands from an SDS-PAGE gel and trypsin was used to digest the protein in the gel.

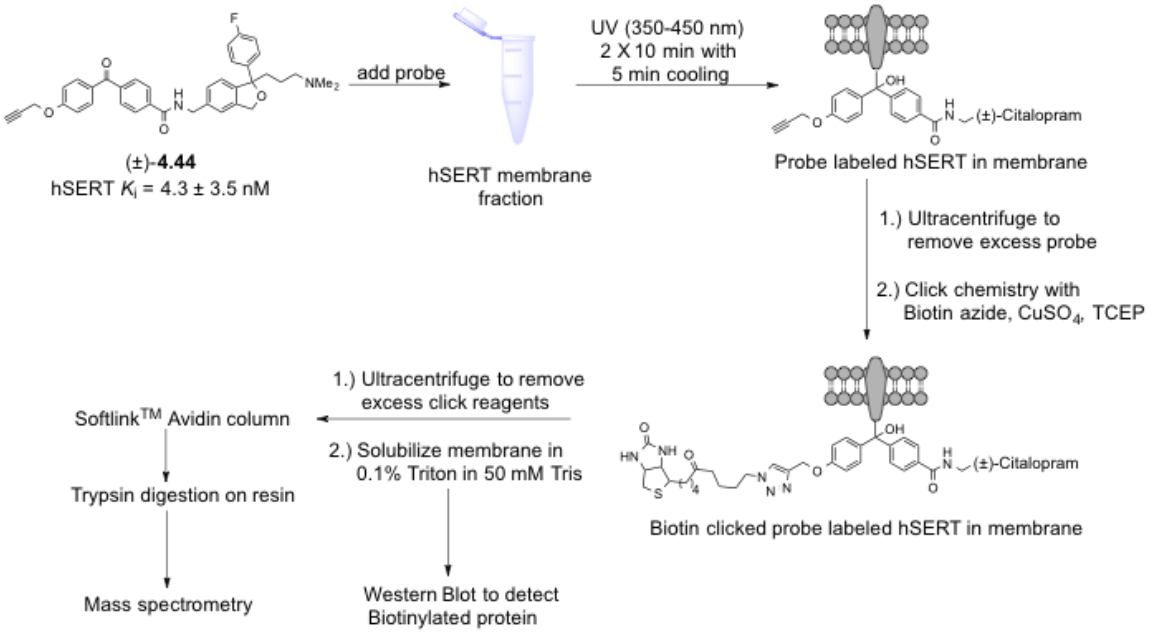

Scheme 5.25. Initial attempt of SERT tandem photoaffinity labeling-bioorthogonal conjugation using (±)-citalopram based photoprobe (±)-**4.44**.

As described, samples from Scheme 5.25 were analyzed by Western blot to detect biotinylated proteins *via* a streptavidin IR dye (Figure 5.1). Although a biotinylated protein band was detected in lane 1 (hSERT labeled with photoprobe (±)-**4.44** and click reacted with biotin azide), unfortunately this band did not match the molecular weight of hSERT (70 kDa). In particular, it was assumed that hSERT was present as its oligomer (*i.e.*, a higher molecular weight band) instead of the monomer. This higher molecular weight band was subsequently excised in order to generate samples for mass spectrometry analysis.

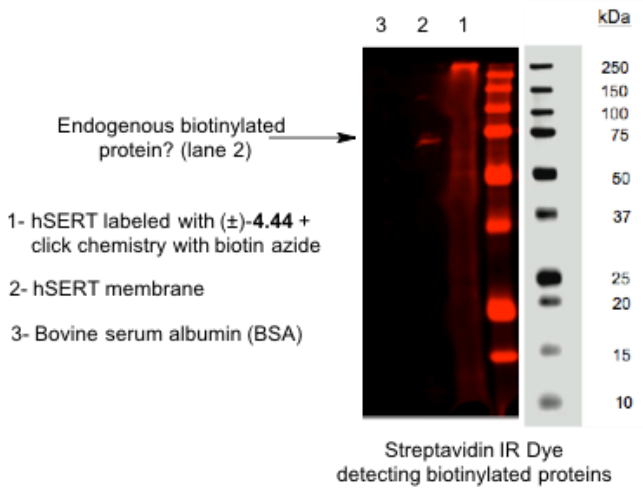

Figure 5.1. Initial results of attempted SERT tandem photoaffinity labeling-bioorthogonal conjugation using (±)-citalopram based photoprobe (±)-**4.44**. These results indicate that the T-Rex cells used in the experiment express endogenously biotinylated proteins.

Careful observation from these experiments indicated that the negative control lane (*i.e.*, lane 2; hSERT membrane without any photolabeling) showed some biotinylated proteins. This prompted subsequent utilization of an hSERT antibody for simultaneous detection of hSERT (*i.e.*, in addition to potential probe-labeled proteins) in future Western blots, such that other endogenously biotinylated proteins were not excised for mass spectrometry analysis.

5.3.2. Attempted Adaptation of a Protocol Used for DAT Photoaffinity Labeling Experiments to SERT Tandem Photoaffinity Labeling-Bioorthogonal Conjugation

Since multiple attempts using the protocol described in Scheme 5.25 did not lead to successful photoaffinity labeling or detection of hSERT *via* Western blot, the next strategy attempted was to adapt a protocol that gave successful results in DAT photoaffinity labeling using (±)-4-azido-3-iodo-methylphenidate ((±)-**4.35**; Lapinsky, *et al*., 2012) as a photoprobe (Scheme 5.26).

For this experimental protocol, the media was initially removed from the HEK-293 cells and the cells were subsequently washed with Krebs Ringer HEPES (KRH) buffer. Citalopram photoprobe (±)-**4.44** was then added to the cells in KRH buffer at two different concentrations (experiment 1a = 10 nM of photoprobe (±)-**4.44**; experiment 2a = 100 nM of photoprobe (±)-**4.44**). Competition experiments were also performed using escitalopram at a high concentration (1 µM) in the presence of photoprobe (±)-**4.44** (experiment 1b = 10 nM of photoprobe (±)-**4.44** + 1 µM escitalopram as a competitor; experiment 2b = 100 nM of photoprobe (±)-**4.44** + 1 µM escitalopram as a competitor). After incubating on ice for 1 hour, the six-well plate containing the HEK-293 cells was exposed to UV light (350-450 nm for 5 minutes). The KRH buffer with the probe was subsequently discarded and the cells were washed with KRH buffer. The cells were then collected in a microcentrifuge tube and lysed with RIPA buffer along with an anti-proteolytic cocktail. Specifically, the cell lysate was centrifuged at 14,000g for 15 minutes and the supernatant was transferred to a fresh microcentrifuge tube. The procedure was then modified as follows from the known DAT photoaffinity labeling

protocol, as photoprobe (±)-**4.44** contains a terminal alkyne instead of ^{125}I as a reporter group.

Specifically, the cell lysates were subjected to click chemistry reaction conditions by adding biotin azide, TBTA (tris[91-benzyl-1H-1,2,3-triazol-4-yl)methyl]amine), $CuSO_4$, and TCEP (tris(2-carboxyethy)phosphine hydrochloride) (Weerapana *et al*., 2007). After click chemistry, excess click chemistry reagents were removed by adding trichloroacetone/acetone (1:1) to the aforementioned reaction mixture followed by centrifuge for 5 min at 10,000g at 4˚C to pellet the protein (Koopmans *et al*., 2012). The resulting protein pellet was then solubilized in 50 mM Tris containing 0.1% Triton for analysis.

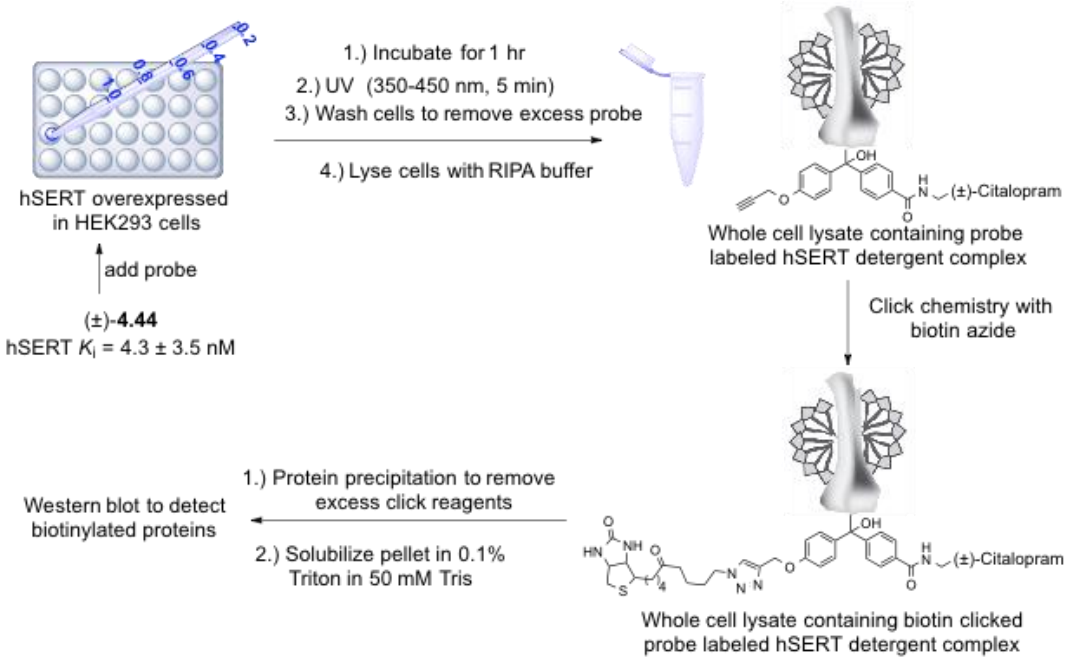

Scheme 5.26. Attempted adaptation of a known protocol from DAT photoaffinity labeling for attempted SERT tandem photoaffinity labeling-bioorthogonal conjugation using (±)-citalopram based photoprobe (±)-**4.44**.

Final samples from the experimental protocol highlighted in Scheme 5.26 were analyzed using Western blot to detect biotinylated proteins *via* a streptavidin IR dye (Figure 5.2). In particular, the Western blot indicated multiple bands of biotinylated proteins, and since these bands did not disappear with excess cold escitalopram present as a photoaffinity labeling competitor (*i.e.*, lanes 1b and 2b), these experimental results appear to indicate non-specific protein labeling. However, these results are not definitively conclusive, as an alternative possibility is that the whole cell lysate may contain a significant number endogenously biotinylated proteins. Simultaneously, similar experiments were carried out in other wells of the six-well plate using citalopram photoprobe (*S*)-**4.44**; however, similar results were obtained compared to that of the racemic version of the citalopram photoprobe.

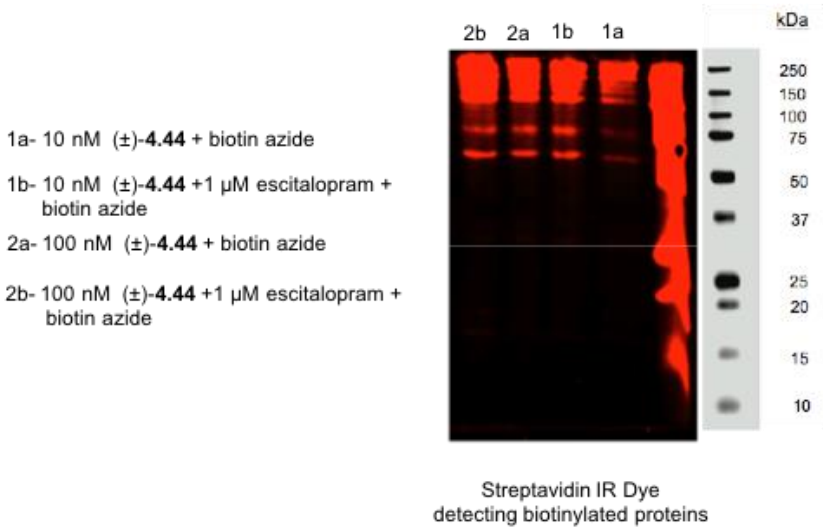

Figure 5.2. Potential results of non-specific labeling from attempted SERT tandem photoaffinity labeling-bioorthogonal conjugation using (±)-citalopram based photoprobe (±)-**4.44**.

In order to rule out the possibility of non-specific protein labeling, the protocol described in Scheme 5.26 was subsequently modified to incorporate a washing step prior to exposing the cells to UV light (lanes 1a and 1b, Figure 5.3). The rationale behind this

experimental modification was to keep only reversibly-bound probe in the binding pocket of SERT to be available for photoaffinity labeling, wherein washing away any excess photoprobe would be expected to reduce the likelihood of non-specific protein labeling. Appropriate control experiments were also performed by washing the cells after UV light exposure (lanes 2a and 2b, Figure 5.3). Unfortunately, the Western blot indicated that this attempted variation in experimental conditions did not result in any significant difference in terms of improved photoaffinity labeling (Figure 5.3).

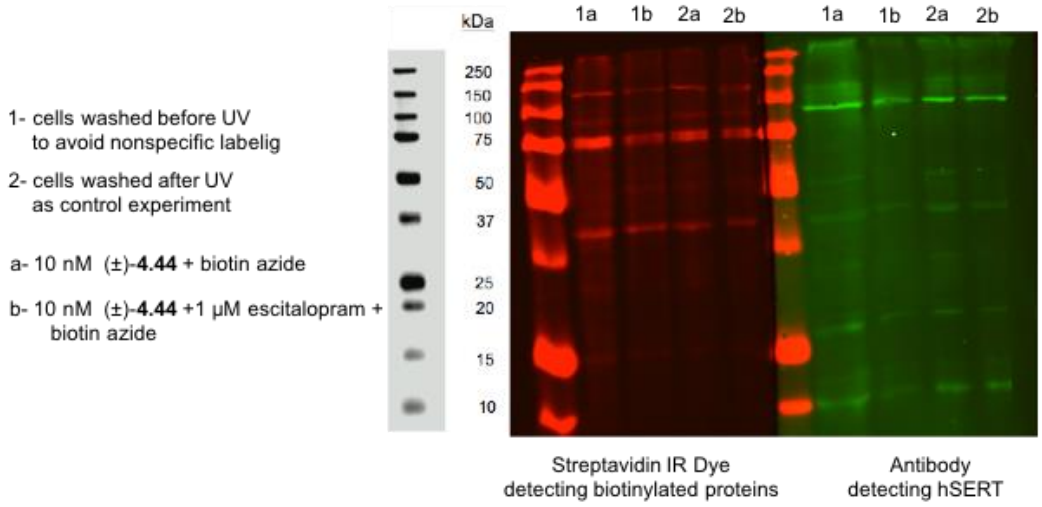

Figure 5.3. Results of attempted SERT tandem photoaffinity labeling-bioorthogonal conjugation using (±)-citalopram based photoprobe (±)-**4.44**. Results appear to indicate that the whole cell lysate contains numerous biotinylated proteins.

By comparing the bands detected by hSERT antibody (*i.e.*, detecting hSERT) to the bands detected by streptavidin IR dye (*i.e.*, detecting biotin) and previous results, it was concluded that the whole cell lysate has a significant amount of endogenously biotinylated proteins *versus* the membrane fraction alone. Even experiments utilizing citalopram photoprobe (*S*)-**4.44** indicated either non-specific protein labeling, or that photolabeled biotinylated protein would be very difficult to isolate from other endogenously biotinylated proteins present in the whole cell lysate. As a result,

subsequent photoaffinity labeling experiments from this point forward were modified to collect just the membrane fraction of lysed cells, instead of generating a whole cell lysate.

5.3.3. Adaptation of an Activity-Based Protein Profiling / Click Chemistry Protocol for Attempted SERT Tandem Photoaffinity Labeling-Bioorthogonal Conjugation

After learning that the whole cell lysate might contain numerous biotinylated proteins that could confound data interpretation, an experimental protocol outlined in Scheme 5.7 was subsequently implemented. This particular experimental protocol is based on well-established protocols developed for activity-based protein profiling and click chemistry for mass spectrometry analysis (Speers and Cravatt, 2009).

Specifically for this protocol, cells were initially grown to 90% confluency in a six well plate, washed with KRH buffer before photoaffinity labeling, followed by addition of fresh KRH buffer. To these cells, citalopram photoprobe (*S*)-**4.44** was added yielding a final concentration of 500 nM, and for competition experiments, (*S*)-citalopram was added to give a concentration of 10 μM. The cells were then incubated on ice for 1 hour and subjected to UV light (350-450 nm for 1 hour on ice) (Tantama *et al*., 2008). After photoaffinity labeling, the cells were then washed to remove excess probe, lysed, and then ultra-centrifuged in order to obtain the membrane fraction. The membrane fraction was then subsequently dissolved in PBS buffer containing 0.1% Triton X-100 in order to carry out the click chemistry reaction with biotin azide (Weerapana *et al*., 2007). In particular, the proteome sample was subjected to chloroform/methanol protein precipitation conditions in order to remove excess click reagents (Speers and Cravatt, 2009).

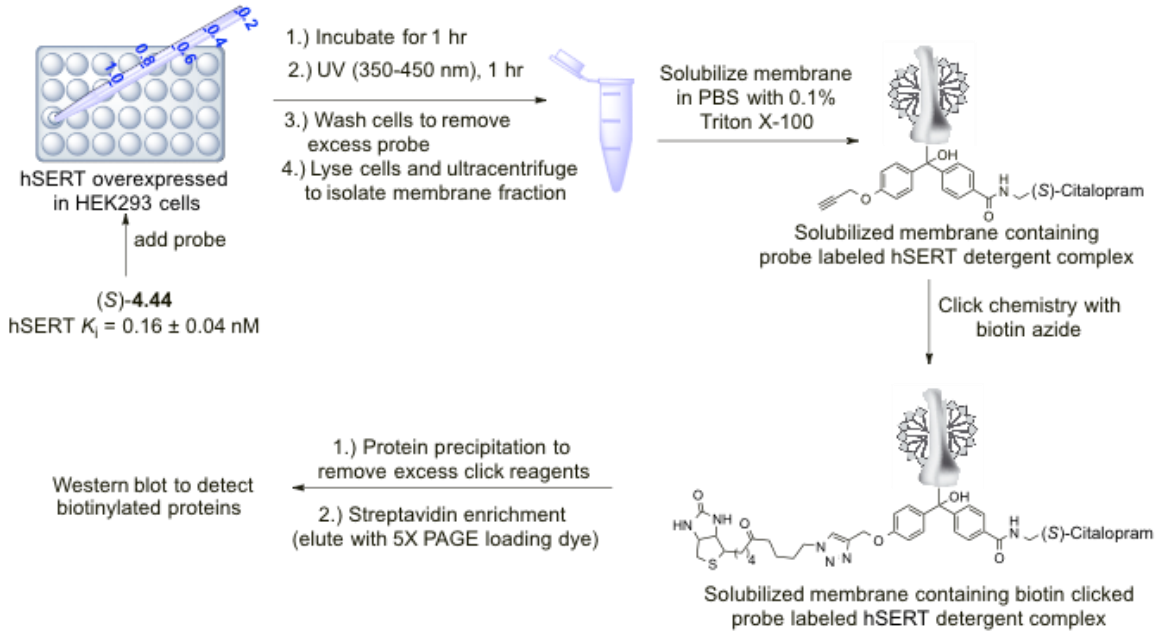

Scheme 5.27. Attempted activity-based protein profiling / click chemistry protocol for SERT tandem photoaffinity labeling-bioorthogonal conjugation.

The protein pellet from Scheme 5.27 in turn was resuspended in PBS with 2.5% SDS (sodium dodecyl sulfate) with the aid of heating and sonication, then the proteome sample was subjected to a streptavidin enrichment protocol in order to isolate biotinylated proteins (Speers and Cravatt, 2009). Specifically, the eluents from the streptavidin beads were analyzed by Western blot in order to detect biotinylated proteins *via* a streptavidin IR dye, and also hSERT antibody for confirmation of hSERT.

In particular for this experimental protocol, the eluents from the streptavidin resin (lanes 1a and 1b, Figure 5.4) did not show any bands corresponding to hSERT. Additionally, the bands being detected by hSERT antibody from samples unbound to streptavidin resin (lanes 2a and 2b, Figure 5.4) corresponded to a molecular weight below 50 kDa. As a result, experimental results from this attempted protocol in turn prompted

subsequent use of FLAG epitope within the SERT being used for detection in future photoaffinity labeling experiments (Section 5.2.4).

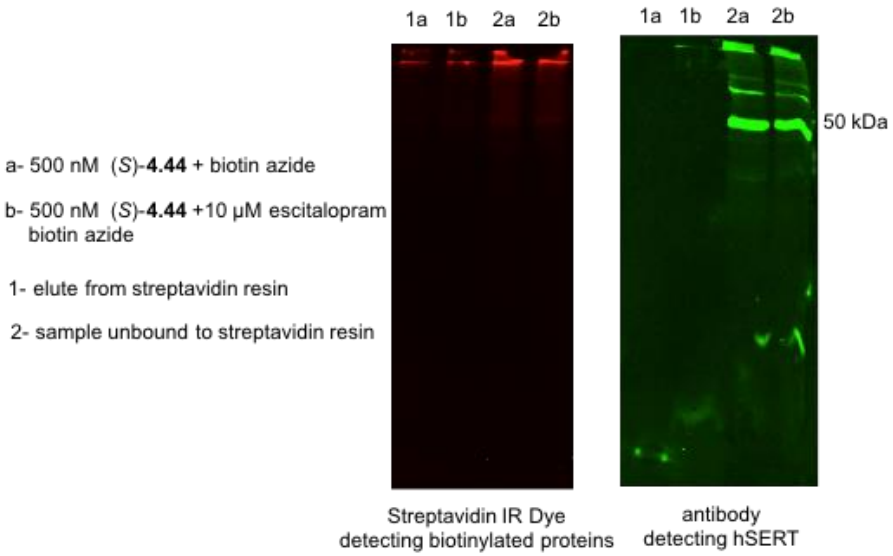

Figure 5.4. Results from applying an activity-based protein profiling / click chemistry protocol for attempted SERT tandem photoaffinity labeling-bioorthogonal conjugation.

5.3.4. Single-Step Affinity Chromatography Purification of hSERT Bearing a FLAG-Epitope Tag

It should be noted that the T-Rex (tetracycline inducible) HEK 293 cell line expressing hSERT being used for this part of the dissertation was developed using a synthetic human SERT gene produced by a PCR-based self-assembly method (Takayama and Sugio, 2011). Specifically, the synthetic DNA sequence corresponding to the human SERT gene was modified to include a FLAG-epitope tag, followed by two glycine spacer linkers, and a Tobacco Etch Virus (TEV) protease cleavage site just prior to the N-terminus of SERT (Figure 5.5). Subsequent overexpression of this modified hSERT was achieved by transfecting the expression vector pCDNA4TO-FLAG-gg-TEV-SERT into

the T-Rex HEK 293 cell line, followed by purification using anti-FLAG M2 antibody beads.

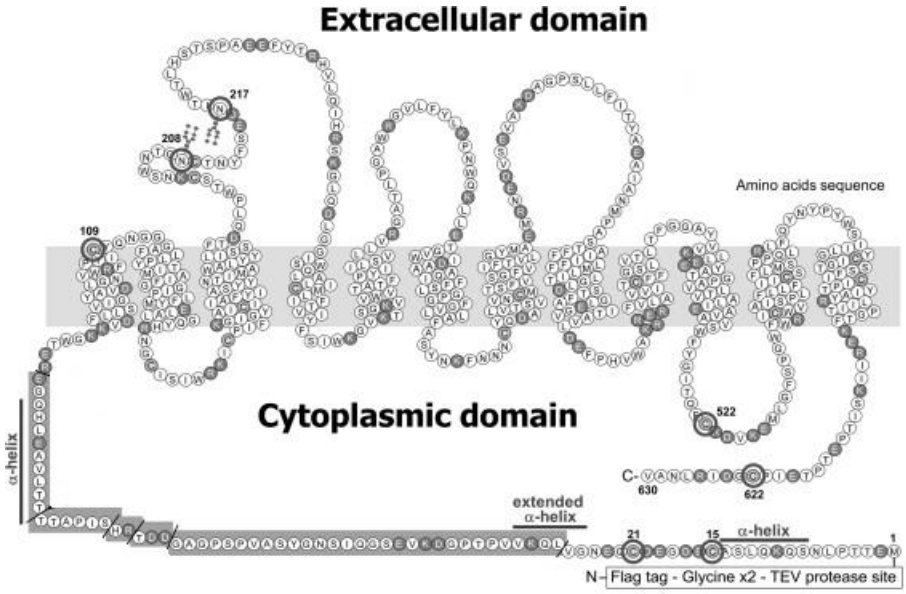

Figure 5.5. Topologocal representation of SERT indicating the FLAG-epitope tag and TEV protease cleavage site attached to the N-terminus (Takayama and Sugio, 2011. Adapted with permission from *Protein Expression and Purification* **2011**, *76*, 211-220. Copyright 2010, Elsevier).

Specifically, T-Rex HEK 293 cells were lysed and ultra-centrifuged to obtain the membrane fraction, followed by solubilizing this membrane fraction in a solubilization buffer containing 1% digitonin detergent. This solution was then absorbed onto anti-FLAG affinity beads in a batch mode. The beads were subsequently washed with a wash buffer then eluted with an elution buffer (*i.e.*, wash buffer containing 3X FLAG peptide). As a positive control experiment to detect a known protein bearing a FLAG epitope, a solubilizing buffer solution of commercially available FLAG-fusion protein of *E. coli* bacterial alkaline phosphatase (BAP) was used, which bears a molecular weight of 49.1 kDa. For a negative control experiment, solubilizing buffer was used as is.

Specifically, eluents from the affinity beads were analyzed using Western blot to detect FLAG-fused proteins *via* an anti-FLAG antibody (Figure 5.6, C). In particular, results depicted in part C of Figure 5.6 indicate that this single-step affinity purification protocol proved successful for purifying the modified hSERT from the T-Rex HEK 293 cells. Additionally, all fractions from this purification protocol, including whole cell lysate, cytosolic supernatant, crude soluble membrane, cell debris, solubilized membrane, material unbound to anti-FLAG beads, washes of the beads, and elution of the beads, were analyzed using coommassie blue staining (Figure 5.6, A) and Western blot for detecting FLAG peptides (Figure 5.6, B).

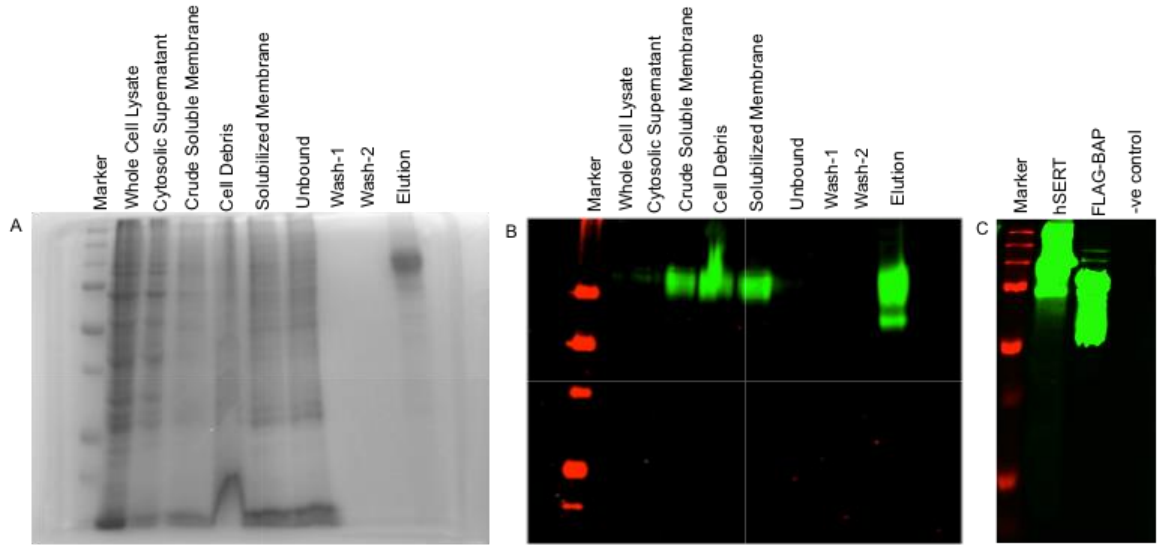

Figure 5.6. Single-step affinity chromatography purification of hSERT bearing a FLAG-epitope tag *via* anti-FLAG M2 antibody beads. (A) Proteins detected via coommassie staining; (B) Western blot detection of proteins bearing a FLAG epitope using an anti-FLAG antibody; (C) Western blot detection of control experiments using an anti-FLAG antibody.

To conclude, results from this work indicate development of a single-step affinity purification protocol that is able to purify hSERT from multiple proteins found in the cell lysate (Figure 5.6, A). After this affinity purification, the concentration of eluted SERT protein was found to be 155 µg/mL using a modified Lowry's assay (see Section 6.2.4).

Additionally, it was found that 71% of the SERT protein purified *via* this protocol was fully functional based on [^{3}H]-imipramine radioligand binding experiments.

5.3.5. Attempted SERT Tandem Photoaffinity Labeling-Bioorthogonal Conjugation Based on an Activity-Based Protein Profiling / Click Chemistry Protocol Involving Solubilizing Buffer That Contains Digitonin

As described in the previous section of this research dissertation, the single-step affinity chromatography protocol employed for purification of hSERT confirmed that: 1.) hSERT protein expressed in the T-Rex HEK293 cells being used for photoaffinity labeling bears a FLAG epitope tag attached to its N-terminus, and 2.) this hSERT protein moves as a good monomeric band corresponding to 70 kDa *via* SDS-PAGE. As a result, the next photoaffinity labeling experiments were modified to incorporate the previously mentioned solubilizing buffer into an attempted activity-based protein profiling / click chemistry photoaffinity labeling protocol (Scheme 5.28, routes "a" and "b").

For this work, a hSERT membrane fraction was initially prepared as previously discussed in Section 5.2.1. For route "a", enantiomerically pure citalopram photoprobe (*S*)-**4.44** was first added to the hSERT membrane fraction dispersed in Tris-buffered saline (TBS), incubated for 1 hour, then exposed to UV light for photoaffinity labeling. The reaction mixture was then ultracentrifuged to remove excess photoprobe (route "a", Scheme 5.28). The resultant membrane fraction was then dissolved in the solubilizing buffer containing 1% digitonin and subjected to click chemistry reaction with biotin azide (Weerapana *et al*., 2007). The click reaction was ultimately quenched by adding 5X loading dye and the samples were analyzed using Western blot (*i.e.*, anti-FLAG antibody

for detecting FLAG-tagged hSERT and Streptavidin IR dye for detecting biotinylated proteins) (Figure 5.7).

As previously mentioned, affinity purified hSERT protein solubilized in solubilizing buffer is still fully functional (> 70%) based on [^{3}H]-imipramine radioligand binding (Takayama and Sugio, 2011). As a result, an alternative route was also investigated wherein the hSERT membrane fraction was dissolved in solubilizing buffer prior to photoaffinity labeling (*i.e.*, route "b"; Scheme 5.28).

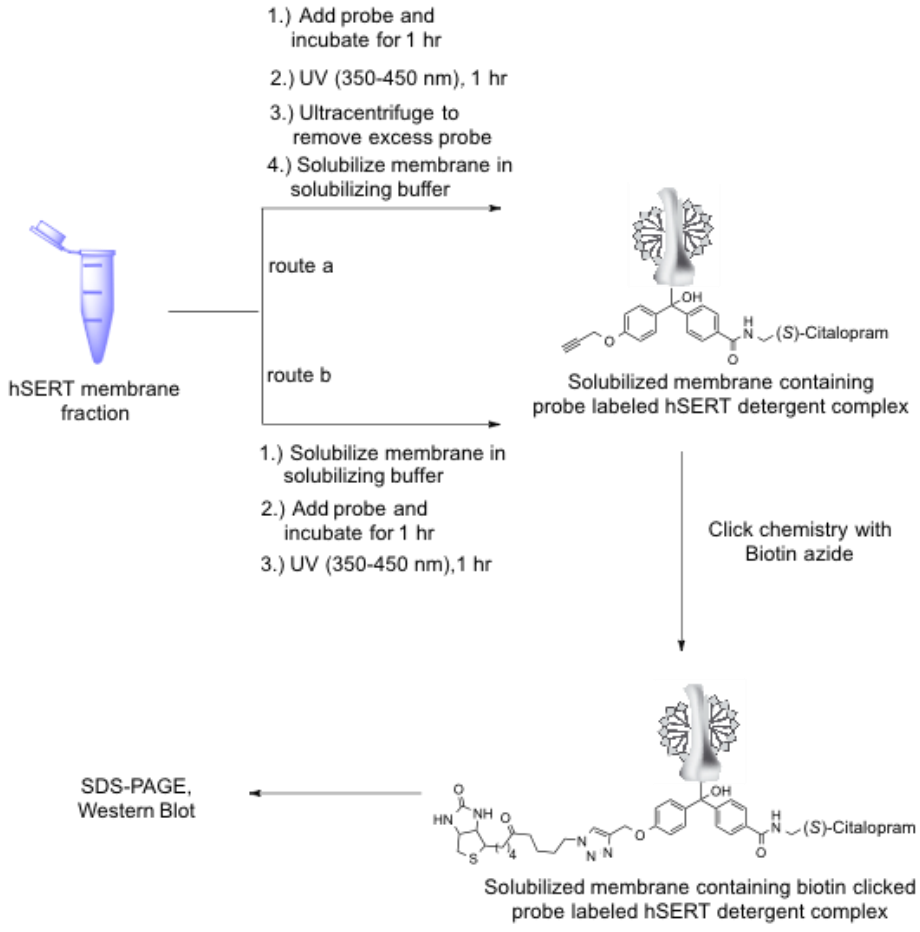

Scheme 5.28. Attempted SERT tandem photoaffinity labeling-bioorthogonal conjugation employing an activity-based protein profiling / click chemistry protocol using solubilizing buffer.

As indicated in Figure 5.7, results from route "a" and route "b" of Scheme 5.28 did not indicate any SERT photoaffinity labeling with citalopram photoprobe (*S*)-**4.44** at 5 μM and 100 μM concentrations. In particular, the use of solubilizing buffer and the anti-FLAG antibody for Western blot did confirm that these samples do contain hSERT; however, the SERT present was clearly not being photolabeled by photoprobe (*S*)-**4.44**.

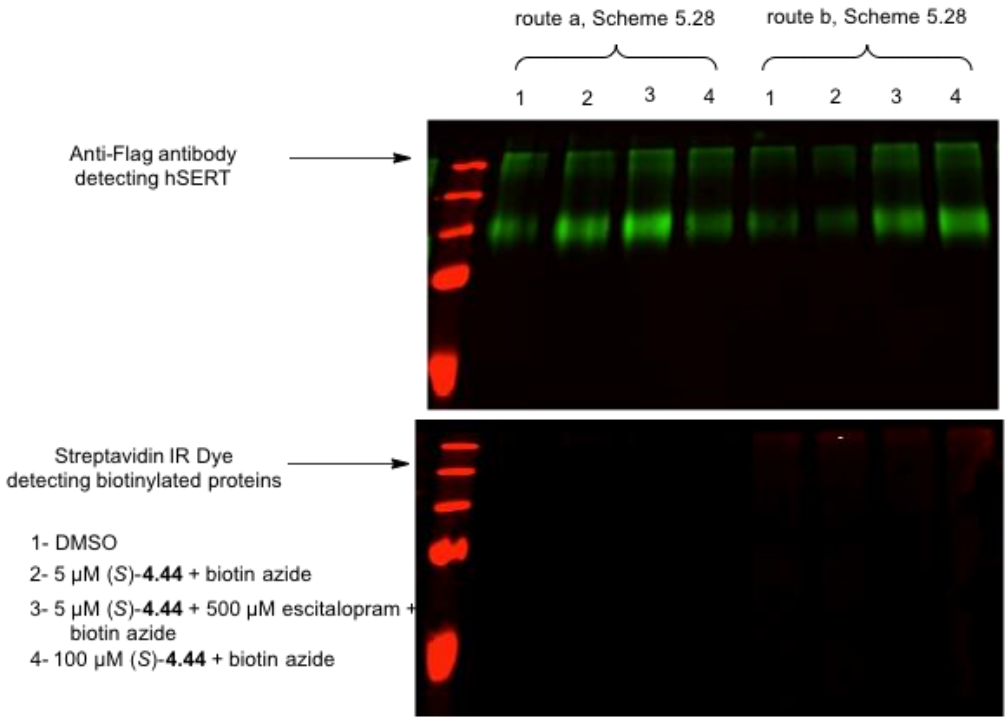

Figure 5.7. Results from attempted SERT tandem photoaffinity labeling-bioorthogonal conjugation using solubilizing buffer with 1% digitonin plus (*S*)-citalopram-based photoprobe (*S*)-**4.44**.

One possible explanation for these experimental results observed was that photoaffinity labeling was not efficient enough to be detected *via* Western blot. Therefore, the next strategy pursued was to attempt photoaffinity labeling of purified hSERT protein (*i.e.*, instead of a hSERT membrane fraction), as this would be expected to improve the efficiency of detection of probe-labeled protein after photoaffinity labeling *via* Western blot. Another strategy employed to potentially improve detection of

probe-labeled protein after photoaffinity labeling was to utilize an IRDye® 800CW azide during the click chemistry reaction instead of biotin azide, as this IRDye would allow direct scanning of an SDS-PAGE gel for probe-labeled proteins and avoid relying on streptavidin-biotin interactions needed for detection.

5.3.6. Successful Tandem Photoaffinity Labeling-Bioorthogonal Conjugation of Purified hSERT Using a Clickable (*S*)-Citalopram-Based Photoprobe

For this part of the research, hSERT was initially purified in its fully functional form (as previously described in Section 5.2.4) and utilized for attempted tandem photoaffinity labeling-bioorthogonal conjugation according to a protocol similar that described for route "b" in Scheme 5.28. Initial experiments were tried using racemic citalopram photoprobe (±)-**4.44** and enantiomerically pure escitalopram photoprobe (*S*)-**4.44** at various concentrations.

Briefly, probe (±)-**4.44** or (*S*)-**4.44** was added to purified hSERT in a 96 well plate, incubated for 1 hour, then exposed to UV light for photoaffinity labeling. The resulting mixture was then subjected to click chemistry reaction with biotin azide (Weerapana *et al*., 2007) and quenched by adding 5X loading dye. Samples were then analyzed using Western blot (*i.e.*, anti-FLAG antibody to detect the FLAG epitope within the modified SERT being used and Streptavidin IR dye to detect biotinylated proteins) (Figure 5.8).

In particular, the results from these experiments indicated that lower concentrations (50 nM and 500 nM) of the photoprobes (lanes 2 and 3) did not show any

photoaffinity labeling, whereas higher concentration (0.2 mM) of the photoprobe (lanes 4) showed some degradation of protein (Figure 5.8).

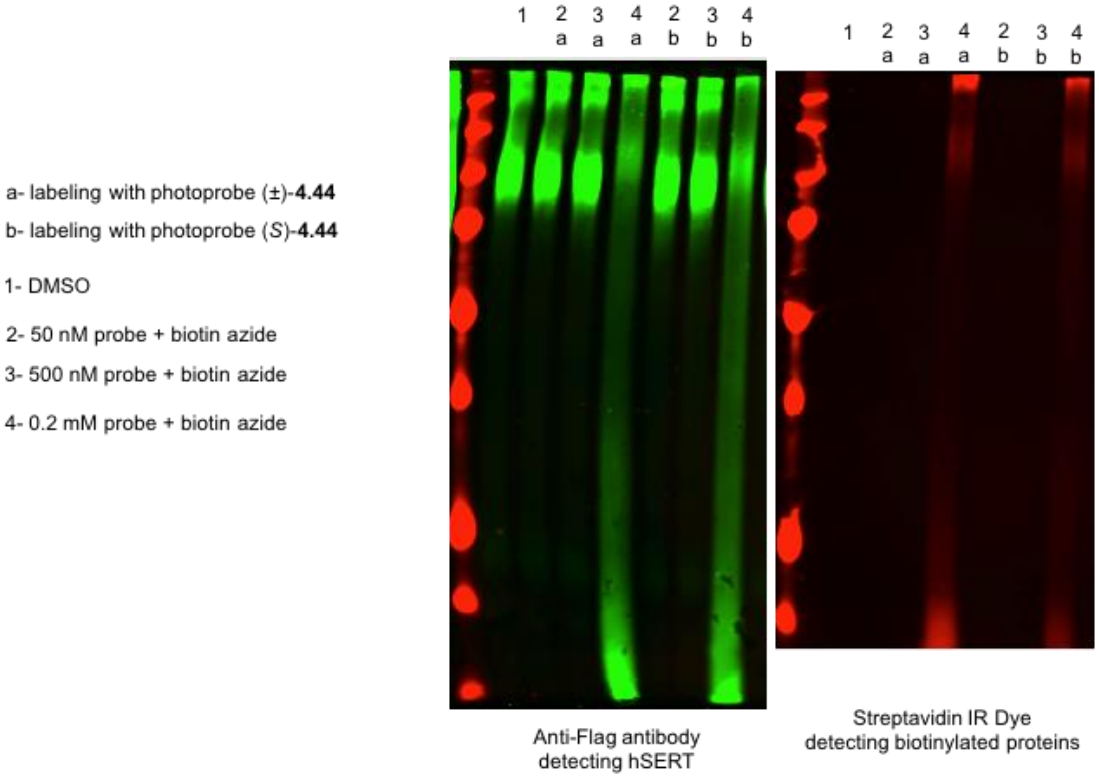

Figure 5.8. Attempted tandem photoaffinity labeling-bioorthogonal conjugation of purified hSERT using 5-substituted racemic/(*S*)-citalopram-based benzophenone-alkyne photoprobes.

Subsequently, intermediate concentrations of enantiomerically pure escitalopram photoprobe (*S*)-**4.44** were utilized in attempted SERT photoaffinity labeling. In particular, successful SERT photoaffinity labeling was observed at a concentration of 1 µM for citalopram photoprobe (*S*)-**4.44**, wherein click chemistry was performed with biotin azide or IRDye® 800CW azide (Scheme 5.29). Thus, the optimum concentration of citalopram photoprobe (*S*)-**4.44** required for SERT photoaffinity labeling was determined to be 1µM.

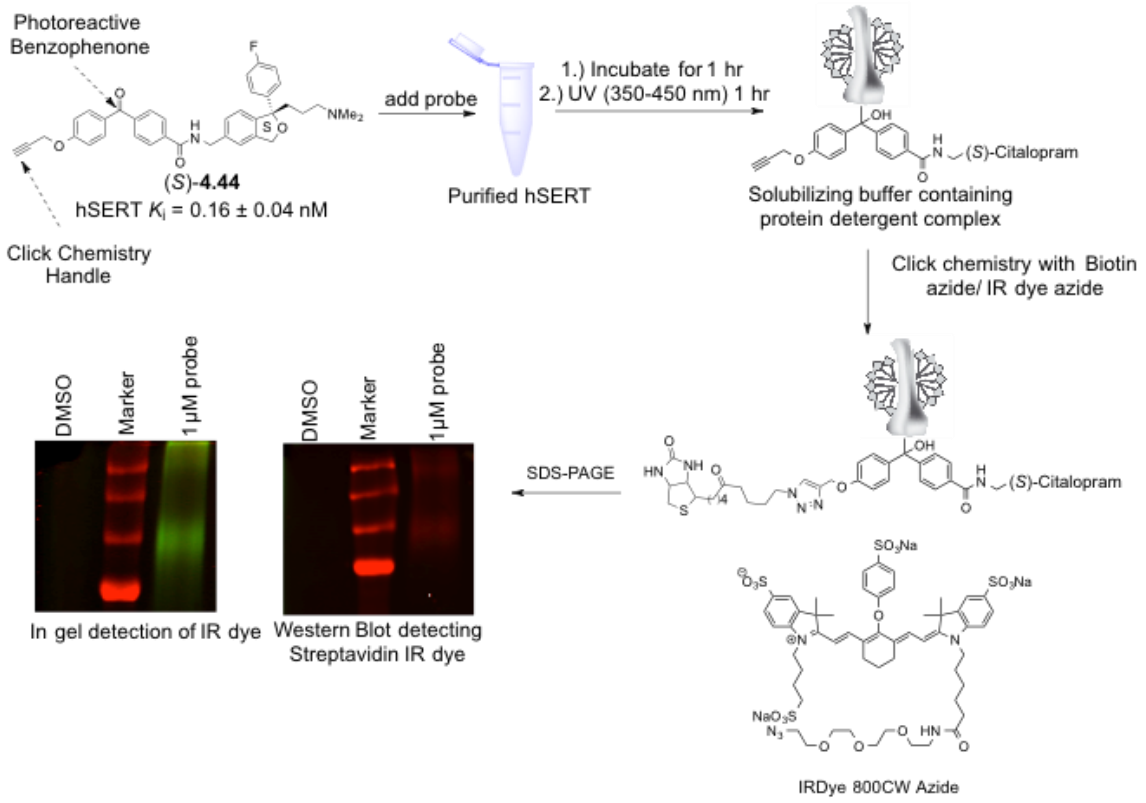

Scheme 5.29. Tandem photoaffinity labeling-bioorthogonal conjugation of purified hSERT using an optimum concentration (1 µM) of (*S*)-citalopram based photoprobe (*S*)-**4.44**.

Additionally, experiments were carried out to determine the optimum time required for UV light exposure during photoaffinity labeling of purified hSERT modified with a FLAG epitope. Specifically, samples were removed from UV light at 10 minute time intervals, and it was identified that 20 minutes of UV light exposure was optimum for SERT photoaffinity labeling to occur using benzophenone-alkyne photoprobe (*S*)-**4.44** (Figure 5.9). These experiments also indicate the specificity of escitalopram photoprobe (*S*)-**4.44** for labeling SERT, since SERT photoaffinity labeling by probe (*S*)-**4.44** was completely blocked by the presence of escitalopram as a competing ligand (lanes b, Figure 5.9).

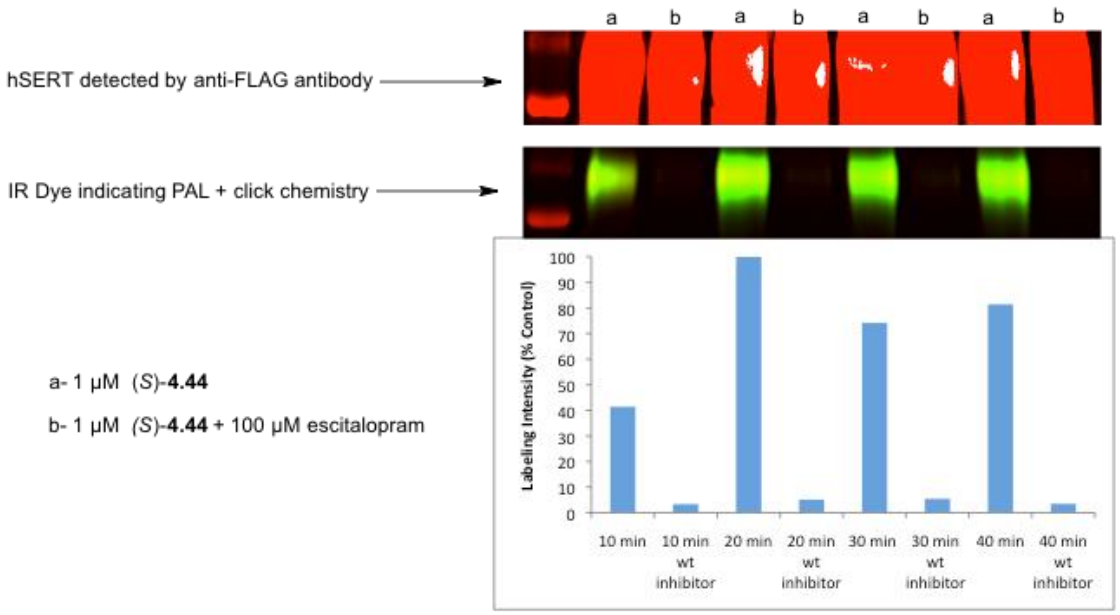

Figure 5.9. Successful tandem photoaffinity labeling-bioorthogonal conjugation of purified hSERT: Optimization of time required for UV exposure using 1 μM of (*S*)-citalopram based photoprobe (*S*)-**4.44**.

As a final effort, photoaffinity labeling was performed for 20 minutes of UV light exposure and click chemistry was carried using IR-dye 800CW azide (see Section 6.2.6) (Figure 5.10) with respect to the following experiments: 1.) without UV (lane "a"; a control experiment to show that UV light is indeed needed to covalently link the benzophenone functional group within the citalopram photoprobe to the SERT protein), 2.) DMSO (lane "b"; no photoprobe is present, only hSERT protein is present), 3.) 1 μM of escitalopram photoprobe (*S*)-**4.44** (lane "c"), and 4.) 1 μM of escitalopram photoprobe (*S*)-**4.44** in the presence of 100 μM of (*S*)-citalopram as a competitor (lane d).

In particular, results from these experiments indicate that escitalopram photoprobe (*S*)-**4.44** is photoaffinity labeling SERT only in lane "c" as expected / desired, whereas control experiments (*i.e.*, lanes "a" and "b") show negligible SERT photoaffinity labeling by the photoprobe. Additionally, SERT photoaffinity labeling by escitalopram photoprobe (*S*)-**4.44** was also successfully inhibited in lane "d", due to the presence of

100-fold excess of (*S*)-citalopram as a competitor to displace photoprobe (*S*)-**4.44** from photolabeling hSERT.

Subsequently, the probe-labeled protein bands that were visualized with the aid of the IR-dye were excised from the SDS-PAGE gel and subjected to trypsin digestion in order to generate samples for mass spectrometry analysis (see Section 6.2.7). These samples are currently in the hands of Dr. Michael Cascio's laboratory (Duquesne University) for mass spectrometric analysis of the generated photoprobe-SERT complex.

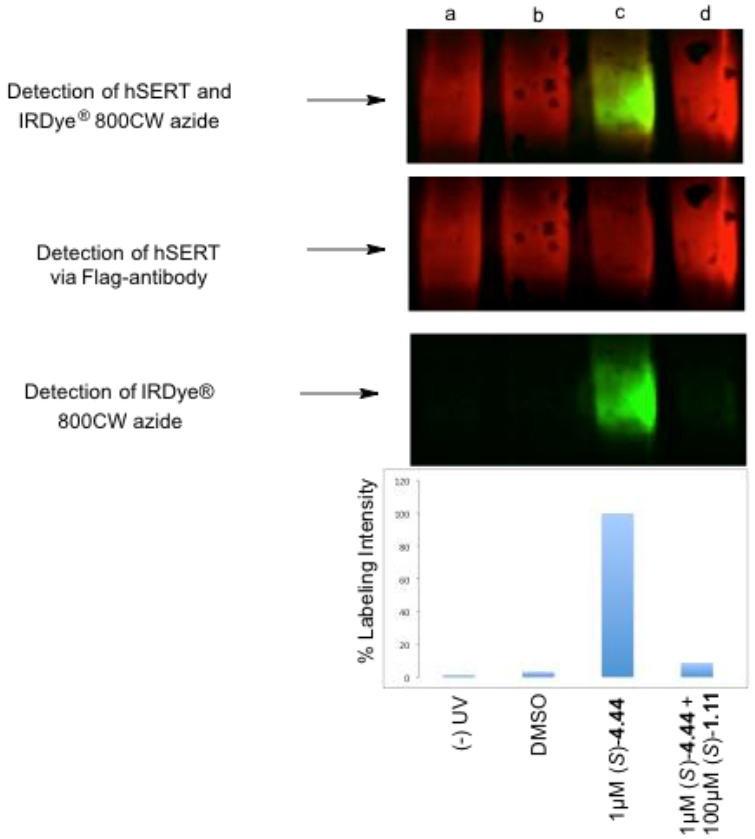

Figure 5.10. Successful tandem photoaffinity labeling-bioorthogonal conjugation of purified hSERT using 1 μM of (*S*)-citalopram based photoprobe (*S*)-**4.44** in the presence (lane "d") or absence (lane "c") of 100 μM of (*S*)-citalopram as a competitor. Control experiments such as a negative control experiment (*i.e.*, lane "b", DMSO solution of hSERT without probe (*S*)-**4.44** present) and a UV control experiment (*i.e.*, lane "a", 1 μM of (*S*)-citalopram based photoprobe (*S*)-**4.44** in the presence of hSERT, but not exposed to UV light conditions for photoaffinity labeling) are also included.

5.4. Summary of the Significance, Innovation, and Research Accomplishments Associated With This Dissertation Work

Despite decades of research, 3D structural details of how the dopamine transporter (DAT) and the serotonin transporter (SERT) interact with therapeutically relevant drugs, is not well understood. Specifically, there are fundamental gaps in understanding: 1) the mechanism of DAT and SERT inhibitors at the molecular level, 2) 3D structural details with respect to ligand-binding sites within DAT and SERT, and 3) conformational states associated with DAT and SERT. These prodigious voids, in turn, hinder rational structure-based drug discovery efforts for numerous disease states associated with DAT and SERT. As a result, a detailed understanding of the ligand-binding sites within DAT and SERT is essential for developing new therapeutics to treat a host of diseases traditionally associated with these proteins (*e.g.*, drug abuse, anxiety, depression, and ADHD).

The overall aim of this dissertation was to develop irreversible chemical probes and chemical proteomic methods in order to understand how the pharmacology profile (*i.e.*, binding affinity, potency, selectivity, behavioral phenotype, etc.) of therapeutically significant DAT and SERT inhibitors is dictated by their reversible, non-covalent interactions with DAT and SERT at the molecular level. In particular, this aim was pursued *via* rational design and chemical synthesis of photoaffinity ligands based on methylphenidate, a well-known ADHD drug and DAT inhibitor, and citalopram, a well-known antidepressant and SERT inhibitor, in order to map the binding sites and poses of these compounds within the DAT or SERT. Additionally, a chemical proteomics method was developed as part of this dissertation for irreversibly labeling hSERT *via* a tandem

photoaffinity labeling-bioorthogonal conjugation experimental approach by employing clickable citalopram-based photoprobes.

One of the long-term research goals of the Lapinsky group is to understand how the DAT discriminates abused (*e.g.*, cocaine, amphetamine, cathinones) *versus* therapeutic compounds (*e.g.*, methylphenidate, bupropion) at the molecular level. With this goal in mind, the initial objective of this research dissertation was to continue the group's chemical development of non-tropane-based DAT inhibitor photoaffinity ligands in order to map the drug-binding pocket(s) of these compounds within the DAT at the molecular level. Specifically, the rationale for this portion of the dissertation was that non-tropane-based DAT inhibitor photoaffinity ligands could serve as complimentary probes to known tropane-based (*e.g.*, cocaine, benztropine) DAT inhibitor photoaffinity ligands, which have previously proved valuable in several 3D DAT structure-function studies.

In particular, the non-tropane DAT inhibitor methylphenidate was chosen as a lead compound for the design of potential DAT photoaffinity ligands by carefully considering previous SAR studies in the chemical literature (*e.g.*, Misra *et al.*, 2010). Specifically, the hypothesis for this portion of work was that methylphenidate could be structurally modified, without significant loss in DAT binding affinity, to contain an aryl azide as a photoreactive functional group and an ^{125}I atom as a radiotracer reporter group, such that the resulting photoprobes could potentially covalently label DAT *via* photoaffinity labeling. Synthesized methylphenidate-based photoprobes bearing these functionalities were then evaluated for their DAT binding affinity by Dr. Christopher Surratt's laboratory (Duquesne University). Subsequently, candidate photoprobes (*i.e.*,

compounds whose DAT binding affinity was ≤100 nM and within 10-fold of methylphenidate's DAT binding affinity) were identified for DAT photoaffinity labeling experiments performed by Dr. Roxanne Vaughan's laboratory (University of North Dakota).

It should be noted that within this dissertation, several innovative methylphenidate-based DAT photoaffinity ligands were systematically designed in order to address experimental shortcomings associated with previously established tropane-based DAT photoaffinity ligands. Most notably, essentially all previously established tropane-based DAT photoaffinity ligands prior to this dissertation employed a variable length methylene linker between the photoreactive functional group and the DAT pharmacophore. As a result, such photoprobes potentially possess an inherent disadvantage when trying to optimally model the DAT-photoprobe complex *via* BEProFL or definitively map the amino acids of the DAT inhibitor-binding pocket. Additionally, methylphenidate-based DAT photoaffinity ligands are expected to be scientifically significant because the binding sites and conformational preferences for non-tropane DAT inhibitors (*e.g.*, methylphenidate, bupropion, pyrovalerone) are unknown relative to tropane-based DAT inhibitors (*e.g.*, cocaine, benztropine). With these thoughts in mind and as previously described in Section 5.1.3, racemic *threo*-3-iodo-4-azido-methylphenidate ((±)-**4.35**) represents the first successful example of a DAT photoaffinity ligand, either tropane- or non-tropane-based, wherein the photoreactive azide and iodine tag are placed directly on the DAT inhibitor pharmacophore (Lapinsky *et al*., 2012). As a result, photoprobe (±)-**4.35** is expected to: 1.) covalently attach to amino acids directly within the methylphenidate-binding site of

DAT, and 2.) result in a more conformationally restricted DAT-photoprobe complex during 3D hDAT molecular modeling studies, thus representing an important contribution to the growing battery of chemical probes for understanding DAT structure and function at the molecular level.

In terms of practical organic synthesis and as previously described in Section 5.1.1, a novel, efficient large-scale synthesis of racemic *threo*-3-iodo-methylphenidate ((±)-**4.29**) was developed in order to generate a series of racemic *threo*-*N*-azidobenzyl-3-or-4-iodo-methylphenidate photoaffinity ligands ((±)-**4.17** to (±)-**4.22**) as potential candidates for DAT structure-function studies. This novel synthesis of racemic *threo*-3-iodo-methylphenidate (Scheme 5.2) utilized four steps and produced the target compound in 30% overall yield (Lapinsky *et al*., 2011). Additionally and as previously described in Section 5.1.3, synthesis of racemic *threo*-4-nitro-methylphenidate ((±)-**4.39**) was needed towards producing racemic *threo*-3-iodo-4-azido-methylphenidate ((±)-**4.35**) as a potential DAT photoprobe. However, initial syntheses of *threo*-4-nitro-methylphenidate ((±)-**4.39**) were problematic wherein global hydrolysis of *N*-benzoyl *threo*-4-nitro-methylphenidate ((±)-**3.25**) lead to epimerization (Scheme 5.7) and direct nitration of racemic *threo*-ritalinic acid ((±)-**5.12**) lead to a mixture of positional nitro isomers (Scheme 5.8). Therefore, in order to overcome these problems, a novel, efficient large-scale synthesis of racemic *threo*-4-nitro-methylphenidate ((±)-**4.39**) was developed (Scheme 5.9) by employing previously disclosed methodology (Axten *et al.*, 1998; Gutman *et al.*, 2004) for the synthesis of methylphenidate analogs *via* alpha-keto amides as starting materials.

Another long-term research goal of the Lapinsky group is to understand how selective serotonin reuptake inhibitors (SSRIs, well-known clinically significant antidepressants) interact with their major target protein (*i.e.*, SERT) at the molecular level. In particular, the SSRI (±)-citalopram, which displays a very unique binding profile with respect to the S1 and S2 binding sites of SERT (*i.e.*, (*R*)-citalopram is proposed to bind to the S2 binding site within SERT, whereas the (*S*)-enantiomer is proposed to bind to the S1 binding site of SERT), was chosen as lead compound for developing SSRI-based photoprobes. Therefore, much like the methylphenidate / DAT work, photoaffinity ligands based on the enantiomers of citalopram would be expected to be important tool compounds for mapping the binding sites and poses of SSRIs within SERT *via* BEProFL and give important structural information regarding the primary substrate binding site (S1) and allosteric binding site (S2) within this protein.

Analogous to the previously mentioned methylphenidate / DAT work, the hypothesis for this portion of the dissertation was that racemic and enantiomerically pure (*S*)-citalopram could be derivatized, without significant loss in SERT binding affinity, to contain a photoreactive functional group (*i.e.*, an aryl azide or a benzophenone) capable of forming a covalent bond to hSERT *via* photoaffinity labeling and a reporter group (*i.e.*, ^{125}I, a terminal alkyne, or an aliphatic azide) for application of a BEProFL experimental approach with respect to SERT. In turn, several citalopram-based probes were rationally designed based on previously disclosed citalopram-SERT SAR studies. These compounds were then chemically synthesized and pharmacologically evaluated in order to identify appropriate candidates for SERT photoaffinity labeling studies. In particular, the SERT binding affinity of synthesized citalopram analogs were pharmacologically

determined by the laboratory of Dr. Christopher Surratt (Duquesne University) in order to identify candidate photoprobes for SERT photoaffinity labeling experiments performed by Dr. Roxanne Vaughan's lab (North Dakota University; *i.e.*, for ^{125}I probes) or within Dr. Michael Cascio's lab (Duquesne University; *i.e.*, for clickable photoprobes).

Once again and analogous to the DAT / methylphenidate work, an innovative, systematic design of citalopram-based SERT photoaffinity ligands was employed in this dissertation towards ultimately determining the exact binding site(s) of citalopram as an SSRI within SERT in the future. This is significant because the binding sites and conformational preferences for citalopram, particularly with respect to the enantiomers of citalopram and the S1 *versus* S2 binding sites within SERT, are not well understood. Additionally, it should be noted that radioisotopes have been the primary reporter groups used in the development of DAT and SERT photoprobes prior to this dissertation. However, given the recent development of numerous click chemistry reactions / bioorthogonal conjugation methodologies, radioactive tags are no longer needed for the detection of probe-labeled proteins after photoaffinity labeling. Instead, "clickable" reporter functional groups, such as aliphatic azides and terminal alkynes, have been routinely shown to readily enable click chemistry techniques post photoaffinity labeling and are mainstream in current photoprobe development. Specifically with respect to this dissertation, once an irreversible SERT-photoprobe complex is generated *via* SERT photoaffinity labeling and then "clicked" with an appropriate detection or purification moiety (*e.g.*, biotin for easy enrichment, isolation, and detection, or fluorophores for sensitive detection and imaging applications), the irreversible SERT-photoprobe complex can be then purified, proteolyzed, and analyzed by mass spectrometry in order to

determine the exact sites of covalent photoprobe ligation to SERT with a reliable level of sensitivity.

Importantly, it must be noted that previous attempts to determine the adduction sites of radioisotope-based DAT photoprobes in DAT has relied on labor-intensive peptide mapping strategies or the construction of mutant proteins, constraints of which limit the utility and resolution of proteomic analysis. In particular and as described in this dissertation, the ability to attach biotin as a purification and detection moiety to a photoprobe *via* click chemistry after SERT photoaffinity labeling is expected to permit microlevel analysis of probe-labeled protein fragments when coupled to sequential LC-MS/MS. In this regard and as previously described in Section 5.2, 5-substituted benzophenone-alkyne (±)-citalopram analog (±)-**4.44**, 5-substituted benzophenone-alkyne (*S*)-citalopram analog (*S*)-**4.44**, *N*-substituted benzophenone-alkyne (*S*)-citalopram analog (*S*)-**4.47**, and 5-substituted diazido (*S*)-citalopram analog (*S*)-**4.50** represent the first clickable photoaffinity ligands for SERT structure-function studies, thus representing an important contribution towards understanding the binding site(s) and pose(s) of SSRIs as clinically important antidepressants by coupling future SERT photoaffinity labeling experiments with SERT molecular modeling studies. Additionally, 5-substituted azido-iodo (*S*)-citalopram-based photoprobe (*S*)-**4.51** was also synthesized as part of this dissertation and evaluated for SERT binding affinity by Dr. Christopher Surratt's laboratory. Subsequently, photoprobe (*S*)-**4.51** was also synthesized in its ^{125}I form by Dr. John Lever (University of Missouri) and preliminary irreversible SERT photoaffinity labeling experiments were performed by Dr. Roxanne Vaughan's laboratory (University of North Dakota).

The final aim of this dissertation was to examine whether 5-substituted benzophenone-alkyne (*S*)-citalopram analog (*S*)-**4.44** could be successfully employed in a SERT tandem photoaffinity labeling-bioorthogonal conjugation experiment. As discussed in Section 5.3 and after numerous attempts, a successful tandem photoaffinity labeling-bioorthogonal conjugation protocol was ultimately developed using purified hSERT protein and (*S*)-citalopram-based clickable photoprobe (*S*)-**4.44** (Scheme 5.30). In this regard, this represents the first time tandem photoaffinity labeling-bioorthogonal conjugation techniques have ever been successfully applied to the monoamine transporter field, thus representing a significant advance *versus* previously mentioned photoaffinity labeling experiments involving radioactive DAT or SERT photoprobes.

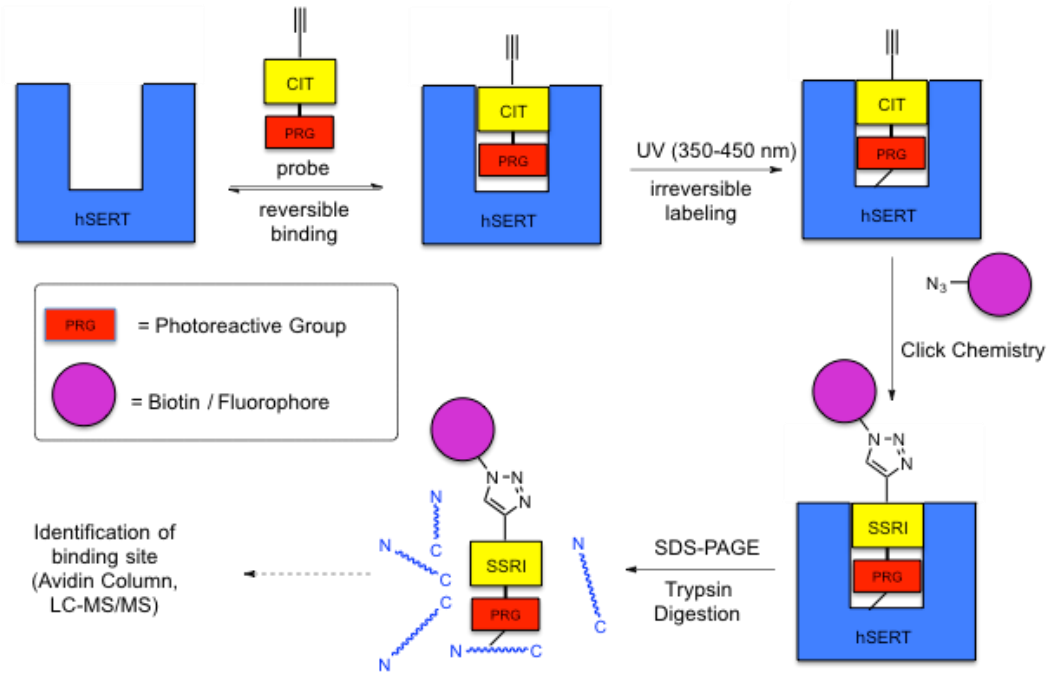

Scheme 5.30. Tandem photoaffinity labeling-bioorthogonal conjugation of hSERT *via* citalopram (CIT)-based photoprobes.

To conclude, the chemical development of DAT and SERT compounds to date has been limited to a ligand-based perspective. However, the photoaffinity ligands and

biochemical proteomic experiments described in this dissertation are expected to: 1.) facilitate transition of the DAT and SERT fields towards a rational, structure-based perspective, and 2.) experimentally validate and further refine current DAT and SERT homology models for improved virtual screening drug discovery efforts. As a result of these expectations, the chemical probes described in this dissertation arguably represent very valuable compounds towards developing improved therapeutics for numerous DAT- and SERT-implicated diseases.

5.5. Summary of Final Compounds Synthesized During This Dissertation

Table 5.1. Final compounds synthesized during this dissertation.

Compound Name	Novel/ Known
(±)-*threo*-3-Iodo-MP hydrochloride ((±)-**4.29**)	Novel
(±)-*threo*-*N*-(*p*-Azido-benzyl)-3-iodo-MP ((±)-**4.22**)	Novel
(±)-*threo*-4-Nitro-MP hydrochloride ((±)-**4.39**)	Known
(±)-*threo*-4-Amino-MP ((±)-**4.36**)	Novel
(±)-*threo*-4-Amino-3-iodo-MP ((±)-**4.40**)	Novel
(±)-*threo*-4-Azido-3-iodo-MP ((±)-**4.35**)	Novel
(±)-*threo*-4-Azido-MP ((±)-**4.41**)	Novel
(±)-*N*-((1-(3-(dimethylamino)propyl)-1-(4-fluorophenyl)-1,3-dihydroisobenzofuran-5-yl)methyl)-4-(4-(prop-2-yn-1-yloxy)benzoyl)benzamide ((±)-**4.44**)	Novel
(*S*)-*N*-((1-(3-(dimethylamino)propyl)-1-(4-fluorophenyl)-1,3-dihydroisobenzofuran-5-yl)methyl)-4-(4-(prop-2-yn-1-yloxy)benzoyl)benzamide ((*S*)-**4.44**)	Novel
(*S*)-1-(3-((4-benzoylbenzyl)(methyl)amino)propyl)-1-(4-fluorophenyl)-1,3-dihydroisobenzofuran-5-carbonitrile ((*S*)-**4.46**)	Novel
(*S*)-1-(4-fluorophenyl)-1-(3-(methyl(4-(4-(prop-2-yn-1-yloxy)benzoyl)benzyl)amino)propyl)-1,3-dihydroisobenzofuran-5-carbonitrile ((*S*)-**4.47**)	Novel
(*S*)-3-azido-5-(azidomethyl)-*N*-((1-(3-(dimethylamino)propyl)-1-(4-fluorophenyl)-1,3-dihydroisobenzofuran-5-yl)methyl)benzamide ((*S*)-**4.50**)	Novel
(*S*)-4-azido-*N*-((1-(3-(dimethylamino)propyl)-1-(4-fluorophenyl)-1,3-dihydroisobenzofuran-5-yl)methyl)-3-iodobenzamide ((*S*)-**4.51**)	Novel

5.6. References

- Axten, J.M., Krim, L., Kung, H.F., and Winkler, J.D. A stereoselective synthesis of *dl-threo*-methylphenidate: preparation and biological evaluation of novel analogues. *J. Org. Chem.* **1998**, *63*, 9628-9629.

- Banala, A.K., Zhang, P., Plenge, P., Cyriac, G., Kopajtic, T., Katz, J.L., Loland, C.J., and Newman, A.H. Design and synthesis of 1-(3-(dimethylamino)propyl)-1-(4-fluorophenyl)-1,3-dihydroisobenzofuran-5-carboni trile (citalopram) analogues as novel probes for the serotonin transporter S1 and S2 binding sites. *J. Med. Chem.* **2013**, *56*, 9709-9724.

- Bandyopadhyay, S. and Bong, D. Synthesis of trifunctional phosphatidylserine probes for identification of lipid-binding proteins. *Eur. J. Org. Chem.* **2011**, 4, 751-758.

- Chaikovskii, V.K., Filimonov, V.D., Skorokhodov, V.I., and Ogorodnikov, V.D. Superactivity and dual reactivity of the system *N*-iodosuccinimide-H_2SO_4 in the iodination of deactivated arenes. *Russian J. Org. Chem*. **2007**, *43*, 1278-1281.

- Chen, F., Larsen, M. B., Sánchez, C., and Wiborg, O. The *S*-enantiomer of *R,S*-citalopram, increases inhibitor binding to the human serotonin transporter by an allosteric mechanism. Comparison with other serotonin transporter inhibitors. *European Neuropsychopharmacology* **2005**, *15*, 193-198.

- Deutsch, H.M., Shi, Q., Gruszecka-Kowalik, E., and Schweri, M.M. Synthesis and pharmacology of potential cocaine antagonists. 2. Structure-activity relationship

studies of aromatic ring-substituted methylphenidate analogs. *J. Med. Chem.* **1996**, *39*, 1201-1209.

- Gutman, A., Zaltsman, I., Shalimov, A., Sotrihin, M., Nisnevich, G., Yudovich, L., and Fedotev, I. Process for the preparation of dexmethylphenidate hydrochloride. Patent US 20040180928 A1, **2004**.

- Jin, C., Boldt, K.G., Rehder, K.S., and Brine, G.A. Improved syntheses of *N*-desmthylcitalopram and *N*,*N*-didesmethylcitalopram. *Syn. Commun.* **2007**, 37, 901-908.

- Kim, D.I., Deutsch, H.M., Ye, X., and Schweri, M.M. Synthesis and pharmacology of site-specific cocaine abuse treatment agents: restricted rotation analogues of methylphenidate. *J. Med. Chem.* **2007**, *50*, 2718-2731.

- Koopmans, T., Dekker, F.J., and Martin, N.I. A photocleavable affinity tag for the enrichment of alkyne-modified biomolecules. *RSC Adv.* **2012**, *2*, 2244-2246.

- Kumar, V., Rahbek-Clemmensen, T., Billesbølle, C.B., Jorgensen, T.N., Gether, U., and Newman, A.H. Novel and high affinity fluorescent ligands for the serotonin transporter based on (S)-citalopram. *ACS Med. Chem. Lett.* **2014**, *5*, 696-699.

- Lapinsky, D.J., Velagaleti, R., Yarravarapu, N., Liu, Y., Huang, Y., Surratt, C.K., Lever, J.R., Foster, J.D., Acharya, R., Vaughan, R.A., and Deutsch, H.M. Azido-iodo-*N*-benzyl derivatives of *threo*-methylphenidate (Ritalin, Concerta): rational design, synthesis, pharmacological evaluation, and dopamine transporter photoaffinity labeling. *Bioorg. Med. Chem.* **2011**, *19*, 504-512.

- Lapinsky, D.J., Yarravarapu, N., Nolan, T.L., Surratt, C.K., Lever, J.R., Tomlinson, M., Vaughan, R.A., and Deutsch, H.M. Evolution of a compact photoprobe for the dopamine transporter based on (±)-*threo*-methylphenidate. *ACS Med. Chem. Lett.* **2012**, *3*, 378-382.

- Lippert, W.P., Burshka, C., Gotz, K., Kaupp, M., Ivanova, D., Gaudon, C., Sato, Y., Antony, P., Rochel, N., Moras, D., Gronemeyer, H., and Tacke, R. Silicon analogs of the RXR-selective retinoid agonist SR11237 (BMS649): Chemistry and biology. *ChemMedChem* **2009**, *4*, 1143-1152.

- Misra, M., Shi, Q., Ye, X., Gruszecka-Kowalik, E., Bu, W., Liu, Z., Schweri, M.M., Deutsch, H.M., and Venanzi, C.A. Quantitative structure-activity relationship studies of *threo*-methylphenidate analogs. *Bioorg. Med. Chem.* **2010**, *18*, 7221-7238.

- Moore, J.L., Taylor, S.M., and Soloshonok, V.A. An efficient and operationally convenient general synthesis of tertiary amines by direct alkylation of secondary amines with alkyl halides in the presence of Huenig's base. *ARKIVOC* **2005**, *6*, 287-292.

- Mornet, R., Leonard, N.J., Theiler, J.B., and Doree, M. Specificity of the 1-methyladenine receptors in starfish oocytes: synthesis and properties of some 1,8-disubstituted adenines, 1,6-dimethyl-1*H*-purine, and of the 1-(azidobenzyl)adenines. *J. Chem. Soc. Perkin Trans. 1* **1984**, *5*, 879-885.

- Neelarapu, R., Holzle, D.L., Velaparthi, S., Bai, H., Brunsteiner, M., Blond, S.Y., and Petukhov, P.A. Design, synthesis, docking, and biological evaluation of novel

diazide-containing isoxazole- and pyrazole-based histone deacetylase probes. *J. Med. Chem.* **2011**, *54*, 4350-4364.

- Oyelere, A.K., Chen, P.C., Guerrant, W., Mwakwari, S.C., Hood, R., Zhang, Y., and Fan, Y. Non-peptide macrocyclic histone deacetylase inhibitors. *J. Med. Chem.* **2009**, *52*, 456-468.

- Pan, D., Gatley, S.J., Chen, R., and Ding, Y.S. Iodine-123 labeled derivatives of methylphenidate: potential SPECT radiopharmaceuticals for brain dopamine transporters. *J. Label. Cmpd. Radiopharm.* **1996**, *38*, 523-532.

- Shu, A.Y.L., Yamashita, D.S., Holt, D.A., and Heys, J.R. Synthesis of I-125 labeled photoaffinity rapamycin analogs. *J. Label. Compd. Radiopharm*. **1996**, *38*, 227-237.

- Speers, A.E. and Cravatt, B.F. Activity-based protein profiling (ABPP) and click chemistry (CC)-ABPP by MudPIT mass spectrometry. *Curr. Protoc. Chem. Biol*. **2009**, *1*, 29-41.

- Takayama, H. and Sugio, S. Functional expression of milligram quantities of the synthetic human transporter gene in a tetracycline-inducible HEK293 cell line. *Protein Expression and Purification* **2011**, *76*, 211-220.

- Tantama, M., Lin, W., and Licht, S. An activity-based protein profiling probe for the nicotinic acetylcholine receptor. *J. Am. Chem. Soc.* **2008**, *130*, 15766-15767.

- Thai, D.L., Sapko, M.T., Reiter, C.T., Bierer, D.E., and Perel, J.M. Asymmetric synthesis and pharmacology of methylphenidate and its para-substituted derivatives. *J. Med. Chem.* **1998**, *41*, 591-601.

- Van Scherpenzeel, M., Moret, E.E., Ballell, L., Liskamp, R.M., Nilsson, U.J., Leffler, H., and Pieters, R.J. Synthesis and evaluation of new thiodigalactoside-based chemical probes to label galectin-3. *ChemBioChem.* **2009**, *10*, 1724-1733.

- Weerapana, E., Speers, A.E., and Cravatt, B.F. Tandem orthogonal proteolysis-activity-based protein profiling (TOP-ABPP) – a general method for mapping sites of probe modification in proteomes. *Nat. Protocols* **2007**, *2*, 1414-1425.

- Wilkinson, M.C. "Greener" Friedel-Crafts acylations: a metal- and halogen-free methodology. *Org. Lett.* **2011**, *13*, 2232-2235.

- Zou, M., Kopajtic, T., Katz, J.L., Wirtz, S., Justice, J.J., and Newman, A.H. Novel tropane-based irreversible ligands for the dopamine transporter. *J. Med. Chem.* **2001**, *44*, 4453-4461.

CHAPTER SIX

6. Experimental

6.1. Synthesis

Reaction conditions and yields were not optimized. All reactions were performed using flame-dried glassware under an inert atmosphere of argon unless otherwise noted. All solvents and chemicals were purchased from Aldrich Chemical Co. or Fisher Scientific and used without further purification unless otherwise noted. Flash column chromatography was performed according to the method of Still et al., 1978 using Fisher S826-25 silica gel sorbent (70–230 mesh) and eluting solvent mixtures as specified. Thin-layer chromatography (TLC) was performed using TLC Silica Gel 60 F_{254} plates obtained from EMD Chemicals, Inc. and compounds were visualized under UV light and/or I_2 stain. Proportions of solvents used for TLC are by volume. ^{1}H and ^{13}C NMR spectra were recorded on either a Bruker 400 or 500 MHz Oxford spectrospin cryostat, controlled by a Bruker Avance system, and were acquired using Bruker TOPSPIN 2.0 acquisition software. Acquired FIDs were analyzed using MestReC 3.2. Chemical shifts for ^{1}H and ^{13}C NMR spectra are reported as parts per million (δ ppm) relative to tetramethylsilane (0.00 ppm) as an internal standard. Coupling constants are measured in hertz (Hz). HRMS samples were analyzed at Old Dominion University (Norfolk, VA) by positive ion electrospray on a Bruker 12 Tesla APEX-Qe FTICR-MS with an Apollo II ion source. Combustion analyses of selected solid compounds were performed by Atlantic Microlab, Inc. (Norcross, GA) and are in agreement within 0.4% of calculated values. Melting point determinations were conducted using a Thomas-Hoover melting

point apparatus and are uncorrected. Infrared spectra were recorded using a Perkin–Elmer Spectrum RZ I FT-IR spectrometer. On the basis of NMR and combustion data, all compounds were ≥ 95% pure.

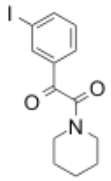

5.4

1-(3-Iodophenylglyoxylyl)piperidine (5.4)

N-iodosuccinimide (0.23g, 1 mmol) was added to 96% H_2SO_4 (3 mL) and cooled to 0 °C. The resulting suspension was stirred for 20-30 min until it became homogeneous black solution. 1-(Phenylglyoxylyl)piperidine (**3.8**, Axten, *et al*., 1998; Gutman, *et al*., 2004) (0.11g, 0.5 mmol) was added to the solution and the mixture was stirred at 0 °C for 20 min. The reaction mixture was poured into 10 mL of ice-H_2O mixture and treated with Na_2SO_3 to adjust the pH to 7. This mixture was then extracted with CH_2Cl_2, washed with brine, dried ($MgSO_4$), and concentrated to obtain 0.13g of **5.4** as yellow oil (77%). R_f = 0.45 (EtOAc/hexanes, 3:7). ^{1}H NMR ($CDCl_3$, 400 MHz): δ 8.27 (s, 1H), 7.95 (d, 1H, *J* = 7.8 Hz), 7.89 (d, 1H, *J* = 7.8 Hz), 7.26 (t, 1H, *J* = 7.8 Hz), 3.3.69 (t, 2H, *J* = 4.79 Hz), 3.27 (t, 2H, *J* = 5.54 Hz), 1.80-1.60 (m, 4H), 1.60-1.50 (m, 2H). ^{13}C NMR ($CDCl_3$, 100 MHz): δ 190.2, 164.5, 143.2, 138.0, 134.9, 130.6, 128.7, 94.5, 47.0, 42.2, 26.1, 25.4, 24.2. HRMS calcd for $C_{13}H_{14}INO_2Na^+$ 365.9961, found 365.9960

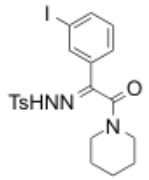

5.5

1-(3-Iodophenylglyoxylyl)piperidine *p*-toluenesulfonylhydrazone (5.5)

Ketone **5.4** (7.3 g, 21.2mmol) was added to a stirred mixture of *p*-toluenesulfonyl hydrazide (4.26 g, 22.89 mmol) in EtOH (194 mL) containing H_2SO_4 (0.03g, 0.3 mmol). The mixture was refluxed at 85 °C overnight, then cooled to room temperature. The precipitated solid was filtered, washed with cold MeOH and cold hexanes, then dried under reduced pressure to give 7.8 g of **5.5** (72%). R_f = 0.1 (EtOAC/hexanes, 3:7). ^{1}H NMR ($CDCl_3$, 400 MHz): δ 8.93 (s, 1H), 7.94 (s, 1H), 7.78 (d, 2H, *J* = 8.25 Hz), 7.69 (d, 1H, *J* = 7.88 Hz), 7.51 (d, 1H, *J* = 7.88 Hz), 7.19 (d, 2H, *J* = 8.14 Hz), 7.09 (t, 1H, *J* = 7.87 Hz), 3.70-3.60 (m, 2H), 3.20-3.10 (m, 2H), 2.34 (s, 3H), 1.76-1.52 (m, 4H), 1.48-1.38 (m, 2H). ^{13}C NMR ($CDCl_3$, 100 MHz): δ 161.3, 148.4, 144.1, 139.2, 135.0, 134.7, 134.2, 130.3, 129.4, 127.9, 127.9, 125.5, 94.5, 47.2, 42.3, 26.2, 25.4, 24.0, 21.5. HRMS calcd for $C_{20}H_{22}IN_3O_3SNa^+$ 534.0319, found 534.0314. Mp: 158-159 °C.

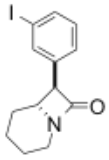

(±)-**5.6**

(±)-7-(3-Iodophenyl)-1-azabicyclo[4.2.0]octan-8-one ((±)-5.6)

50% aq NaOH (1.3 mL, 15.96 mmol) was added to a stirred mixture of hydrazone **5.5** (7.8 g, 15.2 mmol) and Aliquat 336® (61 mg, 0.16 mmol) in toluene (140 mL). The

mixture was refluxed at 130 °C overnight, then cooled to room temperature, diluted with H_2O, and extracted with toluene. The organic layer was dried ($MgSO_4$), filtered, concentrated and chromatographed (EtOAc/hexanes, 2:8) to afford (±)-**5.6** as a yellow solid. Further recrystallization from Et_2O provided 2.7 g of (±)-**5.6** (55%). This reaction provided a mixture of threo and erythro diastereomers and the relative configuration is easily determined by ^{1}H NMR spectrum analysis of the coupling constants between the benzylic and bridge-head protons. The coupling constant for *trans* diastereomers ((±)-**5.6**) is 2-2.5 Hz and the impurity which are the *cis* diastereomers have a coupling constant of 4.5-6 Hz (Backes, 2014). R_f = 0.13 (EtOAc/Hexanes, 2:8). ^{1}H NMR ($CDCl_3$, 400 MHz): δ 7.63-7.57 (m, 2H), 7.25 (d, 1H, *J* = 7.65 Hz), 7.05 (t, 1H, *J* = 7.76 Hz), 4.05-3.80 (m, 2H), 3.40-3.30 (m, 1H), 2.85-2.70 (m, 1H), 2.20-2.10 (m, 1H), 2.05-1.90 (m, 1H), 1.72-1.65 (m, 1H), 1.45-1.35 (m, 3H). ^{13}C NMR ($CDCl_3$, 100 MHz): δ 165.4, 137.9, 136.3, 136.1, 130.4, 126.6, 94.6, 62.6, 56.5, 39.0, 30.4, 24.3, 22.1. HRMS calcd for $C_{13}H_{14}INONa^+$ 350.0012, found 350.0013. Mp: 126-127 °C.

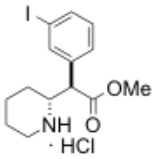

(±)-**4.29**

(±)-*threo*-3-Iodomethylphenidate hydrochloride ((±)-4.29)

(±)-*threo*-β-Lactam (±)-**5.6** (0.19 g, 0.58 mmol) was refluxed with 1.25 M HCl in MeOH for 7 hrs, then concentrated under reduced pressure to afford 229 mg of (±)-**4.29** (99%). This *threo*-iodomethylphenidate was determined to be >95% diastereomerically pure by ^{1}H NMR upon comparison to the known data for enantiomerically pure *threo*-

and *erythro*-methylphenidate and its *para*-substituted derivatives (Thai *et al*., 1998). R_f = 0.55 (MeOH/$CHCl_3$, 1:9). ^{1}H NMR (CD_3OD, 400 MHz): δ 7.74 (d, 1H, *J* = 9.6 Hz), 7.70 (t, 1H, *J* = 1.68 Hz), 7.31 (d, 1H, *J* = 8.37 Hz), 7.18 (t, 1H, *J* = 7.8 Hz), 3.89-3.81 (m, 2H), 3.74 (s, 3H), 3.43 (d, 1H, *J* = 12.81 Hz), 3.10 (t, 1H, *J* = 12.89 Hz), 1.91-1.79 (m, 2H), 1.74-1.63 (m, 1H), 1.57-1.46 (m, 2H), 1.41-1.32 (m, 1H). ^{13}C NMR (CD_3OD, 100 MHz): δ 172.8, 139.0, 138.6, 137.4, 132.2,128.9, 95.6, 58.9, 54.7, 53.6, 46.7, 27.8, 23.3, 22.7. HRMS calcd for $C_{14}H_{19}INO_2Na^+$ 382.0274, found 382.0271. Mp: 191-192ºC.

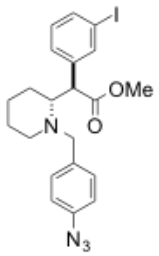

(±)-**4.22**

(±)-*threo*-*N*-(*p*-Azido-benzyl)-3-iodomethylphenidate ((±)-4.22)

(±)-*threo*-3-Iodomethylphenidate hydrochloride ((±)-**4.29**) (0.14 g, 0.35 mmol) was added to a suspension of K_2CO_3 (0.19 g, 1.43 mmol) in DMF (7 mL). The mixture was stirred at room temperature for 10 min then *p*-N_3-*N*-BnBr (Mornet *et al*., 1984) (80 mg, 0.39 mmol) was added. The reaction was allowed to stir at room temperature in the dark for 30 hrs, Et_2O (20 mL) was added and the mixture was decanted followed by rinsing with Et_2O (2 × 20 mL). The combined organic layers were washed with H_2O, dried (MgSO4), concentrated and chromatographed (EtOAc/hexanes, 5: 95) to give 0.11 g of (±)-**4.22** as a yellow gum (63%). R_f = 0.23 (EtOAc/hexanes, 5: 95). ^{1}H NMR ($CDCl_3$, 400 MHz): δ 7.74 (s, 1H), 7.60 (d, 1H, *J* = 7.89 Hz), 7.36 (d, 1H, *J* = 7.83 Hz), 7.26 (d, 2H, *J* = 8.62 Hz), 7.05 (t, 1H, *J* = 7.81 Hz), 6.97 (d, 1H, *J* = 8.41 Hz), 4.08 (d,

1H, *J* = 11.52 Hz), 3.89 (d, 1H, *J* = 13.60 Hz), 3.74 (d, 1H, *J* = 13.60 Hz), 3.66 (s, 3H), 3.46-3.42 (m, 1H), 2.97-2.90 (m, 1H), 2.53-2.49 (m, 1H), 1.58-1.48 (m, 5H), 1.07-1.03 (m, 1H). ^{13}C NMR ($CDCl_3$, 100 MHz): δ 173.4, 139.2, 138.4, 137.0, 136.6, 130.3, 129.9, 128.0, 118.7, 94.5, 62.5, 55.9, 52.5, 51.9, 44.6, 21.1, 20.6, 19.4. HRMS calcd for $C_{21}H_{23}IN_4O_2H^+$ 491.0938, found 491.0945. IR: azide, 2111 cm^{-1}.

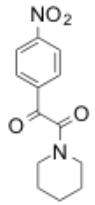

5.17

1-(4-Nitrophenylgloxylyl)piperidine (5.17)

A solution of 4- nitrophenylglyoxylate **5.16** (1 g, 4.48 mmol) in EtOH (6 mL) was treated with piperidine (1.3 mL, 13.44 mmol). The mixture was stirred at 68 °C overnight then cooled to room temperature, diluted with 1 M aq. HCl, and extracted with EtOAc. The combined organic extracts were washed with H_2O and brine, then dried ($MgSO_4$), filtered, and concentrated. The crude material was chromatographed (EtOAc/hexanes, 3:7) to provide 1.07 g of amide **5.17** as a yellow solid (91%). R_f = 0.2 (EtOAc/hexanes, 3:7). ^1H NMR data proved identical to that previously reported (Song *et al*., 2007).

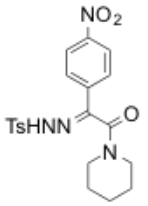

5.18

1-(4-Nitrophenylglyoxylyl)piperidine *p*-toluenesulfonylhydrazone (5.18)

Ketone **5.17** (5.7 g, 21.86 mmol) was added to a stirred mixture of *p*-toluenesulfonyl hydrazide (4.4 g, 23.6 mmol) and H_2SO_4 (0.03 g, 0.33 mmol) in EtOH (170 mL). The reaction mixture was refluxed at 85 °C overnight, then cooled to room temperature. The yellow solid precipitate was collected by filtration, washed with cold MeOH then cold hexanes, and dried in vacuo to give 9.4 g of hydrazone **5.18** (59%). R_f = 0.18 (EtOAc/hexanes, 1:1). ^{1}H NMR ($CDCl_3$, 400 MHz): δ 8.51 (s, 1H), 8.23 (d, 2H, J = 8.88 Hz), 7.85 (d, 2H, J = 8.27 Hz), 7.74 (d, 2H, J = 8.76 Hz), 7.30 (d, 2H, J = 8.37 Hz), 3.75-3.70 (m, 2H), 3.20-3.15 (m, 2H), 2.40 (s, 3H), 1.70-1.65 (m, 4H), 1.55-1.45 (m, 2H). ^{13}C NMR ($CDCl_3$, 100 MHz): δ 161.0, 148.6, 147.2, 144.5, 138.1, 134.9, 129.7, 127.9, 127.0, 124.1, 47.3, 42.5, 26.4, 25.5, 24.0, 21.6. HRMS calcd for $(C_{20}H_{22}N_4O_5S)Na^+$ 453.1203, found 453.1206. Mp: 179-180 °C.

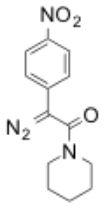

5.19

2-Diazo-2-(4-nitrophenyl)-1-(piperidin-1-yl)ethanone (5.19)

50% aq. NaOH (0.7 mL, 9.02 mmol) was added to a stirred mixture of hydrazone **5.18** (3.7 g, 8.6 mmol) and Aliquat 336® (0.035 g, 0.086 mmol) in toluene (60 mL). The reaction mixture was refluxed at 130 °C for 20 minutes, then cooled to room temperature, diluted with H_2O, and extracted with toluene. The combined organic layers were dried ($MgSO_4$), filtered, concentrated, and recrystallized in Et_2O to give 2.24 g of α-diazo amide **5.19** as a reddish brown solid (95%). R_f = 0.33 (EtOAc/hexanes, 3:7). ^{1}H NMR ($CDCl_3$, 400 MHz): δ 8.19 (d, 2H, *J* = 9.06 Hz), 7.33 (d, 2H, *J* = 9.1 Hz), 4.00-3.45 (m, 4H), 1.70- 1.65 (m, 2H), 1.65-1.60 (m, 4H). ^{13}C NMR ($CDCl_3$, 100 MHz): δ 162.8, 144.7, 136.2, 124.4, 123.1, 46.7, 25.8, 24.4. HRMS calcd for $(C_{13}H_{14}N_4O_3)_2Na^+$ 571.2024, found 571.2027. Anal. calcd for: $C_{13}H_{14}N_4O_3$: C, 56.93; H, 5.14; N, 20.43. Found: C, 57.13; H, 5.2; N, 20.2. Mp: 62-65 °C.

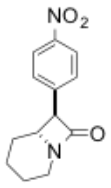

(±)-**5.20**

(±)-*threo*-(6S,7S)-7-(4-Nitrophenyl)-1-azabicyclo[4.2.0]octan-8-one ((±)-5.20)

A solution of α-diazo amide **5.19** (2.24 g, 8.16 mmol) in toluene (60 mL) was refluxed overnight, cooled to room temperature, then concentrated, chromatographed (EtOAc/hexanes, 1:1), and recrystallized from Et_2O to give 1.07 g of (±)- *threo*-β-lactam (±)-**5.20** as a yellow solid (53%). This reaction provided a mixture of threo and erythro diastereomers and the relative configuration is easily determined by ^{1}H NMR spectrum analysis of the coupling constants between the benzylic and bridge-head protons. The coupling constant for *trans* diastereomers ((±)-**5.20**) is 1.4 Hz and the impurity which are

the *cis* diastereomers have a coupling constant of 5.0 Hz (Backes, 2014). R_f = 0.3 (EtOAc/hexanes, 1:1). ^{1}H NMR ($CDCl_3$, 400 MHz): δ 8.19 (d, 2H, *J* = 8.78 Hz), 7.47 (d, 2H, *J* = 8.68 Hz), 4.08-4.07 (m, 1H), 3.95-3.90 (m, 1H), 3.45- 3.40 (m, 1H), 2.85-2.75 (m, 1H), 2.25-2.21 (m, 1H), 2.00-1.94 (m, 1H), 1.75-1.71 (m, 1H), 1.50-1.40 (m,3H). ^{13}C NMR ($CDCl_3$, 100 MHz): δ 164.7, 147.1, 143.1, 128.2, 123.9, 62.8, 56.3, 39.2, 30.5, 24.3, 22.0. HRMS calcd for $(C_{13}H_{14}N_2O_3)_2Na^+$ 515.1901, found 515.1902. Mp: 115-116 °C.

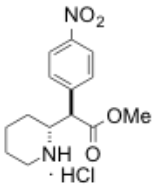

(±)-**4.39**

(±)-*threo*-4-Nitromethylphenidate hydrochloride ((±)-4.39)

(±)-*threo*-β-lactam (±)-**5.20** (0.5 g, 2.03 mmol) was refluxed in 1.25 M HCl in MeOH (40 mL) for 7 hrs, cooled to room temperature, then concentrated to provide 0.63 g of (±)-**4.39** (99%) as the HCl salt. R_f = 0.39 ($CHCl_3$/MeOH, 9:1). ^{1}H NMR ($CDCl_3$, 400 MHz): δ 8.28 (d, 2H, *J* = 8.79 Hz), 7.60 (d, 2H, *J* = 8.79 Hz), 4.15-4.10 (m, 1H), 4.0-3.9 (m, 1H), 3.75 (s, 3H), 3.5-3.4 (m, 1H), 3.2-3.0 (m, 1H), 2.0-1.3 (m, 6H). ^{13}C NMR (MeOD, 100 MHz): δ 172.3, 142.2, 131.2, 125.3, 58.8, 54.8, 53.8, 46.8, 27.7, 23.2, 22.7. HRMS calcd for $(C_{14}H_{19}N_2O_2)^+$ 279.1339, found 279.1340. Anal. calcd for: $C_{14}H_{19}ClN_2O_4$: C, 53.42; H, 6.08; N, 8.90; Cl, 11.26. Found: C, 53.5; H, 6.0; N, 9.01; Cl, 11.02. Mp: 163-165 °C.

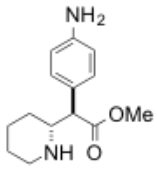

(±)-**4.36**

(±)-*threo*-4-Aminomethylphenidate ((±)-4.36)

Concentrated HCl (5.8 mL) was slowly added to a 0˚C solution of hydrochloride salt (±)-**4.39** (0.5 g, 1.58 mmol) in MeOH (11.7 ml). The mixture was then treated with $SnCl_2$ (1.16 g, 6.11 mmol) and stirred at room temperature overnight. The reaction was quenched with H_2O (50 mL), adjusted to pH >12 using solid NaOH, then extracted with EtOAc (50 mL x 2). The combined organic layers were washed with brine (50 mL), then dried ($MgSO_4$), filtered, and concentrated to give 0.24 g of aniline (±)-**4.36** as a yellow solid (61%). R_f = 0.42 ($CHCl_3$/MeOH/Et_3N, 95:3:2). ^{1}H NMR ($CDCl_3$, 400 MHz): δ 7.06 (d, 2H, *J* = 8.45 Hz), 6.62 (d, 2H, *J* = 8.47 Hz), 3.63 (s, 5H), 3.35-3.25 (m, 1H), 3.1-3.0 (m, 2H), 2.8-2.6 (m, 1H), 2.0-1.9 (br s, 1H), 1.75-1.65 (m, 1H), 1.6-1.5 (m, 1H), 1.45-1.15 (m, 3H), 1.0-0.85 (m, 1H). ^{13}C NMR (MeOD, 100 MHz): δ 174.3, 145.7, 129.4, 126.3, 115.2, 58.9, 57.8, 51.8, 46.9, 29.9, 26.2, 24.4. HRMS calcd for $(C_{14}H_{20}N_2O_2)Na^+$ 271.1417, found 271.1420. Anal. calcd for: $C_{14}H_{19}ClN_2O_4$: C, 67.71; H, 8.12; N, 11.28. Found: C, 67.62; H, 8.02; N, 11.09. Mp: 123-125˚C.

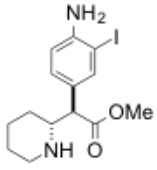

(±)-**4.40**

(±)-*threo*-4-Amino-3-iodomethylphenidate ((±)-4.40).

Iodine monochloride (36 mg, 0.2 mmol) was added to a solution of aniline (±)-**4.36** (50 mg, 0.2 mmol) in glacial AcOH (3.5 mL). The mixture was stirred overnight at room temperature, then concentrated to dryness. The residue was partitioned between 1 M aq. NaOH and EtOAc, then the separated organic layer was washed with brine, dried ($MgSO_4$), filtered, concentrated, and chromatographed ($CHCl_3$/MeOH/Et_3N, 95:3:2) to give 26 mg of iodo-aniline (±)-**4.40** as brown gum (35%). R_f = 0.45 ($CHCl_3$/MeOH/Et_3N, 95:3:2). ^1H NMR ($CDCl_3$, 400 MHz): δ 7.54 (d, 1H, *J* = 2.01 Hz), 7.05 (dd, 1H, *J* = 2.03 Hz, 8.22 Hz), 6.67 (d, 1H, *J* = 8.21 Hz), 4.11 (s, 2H), 3.64 (s, 3H), 3.3-3.2 (m, 1H), 3.1-2.9 (m, 2H), 2.75-2.60 (m, 1H), 2.0-1.9 (br s, 1H), 1.75-1.65 (m, 1H), 1.60-1.55 (m, 1H), 1.4-1.2 (m, 3H), 1.0-0.85 (m, 1H). ^{13}C NMR ($CDCl_3$, 100 MHz): δ 173.8, 146.2, 138.5, 129.4, 127.7, 114.5, 84.0, 58.8, 57.2, 51.9, 46.8, 29.9, 26.1, 24.3. HRMS calcd for $(C_{14}H_{19}IN_2O_2)Na^+$ 397.0383, found 397.0381. Anal. calcd for: $C_{14}H_{19}ClN_2O_4$: C, 44.93; H, 5.12; N, 7.49; I, 33.91. Found: C, 45.00; H, 5.19; N, 7.48; I, 31.91.

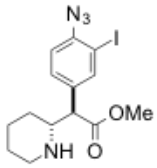

(±)-**4.35**

(±)-*threo*-4-Azido-3-iodomethylphenidate ((±)-4.35)

A solution of iodo-aniline (±)-**4.40** (0.14 g, 0.38 mmol) in 1 M aq. HCl (2 mL) at 0˚C was treated with $NaNO_2$ (29 mg, 0.42 mmol). The mixture was stirred in the dark for 1 hr at 0˚C, then treated with NaN_3 (26 mg, 0.39 mmol), stirred for 2 hrs at 0˚C, and diluted sat. aq. $NaHCO_3$ solution. The resulting mixture was extracted with EtOAc and

the combined organic layers were washed with brine, dried ($MgSO_4$), filtered, and concentrated to provide 150 mg of azido-iodo (±)-**4.35** as a gray solid (99%). R_f = 0.30 ($CHCl_3$/MeOH/Et_3N, 95:3:2). ^1H NMR ($CDCl_3$, 400 MHz): δ 7.72 (d, 1H, *J* = 1.98 Hz), 7.33 (dd, 1H, *J* = 2.00 Hz, 8.26 Hz), 7.08 (d, 1H, *J* = 8.23 Hz), 3.66 (s, 3H), 3.40-3.35 (m, 1H), 3.1-3.0 (m, 2H), 2.75-2.60 (m, 1H), 2.0-1.9 (br s, 1H), 1.75-1.65 (m, 1H), 1.65-1.55 (m, 1H), 1.4-1.2 (m, 3H), 1.0-0.85 (m, 1H). ^{13}C NMR ($CDCl_3$, 100 MHz): δ 173.1, 141.0, 139.7, 134.8, 129.7, 118.4, 88.0, 58.8, 57.4, 52.2, 46.8, 30.0, 26.0, 24.2. HRMS calcd for $(C_{14}H_{17}IN_4O_2)Na^+$ 423.0288, found 423.0284. Anal. calcd for: $C_{14}H_{17}IN_4O_2$•0.1535 EtOAc: C, 42.42; H, 4.44; N, 13.54; I, 30.67. Found: C, 42.67; H, 4.38; N, 13.65; I, 30.71. IR: azide, 2124 cm^{-1}. Mp: 98-100˚C.

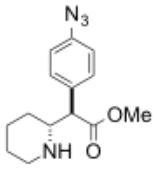

(±)-**4.41**

(±)-*threo*-4-Azidomethylphenidate ((±)-4.41)

A solution of aniline (±)-**4.36** (0.11 g, 0.44 mmol) in 1 M aq. HCl (2 mL) at 0˚C was treated with $NaNO_2$ (33 mg, 0.48 mmol). The mixture was stirred in the dark for 1 hr at 0˚C then treated with NaN_3 (30 mg, 0.46 mmol). The resulting mixture was stirred for 2 hrs at 0˚C, diluted sat. aq. $NaHCO_3$ solution, then extracted with EtOAc. The combined organic layers were washed with brine, dried ($MgSO_4$), filtered, and concentrated to provide 0.12 g of azide (±)-**4.41** as a brown gum (99%). R_f = 0.45 ($CHCl_3$/MeOH/Et_3N, 95:3:2). ^1H NMR ($CDCl_3$, 400 MHz): δ 7.28 (d, 2H, *J* = 8.52 Hz), 6.98 (d, 2H, *J* = 8.55 Hz), 3.65 (s, 3H), 3.45-3.4(m, 1H), 3.15-3.0 (m, 2H), 2.75-2.65 (m,

1H), 2.05-1.95 (br s, 1H), 1.75-1.65 (m, 1H), 1.65-1.55 (m, 1H), 1.45-1.15 (m, 3H), 1.05-0.85 (m, 1H). ^{13}C NMR ($CDCl_3$, 100 MHz): δ 173.6, 139.4, 133.2, 129.9, 119.2, 58.9, 58.0, 52.0, 46.8, 30.0, 26.1, 24.3. HRMS calcd for $(C_{14}H_{18}N_4O_2)Na^+$ 297.1322, found 297.1329. IR: azide, 2121 cm^{-1}.

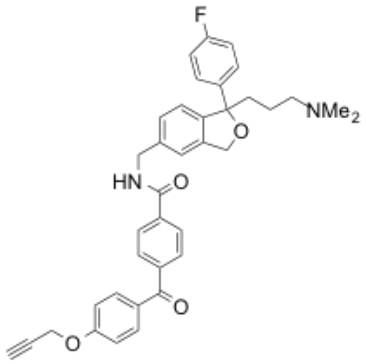

(±)-**4.44**

***N*-((1-(3-(dimethylamino)propyl)-1-(4-fluorophenyl)-1,3-dihydroisobenzofuran-5-yl)methyl)-4-(4-(prop-2-yn-1-yloxy)benzoyl)benzamide ((±)-4.44)**

To a solution of carboxylic acid **5.22** (Bandyopadhyay and Bong, 2011) (84 mg, 0.30 mmol) in DMF (2 mL) at 0˚C was added EDC (49 mg, 0.31 mmol) and HOBT (43 mg, 0.31 mmol) and the mixture was stirred in the dark for 1 hr. To this mixture, a solution of (±)-5-(aminomethyl)-citalopram (±)-**5.21** (Banala *et al*., 2013) (119 mg, 0.36 mmol) in DMF (1 mL) and Et_3N (0.2 mL) were added and the mixture was stirred in the dark at room temperature overnight. The mixture was partitioned between H_2O and EtOAc and the combined organic layers were washed with 1 M NaOH, brine, dried (MgSO4), concentrated and chromatographed ($CHCl_3$/MeOH/Et_3N, 95:3:2) to give 112 mg of (±)-**4.44** as a pale yellow semisolid (63%). R_f = 0.19 ($CHCl_3$/MeOH/Et_3N, 95:3:2). ^{1}H NMR ($CDCl_3$, 400 MHz): δ 7.87 (d, 2H, J = 8.4 Hz), 7.77 (d, 2H, J = 8.9 Hz), 7.71 (d, 2H, J = 8.4 Hz), 7.46-7.40 (m, 2H), 7.28-7.18 (m, 3H), 7.11 (t, 1H, J = 5.7 Hz), 7.02 (d,

2H, *J* = 8.9 Hz), 6.95 (t, 2H, *J* = 8.7 Hz), 5.12 (d, 1H, *J* = 12.6 Hz), 5.07 (d, 1H, *J* = 12.5 Hz), 4.76 (d, 2H, J_1 = 18.1 Hz), 4.61 (d, 2H, J_1 = 5.7 Hz), 2.58 (d, 2H, J_1 = 2.4 Hz) 2.30-2.0 (m, 10H), 1.60-1.20 (m, 2H). ^{13}C NMR ($CDCl_3$, 100 MHz): δ 194.7, 166.6, 162. 9, 161.3, 160.5, 143.7, 141.0, 140.9, 140.6, 139.8, 137.8, 137.2, 132.5, 130.2, 129.7, 127.4, 127.0, 126.8, 126.7, 122.1, 120.7, 115.1, 114.8, 114.6, 90.8, 77.7, 76.4, 71.7, 59.6, 55.9, 45.4, 43.9, 39.3, 22.3. HRMS calcd for $(C_{37}H_{35}FN_2O_4)Na^+$ 613.2473, found 613.2476. Anal. calcd for: $C_{37}H_{35}FN_2O_4$•0.5506$CH_3CO_2C_2H_5$: C, 73.66; H, 6.21; N, 4.38; F, 2.97. Found: C, 73.53; H, 5.99; N, 4.68; F, 3.11.

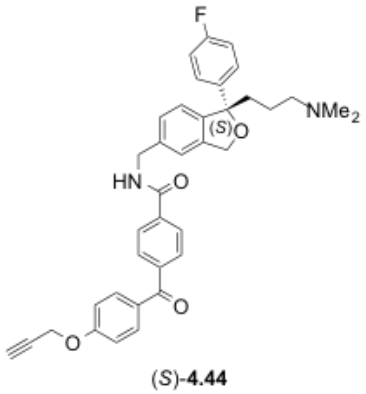

(*S*)-**4.44**

(*S*)-*N*-((1-(3-(dimethylamino)propyl)-1-(4-fluorophenyl)-1,3-dihydroisobenzofuran-5-yl)methyl)-4-(4-(prop-2-yn-1-yloxy)benzoyl)benzamide ((*S*)-4.44)

Propargyloxy benzophenone carboxylic acid **5.22** (Bandyopadhyay and Bong, 2011) (0.43 g, 1.52 mmol) was activated with EDC (0.25 g, 1.6 mmol) and HOBT (0.22 g, 1.6 mmol), by dissolving in 4 mL DMF and stirring at 0 °C for 1 hr in dark. A solution of 5-(aminomethyl)-*S*-Citalopram (*S*)-**5.21** (Kumar *et al*., 2014) (0.5 g, 1.52 mmol) in DMF was added to this mixture, followed by Et_3N (1 mL) and allowed to stir at room temperature overnight. The reaction is quenched with 100 mlL water and extracted with ethylacetate (2 x 100 mL). The combined organic layers were washed with 1 M NaOH,

Brine, dried ($MgSO_4$), concentrated and chromatographed (EtOAc:Et_3N, 95:05) to give 724 mg probe (*S*)-**4.44** as pale yellow semisolid (80.5%). R_f = 0.258 (EtOAc:Et_3N, 95:05). ^1H NMR ($CDCl_3$, 400 MHz) 7.87 (d, 2H, *J* = 8.3 Hz), 7.74 (d, 2H, *J* = 8.9 Hz), 7.67 (d, 2H, *J* = 8.32 Hz), 7.55-7.45(m, 1H), 7.44-7.40 (m, 2H), 7.3-7.20 (m, 2H), 7.16 (s, 1H), 7.0 (d, 2H, *J* = 8.9 Hz), 6.96-6.91 (m, 2H), 5.1 (d, 1H, *J* =12.7 Hz), 5.05 (d, 1H, *J* = 12.7 Hz), 4.75(d, 2H, *J* = 2.4 Hz) 4.58 (d, 2H, *J* = 5.74 Hz), 2.6 (t, 1H, *J* = 2.4 Hz), 2.26-2.0 (m, 10H), 1.5-1.2 (m, 2H). ^{13}C NMR ($CDCl_3$, 100 MHz): 194.7, 166.7, 162.9, 161.3, 160.4, 143.6, 141.0, 140.9, 140.5, 139.7, 137.9, 137.2, 132.4, 130.2, 129.6, 127.3, 127.1, 126.7, 126.6, 121.9, 120.6, 115.0, 114.8, 114.5, 90.7, 77.7, 76.4, 71.7, 59.6, 55.8, 45.3, 43.8, 39.3, 22.2. HRMS calcd for $C_{37}H_{35}FN_2O_4H^+$ 591.265362, found 591.264776. Anal. calcd for: $C_{37}H_{35}FN_2O_4 \bullet 0.5815CH_3CO_2C_2H_5$: C, 73.58; H, 6.22; N, 4.36; F, 2.95. Found: C, 73.38; H, 5.96; N, 4.72; F, 3.34. $[\alpha]^{23}_D$ = +0.22 (c = 10, $CHCl_3$).

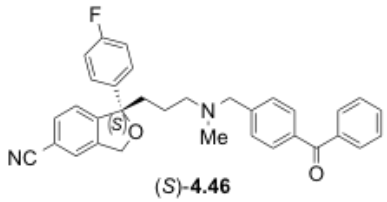

(*S*)-**4.46**

(*S*)-1-(3-((4-benzoylbenzyl)(methyl)amino)propyl)-1-(4-fluorophenyl)-1,3-dihydroisobenzofuran-5-carbonitrile ((*S*)-4.46)

To a solution of (*S*)-Desmethylcitalopram (*S*)-**5.33** (Jin *et al*., 2007) (150 mg, 0.48 mmol) in CH_3CN (3 mL) and *N*,*N*-diisopropylethylamine (0.12 mL) was added 4-(bromomethyl)benzophenone **5.34** (136 mg, 0.53 mmol) and the mixture was stirred at room temperature for 5 hrs. The mixture is then concentrated, diluted with saturated $NaHCO_3$, extracted with EtOAc, washed with brine, dried ($MgSO_4$), filtered,

concentrated, and chromatographed (EtOAc/hexanes, 2:8) to give 143 mg of (*S*)-**4.46** as a pale yellow gum (59%). R_f = 0.325 (EtOAc/hexanes, 2:8). ^{1}H NMR ($CDCl_3$, 400 MHz): δ 7.81-7.74 (m, 4H), 7.61-7.57 (m, 2H), 7.51-7.46 (m, 3H), 7.44-7.36 (m, 5H), 7.0 (t, 2H, *J* = 8.6 Hz), 5.18 (d, 1H, *J* = 12.9 Hz), 5.14 (d, 1H, *J* = 12.9 Hz), 3.48 (s, 2H), 2.36 (t, 2H, *J* = 7.1 Hz), 2.30-2.10 (m, 5H), 1.60-1.35 (m, 2H). ^{13}C NMR ($CDCl_3$, 100 MHz): δ 196.5, 163.2, 149.5, 144.3, 140.3, 139.5, 137.7, 136.3, 132.4, 131.9, 130.2, 129.9, 128.6, 128.3, 126.8, 126.7, 125.2, 122.7, 118.6, 115.5, 115.2, 111.7, 91.1, 71.3, 62.0, 57.2, 42.2, 38.9, 21.9. HRMS calcd for $(C_{33}H_{29}FN_2O_2)H^+$ 505.2286, found 505.2279. $[\alpha]^{24}_D$ = -1.7 (c = 5.7, $CHCl_3$).

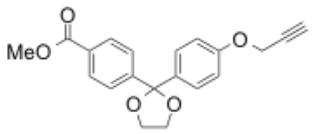

5.35

Methyl 4-(2-(4-(prop-2-yn-1-yloxy)phenyl)-1,3-dioxolan-2-yl)benzoate (5.35)

A mixture of benzophenone analog **(5.28)** (Bandyopadhyay and Bong, 2011) (100 mg, 0.34 mmol), ethane-1,2-diol (1.67 g, 26.9 mmol), 1,2-bis(trimethylsilyloxy)ethane (2.52 g, 12.2 mmol), *p*-toluenesulfonic acid hydrate (4.5 mg, 0.024 mmol), and toluene (1.6 mL) was heated under reflux for 4 hrs. The mixture was then cooled to room temperature and washed with a sat. aq. $NaHCO_3$ solution (10 mL). The organic layer was separated, the aqueous layer was extracted with hexanes/EtOAc (6:4 (v/v); 3 x 20 mL). The combined organic layers were dried ($MgSO_4$), filtered, concentrated and chromatographed (EtOAc/hexanes, 1:9) to give 87 mg of cyclic ketal **5.35** as a colorless oil (75%). R_f = 0.26 (EtOAc/hexanes, 2:8). ^{1}H NMR ($CDCl_3$, 400 MHz): *δ* 7.99 (d, 2H, *J* = 8.6 Hz), 7.60 (d, 2H, *J* = 8.6 Hz), 7.40 (d, 2H, *J* = 8.9 Hz), 6.90 (d, 2H, *J* = 8.9 Hz),

4.65 (d, 2H, J = 2.4 Hz), 4.10-4.0 (m, 4H), 3.90 (s, sH), 2.50 (t, 1H, J = 2.4 Hz). ^{13}C NMR ($CDCl_3$, 100 MHz): δ 166.7, 157.4, 147.1, 134.6, 129.7, 129.5, 127.4, 126.1, 114.4, 108.8, 78.3, 75.6, 64.9, 55.6, 52.0. HRMS calcd for $(C_{20}H_{18}O_5)Na^+$ 361.1046, found 361.1044.

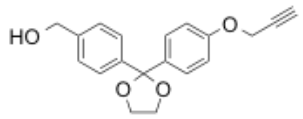

5.36

(4-(2-(4-(Prop-2-yn-1-yloxy)phenyl)-1,3-dioxolan-2-yl)phenyl)methanol (5.36)

Lithium Aluminium Hydride (1 M in THF, 3.98 mL) was added to a solution of ester **5.35** (290 mg, 0.86 mmol) in THF (16 mL) and Et_2O (32 mL) at 0˚C. The mixture was then removed from ice bath and refluxed at 70˚C for 5 hrs. The mixture was cooled to room temperature, quenched by sequential addition of H_2O (0.16 mL), 15% aqueous NaOH (0.16 mL) and H_2O (0.4 mL). The mixture is then filtered, washed with brine, dried ($MgSO_4$), filtered, concentrated and chromatographed (EtOAc/hexanes, 2:8) to provide 168 mg of alcohol **5.36** as colorless oil (70%). R_f = 0.31 (EtOAc/hexanes, 4:6). ^{1}H NMR ($CDCl_3$, 400 MHz): δ 7.47 (d, 2H, J = 8.3 Hz), 7.40 (d, 2H, J = 8.9 Hz), 7.30 (d, 2H, J = 8.4 Hz), 6.90 (d, 2H, J = 8.9 Hz), 4.64 (d, 2H, J = 2.4 Hz), 4.60 (s, 2H), 4.10-3.90 (m, 4H), 2.50 (t, 1H, J = 2.4 Hz), 2.06 (s, 1H). ^{13}C NMR ($CDCl_3$, 100 MHz): δ 157.3, 141.5, 140.6, 135.1, 127.5, 126.7, 126.4, 114.3, 109.1, 78.4, 75.5, 64.9, 64.7, 55.7. HRMS calcd for $(C_{19}H_{18}O_4)Na^+$ 333.1097, found 333.1096.

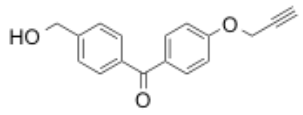

5.37

(4-(Hydroxymethyl)phenyl)(4-(prop-2-yn-1-yloxy)phenyl)methanone (5.37)

A solution of cyclic ketal **5.36** (220 mg, 0.72 mmol) in 10% aqueous HCl (4 mL) was refluxed at 120˚C for 4 hrs. The mixture was then cooled to room temperature, diluted with H_2O and extracted with EtOAc. The organic layer was washed with brine, dried ($MgSO_4$), filtered, concentrated and chromatographed (EtOAc/hexanes, 4:6) to give 128 mg of ketone **5.37** as a colorless gum (67%). R_f = 0.15 (EtOAc/hexanes, 4:6). ^{1}H NMR ($CDCl_3$, 400 MHz): δ 7.78 (d, 2H, J = 8.9 Hz), 7.70 (d, 2H, J = 8.2 Hz), 7.42 (d, 2H, J = 8.4 Hz), 7.02 (d, 2H, J = 8.9 Hz), 4.80-4.70 (m, 4H), 2.91 (s, 1H), 2.58 (t, 1H, J = 2.4 Hz). ^{13}C NMR ($CDCl_3$, 100 MHz): δ 195.5, 161.0, 145.4, 136.9, 132.4, 130.8, 130.4, 126.3, 114.4, 77.8, 76.3, 64.5, 55.9. HRMS calcd for $(C_{17}H_{14}O_3)Na^+$ 289.0835, found 289.0835.

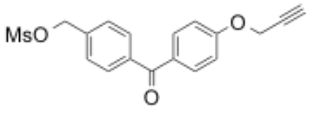

5.38

4-(4-(prop-2-yn-1-yloxy)benzoyl)benzyl methanesulfonate (5.38)

To a solution of alcohol **5.37** (125 mg, 0.47 mmol) in CH_2Cl_2 (5 mL) and triethylamine (0.07 mL, 0.52 mmol) was added mesyl chloride (0.04 mL, 0.52 mmol) at 0 °C, and the mixture was allowed to warm to room temperature. Stirring continued for 2 hrs and the mixture was then partitioned between saturated $NaHCO_3$ and CH_2Cl_2. The organic layer was washed with brine, dried (MgSO4), filtered, concentrated and

chromatographed (EtOAc/hexanes, 4:6) to give 106 mg of mesolate **5.38** as a colorless gum (66%). R_f = 0.27 (EtOAc/hexanes, 4:6). ^{1}H NMR ($CDCl_3$, 400 MHz): δ 7.83 (d, 2H, J = 8.9 Hz), 7.80 (d, 2H, J = 8.3 Hz), 7.53 (d, 2H, J = 8.3 Hz), 7.10 (d, 2H, J = 8.9 Hz), 5.32 (s, 2H), 4.80 (d, 2H, J = 2.4 Hz), 3.02 (s, 3H), 2.58 (t, 1H, J = 2.4 Hz). ^{13}C NMR ($CDCl_3$, 100 MHz): δ 194.7, 161.2, 138.9, 137.2, 132.5, 130.5, 130.215, 128.3, 114.5, 77.7, 76.3, 70.3, 55.6, 38.3.

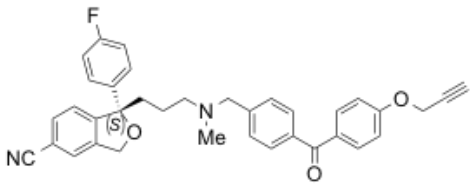

(*S*)-**4.47**

(*S*)-1-(4-Fluorophenyl)-1-(3-(methyl(4-(4-(prop-2-yn-1-yloxy)benzoyl)benzyl)amino) propyl)-1,3-dihydroisobenzofuran-5-carbonitrile ((*S*)-4.47)

To a solution of (*S*)-Desmethylcitalopram (*S*)-**5.33** (Jin *et al*., 2007) (110 mg, 0.35 mmol) in CH_3CN (5 mL) and *N*,*N*-Diisopropylethylamine (0.09 mL) was added mesylate **5.38** (134 mg, 0.39 mmol) and the mixture was stirred at room temperature for 12 hrs. The mixture was then concentrated, diluted with saturated $NaHCO_3$, extracted with EtOAc, washed with brine, dried ($MgSO_4$), filtered, concentrated, and chromatographed (EtOAc/hexanes, 2:1) to give 62 mg of (*S*)-**4.47** as a pale yellow gum (31%). R_f = 0.15 (EtOAc/hexanes, 2:1). ^{1}H NMR ($CDCl_3$, 400 MHz): δ 7.83 (d, 2H, J = 8.9 Hz), 7.71 (d, 2H, J = 8.2 Hz), 7.58 (d, 1H, J = 7.9 Hz), 7.50 (s, 1H), 7.44-7.34 (m, 5H), 7.06-6.90 (m, 4H), 5.18 (d, 1H, J = 12.9 Hz), 5.14 (d, 1H, J = 12.9 Hz), 4.78 (d, 2H, J = 2.4 Hz), 3.48 (s, 2H), 2.57 (t, 1H, J = 2.4 Hz), 2.35 (t, 2H, J = 7.1 Hz), 2.30-2.10 (m, 4H), 1.60-1.30 (m, 2H). ^{13}C NMR ($CDCl_3$, 100 MHz): δ 195.2, 163.1, 160.9, 160.7,

149.4, 143.8, 140.2, 139.5, 136.7, 132.3, 131.8, 130.9, 129.8, 128.5, 126.7, 126.6, 125.2, 122.6, 118.6, 115.4, 115.2, 114.3, 111.6, 91.0, 77.7, 76.1, 71.2, 61.9, 57.1, 55.8, 42.2, 38.8, 21.8. HRMS calcd for $(C_{36}H_{31}FN_2O_3)H^+$ 559.2391, found 559.2389. $[\alpha]^{24}_D$ = -3.36 (c = 5.8, $CHCl_3$).

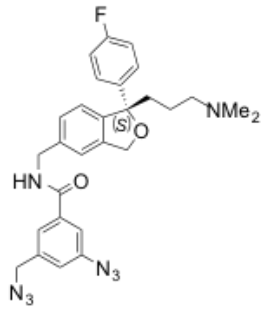

(*S*)-**4.50**

(*S*)-3-azido-5-(azidomethyl)-*N*-((1-(3-(dimethylamino)propyl)-1-(4-fluorophenyl)-1,3-dihydroisobenzofuran-5-yl)methyl)benzamide ((*S*)-4.50)

To a solution of carboxylic acid **5.39** (Neelarapu *et al*., 2011) (78 mg, 0.36 mmol) in DMF (2 mL) at 0 °C was added EDC (59 mg, 0.38 mmol) and HOBT (51 mg, 0.38 mmol) and the mixture was stirred in the dark for 1 hr. To this mixture, a solution of (*S*)-5-(aminomethyl)-citalopram (*S*)-**5.21** (Kumar *et al*., 2014) (118 mg, 0.36 mmol) in DMF (1 mL) and Et_3N (0.25 mL) were added and the mixture was stirred in the dark at room temperature overnight. The mixture was partitioned between H_2O and EtOAc and the combined organic layers were washed with 1 M NaOH, brine, dried ($MgSO_4$), concentrated and chromatographed (EtOAc/Et_3N, 95:5) to give 142 mg of (*S*)-**4.50** as a pale yellow semisolid (75%). R_f = 0.26 (EtOAc/Et_3N, 95:5). ^1H NMR ($CDCl_3$, 400 MHz): δ 7.47-7.41 (m, 4H), 7.27-7.20 (m, 2H), 7.17 (s, 1H), 7.07 (s, 1H), 7.00-6.93 (m, 2H), 6.72 (t, 1H, *J* = 5.5 Hz), 5.14 (d, 1H, *J* = 12.8 Hz), 5.09 (d, 1H, *J* = 12.8 Hz),

4.58 (d, 2H, J = 17.5 Hz), 4.36 (s, 2H), 2.29-2.00 (m, 10H), 1.6-1.2 (m, 2H). ^{13}C NMR ($CDCl_3$, 100 MHz): δ 165.9, 163.0, 160.6, 143.9, 141.4, 141.0, 140.9, 139.9, 138.1, 137.5, 136.6, 127.4, 126.8, 126.7, 122.6, 122.1, 121.2, 120.8, 117.6, 115.1, 114.9, 90.8, 71.7, 59.7, 53.9, 45.4, 43.9, 39.3, 22.3. HRMS calcd for $(C_{28}H_{29}FN_8O_2)H^+$ 529.2470, found 529.2468. IR: azide, 2100 cm^{-1}. $[\alpha]^{24.5}_D$ = +1.3 (c = 4.3, $CHCl_3$).

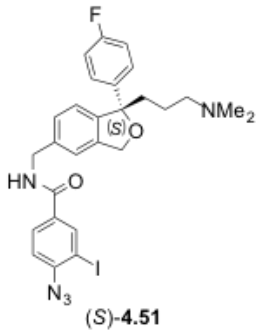

(*S*)-**4.51**

(*S*)-4-azido-*N*-((1-(3-(dimethylamino)propyl)-1-(4-fluorophenyl)-1,3-dihydroisobenzofuran-5-yl)methyl)-3-iodobenzamide ((*S*)-4.51)

To a solution of 4-azido-3-iodobenzoic acid **5.44** (Shu *et al*., 1996) (87 mg, 0.30 mmol) in DMF (2 mL) at 0 °C was added EDC (49 mg, 0.31 mmol) and HOBT (43 mg, 0.31 mmol) and the mixture was stirred in the dark for 1 hr. To this mixture, a solution of (*S*)-5-(aminomethyl)-citalopram (*S*)-**5.21** (kumar *et al*., 2014) (99 mg, 0.30 mmol) in DMF (1 mL) and Et_3N (0.2 mL) were added and the mixture was stirred in the dark at room temperature overnight. The mixture was partitioned between H_2O and EtOAc and the combined organic layers were washed with 1 M NaOH, brine, dried (MgSO4), concentrated and chromatographed (EtOAc/Et_3N, 95:5) to give 120 mg of (*S*)-**4.51** as a colorless semisolid (67%). R_f = 0.257 (EtOAc/Et_3N, 95:5). ^{1}H NMR ($CDCl_3$, 400 MHz): δ 8.18 (d, 1H, J = 1.9 Hz), 7.81 (dd, 1H, J_1 = 8.3, J_2 = 1.9 Hz), 7.50-7.40 (m, 2H), 7.30-

7.20 (m, 2H), 7.16 (s, 1H), 7.10 (d, 1H, J = 8.3 Hz), 6.97 (t, 2H, J = 8.7 Hz), 6.75 (t, 1H, J = 5.5 Hz), 5.12 (d, 1H, J = 12.6 Hz), 5.09 (d, 1H, J = 12.6 Hz), 4.56 (d, 2H, J = 5.7 Hz), 2.3-2.0 (m, 10H), 1.5-1.2 (m, 2H). ^{13}C NMR ($CDCl_3$, 100 MHz): δ 164.9, 162.9, 144.9, 143.8, 140.9, 139.8, 138.7, 137.6, 131.9, 128.5, 127.4, 126.7, 126.6, 122.1, 120.8, 117.9, 115.1, 114.8, 90.8, 87.5, 71.7, 59.6, 45.4, 43.9, 39.3, 22.3. HRMS calcd for $C_{27}H_{27}FIN_5O_2H^+$ 600.1266, found 600.1268. IR: azide, 2117 cm^{-1}. The oxalate salt was precipitated from acetone; Mp: 83-84 °C. Anal calcd for: $C_{29}H_{29}FIN_5O_6$•0.78CH_3COCH_3 •0.40$C_2O_4H_2$: C, 50.07; H, 4.51; N, 9.07; F, 2.46; I, 16.44. Found: C, 50.09; H, 4.46; N, 9.18; F, 2.39; I, 16.39. $[\alpha]^{23.5}_D$ = +2.13 (c = 6, MeOD).

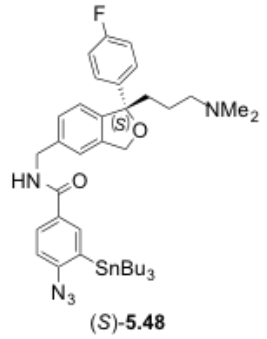

(*S*)-**5.48**

(*S*)-4-azido-*N*-((1-(3-(dimethylamino)propyl)-1-(4-fluorophenyl)-1,3-dihydroisobenzofuran-5-yl)methyl)-3-(tributylstannyl)benzamide ((*S*)-5.48)

A mixture of (*S*)-4-azido-*N*-((1-(3-(dimethylamino)propyl)-1-(4-fluorophenyl)-1,3-dihydroisobenzofuran-5-yl)methyl)-3-iodobenzamide (*S*)-**4.51** (170 mg, 0.28 mmol), $Pd(PPh_3)_2Br_2$ (13.5 mg, 0.02 mmol), and bis(tri-*n*-butyltin) (0.26 mL, 0.51 mmol) in toluene (10 mL) was heated at 105˚C for 4 hrs. The mixture was then cooled to room temperature, diluted with saturated aq. K_2CO_3 solution, and then extracted with EtOAc. The organic phase was washed with brine, dried ($MgSO_4$), filtered, concentrated, and

chromatographed (EtOAc/Et_3N, 95:5) to give 110 mg of organostannane (*S*)-**5.48** as a brown oil (52%). R_f = 0.25 (EtOAc/Et_3N, 95:5). ^1H NMR ($CDCl_3$, 400 MHz): δ 7.83 (d, 1H, J = 2.1 Hz), 7.74 (dd, 1H, J_1 = 8.3 Hz, J_2 = 2.1 Hz), 7.50-7.40 (m, 2H), 7.25 (s, 2H), 7.19 (s,1H), 7.13 (d, 1H, J = 8.3 Hz), 6.97 (t, 2H, J = 8.7), 6.42 (t, 1H, J = 5.6 Hz), 5.14 (d, 1H, J = 12.8 Hz), 5.10 (d, 1H, J = 12.8 Hz), 4.62 (d, 2H, J = 5.7 Hz), 2.30-2.0 (m, 10H), 1.60-1.40 (m, 7H), 1.4-1.2 (m, 7H), 1.2-1.0 (m, 6H), 0.9-0.8 (m, 9H). ^{13}C NMR ($CDCl_3$, 100 MHz): δ 166.9, 162.9, 160.5, 149.2, 143.6, 140.9, 139.7, 137.9, 136.3, 135.1, 130.0, 128.5, 127.2, 126.7, 126.6, 121.9, 120.6, 116.5, 114.9, 114.7, 90.7, 71.6, 59.6, 45.3, 43.7, 39.3, 28.9, 27.2, 22.3,13.6, 10.1. HRMS calcd for $C_{39}H_{54}FN_5O_2SnH^+$ 764.3356, found 764.3369. IR: azide, 2109 cm^{-1}. $[\alpha]^{23}_D$ = +1.3 (c = 2.25, $CHCl_3$)

6.2. Materials and Methods for Proteomics

6.2.1. Materials and Equipment

Materials

Cell line

TRex- HEK 293 cell line (HEK 293 cells stably expressing synthetic human serotonin transporter)

Chemicals

3X FLAG® Peptide
Sigma-Aldrich Co., St. Louis, MO

Acetic acid
Fisher Scientific, Waltham, MA

Acetonitrile HPLC grade
Fisher Scientific, Waltham, MA

Acrylamide:Bis 37.5:1
Calbiochem, Gibbstown, NJ

Albumin standard
Thermo Scientific, Rockford, IL

Ammonium bicarbonate
Fisher Scientific, Waltham, MA

Ammonium persulfate
Fisher Scientific, Waltham, MA

ANTI-FLAG® M2 Affinity Gel,
Sigma-Aldrich Co., St. Louis, MO

Aprotinin
MP Biomedicals Inc., Santa Ana, CA
Benzamidine
Sigma-Aldrich Co., St. Louis, MO

Benzethonium chloride
Sigma-Aldrich Co., St. Louis, MO

Bromophenol blue
Fisher Scientific, Waltham, MA

Copper sulfate
Sigma-Aldrich Co., St. Louis, MO

Deoxycholic acid
Sigma-Aldrich Co., St. Louis, MO

Digitonin
Calbiochem, La Jolla, CA

Dithiothreitol (DTT)
Fisher Scientific, Waltham, MA

DMSO
Sigma-Aldrich Co., St. Louis, MO

Dulbecco's modified eagle medium (DMEM)
Hyclone, Logan, UT

EDTA
Fisher Scientific, Waltham, MA

Fetal Bovine Serum (FBS)
Hyclone, Logan, UT

Folin-Ciocalteu's phenol reagent 2N
Sigma-Aldrich Co., St. Louis, MO

Glycerol
Sigma-Aldrich Co., St. Louis, MO

Glycine
Invitrogen, Carlbad, CA

HBSS/Modified
Hyclone, Logan, UT

HEPES Free acid
Amresco, Solon, OH

Iodoacetamide
Sigma-Aldrich Co., St. Louis, MO

IRDye® 680LT goat anti mouse IgG (H+L)
LI-COR, Lincoln, NE

IRDye® 800CW azide infrared dye
LI-COR, Lincoln, NE

IRDye® 800CW goat anti mouse IgG (H+L)
LI-COR, Lincoln, NE

MeOH HPLC grade
Fisher Scientific, Waltham, MA

Modified lowry protein assay reagent
Thermo Scientific, Rockford, IL

Molecular weight markers (928-40000)
LI-COR, Lincoln, NE

Monoclonal ANTI-FLAG® M2, Clone M2
Sigma-Aldrich Co., St. Louis, MO

Odyssey® blocking buffer
LI-COR, Lincoln, NE

Odyssey® nitrocellulose membrane
LI-COR, Lincoln, NE

Penicillin-Streptomycin-Glutamine (PSQ)
Gibco-BRL, Grand Island, NY

Phenylmethylsulfonyl fluoride (PMSF)
Sigma-Aldrich Co., St. Louis, MO

Potassium chloride
Fisher Scientific, Waltham, MA

Potassium phosphate monobasic
Fisher Scientific, Waltham, MA

Sodium chloride
VWR Scientific, Bridgeport, NJ

Sodium dodecyl sulfate
Fisher Scientific, Waltham, MA

Sodium phosphate dibasic
Fisher Scientific, Waltham, MA

Temed (JT Baker)
Capitol Scientific, Inc. Austin, TX

Tetracycline hydrochloride
Sigma-Aldrich Co., St. Louis, MO

Trichloroacetic acid
MP Biomedicals Inc., Santa Ana, CA

Trifluoroacetic acid (TFA)
Sigma-Aldrich Co., St. Louis, MO

Tris[1-benzyl-1H-1,2,3 triazol-4yl)methyl]amine (TBTA)
Sigma-Aldrich Co., St. Louis, MO

Tris-2-carboxyethyl phosphine hydrochloride (TCEP)
Molecular Probes, Grand Island, NY

Tris base
Sigma-Aldrich Co., St. Louis, MO

Tris hydrochloride
Sigma-Aldrich Co., St. Louis, MO

Trypsin-EDTA 10X
Gibco-BRL, Grand Island, NY

Trypsin gold, mass spectrometry grade
Prmega, Madison, WI

Tween-20
Biorad, Hercules, CA

Zeocin
Invitrogen, Carlbad, CA

Equipment

Biorad power PAC 300
Biorad, Hercules, CA

Branson sonifier 250
Branson Ultrasonics Corporation, Danbury, CT

Cell culture incubator
Forma Scientific, Worcester, MA

Dry bath incubator
Fisher Scientific, Waltham, MA

Newport mercury arc lamp, Model 97435-1000-1
Newport Corporation, Irvine, CA

Odyssey classic imager
LI-COR, Lincoln, NE

Optima XE-90 ultracentrifuge
Beckman Coulter, Inc. Brea, CA

Refrigerated tabletop centrifuge, Model 5810R
Eppendorf Scientific, Hauppauge, NY

Themolyne rotomix type 48200
SER, Mountain View. CA

Thermix stirring hot plate, Model 210T
Fisher Scientific, Waltham, MA

Type 70.1 Ti rotor, Titanium, Fixed angle
Beckman Coulter, Inc. Brea, CA

UV-visible spectrophotometer DU 530
Beckman Instruments Inc., Fullerton, CA

Vacufuge concentrator 5301
Eppendorf, Hamburg, Germany

Vortex genie-2, Model G560
VWR Scientific, Bridgeport, NJ

VWR® mini vertical PAGE system
VWR Scientific, Bridgeport, NJ

6.2.2. Cell Culture

A T-Rex-HEK-293-human SERT cell line employed in the study was kindly provided by Dr. Shigetoshi Sugi's laboratory, Mitsubishi Chemical Group Science and Technology Research Center, Inc., Yokohama, Japan. The cells were grown in growth media (DMEM media supplemented with 10% fetal bovine serum (FBS), 1X PSQ, zeocin (100µg/ml)). Cells were grown as monolayers in 75 cm^2 flasks at 37˚C and 5% CO_2 and subcultured twice a week or every 3 days. For subculturing the cells, the exhausted media in the flask was aspirated and the confluent adherent cells were washed with 10 mL of Hanks buffered salt solution (HBSS). To detach the cells from the flask, 2 mL of trypsin-EDTA was added and swirled to cover the cell monolayers. When the cells were detached from the flask, 8 mL of growth media was added to inactivate the trypsin-EDTA. The cell suspension was then transferred into a 15 mL tube and centrifuged at 1000g for 5 minutes. The supernatant was decanted and cell pellet was resuspended in 10 mL growth media. From this cell suspension, 2 mL was then transferred into a new flask containing 18 mL of fresh growth media. The flask was

tightly capped and then gently swirled to evenly suspend the cells. The flask was placed in the incubator and the cells were allowed to grow until the next subculture.

For tetracycline-induction, cells were grown in growth media as monolayers in 10 cm-diameter-tissue culturing plates at 37˚C and 5% CO_2. At around 90% confluence, the exhausted media in the flask was aspirated and new tetracycline-containing induction medium (DMEM media supplemented with 10% fetal bovine serum (FBS), 1X PSQ, tetracycline (1 µg/ml)) was added to the cells. The cells were grown at 37˚C and 5% CO_2 for 24 hrs and then harvested for experiments. The medium was completely removed by aspiration, added phosphate buffrered saline (1X PBS, 137 mm NaCl, 2.7mm KCl, 8.1mM Na_2HPO_4, 1.47 mM KH_2PO_4) (4 °C) and scraped cells to 50 mL falcon tube. Centrifuged at 1000g for 5 minutes to collect cells and discarded the supernatant. The cell pellet in the falcon tube was then dipped into liquid nitrogen for 4 sec to snap freeze and stored at -80 °C until used.

6.2.3. Purification of hSERT: Single-Step Immuno-Affinity Chromatography with FLAG-Epitope Tag

The HEK293 cell pellet (collected from 10 plates) was dispersed in 10 mL lysis buffer (10 mM Tris-HCl, 1 mM EDTA, pH = 7.4, anti-proteolytic cocktail (APC) containing 1.6 µu/mL aprotinin, 100 µM phenylmethylsulfonyl fluoride, 1 mM benzamidine and 100 µM benzethonium chloride) and sonicated using a probe sonicator microtip at maximum power and 50% cycle setting (15 strokes). The cell homogenate was ultracentrifuged at 100,000g for 20 min at 4 °C, and membrane fraction was again homogenized and centrifuged in the same way. The resultant membrane fraction can be

snap frozen in liquid nitrogen and stored at -80 °C until further use. The membrane fraction was then solubilized by resuspending and incubating at 4 °C overnight in 10 mL of solubilization buffer (20 mM Tris-HCl, pH = 7.4, 500 nM NaCl, 10% v/v glycerol, 1 mM EDTA, APC, 1% w/v digitonin). The solubilized SERT was ultracentifuged at 100,000g for 20 min at 4 °C and the supernatant was subjected to affinity chromatography using ANTI-FLAG M2 affinity gel according to the manufacturer instructions for batch mode. Briefly, 1 mL resin (50% solution) was transferred to a 15 mL falcon tube. Centrifuged at 3200g for 2 min at 4 °C and removed the supernatant without discarding any resin. The resin was then washed (2X) with 10 mL of TBS (50 mM Tris HCl, 150 mM NaCl, pH = 7.4) at 4 °C. To this resin, 10 mL of solubilized hSERT was added and incubated for 2 hrs at 4 °C with gentle agitation (nutator). The sample was centrifuged at 3200g for 2 min at 4 °C and unbound supernatant was removed from the resin. The resin was then washed (2X) with 8 mL wash buffer (25mM HEPES, 150 mM NaCl, 10% glycerol, pH 7.4, 0.07 % digitonin). The resin was then incubated with 2 mL elution buffer (the wash buffer with 250 ng/µL 3X FLAG-peptide) for 30 min at room temperature. The sample was centrifuged at 3200g for 2 min at 4°C and elute (purified hSERT) was stored at -20 °C until further use.

6.2.4. Protein Assay: Modified Lowry Assay

Protein concentrations were determined using modified Lowry assay (Peterson, 1977). Protein samples or bovine serum albumin (BSA) standards were diluted to 1.0 mL with distilled H_2O and proteins were precipitated by adding 0.15 mL 1.0% deoxycholate and vortexed and incubated for 10 min at room temperature. Then 0.1 mL 72% tricholoracetic acid was added, mixed by vortexing and centrifuged at 11,000 rpm for 10

min. The supernatant was discarded and the pellet was resuspended in 0.2 ml distilled H_2O. At 15 sec intervals, 1 mL of modified lowry protein assay reagent was added to each sample. The samples were mixed by vortexing and allowed to stand for exactly 10 min at room temperature. Exactly, after the end of each sample's 10 min incubation period, 100 µL of 1X Folin-Ciocalteu reagent was added and immediately mixed vigorously. The color was developed for 30 min in the dark and absorbance at 750 nm was recorded. All samples were run in duplicate. To determine protein sample concentration, the standard curve was plotted using various concentrations of BSA standard. The concentration of protein samples was determined by fitting the experimentally obtained absorbance of protein samples to the BSA standard curve.

6.2.5. SDS-PAGE and Western blot

All protein samples were treated with SDS-PAGE sample buffer containing 2% SDS. Proteins were separated on 10% SDS-PAGE gels at a constant voltage of 120 V and transferred to a nitrocellulose membrane at 90 mA constant current overnight at 4 °C. The membrane was blocked with Odyssey blocking buffer, washed twice and incubated with the primary antibody with a dilution of 1 µg/mL (monoclonal ANTI-FLAG M2, Clone M2 produced in mouse, Sigma-Aldrich) for 2 hr at room temperature in blocking buffer with 0.1% Tween-20. The membrane was washed with PBS-T (Phosphate buffered saline with 0.1% Tween-20) buffer for 5 min (4X) and incubated with the IR-conjugated 680LT goat anti-mouse secondary antibody with a dilution of 1:5,000 for 1 hr. The membrane was again washed with PBS-T buffer for 5 min (4X) and scanned on Odyssey imager.

6.2.6. SERT Photoaffinity Labeling and Click-Chemistry

Purified hSERT (100 µL) was taken in 96 well-plate and add (*S*)-**4.44** (1 µL of 100 mM stock in DMSO) and incubate on ice for 1 hr. Then, the 96 well-plate without lid (on ice) was irradiated with UV light (350-450 nm) for 20 min. The click reaction was initiated by adding IRDye® 800CW azide (1 µL of 2.5 mM stock in H_2O, LI-COR), TCEP (2 µL of 50 mM stock in H2O), tris((1-benzyl-1H-1,2,3-triazol-4-yl)methyl)amine (6 µL of 2 mM stock in DMSO:t-BuOH, 1:4), $CuSO_4$ (2 µL of 50 mM stock in H_2O) and allowed to react for 1 hr at room temperature. The reaction was quenched by adding 28 µL of 5X loading dye and the samples were analysed within two days by storing at -20ºC to visualize crosslinking using Western blot. For in-gel scanning, proteins separated by SDS-PAGE were visualized by first soaking the gel in 40% MeOH, 10% acetic acid in water with shaking for 20 mins and directly scanning the gel on Odyssey imager.

6.2.7. In-gel Trypsin Digestion

Before trypsin digestion, cysteine residues were reduced and alkylated with iodoacetamide. Briefly, the gel pieces (each band) were incubated with 100 % acetonitrile (300 µL), and then 50 µL of 10 mM DTT in 100 mM ammonium bicarbonate at 60 °C for 1 hr. After two washes with 100 mM ammonium bicarbonate, the gel pieces were incubated with 50 µL of 50 mM iodoacetamide in 100 mM ammonium bicarbonate for 30 min in dark at room temperature. Then, the gel pieces were washed with 300 µL of wash buffer (20 mM ammonium bicarbonate in 50% acetonitrile) twice for 10 min with gentle agitation. The gel plugs were dehydrated by adding 100 µL acetonitrile. After the gel plugs turned whitish, acetonitrile was removed and dried in a SpeedVac for

about 15 min. Then 20 μL of trypsin buffer (20 μg/mL of trypsin gold in 40 mM ammonium bicarbonate in 10 % acetonitrile) was added to each sample and incubated at room temperature for 1 hr. Then 40 mM ammonium bicarbonate in 10% acetonitrile was added to cover the gel pieces and incubated overnight at 37 °C. The trypsin buffer was transferred to a new tube (labeled). Later, 60 μL of extraction buffer (1% TFA in 50:50 acetonitrile: H_2O) was added to the gel plugs and incubated for 30 min with gentle agitation. Then the 60 μL of extraction buffer was transferred to the above labeled sample tube and the gel plugs were incubated with 40 μL of extraction buffer (1% TFA in acetonitrile/H_2O, 50:50) for 30 min with gentle agitation and then transferred to the above labeled sample tube. Samples were dried in SpeedVac for about 3 hr.

6.3. References

- Axten, J.M., Krim, L., Kung, H.F., and Winkler, J.D. A stereoselective synthesis of *dl-threo*-methylphenidate: preparation and biological evaluation of novel analogues. *J. Org. Chem.* **1998**, *63*, 9628-9629.

- Backes, J. 2-Oxo-azetidine (*β*-Lactame). Houben-Weyl, Science of Synthesis **2014**, 31-942.

- Banala, A.K., Zhang, P., Plenge, P., Cyriac, G., Kopajtic, T., Katz, J.L., Loland, C.J., and Newman, A.H. Design and synthesis of 1-(3-(dimethylamino)propyl)-1-(4-fluorophenyl)-1,3-dihydroisobenzofuran-5-carbonitrile (citalopram) analogues as novel probes for the serotonin transporter S1 and S2 binding sites. *J. Med. Chem.* **2013**, *56*, 9709-9724.

- Bandyopadhyay, S. and Bong, D. Synthesis of trifunctional phosphatidylserine probes for identification of lipid-binding proteins. *Eur. J. Org. Chem.* **2011**, 4, 751-758.

- Gutman, A., Zaltsman, I., Shalimov, A., Sotrihin, M., Nisnevich, G., Yudovich, L., and Fedotev, I. Process for the preparation of dexmethylphenidate hydrochloride. Patent US 20040180928 A1, **2004**.

- Jin, C., Boldt, K.G., Rehder, K.S., and Brine, G.A. Improved syntheses of *N*-desmthylcitalopram and *N*,*N*-didesmethylcitalopram. *Syn. Commun*. **2007**, 37, 901-908.

- Kumar, V., Rahbek-Clemmensen, T., Billesbølle, C.B., Jorgensen, T.N., Gether, U., and Newman, A.H. Novel and high affinity fluorescent ligands for the serotonin transporter based on (*S*)-citalopram. *ACS Med. Chem. Lett.* **2014**, *5*, 696-699.

- Mornet, R., Leonard, N.J., Theiler, J.B., and Doree, M. Specificity of the 1-methyladenine receptors in starfish oocytes: synthesis and properties of some 1,8-disubstituted adenines, 1,6-dimethyl-1*H*-purine, and of the 1-(azidobenzyl)adenines. *J. Chem. Soc. Perkin Trans. 1* **1984**, *5*, 879-885.

- Neelarapu, R., Holzle, D.L., Velaparthi, S., Bai, H., Brunsteiner, M., Blond, S.Y., and Petukhov, P.A. Design, synthesis, docking, and biological evaluation of novel diazide-containing isoxazole- and pyrazole-based histone deacetylase probes. *J. Med. Chem.* **2011**, *54*, 4350-4364.

- Peterson, G.L. A simplification of the protein assay method of Lowry *et al*. which is more generally applicable. *Anal. Biochem.* **1977**, *83*, 346-356.

- Shu, A.Y.L., Yamashita, D.S., Holt, D.A., and Heys, J.R. Synthesis of I-125 labeled photoaffinity rapamycin analogs. *J. Label. Compd. Radiopharm*. **1996**, *38*, 227-237.

- Song, B., Wang, S., Sun, C., Deng, H., and Xu, B. Cesium carbonate promoted aerobic oxidation of arylacetamides: an efficient access to *N*-substituted α-keto amides. *Tetrahedron Lett*. **2007**, *48*, 8982-8986.

- Still, W.C., Kahn, M., and Mitra, A. Rapid chromatographic technique for preparative separations with moderate resolution. *J. Org. Chem.* **1978**, *43*, 2923-2925.

- Thai, D.L., Sapko, M.T., Reiter, C.T., Bierer, D.E., and Perel, J.M. Asymmetric synthesis and pharmacology of methylphenidate and its *para*-substituted derivatives. *J. Med. Chem.* **1998**, *41*, 591−601.

APPENDIX

A.1. Radiosynthesis, Pharmacological Evaluation, and Photoaffinity Labeling Experiments of Racemic 4-Azido-3-Iodo-Methylphenidate ((±)-[^{125}I]-4.35) for DAT Structure-Function Studies

With methylphenidate derivatives aniline (±)-**4.36**, 4-amino-3-iodo (±)-**4.40** and target 4-azido-3-iodo (±)-**4.35** in hand, ligand affinities (K_i values) were determined for inhibition of [^{3}H]-WIN-35,428 (**1.25**) binding to hDAT expressed in N2A neuroblastoma cells by Dr. Christopher Surratt's group (Duquesne University). These results indicated that (±)-**4.35** (K_i = 4.0 ± 0.8 nM) displays 4-fold higher hDAT affinity than (±)-*threo*-methylphenidate ((±)-**1.18**). Given that racemic threo-4-azido-3-iodo-MP ((±)-**4.35**) represented one of the highest affinity DAT photoprobes synthesized to date, further development of this compound into a potential DAT photoprobe was pursued.

Table A.1. Inhibition of [^{3}H]-WIN 35,428 binding of methylphenidate-based compounds at hDAT N2A neuroblastoma cells (Lapinsky, Yarravarapu *et al.*, 2012).

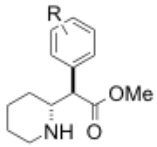

racemic *threo* MP analogs

Compound No.	Aromatic substituent (R)	[^{3}H]-WIN binding inhibition K_i (nM)
(±)-**4.35**	4-N_3-3-I	4.0 ± 0.8
(±)-**4.36**	4-NH_2	6.3 ± 2.0
(±)-**4.40**	4-NH_2-3-I	9.1 ± 1.5

Given that wash-resistant binding experiments involving non-radioactive azido-containing compounds frequently give false positives in assessment of covalent

attachment (Agoston *et al.*, 1997), a radio-iodinated [^{125}I] version of (±)-**4.35** was pursued to determine if photoactivation could produce covalent ligation to the hDAT protein. In this regard, (±)-**[^{125}I]-4.35** was synthesized by Dr John Lever (University of Missouri-Columbia) *via* electrophilic radioiodination of aniline (±)-**4.36** with [^{125}I]-NaI (1.49 mCi) under no-carrier-added conditions using Chloramine-T (*N*-chloro-4-toluenesulfonamide trihydrate) as an oxidant, followed by diazotization and subsequent treatment with sodium azide (Scheme A.1). Reversed-phase HPLC purification provided final photoprobe (±)-**[^{125}I]-4.35** in 54% isolated yield with high purity (98%) and high specific activity (1986 mCi/μmol). Furthermore, purified (±)-**[^{125}I]-4.35** co-eluted with a fully characterized sample of non-radioactive (±)-**4.35** under the same reverse-phase HPLC conditions.

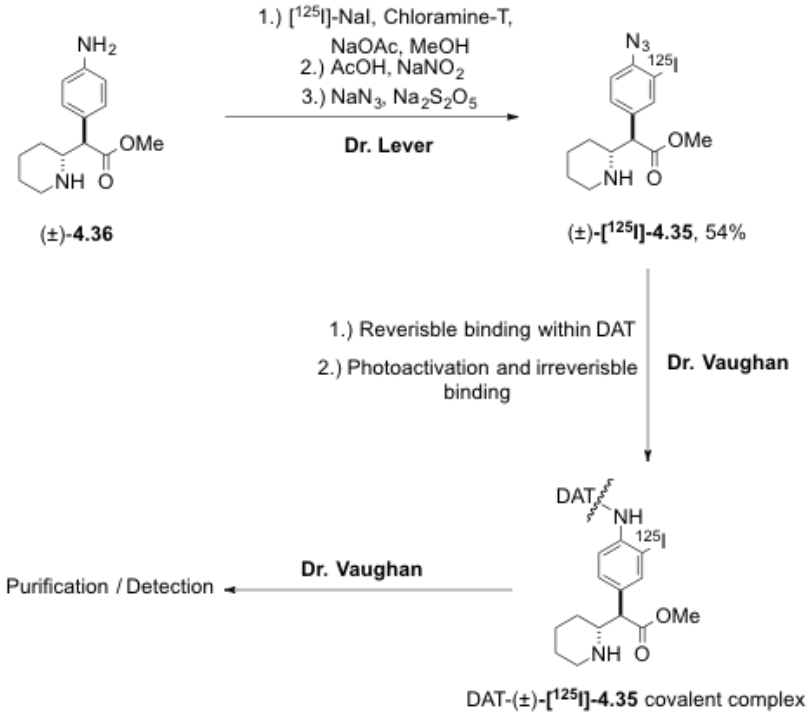

Scheme A.1. Radioiodination and DAT covalent ligation of methylphenidate-based photoprobe **(±)-[^{125}I]-4.35** (Lapinsky, Yarravarapu *et al*., 2012).

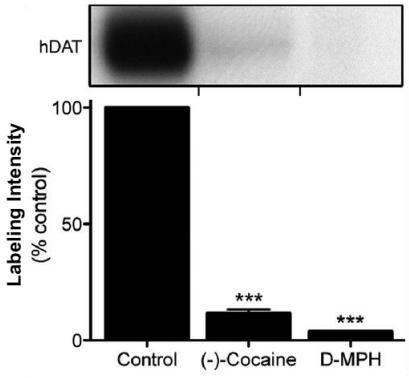

Figure A.1. Photoaffinity labeling of hDAT with **(±)-[^{125}I]-4.35** performed by the Vaughan group. LLCPK1 cells expressing 6Xhis-hDAT were photolabeled with 10 nM (±)-**[^{125}I]-4.35** in the absence or presence of 10 μM (-)-cocaine or D-methylphenidate (D-MPH). Cells were solubilized and DATs were immunoprecipitated followed by analysis by SDS–PAGE and autoradiography. The relevant portion of a representative autoradiograph is pictured followed by a histogram that quantitates relative band intensities (mean ± SE of three independent experiments are shown; ***, $p < 0.001$ *versus* control). (Lapinsky, Yarravarapu *et al*., 2012. Reprinted with permission from *ACS Med. Chem. Lett.* **2012**, *3*, 378-382. Copyright 2012, American Chemical Society).

With radioactive photoprobe (±)-**[^{125}I]-4.35** in hand, Dr Roxanne A. Vaughan's group (University of North Dakota) conducted preliminary photoaffinity labeling experiments with the DAT. In particular, rat striatal membranes and $LLCPK_1$ cells expressing 6Xhis-human DAT were incubated with 10 nM (±)-**[^{125}I]-4.35** in the absence or presence of 10 μM (-)-cocaine or D-(+)-methylphenidate. The membrane and cells were then irradiated with 254 nm UV light for 5 min to photoactivate the azido group and allow irreversible binding of the probe to DAT. Next, the membrane and cells were detergent-solubilized, and the lysates were immunoprecipitated with DAT antibody and analyzed by SDS-PAGE and autoradiography. The isolated ~80 kDa labeled proteins obtained from both $LLCPK_1$ hDAT cells (see Figure A.1) and rat striatal tissue (see Figure A.2) clearly demonstrated the photoincorporation of (±)-**[^{125}I]-4.35** into DAT. Incorporation of photoprobe was >90% blocked by either (-)-cocaine or D-(+)-

methylphenidate, demonstrating the pharmacological specificity of (±)-**[^{125}I]-4.35** attachment to the DAT.

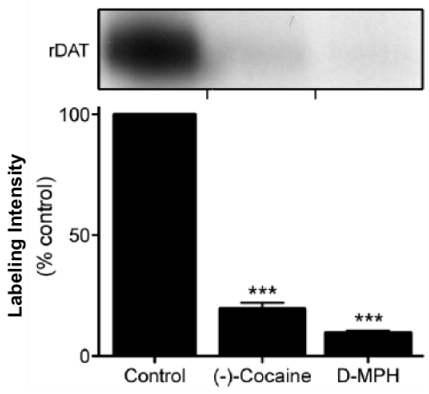

Figure A.2. Photoaffinity labeling of rDAT with (±)-**[^{125}I]-4.35** performed by the Vaughan group. Rat striatal membranes were photolabeled with 10 nM (±)-**[^{125}I]-4.35** in the absence or presence of 10 μM (-)-cocaine or D-methylphenidate (D-MPH). Cells were solubilized and DATs were immunoprecipitated followed by analysis by SDS–PAGE and autoradiography. The relevant portion of a representative autoradiograph is pictured followed by a histogram that quantitates relative band intensities (mean ± SE of three independent experiments are shown; ***, $p < 0.001$ *versus* control). (Lapinsky, Yarravarapu *et al.*, 2012. Reprinted with permission from *ACS Med. Chem. Lett.* **2012**, *3*, 378-382. Copyright 2012, American Chemical Society)

A.2. Radioiodination, and Serotonin Transporter Covalent Ligation of Escitalopram-Based Photoaffinity Ligand ((±)-[^{125}I]-4.51) Containing the Traditional 4-Azido-3-Iodo Photoaffinity Labeling Motif for

Given escitalopram-based photoaffinity ligand (*S*)-**4.51** retained high SERT binding affinity (K_i = 3.45 ± 2.04 nM) when compared to escitalopram (K_i = 1.77 ± 1.14 nM) as a lead compound, further development of this compound into a potential serotonin transporter photoprobe was pursued. Once again, given that wash-resistant binding experiments involving non-radioactive azido-containing compounds frequently give false positives in assessment of covalent attachment (Agoston *et al.*, 1997), synthesis of a radio-iodinated [^{125}I] version of (*S*)-**4.51** was pursued to determine if photoactivation could produce covalent ligation to the hSERT protein. In this regard, tri-*n*-butyl stannyl

analog (*S*)-**5.48** (synthesis described in section 5.2.3) was converted to radioactive iodine derivative (*S*)-[^{125}I]-**4.51** by Dr. John Lever at the University of Missouri-Columbia.

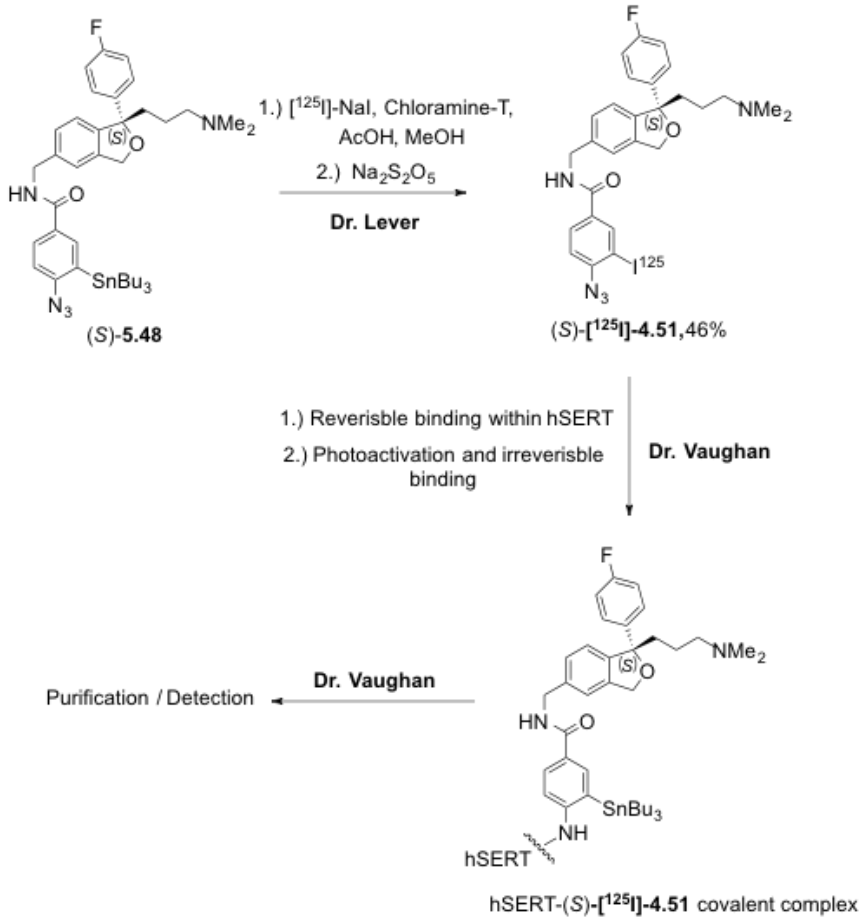

Scheme A.2. Radiosynthesis and SERT covalent ligation of methylphenidate-based photoprobe (*S*)-[^{125}**I**]-**4.51**.

Since carryover of trace amounts of (*S*)-**4.51** would dramatically lower the specific radioactivity of (*S*)-[^{125}I]-**4.51** prepared from (*S*)-**5.48** (Lever, 1996), this material was purified by reversed-phase HPLC prior to radiolabeling. As shown in Scheme A.2, Dr.Lever treated the stannyl derivative (*S*)-**5.48** with [^{125}I]NaI (2.07 mCi) in the presence chloramine-T as the oxidant in methanolic acetic acid, followed by reversed-phase HPLC isolation to provide (*S*)-[^{125}I]-**4.51** in 46% yield with high purity (≥ 98%) and specific

radioactivity of 2096 mCi / μmol. Furthermore, this radioligand exhibited a chromatographic profile identical to that of non-radioactive (*S*)-**4.51**.

To determine if the SERT could be irreversibly labeled (Scheme A.2) with (*S*)-[^{125}I]-**4.51**, Dr. Roxanne Vaughan's group (University of North Dakota) performed photoaffinity labeling with LLCPK cells expressing HA-hSERT incubated with 10 nM (*S*)-[^{125}I]-**4.51** in the absence or presence of 10 μM escitalopram (Scheme A.2). The cells were then detergent-solubilized and the lystates were immunoprecipitated with Anti-HA antibody linked sepharose A beads and samples eluted from the beads were analyzed by SDS-PAGE/autoradiography. Labeled proteins of ~100 kDa were obtained from LLCPK HA-hSERT cells, demonstrating the incorporation of (*S*)-[^{125}I]-**4.51** into the SERT. Incorporation of the enantiomerically pure photoaffinity ligand was blocked by escitalopram, demonstrating the appropriate pharmacological specificity for (*S*)-[^{125}I]-**4.51** attachment to the SERT (Figure A.3). In summary, (*S*)-[^{125}I]-**4.51** represents a successful example of an enantiopure SERT photoaffinity ligand based on a CIT scaffold, thus representing an important contribution to the arsenal of chemical probes useful for characterizing SERT function and 3D structure.

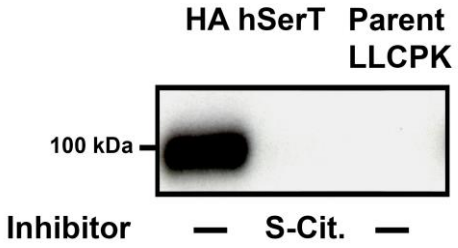

Figure A.3. Photoaffinity labeling of hSERT with (*S*)-**[^{125}I]-4.51** performed by the Vaughan group. LLCPK1 cells expressing HA-hSERT were photolabeled with 10 nM (±)-**[^{125}I]-4.51** in the absence or presence of 10 μM (*S*)-citalopram (S-Cit). Cells were solubilized and DATs were immunoprecipitated followed by analysis by SDS–PAGE and autoradiography.